Host-derived endosymbiont-targeted proteins form part of the division machinery of the bacterial endosymbiont in the trypanosomatid *Angomonas deanei*

Inaugural-Dissertation

Zur Erlangung des Doktorgrades

der Mathematisch-Naturwissenschaftlichen Fakultät

der Heinrich-Heine-Universität Düsseldorf

vorgelegt von

Georg Ehret

Aus Nowo-Iljanowski, Kasachstan

Düsseldorf, August 2023

Aus dem Institut für Mikrobielle Zellbiologie der Heinrich-Heine-Universität Düsseldorf

Gedruckt mit der Genehmigung der

Mathematisch-Naturwissenschaftlichen Fakultät der

Heinrich-Heine-Universität Düsseldorf

Berichterstatter:

1. Prof. Dr. Eva C. M. Nowack

2. Prof. Dr. Johannes Hegemann

Tag der mündlichen Prüfung: _____

Eidesstaatliche Erklärung

Ich versichere an Eides statt, dass die Dissertation von mir selbstständig und ohne unzulässige fremde Hilfe unter Beachtung der „Grundsätze zur Sicherung guter wissenschaftlicher Praxis an der Heinrich-Heine-Universität Düsseldorf“ erstellt worden ist. Die Dissertation wurde in ihrer jetzigen oder ähnlicher Form noch bei keiner anderen Hochschule eingereicht. Ich habe zuvor keine erfolglosen Promotionsversuche unternommen.

Ort, Datum	Georg Ehret

Die Untersuchungen zur vorliegenden Arbeit wurden von Mai 2017 bis August 2022 in Düsseldorf an der Heinrich-Heine-Universität im Institut für Mikrobielle Zellbiologie unter der Betreuung von Prof. Dr. Eva C. M. Nowack durchgeführt.

Teile dieser Arbeit wurden veröffentlicht in:

Morales, J.*, Ehret, G.*, Poschmann, G., Reinicke, T., Maurya, A.K., Kröninger, L., Zanini, D., Wolters, R., Kalyanaraman, D., Krakovka, M., Bäumers, M., Stühler, K., and Nowack, E.C.M. et al. (2023) 'Host-symbiont interactions in Angomonas deanei include the evolution of a host-derived dynamin ring around the endosymbiont division site', Current Biology 33: 28-40. doi: 10.1016/j.cub.2022.11.020.

*Authors contributed equally.

Summary

As life of all cells is finite, cost-intense cellular division is essential for survival. Most often availability of nutrients and habitats is limiting and inter– or intraspecific competition is unavoidable. In some cases tightly associated consortia of organisms of different species have developed in this race for resources by all organisms. These multi-species microbial communities can be classified by its effect on the interactors. If one or several parties' benefit, it is called symbiosis. On the other hand, if one party is damaged for the benefit or another, it is called parasitism.

The longer a consortia of organisms is found in the same biome, the more adaptions occur, slowly refining their abilities during the evolutionary arms race. The evolution of an interaction, especially in its early steps may allow newcomers to obtain growth limiting factors. It is much easier to scavenge a limited resource from another organism than to evolve an entire pathway for de novo synthesis, leading to a dependence, which can become obligate for survival. Often, this is linked to predatory behavior, either by phagocytosis-like processes or by invasion of one organism into another in the cases of single cell organisms and death of the exploited organism is very common. In some cases the retainment and survival of one organism inside another instead seems to be beneficial for both parties. This process has been termed endosymbiosis and is believed to be a key element in the evolution of eukaryotes through the acquisition of mitochondria and chloroplasts more than one billion years ago. Interest in the research of the early steps of endosymbiosis lead to a search for organisms featuring more recent cases of symbiont incorporation.

Two cases of unicellular organisms harboring bacterial endosymbionts (ES) have been the center of attention in our institute: on the one hand *Paulinella chromatophora* with its photosynthetically active ES of α–cyanobacterial origin and on the other hand *Angomonas deanei* – a flagellated trypanosomatid with a β–proteobacterial ES. Genetic tractability made *A. deanei* a perfect candidate as a model organism for a very young but stable endosymbiotic relationship of unknown origin. As *Candidatus* Kinetoplastibacterium crithidii, the bacterial ES originates from a lineage of mainly intracellular pathogens and trypanosomatida have not been observed yet to engulf bacteria, the ES may initially have entered the host as pathogen. Mass spectrometric analysis by whole proteome comparison was performed to understand the level of control, that the host has established over the ES, and revealed only very few putative host-encoded and ES-targeted proteins, which are potential effector proteins necessary for controlling the ES. Experimental verification of these host-encoded proteins showed that only 7, of these so called endosymbiont targeted proteins (ETPs) can be found at or in the ES. Three proteins, ETP2, ETP7, and ETP9 seem to be located at the site of division of the ES and during this thesis particularly ETP2 and ETP7 were explored in more detail. Several attempts were made to generate

homozygous knockouts of both genes in *A. deanei* as well as substitution of one allele against a resistance marker and insertion of reporter fusion protein constructs into the endogenous loci, to test viability of fusion constructs.

To explore the function of the genes in-vivo a conditional protein stabilization system as well as a conditional gene excision system and an inducible expression system were deployed in *A. deanei*. Knock-outs of ETP2, ETP7 and ETP9 were also tested in the aposymbiotic strain ATCC-30969 of *A. deanei*.

In-silico analyses of ETP2 and ETP7 identified both to be unique to the Strigomonadinae, but even within this small group both proteins are poorly conserved and no predicted function for ETP2 could be identified. ETP7 however was predicted to contain a putative peptidoglycan (PG) hydrolase domain according to Phyre² modelling. Furthermore, identification of interaction partners via Co-immunoprecipitation was tested to find hinds on the mode of action of ETP2 and ETP7 in the ES.

To test PG-hydrolyzing activity, ETP7 was expressed in *E. coli* and *Leishmania tarentolae* and purified for in-gel peptidoglycan hydrolysis assay (zymogram) and via turbidity clearing and dye release in plate reader assays. Furthermore, the ability of ETP7 to bind to β-lactams, as observed in penicillin binding proteins (PBPs), was explored. As all steps involving PG restructuring happen in the intermembrane space of the bacterium, ETP7 must be able to migrate through the outer membrane of the ES. To verify this, immunogold-transmission electron microscopy of *A. deanei* was established, to determine the subcellular localization.

Zusammenfassung

Da das Leben aller Zellen endlich ist, ist die kostenintensive Zellteilung für das Überleben unerlässlich. Meistens ist die Verfügbarkeit von Nährstoffen und Lebensräumen begrenzt, und ein inter- oder intraspezifischer Wettbewerb ist unvermeidlich. In einigen Fällen haben sich in diesem Wettlauf aller Organismen um die Ressourcen eng verbundene Konsortien von Organismen verschiedener Arten entwickelt. Diese artenübergreifenden mikrobiellen Gemeinschaften können nach ihren Auswirkungen auf die Interaktionspartner klassifiziert werden. Wenn eine oder mehrere Parteien davon profitieren, spricht man von einer Symbiose. Wird hingegen eine Partei zum Nutzen einer anderen geschädigt, spricht man von Parasitismus.

Je länger ein Konsortium von Organismen im selben Biotop lebt, desto mehr Anpassungen treten auf und verfeinern langsam ihre Fähigkeiten während des evolutionären Wettrüstens. Die Entwicklung einer Interaktion, vor allem in der Anfangsphase, kann es Neuankömmlingen ermöglichen, wachstumsbegrenzende Faktoren zu erhalten. Es ist viel einfacher, eine begrenzte Ressource von einem anderen Organismus zu erbeuten, als einen kompletten Weg für die De-novo-Synthese zu entwickeln, was zu einer Abhängigkeit führt, die für das Überleben unerlässlich werden kann. Oft ist dies mit räuberischem Verhalten verbunden, entweder durch Phagozytose-ähnliche Prozesse oder durch Invasion eines Organismus in einen anderen, wenn es sich um einzellige Organismen handelt, und den Tod des angegriffenen Organismus häufig bedeutet. In einigen Fällen scheinen das Verbleiben und Überleben eines Organismus im Inneren eines anderen für beide Seiten jedoch von Vorteil zu sein. Dieser Prozess wird als Endosymbiose bezeichnet und ist vermutlich ein Schlüsselelement in der Evolution der Eukaryonten, definiert durch die Aufnahme von Mitochondrien und Chloroplasten vor mehr als einer Milliarde Jahren. Das Interesse an der Erforschung der frühen Schritte der Endosymbiose führte zur Suche nach Organismen, bei denen in jüngerer Zeit eine Symbionten-Inkorporation stattgefunden hat.

Zwei Fälle von einzelligen Organismen, die bakterielle Endosymbionten (ES) beherbergen, standen in unserem Institut im Mittelpunkt des Interesses: zum einen *Paulinella chromatophora* mit seinem photosynthetisch aktiven ES von α–cyanobakteriellem Ursprung und zum anderen *Angomonas deanei* - ein begeißelter Trypanosomatid mit einem β–proteobakteriellen ES. Die genetische Modifizierbarkeit machte *A. deanei* zu einem perfekten Kandidaten als Modellorganismus für eine sehr junge, aber stabile endosymbiotische Beziehung unbekannten Ursprungs. Da *Candidatus* Kinetoplastibacterium crithidii, der bakterielle ES, aus einer Linie von hauptsächlich intrazellulären Krankheitserregern stammt und bei Trypanosomatida bisher nicht beobachtet wurde, dass sie Bakterien aufnehmen, könnte der ES ursprünglich als Krankheitserreger in den Wirt gelangt sein. Eine

massenspektrometrische Analyse des gesamten Proteoms wurde durchgeführt, um das Ausmaß der Kontrolle zu verstehen, die der Wirt über die ES ausübt, und ergab nur sehr wenige mutmaßliche vom Wirt kodierte und zum ES transportierte potenzielle Effektorproteine, die für die Kontrolle der ES erforderlich sind. Die experimentelle Überprüfung dieser vom Wirt kodierten Proteine ergab, dass nur 7 dieser so genannten “Endosymbiont targeted Proteins (ETPs) an oder in dem ES zu finden sind. Drei Proteine, ETP2, ETP7 und ETP9, scheinen sich an der Teilungsstelle des ES zu befinden, und im Rahmen dieser Arbeit wurden insbesondere ETP2 und ETP7 näher untersucht. Es wurden mehrere Versuche unternommen, homozygote Deletionen beider Gene in *A. deanei* zu erzeugen sowie ein Allel gegen einen Resistenzmarker auszutauschen und Reporter-Fusionsprotein-Konstrukte in die endogenen Loci einzufügen, um die Funktionsfähigkeit der Fusionskonstrukte zu testen.

Zur Funktionanalyse der Gene in vivo, wurden in *A. deanei* ein konditionelles Proteinstabilisierungssystem sowie ein konditionelles System zum Ausschneiden des Gens und ein induzierbares Expressionssystem eingesetzt. Knock-outs von ETP2, ETP7 und ETP9 wurden auch im aposymbiotischen Stamm ATCC-30969 von *A. deanei* getestet.

In-silico-Analysen von ETP2 und ETP7 ergaben, dass beide nur bei den Strigomonadinae vorkommen, aber selbst innerhalb dieser kleinen Gruppe sind beide Proteine nur wenig konserviert, und für ETP2 konnte keine Funktion vorhergesagt werden. Für ETP7 wurde jedoch gemäß der Phyre²-Modellierung eine mutmaßliche Peptidoglykan (PG)-Hydrolase-Domäne vorhergesagt. Darüber hinaus wurde die Identifizierung von Interaktionspartnern mittels Co-Immunopräzipitation getestet, um mögliche Hinweise auf die Wirkungsweise von ETP2 und ETP7 in dem ES zu erhalten.

Um die PG-hydrolysierende Aktivität zu testen, wurde ETP7 in *E. coli* und *Leishmania tarentolae* exprimiert und für den In-Gel-Peptidoglykan-Hydrolyse-Assay (Zymogramm) sowie durch Trübungsabbau und Farbstofffreisetzung in Plattenlese-Assays aufgereinigt. Darüber hinaus wurde die Fähigkeit von ETP7 zur Bindung an β–Lactame, wie sie bei Penicillin-bindenden Proteinen (PBPs) beobachtet wird, untersucht. Da alle Schritte der PG-Umstrukturierung im Intermembranraum des Bakteriums stattfinden, muss ETP7 in der Lage sein, durch die äußere Membran des ES zu wandern. Um dies zu überprüfen, wurde Immunogold-Transmissions-Elektronenmikroskopie an *A. deanei* eingesetzt, um die subzelluläre Lokalisierung zu bestimmen.

List of Abbreviations

aa	amino acid
Ad	*Angomonas deanei*
Amp	ampicillin
AP	Alkaline phosphatase
APS	ammonium persulfate
ATC	anhydrotetracycline
BHI	brain heart infused
bp	base pair
BS	blocking solution
BSA	bovine serum albumin
CAM	chloramphenicol
CDP	Disodium 2-chloro-5-(4-methoxyspiro{1,2-dioxetane-3,2'-(5'-chloro)-tricyclo[3.3.1.13,7]decan}-4-yl)-1-phenyl phosphate
Co-IP	co-immunoprecipitation
C-terminal	carboxy terminal
dH_2O	distilled water
DIG	digoxigenin
DMSO	dimethylsulphoxide
DNA	deoxyribonucleic acid
dNTP	deoxynucleoside triphosphate
DTT	dithiothreitol
EDTA	ethylenediaminetetraacetic acid
ES	endosymbiont
EtOH	ethanol
ETP1	endosymbiont targeted protein 1
ETP2	endosymbiont targeted protein 2
ETP7	endosymbiont targeted 7
ETP9	endosymbiont targeted 9
FKBP	FK506 binding protein
FR	flanking region
GA	glutaraldehyde
GAPDH	glyceraldehyde 3-phosphate dehydrogenase
gDNA	genomic DNA
GFP	green fluorescent protein
HR	homologous recombination
HS	horse serum
Hyg	hygromycin
IgG	Immunoglobulin G
IMAC	Immobilized metal affinity chromatography
IPTG	Isopropyl β-D-1-thiogalactopyranoside
IR	intergenic region
kBp	kilo base pair
kDa	kilodalton
KO	knock out
LB	lysogeny broth
LC	lead citrate
LZ	Lysozyme
M	Molar
mA	milliampere
min	minute

MS	mass spectrometry
mS	mScarlet
mya	million years ago
NAG	N-acetylglucosamine
NAM	N-acetylmuramic acid
Neo	geneticin
ng	nanogram
N-terminal	amino terminal
ORF	open reading frame
p.a	pro analysi
PBS	phosphate buffered saline
PFA	paraformaldehyde
PG	peptidoglycan
phl	phleomycin
pmol	picomol
PMSF	phenylmethyl sulfonylfluorid
PVDF	polyvinylidenfluorid
RBB	Remazol brilliant blue
RE	restriction enzyme
RT	room temperature
S. culicis	*Strigomonas culicis*
Stc	*Strigomonas culicis*
SDS	sodiumdodecylsulfate
SHT	symbiont-harboring trypanosomatid
T7P	T7 polymerase promotor
TCA	trichloroacetic acid
TEM	transmission electron microscopy
Tet	tetracycline
TLCK	tosyl phenylalanyl chloromethyl ketone
TSE	Tris, Sucrose, and EDTA
UA	uranyl acetate
WT	wild type

Table of Contents

1 Introduction

1.1 Interaction of microbes

Almost all microbial organisms interact in their natural environment with organisms from other species and many require compounds synthesized by other organisms, forming complex networks of dependencies. These interactions can be harmful for one partner as is the case in predation, parasitism or pathogenesis. Interactions which benefit one or several parties (without harming the other partner), e.g. by the exchange of nutrients or offering protection, are called mutualism or symbiosis (which is the term used throughout this thesis for this type of interaction). When two individuals associate permanently to the point where they become dependent of each other the line starts to blur whether they can still be seen as separate organisms. At some point one of the dependent organisms (the ES) may be hosted inside another (the host), which requires complex adaptions of both, host and ES. This situation can result in the complete fusion of two or several cells into a single entity as was suggested early on by Andreas Franz Wilhelm Schimper (Schimper, 1883) and Konstantin Mereschkowsky (Mereschkowsky, 1905) based on observation of plant cells and hypothesizing on the origin of chloroplasts. Later in the 1960s Lynn Margulis picked up these early proposals and contributed to the establishment of a symbiotic theory of the evolution of eukaryotes (Sagan, 1967).

1.2 Organelles of bacterial origin in modern eukaryotes

Nowadays, it is widely accepted in the scientific community that eukaryotes as we know them today harbor organelles derived from bacterial endosymbionts. These organelles have become a defining feature of eukaryotes. The acquisition of an α-proteobacterial endosymbiont and its evolution into the mitochondrion drastically increased the metabolic abilities of primordial eukaryotes, e.g. allowing for efficient ATP production via aerobic respiration, fatty acid biosynthesis, (Johnson *et al.*, 2005; Osellame, Blacker and Duchen, 2012). Incorporation of the cyanobacterial chloroplast predecessor allowed eukaryotes to harvest light energy for the generation of energy-rich organic compounds. With these events tracing back more than 1 billion years reconstruction of the initial steps in organellogenesis is very difficult.

There are several hypotheses how the initial interaction may have occured, spanning from H_2 exchange to predatory eukaryotes not digesting phagocytosed prey (Embley and Martin, 2006). As these two cases are undisputed the first events of intracellular incorporation that survived of bacteria in eukaryotes, they were not the last ones. While in most cases microorganisms are only allowed to populate open environments like the surface of the skin, the gut lumen, or invaginations like the lungs, which are protected by a rigid barrier against intrusion, several bacteria have been found in between cells of specific tissues or even inside of hosts in both single cell and multi-cellular organisms in recent

years. These organisms living inside another cell are regarded as mutualistic endosymbionts when they bring a benefit to the host.

Even though the transformation of bacterial endosymbionts into organelles happened twice, and both events occurred more than a billion years ago, there are many more recent events found throughout diverse groups of eukaryotes (Moya *et al.*, 2008) that show a lower degree of specialization and adaption.

Probably the most well-known and economically important bacterial endosymbiotic relationship is the one between plants and rhizobia. Leguminosae, to which a lot of agronomically important crops belong, are distinct from non-legumes in terms of their ability to fix nitrogen by root nodules. These nodules have formed around 58 mya (Sprent, 2007) and harbor symbiotic rhizobia that provide the host plants with ammonia, which is a highly limited nutrient in most soils, via fixation of atmospheric N_2. The bacteria are facultative endosymbionts as they can proliferate in the soil without plants. One out of several modes of infection is by root hair curling, producing an infection threat, which allows the bacteria to pass through the epidermis. Once the bacteria have entered through the base of axillary hairs the surrounding plant tissue cell wall becomes more porous and allows bacteria to enter inside of plants cells. Inside the plant cells the N_2 fixation can take place (Sharma *et al.*, 2020). Unlike many free-living diazotrophs, rhizobia fix N_2 only in the endosymbiotic form. The oxygen-sensitive nitrogenase complex is encoded in the bacterial DNA but homocitrate, a crucial component for this complex, is usually derived from the plant host (Hakoyama *et al.*, 2009). This means that the ability to fix N_2 is only possible through cooperation of both partners.

Apart from facultative endosymbiosis, where both parties meet in the environment and form a symbiosis on an individual level, obligate endosymbiosis in many cases involves vertical inheritance of the endosymbiont from one host generation to the next one. Mealybugs, insects feeding exclusively on phloem or xylem plant sap, suffer from a very monotonous diet lacking several essential amino acids. Yet they are still able to obtain all necessary nutrients because they are provided by endosymbionts from one or sometimes several bacterial families. The bacteria are harbored in the cytosol of specialized insect cells called bacteriocytes, which evolved approximately 200 mya (Shigenobu and Stern, 2012). These cells protect the endosymbionts from the immune system of the host and are essential for host-endosymbiont interaction by controlling the amount of nutrients shuttled to the bacteria and limiting their proliferation by expression of antimicrobial peptides (AMPs) (Anselme *et al.*, 2008; Price *et al.*, 2014; Silva *et al.*, 2014). The bacteria are inherited vertically from the mother and fulfill their entire life cycle inside the bacteriocytes. The intracellular lifestyle has led to a massive genome reduction as all genes necessary for adaption to the environment have become obsolete. This evolutionary rabbit hole has made the endosymbionts gradually more dependent on the

host, slowly transitioning from an individual into an organelle (Bennett and Moran, 2015). As the bacteria are strictly clonal, negative and deleterious mutations quickly accumulate and are partially alleviated by higher production levels of chaperones by the host (Kupper *et al.*, 2014). In the worst case, dependence on a slowly deteriorating symbiont gradually increases the burden on the host, which is why some sap-feeding insects have joined or replaced the initial symbionts with a new one (Urban and Cryan, 2012).

There is a plethora of endosymbiotic relationships in all kinds of different intermediate stages of integration. To understand the evolution of early eukaryotes, a more recently established, stable endosymbiosis in a unicellular organism would come in handy, as at least primordial systems to control endosymbiont division and metabolite exchange must have evolved in such a system. In our group, two unicellular model organisms for endosymbiosis have been established: the cercozoan amoeba *Paulinella chromatophora* and the flagellated trypanosomatid *Angomonas deanei*.

1.3 *Paulinella chromatophora*

So far, the one and only identified independent acquisition of a cyanobacterial endosymbiont which evolved into a photosynthetic organelle happened in the cercozoan amoeba *Paulinella chromatophora* more than 100 million years ago (Marin, Nowack and Melkonian, 2005; Delaye, Valadez-Cano and Pérez-Zamorano, 2016). Each *P. chromatophora* cell contains two α-cyanobacterium-derived organelles, referred to as chromatophores. This symbiosis is probably of predatory origin as *Paulinella* species without chromatophores, such as *P. ovalis* (Bhattacharya *et al.*, 2012), phagocytose bacteria, an ability that photoautotrophic *Paulinella* species have lost.

P. chromatophora is an excellent system to study the early the evolution of chloroplasts as the genome of the chromatophore is reduced to roughly one-third compared to free-living cyanobacteria (Nowack, Melkonian and Glöckner, 2008) but there are still five to ten times more genes than the 60 to 200 protein-coding genes found in chloroplasts (Timmis *et al.*, 2004). This suggests that the evolution of the chromatophore into a true organelle is still ongoing.

Genome analyses of *P. chromatophora* revealed that from the approximately 2500 genes lost from the chromatophore compared to free-living ancestors only around 58 genes were transferred to the host nucleus by endosymbiotic gene transfers (EGTs) (Nowack *et al.*, 2011, 2016). EGTs showed a bias towards genes coding for proteins involved in photosynthesis, and for two of these proteins, the photosystem I subunits PsaE and PsaK, translation by the host and localization at the chromatophore thylakoids could be shown (Nowack and Grossman, 2012). However, proteome analyses of isolated chromatophores revealed that besides proteins resulting from EGT, hundreds of proteins of host origin or acquired by HGT are imported into the chromatophore (Singer *et al.*, 2017; Oberleitner *et al.*, 2020).

Although the detailed molecular mechanisms underpinning protein import into the chromatophores are still unclear, immunogold analyses as well as conserved signals at the N-terminus of many chromatophore-targeted proteins suggest the involvement of vesicular transport through the Golgi to be involved in transporting proteins to the chromatophore (Nowack and Grossman 2012, Singer et al. 2017, Oberleitner et al. 2022).

These results demonstrate that in this relatively short time span of ~100 million years the transformation of an endosymbiotic bacterium into a genetically integrated organelle that depends for many biological functions on nucleus-encoded proteins is possible (Nowack, 2014; Gabr, Grossman and Bhattacharya, 2020).

The disadvantage of *P. chromatophora* as a model system for organellogenesis, however, is the large genome of the host estimated to be around 10 Gbp, which has not been fully sequenced and assembled yet. Illumina HiSeq data was generated from cDNA providing a high-quality transcriptome (Nowack *et al.*, 2016).

The slow growth, with just one division every six days, clumping in liquid culture, and the tight, but delicate silicate shell are obstacles during experimental work and make *P. chromatophora* challenging to handle.

1.4 Trypanosomatids

Flagellates of the family of Trypanosomatidae have been a focus of research ever since their discovery as human pathogens in Sub-Saharan Africa and South America. About 70 million people in 36 countries are at risk of infection with sleeping sickness alone (Simarro *et al.*, 2012) but in recent years the number of death cases reduced drastically from over 25,000 per year in 2000 to just 600 in 2020. The decrease comes mainly from projects decreasing the population of the tsetse fly host of *Trypanosoma brucei*, the causative agent of sleeping sickness, in risk areas.

Research focused mainly on dissecting the lifestyle and treatment of the heteroxenous species such as *T. brucei* (sleeping sickness), *Trypanosoma cruzi* (Chagas disease) and *Leishmania* spp. (leishmaniasis). Pathogenic trypanosomatids have a dixenic life cycle alternating between morphologically and biologically distinct life stages from invertebrate host to vertebrate or plant hosts. While pathogenic strains are in the spotlight of general attention most trypanosomatids are actually monoxenic parasites of insects (i.e. are restricted to a single host throughout their entire life cycle) and have been identified to be the ancestral form of the entire family (Flegontov *et al.*, 2013; Maslov *et al.*, 2013; Lukeš *et al.*, 2018).

Continuous research on Trypanosomatids has revealed several interesting biological features either exclusive to Trypanosomatids or rarely found in other species. Trypanosomatids belong to the Kinetoplastea, which all possess a so called kinetoplast, a structure containing mitochondrial DNA (mtDNA) in a highly condensed state. This mtDNA (in trypanosomatids called kDNA) is arranged in several thousand physically interconnected mini (0.2-10 kBp) and a dozen highly similar maxi circles that are interwoven in the network periphery (Hajduk, Klein and Englund, 1984; Lukeš *et al.*, 2002). The single mitochondrion itself is a tubular structure extending along the cell membrane of the trypanosomatid.

Metabolism in trypanosomatids and other kinetoplastea has several peculiarities compared to animal cells e.g glycolysis was transferred from the cytosol into specialized peroxisomes, called glycosomes (Flaspohler *et al.*, 1997; Parsons, 2004).

The genome organization is drastically different to most other eukaryotes as the vast majority of ORFs neither contains introns nor classical promoter structures. In fact cis-splicing was only demonstrated for the poly(A) polymerase (Mair *et al.*, 2000). Instead, functionally unrelated genes are transcribed as polycistronic gene clusters (PGCs) into long pre-mRNAs. Each gene is flanked by a spliced leader acceptor site upstream of the gene and a polyadenylation site downstream of the gene. The spliced leader acceptor sites allow for trans-splicing of the PGC pre-mRNA into individual, mature mRNAs and adds a capped 39-nucleotide long spliced leader (SL) to the 5’ end of the mRNA (Kooter and Borst, 1984; Parsons *et al.*, 1984). While transcription of all genes in a PGC occur at the same level as a consequence of polycistronic transcription, posttranscriptional mRNA processing allows for divergent gene expression of adjacent genes within a PGC. The stability of the mRNA depends on the 3’ untranslated region just downstream of the gene (Clayton, 2002; Jackson, 2015). Interestingly, several reports have shown that the level of mRNA must not necessarily correlate to protein abundance (Gale, Carter and Parsons, 1994; Mayho *et al.*, 2006; Nardelli *et al.*, 2007).

Trypanosomatids show high levels of homologous recombination allowing for straight forward genetic manipulation strategies based on the integration of elements into a specific target locus by addition of upstream and downstream flanking regions (Lee and Van der Ploeg, 1990). This allowed simple and fast adaptation of new techniques in trypanosomes such as RNAi for gene knockdown, Tetracycline-controlled expression of genes, conditional gene excision via a dimerizing Cre recombinase (DiCre) as well as CRISPR/Cas9 (Duncan, Jones and Mottram, 2017). All of this allowed research on flagellate trypanosomatids to dissect numerous features of eukaryotic cells, such as replication of mtDNA, polycistronic transcription and RNA editing (Maslov *et al.*, 2019).

1.5 Symbiont-harboring trypanosomatids

In the group of non-pathogenic monoxenous trypanosomatids four genera have become of particular interest for endosymbiosis research as they harbor bacterial endosymbionts derived from two separate uptake events (Figure 1.1). From these four genera of symbiont-harboring trypanosomatids (SHTs) the three genera *Angomonas*, *Kentomonas* and *Strigomonas* form the subfamily Strigomonadinae. The common ancestor of all members of this subfamily was invaded by a β–proteobacterium of the family Alcaligenaceae that evolved into a beneficial endosymbiont. This endosymbiont is called *Candidatus* Kinetoplastibacterium (Votýpka *et al.*, 2014; Borghesan *et al.*, 2018).

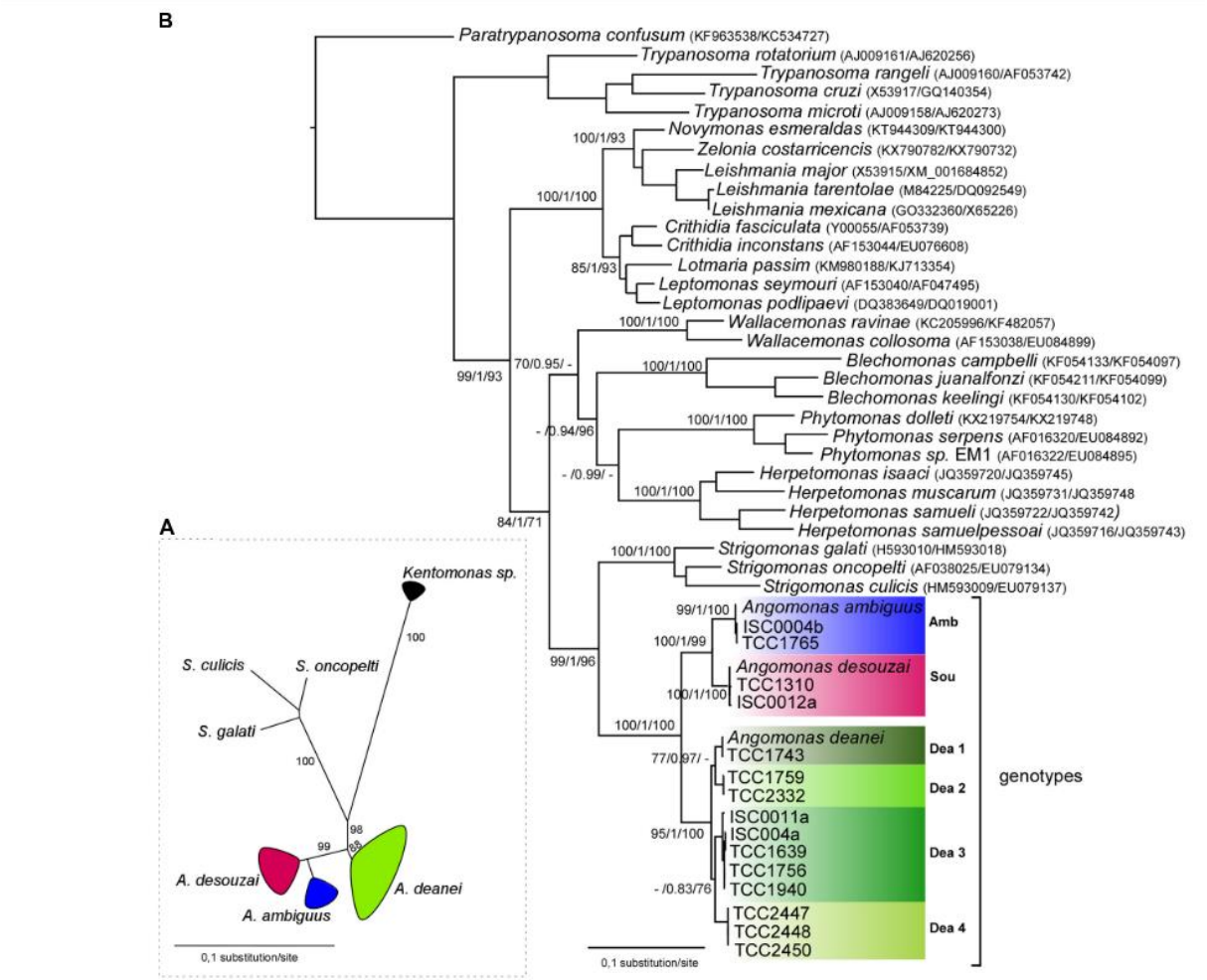

Figure 1.1 Phylogenetic analysis of Angomonas species and genotypes. A: Dendrogram (ML) of V7V8 SSU rRNA sequences (barcodes) from 175 (174 from blowflies) cultures of *A. deanei* (Dea), *A. desouzai* (Amb), and *A. ambiguus* (Sou), and species of the other genera of symbiont harboring trypanosomatids: *Strigomonas culicis*, *Strigomonas oncopelti*, *Strigomonas galati*, and *Kentomonas sorsogonicus*. Numbers at the nodes are ML support values (>50%) from 500 replicates. **B:** Positioning of representatives of each the three *Angomonas* species and four genotypes of *A. deanei* (Dea1–Dea4) were showed in the phylogenetic tree of *Trypanosomatidae* based on concatenated gGAPDH and V7V8 SSU rRNA gene sequences, inferred by maximum likelihood (–Ln = –16564.401081) and Bayesian analyses. Numbers at the nodes correspond, respectively, to ML/BI/P support values

(>50%) from 500 replicates. Figure published by (Borghesan *et al.*, 2018). http://creativecommons.org/licenses/by/4.0/

The presence of *Ca.* Kinetoplastibacterium reduces the nutritional requirements of SHTs of the Strigomonadinae compared to related non-SHTs, providing heme, purine, and at least 6 amino acids essential for some non-SHTs such as *Crithidia fasciculata* (de Menezes and Roitmanz, 1991; Souza *et al.*, 1999; Klein *et al.*, 2013). Host glycosomes are often observed in close association with the ES of SHT, which raised the question if the ES fuels the energy metabolism of the host (Loyola-Machado *et al.*, 2017).

The benefit of the ES to the host cell is clear, exerting great selection pressure on the host to inherit the ES to the daughter cells upon division. All Strigomonadinae have a tightly synchronized division cycle between the host and the ES with one single ES per host cell. The ES always divides first, followed by the basal body, the kinetoplast, and finally the nucleus (Motta *et al.*, 2010; Brum *et al.*, 2014).

The influence of the ES is not limited to nutritional advantages but has been shown to influence the ability to colonize insect hosts (Fampa *et al.*, 2003), regulate oxygen consumption (de Azevedo-Martins *et al.*, 2015) and affect the mitochondrium, protein synthesis, and metalloprotease activities (d'Avila-Levy *et al.*, 2003, 2008; Bombaça *et al.*, 2017; Brunoro *et al.*, 2019). And while several studies in the past have explored the life cycle and the effect of the bacterium on the host, only just recently the molecular mechanisms underlying interaction and communication of the ES and the host have come into spotlight.

The fourth SHT, *Novymonas esmeraldas,* originates from a separate endosymbiotic event and harbors a β-proteobacterium of the family of Burkholderiaceae, called *Ca.* Pandorea novymonadis (Kostygov *et al.*, 2016). In contrast to the Strigomonadinae the mutual adaption between the host and the ES of *N. esmeraldas* appears to be less advanced and stable as the division is not synchronized yet, allowing for *N. esmeraldas* cells with few bacteria up to more than ten in a single host cell. *Ca.* Pandorea novymonadis has undergone a less extensive genome reduction compared to *Ca.* Kinetoplastibacterium, retaining a complete TCA cycle and seven more amino acid synthesis pathways, suggesting a more recent endosymbiotic event when compared to the Strigomonadinae (Zakharova *et al.*, 2021). Clearing *N. esmeraldas* of the bacterial ES by antibiotic treatment leads to a significant growth impairment in RPMI medium, which could be almost fully recovered in a suitable medium (i.e., supplemented M199 medium) (Kostygov *et al.*, 2017).

1.6 *Angomonas deanei* and *Strigomonas culicis*

From the subfamily Strigomonadinae *Angomonas deanei* and *Strigomonas culicis* are the most studied species. *A. deanei* strain PRA-265 has been isolated from the assassin =bug *Zelus leucogrammus* (Carvalho and Deane, 1974), but *A. deanei* is highly prevalent in hemiptera and diptera insects found globally up to the Leningrad region in Russia (Borghesan *et al.*, 2018; Ganyukova, Malysheva and Frolov, 2020). In liquid culture *A. deanei* has an elliptic shape with a single flagellum, roughly the length of the cell itself protruding outside of a flagellar pocket (Figure 1.2). The single β−proteobacterial ES *Ca.* K. crithidii is found at the posterior end of the cell. The ES is surrounded by two membranes of bacterial origin with a reduced peptidoglycan layer in the periplasmic space, essential for division as treatment with β−lactams impaired division (M. C. M. Motta *et al.*, 1997). The genome of the host and ES have been sequenced and the chromosomes of *A. deanei* were assembled (João M.P. Alves *et al.*, 2013; Motta *et al.*, 2013; Davey *et al.*, 2021). Analysis of the ES genome revealed a close relationship with the intracellular bacterium *Taylorella equigenitalis*, found in the reproductive tracts of horses, and *Bordetella* spp., the causative agent of whooping cough. Comparison of the 0.8 MBp genome of *Ca.* K. crithidii to the genomes of *T. equigenitalis* and the closest free-living Alcaligenaceae *Achromobacter xylosoxidans* revealed a 50% decrease of genome size when compare to *T. equigenitalis* (1.7 MBp) and an almost 90% reduction compared to *A. xylosoxidans* (7.3 MBp) (Alves et al., 2013). Some abilities have become less important or even counterproductive when found in a relatively stable and non-hostile environment where genetic integration of several organisms into one functional unity becomes an advantage. The massive genome reduction makes the ES unculturable by itself but the host could be cleared of the ES at least once in the past by treatment with chloramphenicol (Mundim and Roitman, 1977). The aposymbiotic *A. deanei* strain ATCC-30969 is available via the American Type Culture Collection. It shows severe growth deficiency that cannot be alleviated with rich medium (personal experience, data not shown). Aposymbiotic cultures of *A. deanei* ATCC PRA-265 (i.e., the strain worked with in this thesis) could not be obtained by diverse antibiotic treatments (Kokkori, 2018; Morales *et al.*, 2023), suggesting that small differences in the host genome result in an obligate dependence of the host cell on its endosymbiont in our strain.

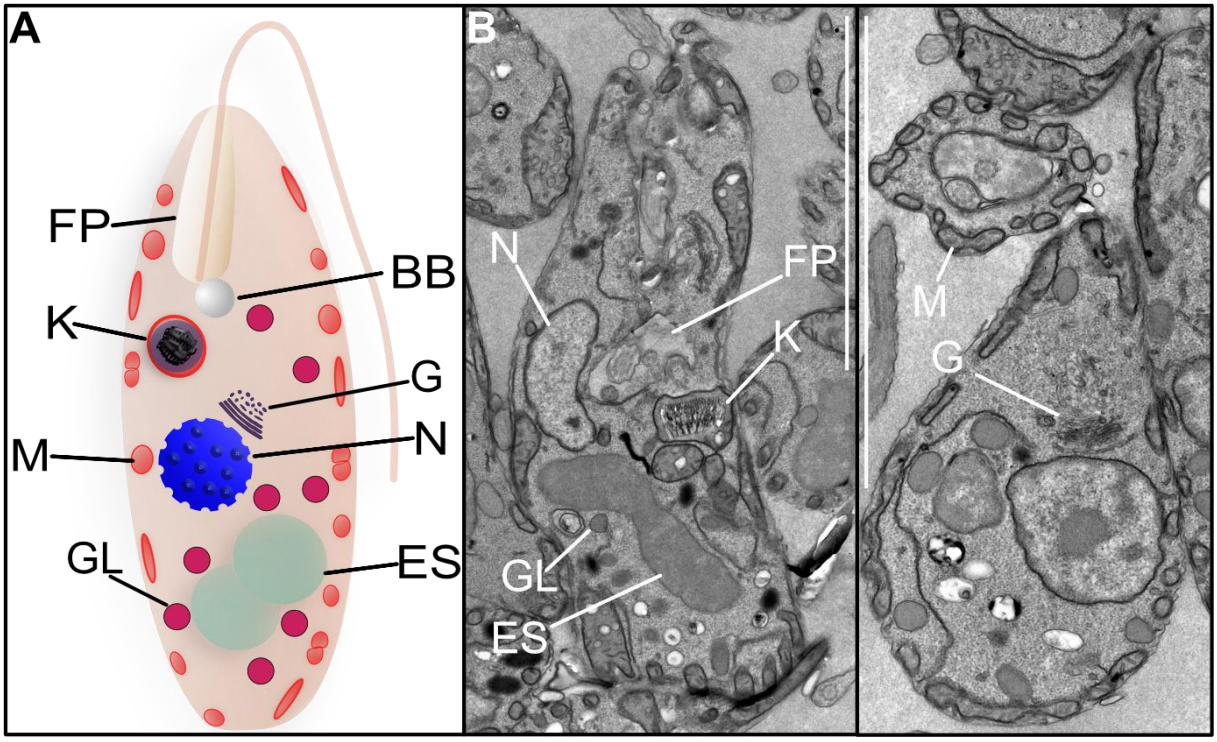

Figure 1.2 (A) *A. deanei* schematic depiction and (B) transmission electron microscopy to visualize structures of interest. The flagellum is surrounded by a flagellar pocket (FP), with a basal body (BB) found at the anterior of the cell. The kinetoplast is surrounded by the membrane of the tubular mitochondrion (m) and is usually located close to the membrane of the host. Anterior to the nucleus (N) the Golgi apparatus is localized (G) and the endosymbiont (ES) is found at the posterior end surrounded by glycosomes (GL).

The undemanding nutritional requirements, a fast dividing time of 6 h, the availability of an aposymbiotic strain and the easy adaption of genetic tools (Morales *et al.*, 2016; Gonçalves *et al.*, 2021) make *A. deanei* an excellent organism to study the early development stages of a permanent endosymbiont in a unicellular eukaryote.

1.7 Bacterial division and restructuring of peptidoglycan

Bacterial division is a multi-protein complex-dependent multi-step process, spanning septation and elongation of daughter cells. The envelope of gram-negative bacteria (incl. the β-proteobacteria) features two membranes in between which the cell wall localizes. The cell wall consists of peptidoglycan (PG) and makes bacteria resilient to osmotic pressure. Together with the membranes, it protects the cells from environmental influences. The rigidity of the structure is due to its 3D layout, where long polymer chains of the two alternating sugar monomers N-acetylglucosamine (NAG) and N-acetylmuramic acid (NAM) are crosslinked by short peptide chains, attached to the N-acetylmuramic acid. The thickness of this cell wall varies drastically between species and makes up to 10 % of the cell wall's dry weight in gram-negative bacteria but anywhere from 40-90 % in gram-positive bacteria (Dworzanski *et al.*, 2005). The PG cage, referred to as sacculus, surrounding the cell must be rigid but still permeable, as bacteria need to shuttle nutrients and metabolites through the layer. During cell

division, the PG strands must be restructured to elongate the cell first and divide in a second step. This process must be carefully balanced as weakening the PG layers by endogenous lytic enzymes (autolysins) can damage the cell due to osmotic pressure, potentially inflating and ripping the cell through water influx. Intact PG strands on the other side will interfere with proper cell elongation, septation and separation of the daughter cells.

While other essential processes like DNA replication and translation take place in the well-shielded cytosol, reactions at the cell surface are much more exposed to the extracellular environment (Typas *et al.*, 2012). To cope with a permanently fluctuating environment bacteria have evolved a redundant set of enzymes for PG restructuring. In *E. coli* synthesis of PG precursors in the cytosol spans 10 reactions in total, covered by 12 enzymes, while 37 enzymes are involved in the 8 reactions in PG metabolism in the periplasm (Mueller and Levin, 2020). Even removal of several enzymes of the same class can lead to mutants without a visible phenotype (Heidrich *et al.*, 2001, 2002; Singh *et al.*, 2012). The gram-positive *B. subtilis* features even more redundancy as from the 45 autolysins and extracellular PG synthases only the three enzymes RodA, FtsW and PBP2b are essential for growth under laboratory standard conditions (Heidrich *et al.*, 2002).

Intracellular bacteria on the other hand inhabit the stable host cytosolic environment allowing them to decrease the number of enzymes for PG restructuring (Otten *et al.*, 2018). Additionally, PG is a major trigger of immune response by pathogen-associated molecular patterns (PAMPs) in the innate immune system of eukaryotes. For intracellular pathogens there is a high selective pressure to reduce possible targets for host recognition. For decades it was not clear why chlamydia, obligately intracellular pathogens of diverse eukaryotes, are sensitive to β–lactams even though PG could never be detected (Ghuysen and Goffin, 1999). Highly sensitive mass spectrometry and cryoelectron tomography revealed that *Chlamydia trachomatis* possess PG-like structures. *C. trachomatis* in particular forms a discrete and transient PG ring during constriction of dividing cells (Liechti *et al.*, 2014). In *Buchnera aphidicola*, the endosymbiotic bacterium of the pea aphid *Acyrthosiphon pisum,* lipopolysaccharides (LPS), another major PAMP-trigger, are not synthesized, probably to further reduce immune system triggering of the host (Otten *et al.*, 2018).

When examining the genome of *Ca.* K. crithidii protein-encoding genes involved in cell division described to be essential in gram-negative bacteria are missing (Motta *et al.*, 2013). Loss of proteins essential for division must be compensated in some way, as proliferation must either be completed by host-derived factors or the division must become less complex in general. This is partially alleviated as free-living bacteria have a plethora of division proteins crucial only in certain situations, often related to environmental stress factors (Typas *et al.*, 2012).

Comparing the elongation and septation machinery encoded on the genomes of the endosymbiotic β–proteobacteria of the Strigomonadinae and *Ca.* P. novymonadis (the independently acquired endosymbiont of *Novymonas esmeraldas*) to close relatives of the genera *Achromobacter*, *Bordetella* and *Taylorella* the loss of several proteins of the septation machinery becomes apparent, while all proteins necessary for cell elongation are retained in the ESs (Figure 1.3). FtsE and FtsX are part of the ABC transporter FtsEX involved in cellular division. They are important for assembly and stability of the septal ring. FtsB recruits downstream divisome proteins. All three are lost when compared to close relatives but they are only essential in free-living relatives (Buddelmeijer *et al.*, 2002; Schmidt *et al.*, 2004), yet still retained in the intracellular *Bordetella* spp. and *Taylorella* spp.. The remaining 5 candidates FtsA, PBP3, FtsW, FtsQ, and TolQ are all missing from the Strigomonadinae ES but still preserved in the ES of *N. esmeraldas*. The one exception is FtsA which is also still found in *Ca.* Kinetoplastibacterium sorsogonicus. With *Ca.* P. novymonadis in control of its division, the loss of these proteins must allow the host to fill in the gap and synchronize the division cycle.

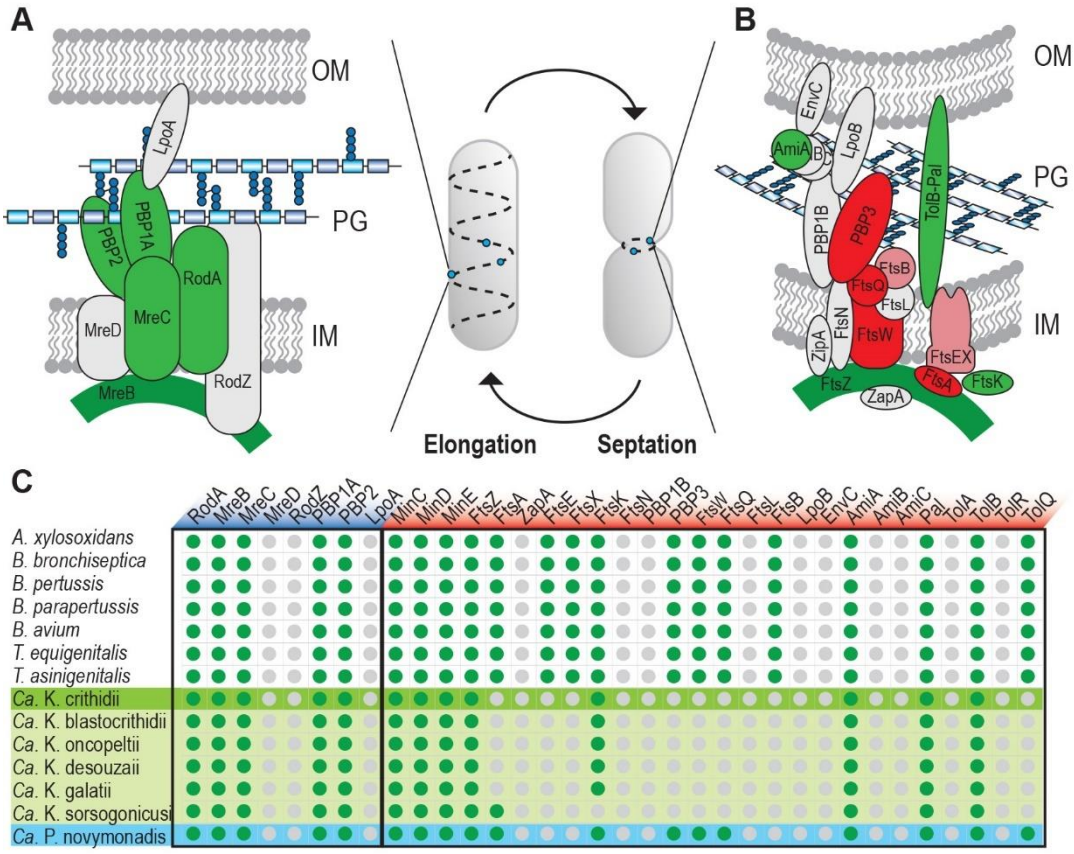

Figure 1.3 Overview of the elongation and septation machinery related proteins of bacterial ES in trypanosomatids to non-endosymbiotic relatives. (**A**) Schematic depiction of the elongation machinery. (**B**) Schematic depiction of the septation machinery. Proteins in green are essential and found in the ES. Grey proteins are missing from the intracellular pathogenic relatives as well as the ES group. In pink are proteins found in the intracellular pathogenic relatives and missing in the ES but are reported to be only essential in free-living bacteria. In red are proteins described to be essential and are missing in the ES group, except for *Ca*. P. novymonadis. OM: outer membrane, IM: inner membrane: PG: peptidoglycan. (**C**) Table listing main components for elongation (proteins on blue background) and septation (proteins on red background). Species in white rows: intracellular pathogenic relatives of the endosymbiotic bacteria. Species in green rows: ES of the Strigomonadinae. The ES of *A. deanei* is highlighted in dark green and the ES of *N. esmeraldas* in light blue. Green dots represent proteins found in a species. Grey dots represent proteins missing in a species. Figure produced by Eva Nowack.

FtsA is necessary for the membrane attachment of the bacterial tubulin analogue FtsZ, which forms the division ring separating the two daughter cells (Pichoff and Lutkenhaus, 2005). PBP3 is a transpeptidase that catalyzes cross-linking of peptidoglycan at the division septum. It is recruited late to the septal ring in an FtsA and FtsZ dependent manner (Weiss *et al.*, 1999). FtsW has been thought for the longest time to flip lipid II (a PG precursor) from the cytosol into the periplasm, but a recent study actually showed its ability to polymerize lipid II into peptidoglycan strands when in a complex with class B PBPs (Taguchi *et al.*, 2019). A major assembly factor of the division machinery is FtsQ. It controls correct divisome assembly and the POTRA domain of FtsQ functions as a chaperone

specifically recognizing secretion or assembly-competent forms of divisome-related polypeptides (D'Ulisse *et al.*, 2007).

TolQ is a part of the Tol-Pal system consisting of an inner membrane motor complex of TolQ, TolR and TolA, the periplasmic TolB and the PG-binding outer membrane lipoprotein Pal (Egan, 2018). Loss of Tol-Pal activity was shown to destabilize the outer membrane of the bacterium, making it hypersensitive to detergents and large antibiotics (Webster, 1991). Loss of Tol-Pal in gram-negative bacteria also resulted in cell chains failing to separate during division (Gerding *et al.*, 2007). In *Bordetella* and *Taylorella* spp. this system is already reduced to just TolB, TolQ and Pal.

With systems impaired in PG polymerization, restructuring and outer membrane invagination, several crucial steps of division are impaired and should make complete division of the ES impossible without host-assistance.

1.8 Aim of this thesis

The evolution of a bacterium into an organelle was critical to the emergence of early eukaryotes. To understand the processes involved in early organellogenesis, *A. deanei* as an organism harboring a bacterial ES, which has been proven to provide the host with nutrients and which has a regulated division cycle, is an ideal system to study these early evolutionary steps. How the host and ES communicate, orchestrate division, and exchange metabolites has not been explored in depth yet, but may elucidate which processes are at the forefront of adaption. To understand these molecular processes, in a previous project in our group, protein mass spectrometry of the purified ES of *A. deanei* was performed and revealed several putative ES-targeted proteins. The previously developed molecular tool box (Morales *et al.*, 2016) allowed to track the localization of host-derived proteins in *A. deanei* by expression of fluorescent protein tag fusion constructs. The Aim of this thesis was to confirm localization of the 7 candidate endosymbiont-targeted proteins (ETPs) via epi- as well as confocal fluorescence microscopy and Western blot. Based on the results ETP2, ETP7 and ETP9s involvement in cell cycle coordination was to be explored further as all three were observed at the constriction side of the eight-shaped (also referred to as peanut-shaped) bacterium. The ETPs found at the constriction site were to be characterized in-depth by co-localization studies and the role of ETP2 and ETP7 in the context of host and ES interaction was analyzed during this thesis. Homozygous knockout strains should help to obtain hints on possible functions. As previous fusion constructs were expressed from the δ– and γ–amastin loci, the viability of the fusion constructs was tested by expression in the endogenous loci. As generation of homozygous knockouts was not possible, several conditional systems were explored in *A. deanei*.

Identification of the ETPs in *A. deanei* hinted that other members of the sub-family of Strigomonadinae likely also contain ETPs. The *Strigomonas culicis* genome was searched for ETPs, to allow comparison of *A. deanei* ETPs to *S. culicis* ETPs.

The *in silico* prediction of ETP7 revealed a putative PG hydrolase function. To test this hypothesis ETP7 was produced in *E. coli* and functional assays were performed. *Leishmania tarentolae* was established as a second expression system for heterologous proteins.

With several ETPs found at the periphery of the ES, a method for exploring the exact subcellular localization needed to be established. Transmission electron microscopy coupled to immunolabeling with colloidal gold particles was established in *A. deanei*.

2 Results

2.1 Identification of putative ES targeted proteins by protein mass spectrometry

As the extent of protein exchange between the bacterial ES and the host was not known, proteins extracted from isolated ES (Figure 2.1 a, b) were compared to whole cell lysates by liquid chromatography coupled to tandem mass spectrometry (LC-MS/MS) by Jorge Morales (Morales *et al.*, 2023). Over two independent proteomic analyses with a total of 9 biological replicates 573 and 638 endosymbiont-encoded proteins were detected with high confidence, from a total of 730 predicted ES proteins (João M.P. Alves *et al.*, 2013). At the same time 2,646 and 2,175 host-encoded proteins from the 10,365 predicted nucleus-encoded proteins (Davey *et al.*, 2021) could be identified. A total of 14 host-encoded proteins were enriched in the ES samples in both experiments (Table 2.1; red crosses figure 2.1 c, d) or at least one but were not detected in the other experiment (orange crosses, Figure 2.1 c, d). Host-encoded proteins found enriched in the endosymbiont in one experiment but host-enriched in the other experiment (yellow crosses, Figure 2.1 c, d) contained several putative glycosomal and mitochondrial proteins. This group was regarded as contaminants and not further analyzed. The integrity of the ESs was judged by the presence of a double membrane surrounding the ES as seen in TEM (Figure 2.1 a, b).

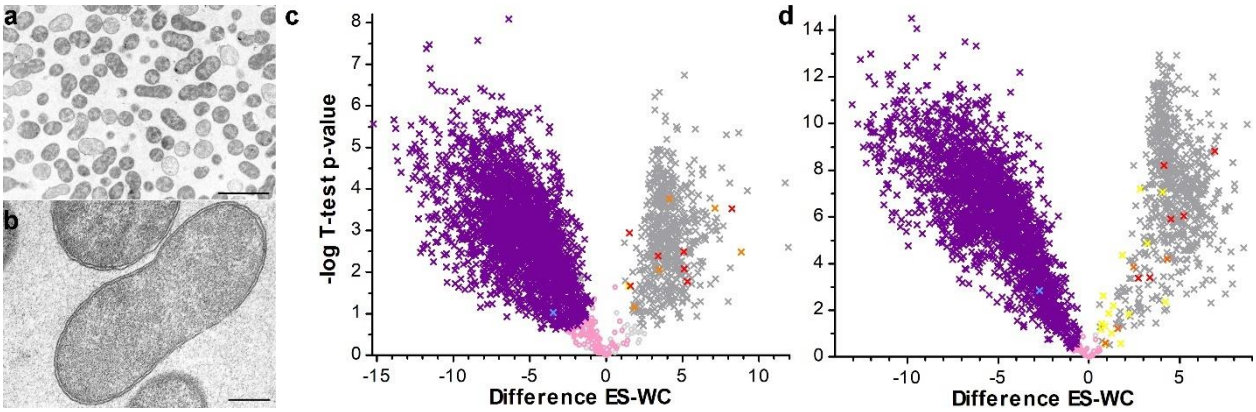

Figure 2.1 Comparative proteome analysis of whole cell lysates (WC) versus purified ES of *A. deanei*. (a-b) Transmission electron microscopy (TEM) of *Ca.* K. crithidii. (a) Overview of the collected endosymbiont fraction. Most of the structures observed in this fraction consist of eight-shaped and round structures that are surrounded by a double membrane consistent with the endosymbiont. Scale bar: 2.5 µm. (b) The endosymbiont outer and inner membrane remained intact in most of the cells during isolation. Scale bar: 250 nm. (c, d) Volcano plots of proteins identified by LC-MS/MS in Experiment 1 (c) and Experiment 2 (d). The difference of intensities of individual proteins between WC and ES samples ($\overline{log2\ (norm\ Int_{ES})}$ - $\overline{log2(norm\ Int_{WC})}$; Difference ES-WC) is plotted against significance (-log10 p-value in Student's T-test) for proteins detected in ES or WC samples. Color code: grey, endosymbiont-encoded proteins; colorful, nucleus-encoded proteins (red, enriched in endosymbiont in both experiments; orange, enriched in ES samples in one experiment, not identified in the other experiment; yellow, enriched in ES samples in one experiment, but depleted in the other experiment; blue, the endosymbiotic gene transfer-derived OCD; purple, remaining nucleus-encoded

proteins). Crosses in bright colors, significant enrichment or depletion; circles in pale colors represent nonsignificant values (rose, nucleus-encoded; light grey, endosymbiont-encoded).

Table 2.1 Mass spectrometric identification of candidate ETPs. Whenever ES-WC difference was higher than 3 or the -log T-test p-value higher than 3 in one experiment the background was highlighted in green.

Accession[a]	Annotation	Exp. 1[b]	Exp. 2[c]	Chr [d]	N-ext [aa][e]	M.W. [kDa][f]	Fluorescent fusions [kDa][g]	ETP[h]
CAD2220707.1	Hypothetical protein, cons.	3.4/2.4	4.1/8.2	18	98	42.7	69.0 (mSCARLET)	ETP1
CAD2221027.1	Hypothetical protein, cons.	8.2/3.5	6.9/8.8	19	-	53.4	80.2 (eGFP)	ETP2
CAD2213480.1	Hypothetical protein, cons.	1.5/2.9	5.2/6.0	02	-	105.1	131.9 (eGFP)	ETP3
CAD2216595.1	Nodulation protein S (NodS)/Methyltransferase domain/Ribosomal protein L11 methyltransferase (PrmA), put.	5.3/1.8	0.1/0.0	07	-	32.9	59.9 (eGFP)	
CAD2216818.1; CAD2216819.1; CAD2216820.1; CAD2216821.1	Kinetoplastid membrane protein 11, put.	0.4/0.3	2.7/3.4	07 07 07 07	-	11.0	37.8 (eGFP)	ETP5
CAD2220712.1	Hypothetical protein, cons.	4.1/3.8	nd	18	-	22.5	49.4 (eGFP)	
CAD2217314.1	Phage tail lysozyme, put.	5.1/2.1	3.4/3.4	08	-	61.0	87.8 (eGFP)	ETP7
CAD2216283.1	Hypothetical protein, cons.	5.1/2.5	4.5/5.9	06	122	22.6	49.4 (eGFP)	ETP8
CAD2212698.1	Dynamin family/Dynamin central region/Dynamin GTPase effector domain containing protein, putative	1.6/1.7	0.5/0.4	01	-	77.4	104.4 (eGFP)	ETP9
CAD2220896.1	Hypothetical protein, cons.	8.8/2.5	nd	19	263	73.9	100.8 (eGFP)	-
CAD2222258.1	WD domain, G-beta repeat, put.	3.5/2.1	nd	25	185	66.2	93.1 (eGFP)	-
CAD2222840.1	Hypothetical protein, cons.	nd	2.5/3.9	28	-	123.8	150.7 (eGFP)	-
CAD2218427.1	Sugar (and other) transporter/Major Facilitator Superfamily/Uncharacterised MFS-type transporter YbfB/Organic Anion Transporter Polypeptide (OATP) family, putative	7.1/3.5	nd	11	-	74.8	101.7 (eGFP)	-
CAD2216215.1	ABC transporter transmembrane region/ABC transporter, putative	nd	4.3/4.2	06	153	67.6	94.5 (eGFP)	-

[a] GenBank accession number.
[b,c] Enrichment of protein in ES fractions in LC-MS/MS Experiment 1 and 2, indicated by (difference ES-WC/-log T-test p-value) as in Figure 2.1 c-d. Nd, not detected.
[d] Chromosomal localization in *A. deanei* nuclear genome assembly GCA_903995115.1.
[e] N-terminal extension of the ORF as predicted by full-length transcript by indicated number of amino acids (see Figure 6.3).
[f] Estimated molecular weight of the protein encoded by the full length ORF (Expasy Protparam).
[g] Estimated molecular weight of the fluorescent fusion protein mSCARLET-ETP1 and eGFP-POI.
[h] Newly assigned name.

2.2 Experimental verification of ETP candidates in *A. deanei*

All 14 putative ETP candidates were to be screened with N- and C-terminal GFP fusion constructs, which resulted in a total of 28 cell lines. Generation of plasmids and downstream analyses were distributed among several lab members to streamline and accelerate the process. Table 6.1 shows the contribution of each researcher to the final dataset. All ETP candidates were transfected into Adea126 (material and methods 4.4.3), expressing CAD2220707.1 (ETP1) fused N-terminally to mSCARLET. ETP1 fusion constructs have been investigated by Sofia Kokkori during her PhD thesis (Kokkori, 2018) and mSCARLET-ETP1 was used in the course of this thesis as a marker for the ES in *A. deanei*. The plasmids were created using Golden Gate cloning with the eGFP-tagging vectors pAdea043 and pAdea235 (material and methods 4.3.4). In some cases, multi fragment Golden Gate or Gibson assembly was used instead, due to incompatibility of internal BsaI restriction sites (Figure 6.1). PCR verified clones of each cell line were analyzed by epifluorescence microscopy (Material and methods 4.4.6) and ES were isolated and compared to whole cell fractions of the same cell line (Morales *et al.*, 2023). If localization at the ES was observed by epifluorescence microscopy and enrichment in the ES fraction was shown via Western blot analysis (Material and methods 4.5.5), confocal microscopy and 3D reconstruction based on focal planes throughout the entire *A. deanei* cell was performed. This multistep analysis identified 7 of the 14 candidates as actual ETPs (Figure 2.2). 3D reconstruction of ETP1 confirmed that the protein localizes at the periphery of the ES. ETP2, ETP7, and ETP9 are found at the constriction site of the ES, where fission during cell division occurs (Motta *et al.*, 2010). ETP3 and ETP8 were observed inside the ES and in a separate dot like structure at the posterior end of the nucleus, at which the Golgi apparatus localizes in trypanosomatids (Sahin *et al.*, 2008). ARL-1, a marker for the trans Golgi network (TGN) established in *A. deanei* by Lucie Hansen (Hansen, 2021) was co-expressed with ETP8-eGFP. The dot like structure of ETP8-eGFP appears between the nucleus and the TGN labelled by ARL1-V5 (

), with some degree of overlapping. This speaks for an accumulation of ETP8-eGFP at the cis site of the Golgi apparatus, which is by similarity of the signal most likely also true for eGFP-ETP3.

The import of ETP3 and ETP8 into the cytosol of the ES was visualized by measuring the fluorescence intensity of the eGFP-tagged ETP3 and ETP8 and comparing the distribution to mSCARLET-ETP1 (

B), as ETP1 is found mainly at the envelope of the ES as described in paragraph 2.5. The decrease in fluorescence intensity between 1 and 3 µm of mSCARLET-ETP1 correlates to the location of the cytosol of the ES. eGFP-ETP3 and eGFP-ETP8 fluorescence intensity peaks do not overlap with the peaks of mSCARLET-ETP1 but were shifted to the center of the ES indicating accumulation in the cytosol (Figure 2.4).

ETP5, known as KMP-11 in other trypanosomatids, has been reported to localize at the basal body of the parasite (Li and Wang, 2008), which seems to be the case in *A. deanei* as well but it is also found throughout the periphery of the bacterium, like ETP1 and seems to interconnect the DNA-bearing compartments of *A. deanei* by a thread like structure that ends in a spot at the posterior end of the host. Localization of all fusion proteins was similar independently of N- or C-terminal fusions except for ETP3, which did not show any fluorescence when tagged at the C-terminus.

All other candidates could only be detected in the whole cell lysate or, in the case of CAD2218427, were not detected at all and thus, were omitted from further analyses (Figure 2.3).

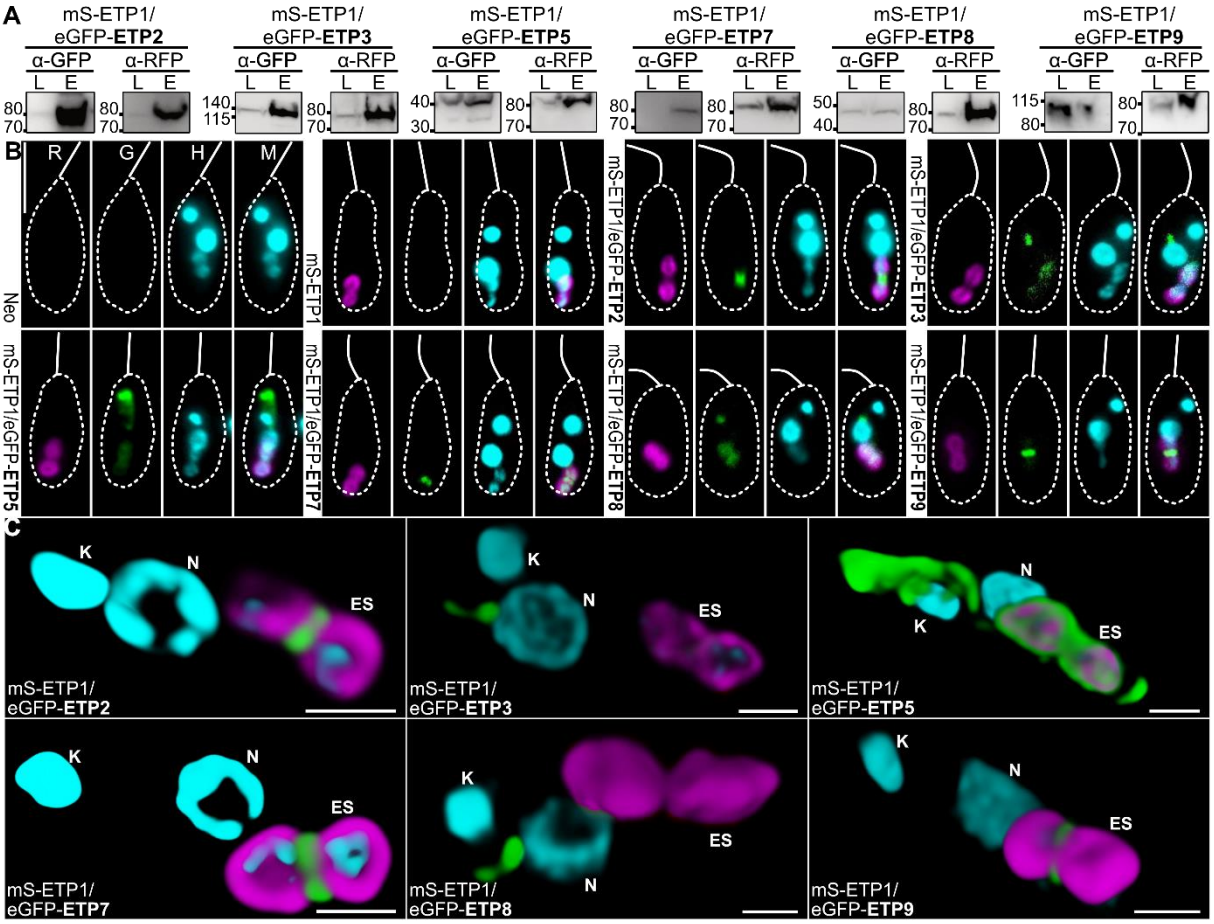

Figure 2.2: Newly identified ETPs show distinct subcellular localizations within *Ca.* K. crithidii and the host cell. (**A**) Protein from whole cell lysate (L) or purified endosymbionts (E) were resolved by SDS-PAGE, transferred onto PVDF-membranes, and recombinant proteins were visualized by Western blot analysis using anti-GFP (α-GFP) or anti-RFP (α-RFP) antibodies (1:1000). (**B**) Epifluorescence microscopic analyses of cell lines expressing the neomycin phosphotransferase (Neo) alone, mS-ETP1, or mS-ETP1 in combination with eGFP-POI constructs. D: differential interference contrast; R: red channel; G: green channel; H: blue channel visualizing Hoechst 33342 staining; M: merge of the three fluorescence channels. Scale bar is 5 μm. (**C**) Three-dimensional reconstruction of the localization of the different recombinant ETPs within *A. deanei* from the superposition of 12-32 Z-stacks after deconvolution. Color code: magenta, mS-ETP1; green, eGFP-POI; cyan, Hoechst 33342. Scale bar is 1 μm. ES, endosymbiont; K, kinetoplast; N, nucleus.

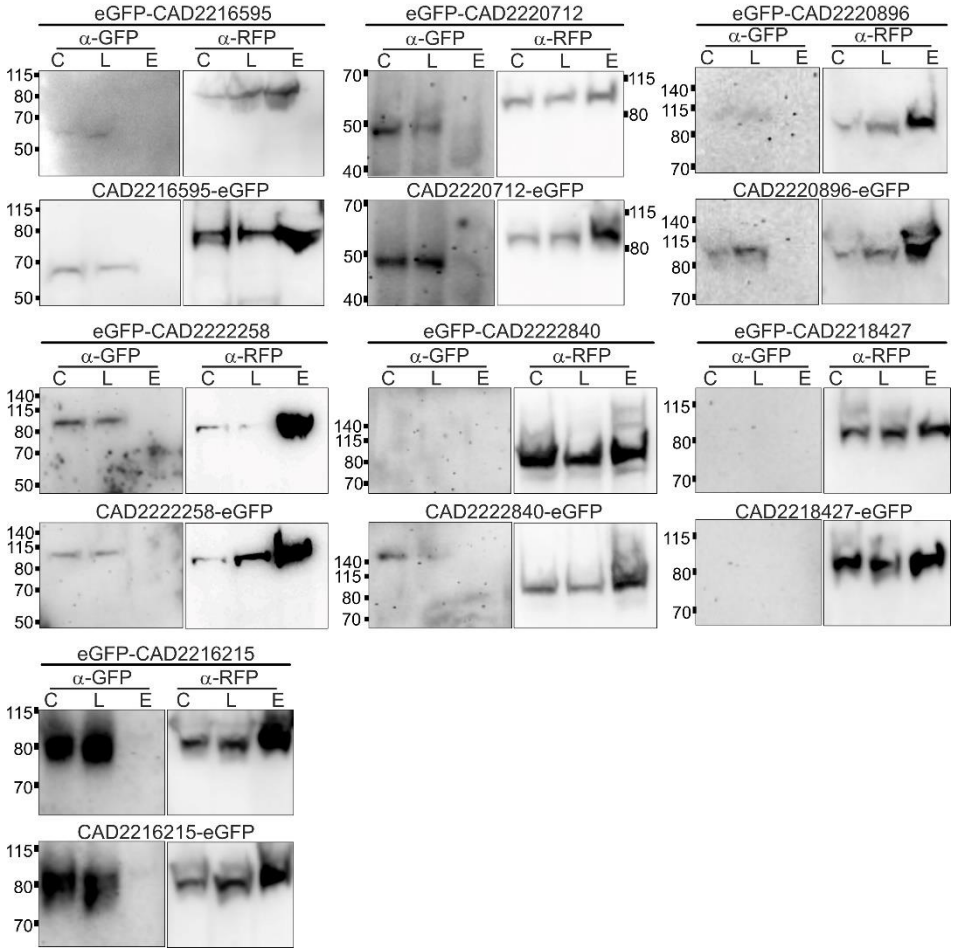

Figure 2.3 Seven candidates did not show accumulation at the ES by Western blot. 30 µg of protein from intact cells (C), whole cell lysate (L) or up to the Percoll step purified endosymbionts (E) were resolved by SDS-PAGE on 4-12% acrylamide gels, transferred onto a PVDF-membrane, and recombinant proteins were visualized using α–GFP or α–RFP antibodies (1:1000) with 2nd AB conjugated to horseradish peroxidase (1:5000). Note that these candidate ETPs for which localization at the endosymbiont was not confirmed did not receive an 'ETP annotation'. α–RFP causes a signal that corresponds to mSCARLET-ETP1. α–GFP produces a signal for eGFP-fusion constructs of ETP candidates. Marker in kDa.

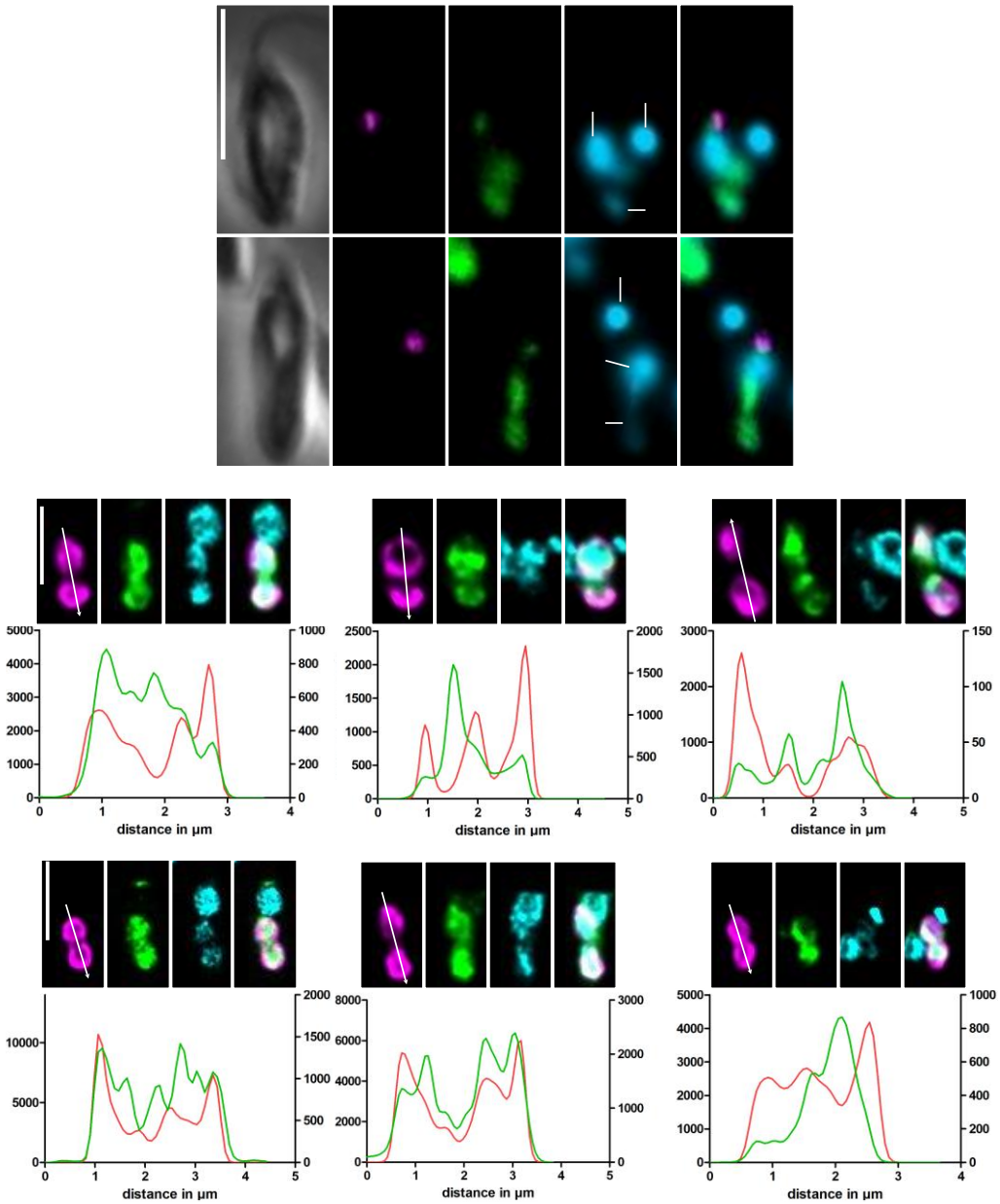

Figure 2.4 (A) Immunofluorescence assay (IFA) shows partial overlap of the subcellular localization of the trans Golgi network (TGN) marker ARL1-V5 with ETP8-eGFP in *A. deanei*. (B) Plotted intensity through the longitudinal axis of the center of the ES of mSCARLET-ETP1 and eGFP-ETP8. (**A**) 1st AB: α–V5 1:100, 2nd AB: CFL-594 1:100. D: differential interference contrast; R: red channel, ARL1-V5; G: green channel, ETP8-eGFP; H: blue channel visualizing Hoechst 33342 staining; M: merge of the three fluorescence channels). ETP8-eGFP fluorescence is found throughout the endosymbiont cytosol as well as a spot between nucleus and TGN, indicative of the Golgi apparatus. Scale bar is 5 µm. ES: endosymbiont; K: kinetoplast; N: nucleus. Two cells of the same cell line representing the typical fluorescence pattern are displayed. (**B**) Confocal microscopy of cells expressing eGFP-ETP3 and eGFP-ETP8 and mSCARLET-ETP1 was performed and 0.1 µm sections throughout the cells were imaged. Focal planes through the center of the ES were chosen according to a decrease in fluorescence of mSCARLET-ETP1 through the cytosol of the ES. A line was drawn through the center (white arrow, orientation correlates to the distance in µm on the X-axis of the graphs) of the ES cytosol and arbitrary intensities were plotted. Intensity of mSCARLET-ETP1 (red graph, left Y-axis) and eGFP-ETP3/eGFP-ETP8 (green graph, right Y-axis). R: mSCARLET-ETP1; G: eGFP-ETP8, H: Hoechst 33342; M: merge. Scale bar 2.5 µm. 3 cells were plotted to represent each cell line.

2.3 Distribution of ETP2, ETP7 and ETP9 throughout the ES

Observation of the epifluorescence pattern of ETP2 fusion constructs revealed that the fluorescence signal was not limited to the constriction site of the ES but also found at the poles of the ES. Since the ES are often in a tilted angle, determination of the distribution of fluorescence signal in a cell by just one focal plane is often difficult. Confocal microscopy was performed to analyze the fluorescence pattern of the ES by imaging of several focal planes covering the entire depth of the cell. The same procedure was performed for ETP7 and ETP9 fusion constructs.

53% of mSCARLET-ETP2 expressing cells showed fluorescence at the constriction site (Figure 2.5 A 1, 2 and 3; B dark green). However, another 34% showed fluorescence at either one or both poles of the ES (Figure 2.5 A 4 light green) and 13% of the cells did not show any fluorescence at all (Figure 2.5 B grey). eGFP-ETP7 is limited to fluorescence at the constriction site in 40% of the cells with 56% of all cells not showing any fluorescence at all. eGFP-ETP9 is found at the constriction site in 50% of the cells and 24% showed evenly distributed fluorescence throughout the ES without accumulation at a specific spot. For the remaining 26% no fluorescence was detected.

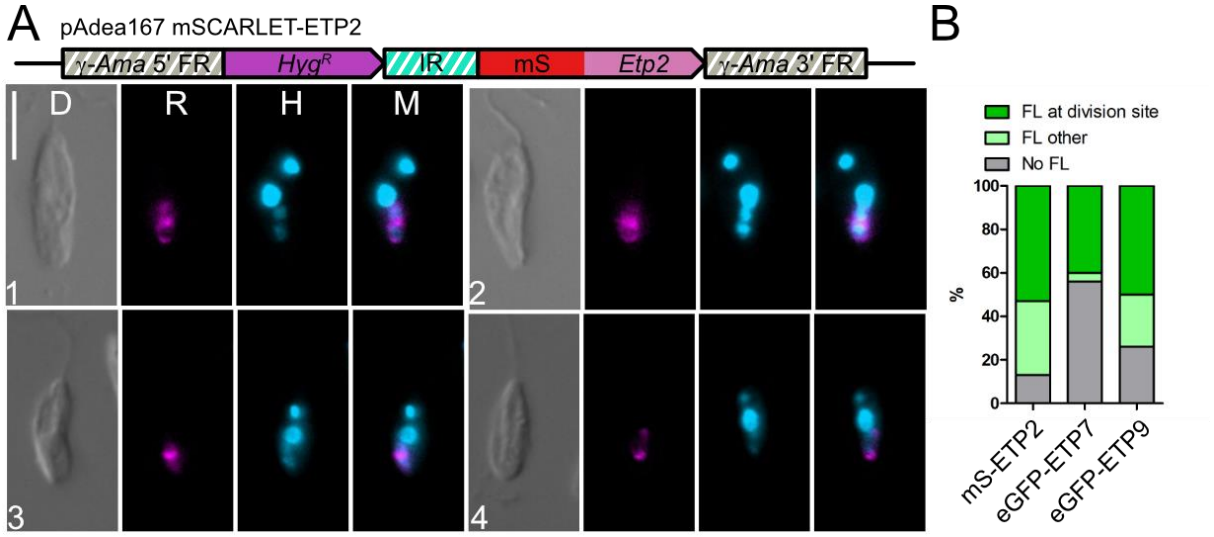

Figure 2.5: (A) Different distributions of *Ad*ETP2 throughout the ES of *A. deanei.* (B) Quantification of fluorescence distribution of mSCARLET-*Ad*ETP2, eGFP-ETP7 and eGFP-ETP9. (**A**) Epifluorescence microscopy of mSCARLET-*Ad*ETP2 expressing cells. mSCARLET-*Ad*ETP2 can be found accumulated at the division site and both poles (1), only one pole (2), limited to the division site (3) or limited to the poles (4). D: Differential interference contrast, R: red channel, H: Hoechst 33342, M: Merge. Scale bar 5 µm. (**B**) mSCARLET-ETP2, eGFP-ETP7 and eGFP-ETP9 expressing cells were imaged via confocal microscopy with focal planes of 0.1 µm distance throughout the length of the cell. Maximum projections were produced from which the fluorescence distribution was categorized accordingly. A total of at least 100 cells per cell line were counted. FL at division site = fluorescence signal accumulation at the constriction site of the bacterium. FL other = fluorescence signal at the ES but no accumulation at the constriction site. No FL = no fluorescence at the ES observed.

2.4 Comparison of ETP7 and ETP9 localization by confocal microscopy

As the localization of ETP7 and ETP9 at the constriction site was similar when co-expressed with mSCARLET-ETP1, their localization was also analyzed in a cell line expressing both, eGFP-ETP7 and mSCARLET-ETP9. ETP9 was observed in the constriction site mainly in the ring structure, characterized by two separate dots co-localizing with mSCARLET-ETP1 or in the ES right before division, as concluded from the separation of the bacterial DNA, in a singular centered spot (Figure 2.6 A and B). eGFP-ETP7 seems to migrate in a similar pattern. When mSCARLET-ETP9 is in the ring structure eGFP-ETP7 is also found in the center spanning the septum, which is not the case for ETP9 (Figure 2.6 C). When ETP9 is showing the dot structure, ETP7 is also in a more restricted dot concentrated between the separating ES (Figure 2.6 D).

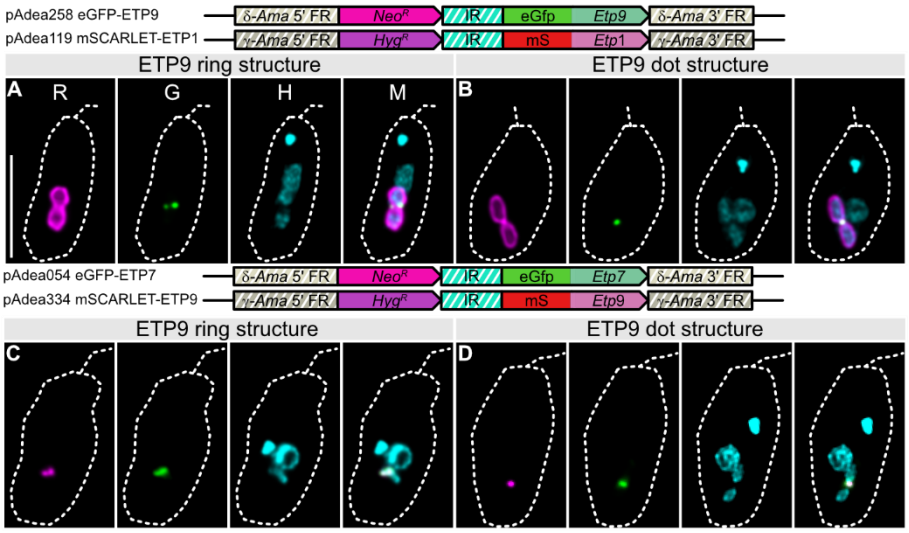

Figure 2.6 Co-expression of eGFP-ETP9/mSCARLET-ETP1 and eGFP-ETP7/mSCARLET-ETP9. Maximum projection of cells imaged by confocal microscopy in focal planes of 0.1 µm distance throughout the depth of the cell. ETP9 is found in a ring (A and C) or dot structure (B and D). eGFP-ETP7 is distributed in a disk like extension at the constriction site or in a concentrated dot. A and B: R: mSCARLET-ETP1; G: green channel; C and D: R: mSCARLET-ETP9; G: eGFP-ETP7; (A-D) H: Hoechst 33342; M: merge. Scale bar 5 µm. Cell shape tracked by a dotted line.

2.5 Establishment of Immunogold transmission electron microscopy in *A. deanei* to determine the subcellular localization of the ETPs

Except for ETP3 and ETP8 all ETPs are found mainly at the periphery of the ES, which is harbored by two bacterial membranes but no host-derived membrane (Soares and De Souza, 1988). Furthermore, phosphatidylcholine (PC), the major phospholipid of eukaryotes, absent in most bacteria that do not interact with eukaryotes, was found to comprise more than 15% of the phospholipid composition of the ES (Palmié-Peixoto *et al.*, 2006). From epifluorescence microscopy it is difficult to pinpoint the localization of the ETPs at the membrane as the intermembrane space is only about 30 nm (Soares and De Souza, 1988) and no dyes specific for any of the ES membranes have been established yet. Previous studies could clearly distinguish between the outer and inner membrane of the bacterium by transmission electron microscopy (M. C. Motta *et al.*, 1997).

To observe the localization of the ETPs along the membranes of the ES, V5-tagged fusion proteins were expressed in *A. deanei*. In IFA studies the localization was identical to the eGFP- and mSCARLET-tagged constructs of the ETPs for all tested candidates (data not shown).

As most epoxy resins are not permeable for antibodies, LR white which was previously successfully applied in immunogold-TEM in *P. chromatophora* (Nowack and Grossman, 2012)**,** was chosen for embedding of *A. deanei* cells expressing V5-ETP1 and ETP1-V5 (4.4.9). Several immunostaining strategies were compared for optimal results in LR-White-embedded cell lines:

Approach 1) 1st AB (mouse, Abcam, ab27671) followed by a 2nd AB coupled to colloidal gold

a) 6 nm gold (goat-α–mouse IgG, Jackson ImmunoResearch, 115-195-146)
b) 15 nm gold (goat-α–mouse IgG, Aurion, 815.022)

Approach 2) 1st AB (mouse, Abcam, ab27671) conjugated with 10 nm colloidal gold (Abcam, ab201808)

Approach 3) 1st AB (mouse, Abcam, ab27671), a bridge AB (rabbit-α–mouse IgG, Dianova, 315-005-048) and Protein A gold (PAG) bound to 15 nm gold (Cell Biology Utrecht)

Application of approach 1 in different concentrations of the 1st and 2nd ABs on LR-White embedded *A. deanei* cells always showed very few gold particles bound to the sample (Figure 2.7 A). No gold particles could be observed for approach 2. Approach 3 could be used to reliably stain ETP1-V5 but the extended period of time in the staining and washing solution led to the formation of wrinkles on the sections, particularly common throughout the ES (Figure 2.7 B).

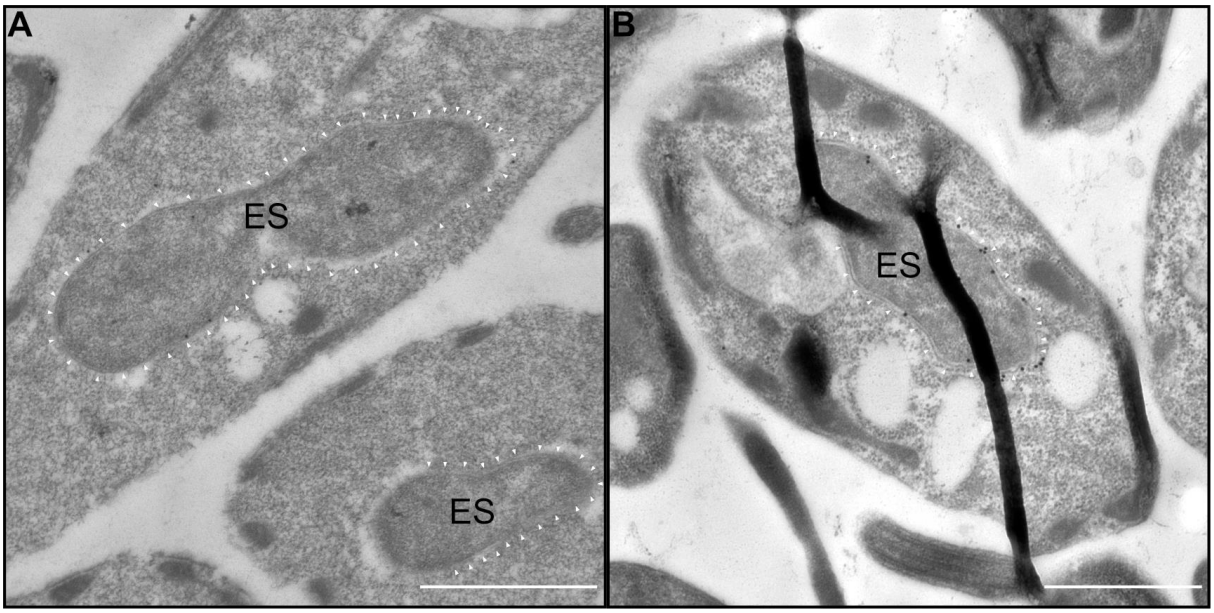

Figure 2.7 Immuno-TEM of LR-White embedded *A. deanei* cells expressing ETP1-V5. (A) 1st AB: 1:4 α–V5 overnight 4°C, 2nd AB: 1:5 goat-α–mouse 15 nm gold 60 min RT. (**B**) 1:10 α–V5 overnight 4°C; 2nd AB: 1:10 rabbit-α–mouse 30 min RT, 3rd: 1:50 PAG 15 nm 30 min. White arrow heads track the outer membrane of the ES. Black spheres correspond to the 15 nm gold particles. ES: endosymbiont. 20,000x magnification. Scale bar 1 µm.

The ES envelope space is a narrow structure and epitope preservation in LR white embedded cells was too low overall. To avoid the strong and long fixation and embedding steps, which all decrease epitope availability, cryosectioning according to (Tokuyasu, 1973) was performed. The accessibility of epitopes was tested on 250 nm rough sections (4.4.11) (Figure 2.8), before applying immunosteps on the grids carrying ultrathin sections.

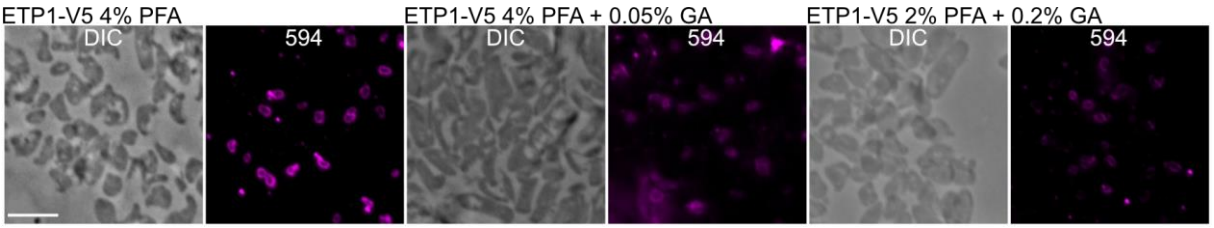

Figure 2.8 IFA of 250 nm rough sections of *A. deanei* expressing ETP1-V5. Fixation with glutaraldehyde (GA) leads to a strong decrease in fluorescence intensity. 1st AB: α–V5 1:20, 2nd AB: goat α–mouse Alexa fluor 594 nm according to manufacturer protocol, undiluted. Scale bar 5 µm.

Fixation omitting GA showed the strongest fluorescence and became the condition of choice for all further Tokuyasu embeddings of *A. deanei* cell lines. Treatment of sections with the previously described combinations of antibodies showed the best results for approaches 1b (Figure 2.9 A, B) and 3 (Figure 2.9 C, D). Approach 1a showed very few and highly dispersed gold particles, and in grids treated according to approach 2 no gold particles were observed (data not shown). Approach 1b showed only few gold particles, but these were very specifically localized at the envelope membranes of the ES (Figure 2.9 A), as previously seen by IFA (Figure 2.8). When grids were incubated without the 1st antibody as a negative control, no gold particles could be observed in the proximity of the ES (Figure

2.9 B). In grids treated according to approach 3 the overall number of gold particles was very high, corresponding to a high background but labelling of the ES membrane was very specific, tracing the envelope (Figure 2.9 C, inlay). As protein A binding is very heterogeneous to the different mouse IgG classes (Duhamel *et al.*, 1979) a rabbit-α–mouse IgG antibody was applied to increase overall binding of PAG. As a negative control for approach 3 only PAG was applied to the grids (Figure 2.9 D). The overall number of gold particles was similar but gold particles at the ES envelope membranes were far less frequent.

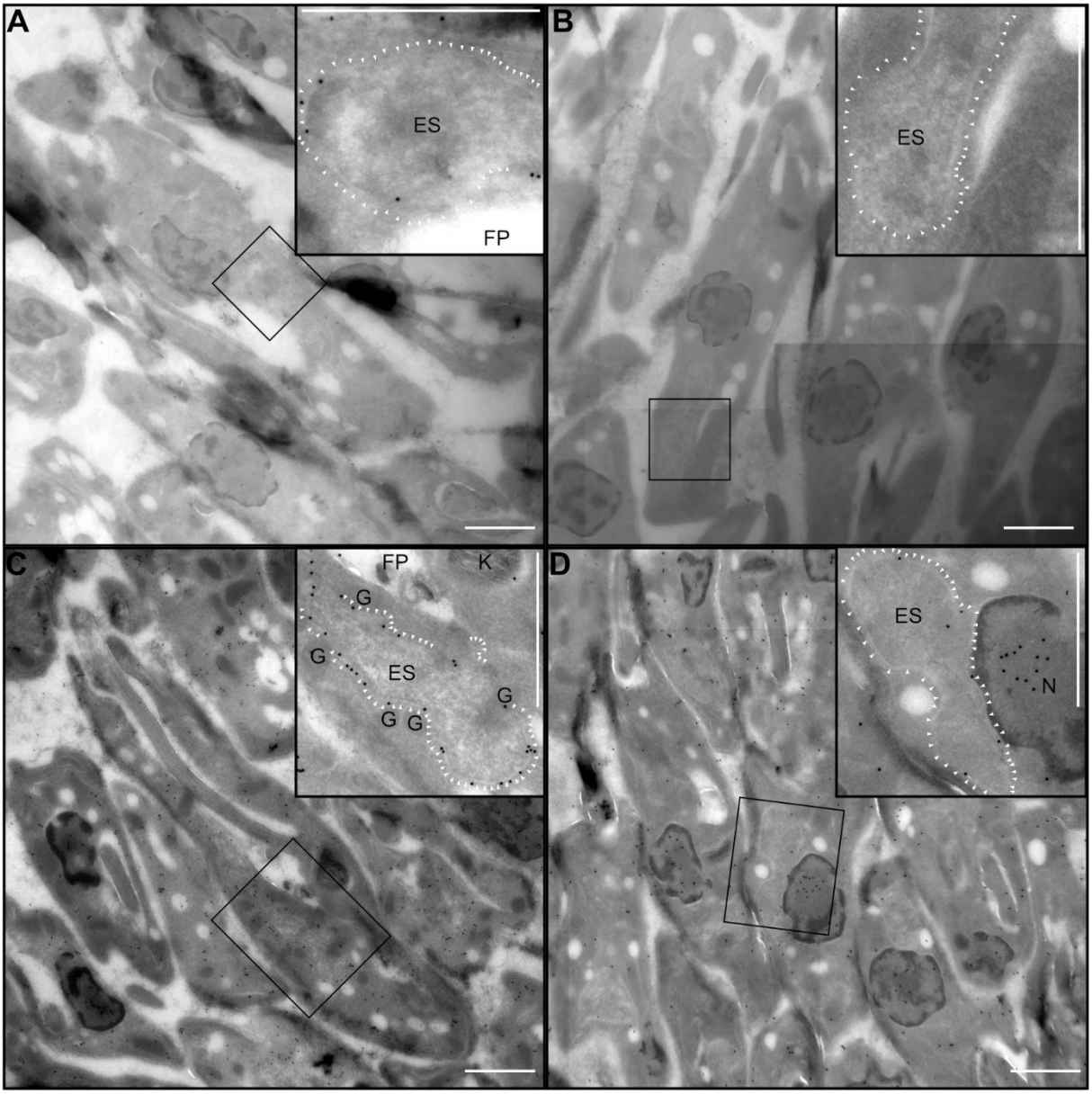

Figure 2.9 Immunogold-TEM of cryosectioned V5-ETP1-expressing *A. deanei* cells. (**A**) 1st AB: 1:20 α-V5 90 min RT, 2nd AB: 1:20 goat-α-mouse 15 nm gold 60 min RT. (**B**) 1:20 goat-α-mouse 15 nm gold 60 min. (**C**) 1st AB: 1:20 α-V5 90 min, 2nd AB: 1:10 rabbit-α-mouse IgG 30 min, 3rd: PAG 15 nm 1:50 30 min. (**D**) PAG 15 nm 1:50 30 min. Black box highlights area of the ES enhanced in inlay. White arrow heads track the outer membrane of the ES. Black spheres correspond to the 15 nm gold particles. ES: endosymbiont; G: glycosome; K: kinetoplast; FP: flagellar pocket; N: nucleus. Scale bar is 1 µm. Overview images: A, C: 12,000x magnification, inlays 30,000x; B, D: Areas were imaged at 20,000x, and

overview images stitched together from 9 images total; inlays enhanced from the original 20,000x image.

2.6 Evolution of the ETPs in the aposymbiotic *A. deanei* strain ATCC-30969

Since ETPs can be assumed to fulfill symbiosis-related functions, an important question is, whether these proteins survive in cells, in which the endosymbiont has been experimentally deleted. Therefore, we ordered the aposymbiotic strain ATCC-30969 form the American Type Culture Collection to study the presence and nucleotide sequence of ETP-coding genes. Previous analysis of the strain ATCC-30969 created doubts regarding its identity (Teng, Wang and Gabriel, 1995; Clark, 1997). To address this, the 18S rRNA gene of this strain was amplified via PCR (4.3.1) from gDNA (4.4.5). The 18S rRNA gene was sent for sequencing (Microsynth) and compared to *A. deanei* subgroups (represented by *A. deanei* TCC080E) as well as other SHTs of the genus *Angomonas* previously published (represented by *A. desouzai* TCC079E) (Teixeira *et al.*, 2011).

The ATCC-30969 18S rRNA gene is identical to the gene found in SHT *A. deanei* strains (Figure 2.10). Bp 166 and 1200 contained mixed signals in sequencing results, with the strongest peak corresponding to the expected bases at said positions (data no shown). With the identity of the strain confirmed, the presence and sequences of the ETP-coding genes were to be investigated. For this purpose, primers binding at the 5' and 3' of each ETP-coding gene were chosen and for the ETP3-coding gene internal primers were additionally used to ensure full sequencing coverage of the length of the gene. The genes were amplified, subcloned into pJET (Fisher Scientific) and transformed into *E. coli* Top10 cells. This subcloning step was necessary, to increase the DNA yield and allow for sequencing of the in some cases varying alleles of the ETPs. Plasmids were finally purified for sequencing (4.4.2)

Previously, an Illumina shotgun library was created (Morales *et al.*, 2016) and assembled into a draft genome resolving both haplotypes of the *A. deanei* nuclear genome. In 2021, a chromosome-level assembly of just one haplotype of the *A. deanei* nuclear genome was published (Davey *et al.*, 2021), which allowed for the comparison of two independently created genome sequences of the SHT *A. deanei* to the sequenced allele from the aposymbiotic strain ATCC-30969 (Figure 2.11). Initially, the sequences of the ATCC-30969 ETP-coding genes were blasted against the NCBI nucleotide collection (nr/nt), which would always show the hit in the assembled genome by Davey *et al.* from 2021. In a second step the ATCC-30969 ETP encoding genes were then blasted against the Illumina shotgun library and the resulting hits inside 2-3 scaffolds were compared to the NCBI hits. With two scaffolds found, usually one referred to each allele. In the cases of ETP9, one allele was partially found at the end of one scaffold and the beginning of another with a gap between bp 572 and 652. In the cases of ETP7 and ETP9 both alleles from the Illumina library were not identical to the assembled genome,

which were listed separately in Figure 2.11. All alleles have the same length, except for ETP1, which contains a 21 bp insertion, that has been previously described as the Q+ allele (Kokkori, 2018). ETP2 and ETP5 do not contain any allelic variation at all, which at least for ETP5 (also known as KMP-11 in other trypanosomatids) is not surprising as there have been previous reports on its involvement in the division of the trypanosomatid (Li and Wang, 2008). ETP5 is also the only ETP which comes in a tandem array of 4 copies on each allele.

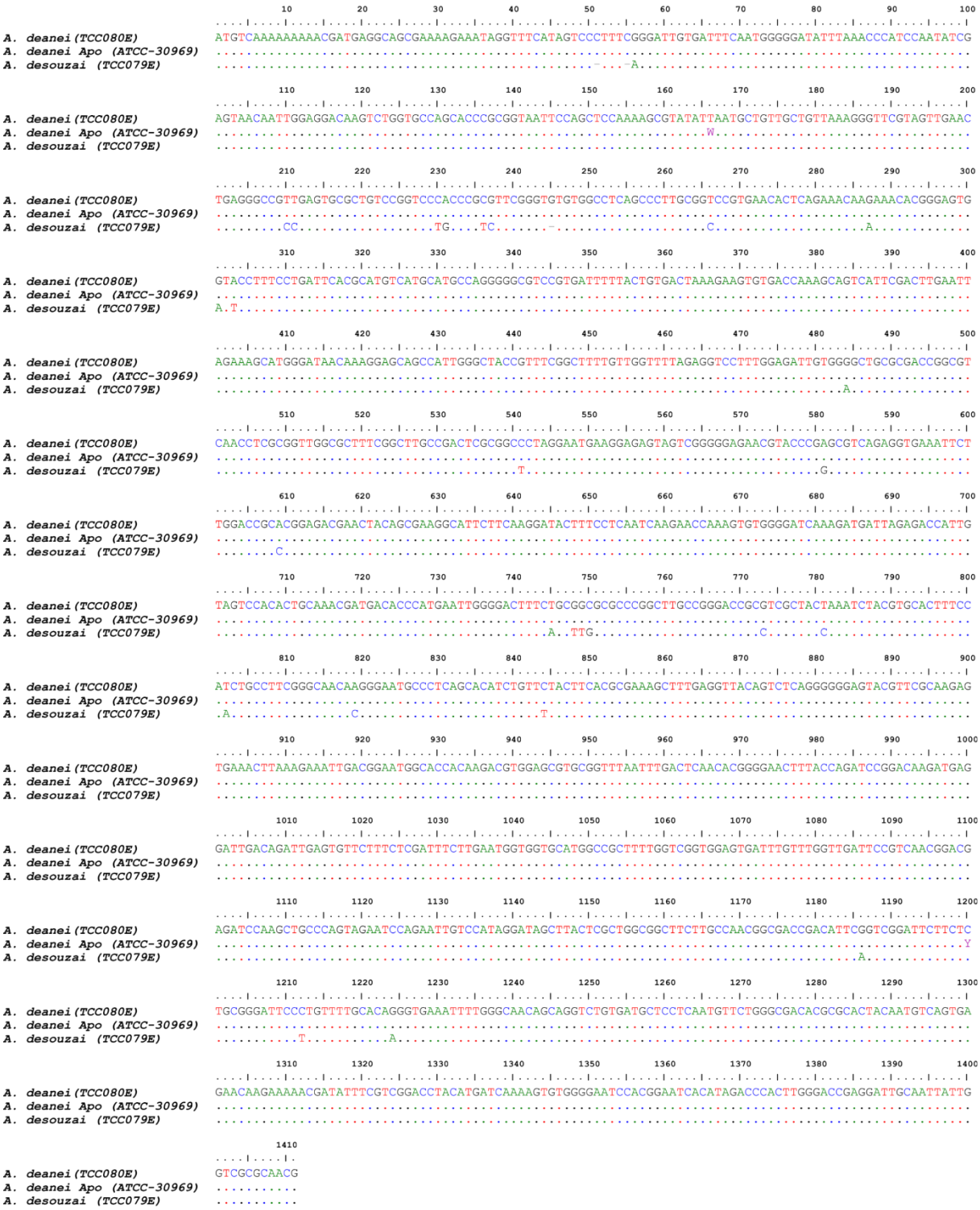

Figure 2.10 Alignment of the 18S rRNA gene of SHT *A. deanei* (TCC080E), aposymbiotic *A. deanei* (ATCC-30969) and *A. desouzai* (TCC079E). Dots (.) correspond to identical positions between the reference gene *A. deanei* (TCC080E) and the corresponding lane. Ruler in bp.

All ETPs were found in the aposymbiotic *A. deanei* strain, and the sequenced alleles did not show any allelic variations, except for ETP3. This means that either not enough time in the evolution of the strain has passed since the loss of the ES to lead to deleterious mutations in now obsolete genes, or that the ETPs do have a yet unknown function for the host.

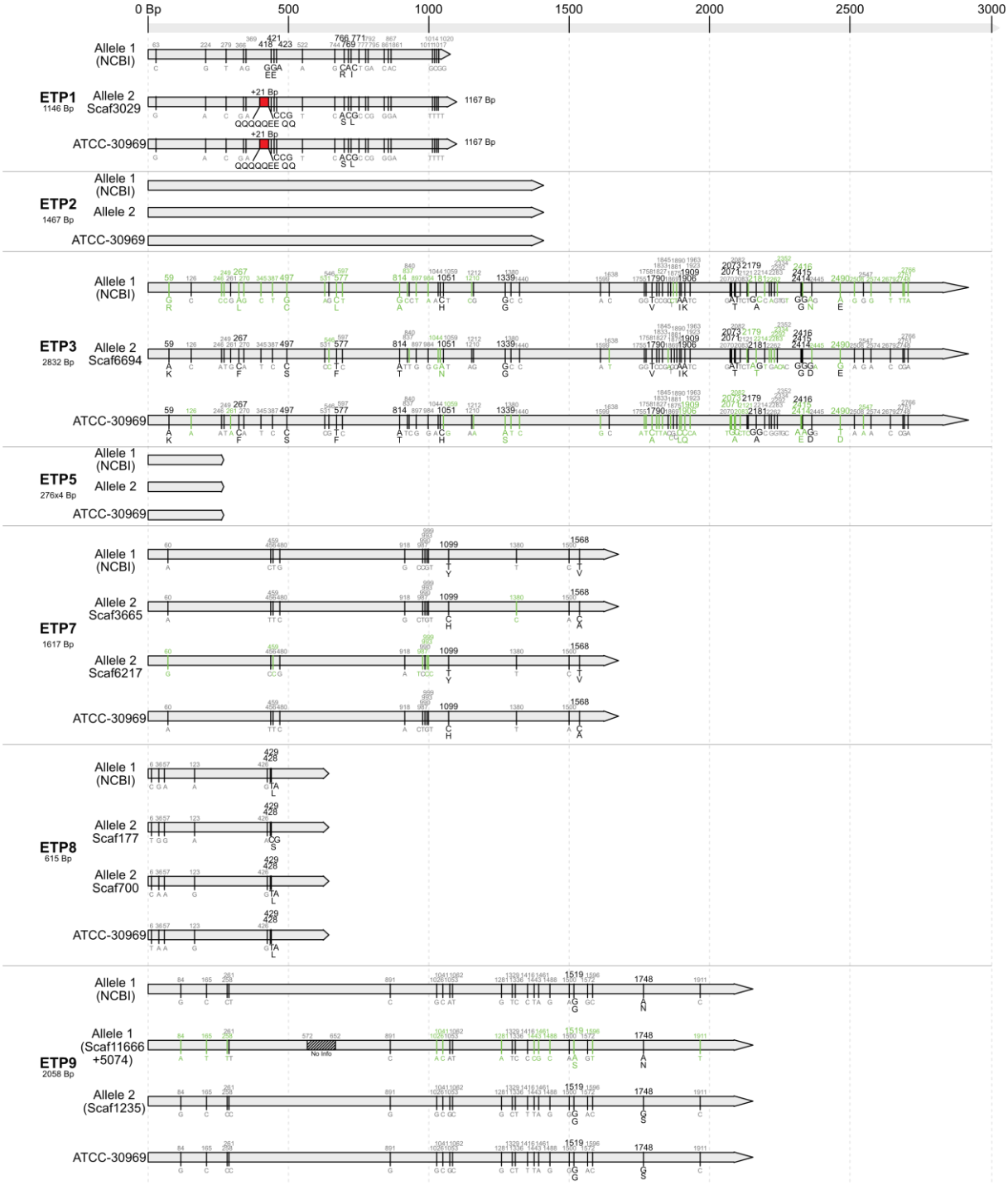

Figure 2.11 Comparison of the ETP alleles of SHT *A. deanei* to the aposymbiotic *A. deanei* strain. Allele 1 corresponds to the BLAST hit retrieved from NCBI and allele 2 to the divergent scaffold from the Illumina shotgun library. ATCC-30969 corresponds to the sequenced allele from the aposymbiotic strain. All allelic variations were highlighted in light grey with the position in bp above the schematic representation and the corresponding base below. Mutations unique to one allele were marked green. Whenever a mutation led to an aa exchange, the aa was named in one letter code below the base. Insertion of the 21 bp at ETP1 marked with a red box. Grey box in Scaf11666+5074 covers the area missing sequence in formation.

2.7 Generation of homozygous knockouts of ETP2 and ETP7

The lack of homology of ETP2 and ETP7 to any known protein domains makes it difficult to understand their role in the context of endosymbiosis in *A. deanei*. A deletion of the gene of interest may trigger a phenotype allowing new hypotheses regarding the function of the corresponding proteins based on the effect on the cells. Therefore, knock-out plasmids were designed to exchange ETP2 and ETP7 by homologous recombination against resistance cassettes. A second round of transfection and selection should produce homozygous knock outs of a verified heterozygous knock out with a second knock-out cassette. The necessary plasmids for generation of *Etp*7 KOs were produced by Dhevi Kalyanaraman during her master thesis (Kalyanaraman, 2018). The plasmids were designed with the FR of one allele.

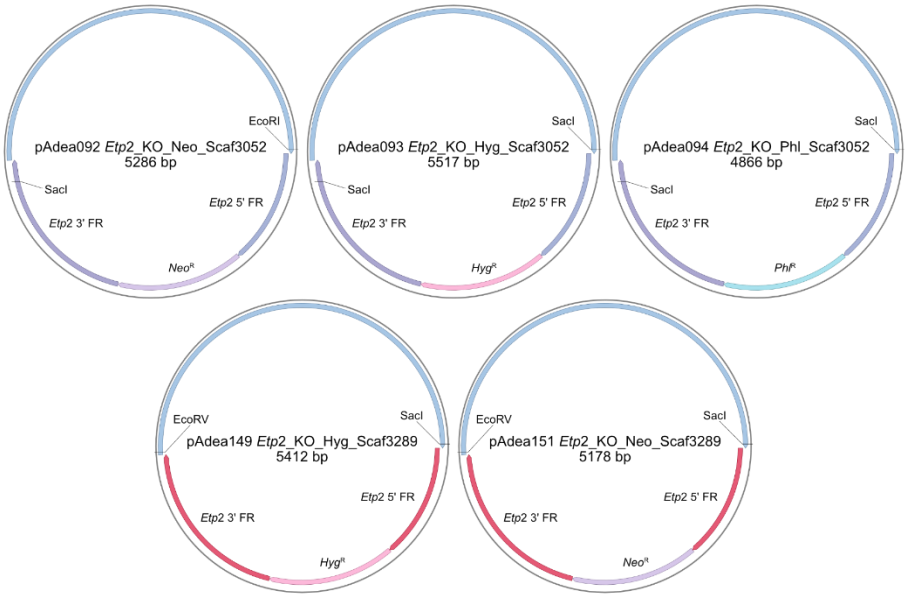

Figure 2.12 Plasmids for generation of *Etp2* KO. Upstream and downstream of the resistance cassettes (*Neo*^{R}, purple arrow; *Hyg*^{R}, pink arrow; *Phl*^{R}, cyan arrow) the plasmids contain *Etp*2 FRs from Scaf3052 (dark blue arrow) or Scaf3289 (red arrow) to target homologous recombination to both alleles of the *Etp2* locus individually. Plasmids were restricted using SacI or SacI and EcoRV to produce linearized cassettes, which were used for transfection into *A. deanei*. Vector backbone: pUMA1467 (Terfrüchte *et al.*, 2014).

Since the efficiency of HR to target the exact scaffold for which the FR were designed has not been previously determined, separate plasmids for both alleles were produced for *Etp2* to explore the possibility of allele-specific targeting during transfection of a heterozygous KO. Instead of an exchange of the second allele of *Etp2* it was speculated that the previously integrated resistance cassette was exchanged again, leading to a non-viable cell line under selection pressure of both antibiotics.

Transfection of SHT *A. deanei* and aposymbiotic *A. deanei* cells according to (4.4.3) produced in total 8 heterozygous *Etp2* and *Etp7* KO cell lines (Table 2.2). Cell lines were verified by PCR and additionally during the establishment phase of this strategy also via Southern blot (4.3.7) (Figure 2.13).

Table 2.2 Generated heterozygous knock-outs of *Etp2* and *Etp7* in *A. deanei*. Strains are arranged by recipient cell line and targeted locus.

Recipient cell line	Plasmid	Resistance	Locus/scaffold (allele)	Generated cell line
ATCC PRA-265	pAdea092	*Neo*^{R}	*Etp2*/Scaf3052	Adea086
ATCC PRA-265	pAdea093	*Hyg*^{R}	*Etp2*/Scaf3052	Adea113
ATCC PRA-265	pAdea094	*Phl*^{R}	*Etp2*/Scaf3052	Adea087
ATCC PRA-265	pAdea102	*Hyg*^{R}	*Etp7*/6217	Adea102
ATCC PRA-265	pAdea103	*Phl*^{R}	*Etp7*/6217	Adea103
ATCC PRA-265	pAdea149	*Hyg*^{R}	*Etp2*/Scaf3289	Adea153
ATCC-30969	pAdea092	*Neo*^{R}	*Etp2*/Scaf3052	Adea361
ATCC-30969	pAdea102	*Hyg*^{R}	*Etp7*/6217	Adea364

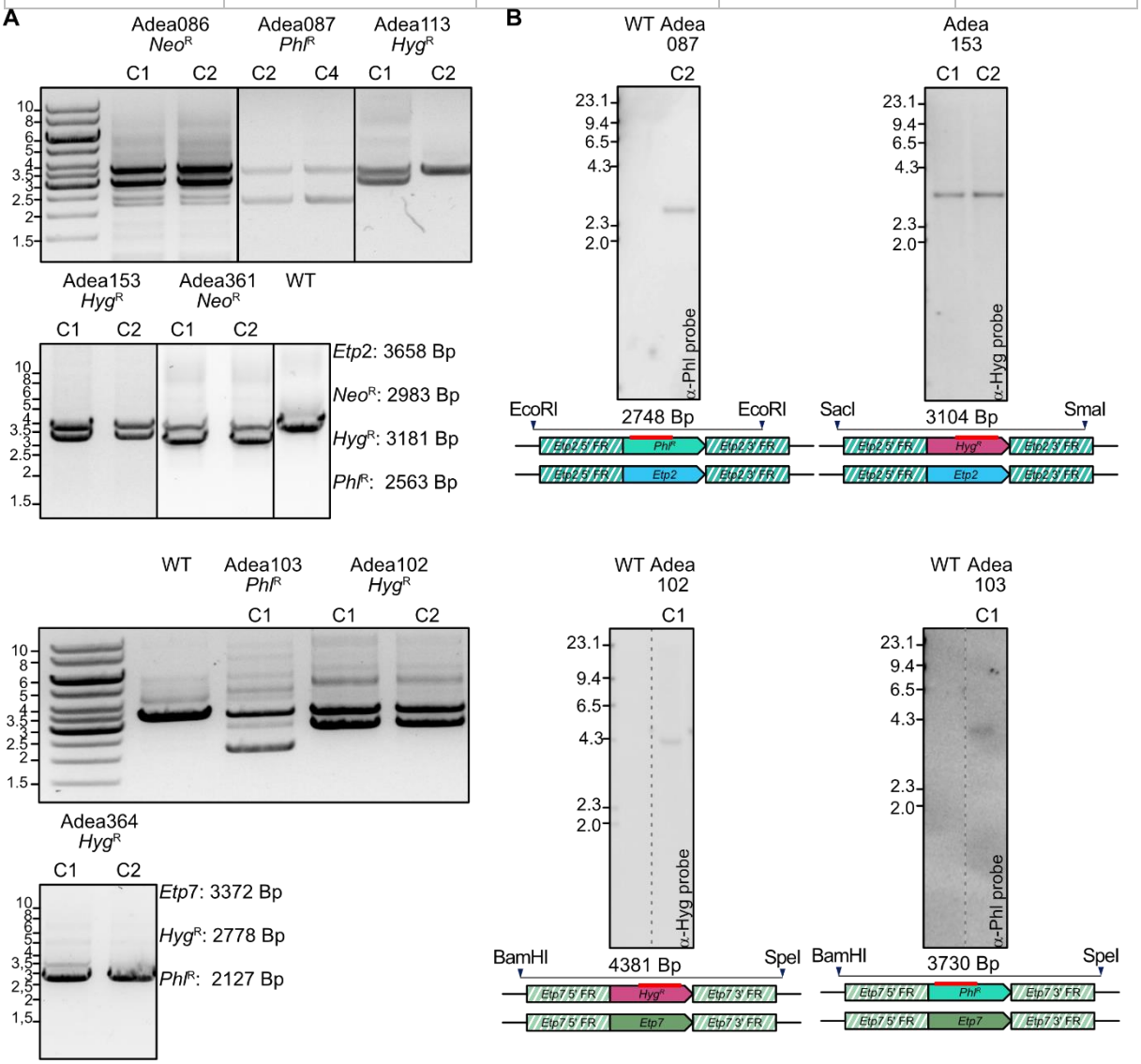

Figure 2.13 (A) PCR and (B) Southern blot verification of heterozygous knockouts of *Etp2* and *Etp7*. (**A**) Diagnostic PCR using primes binding upstream and downstream of the FR used for homologous recombination on gDNA extracted from clonal cultures. Two main products were visible, corresponding to the WT allele of *Etp2* and *Etp7* and the exchanged allele for the resistance cassettes (see legend). Only one or two clones were shown here as representatives of the cell line. (**B**) Southern blot of PCR tested clones to screen for off-target and multiple insertions. Probes were used against the corresponding resistance cassettes. Schematics below the blots show the digest strategy and the expected signal size. Marker in kBp.

All heterozygous knockouts tested did not show any change in growth in BHI medium supplemented with 10% HS and 5 µg/ml hemin. Microscopy studies of the cell lines also failed to observe any changes in cell morphology or DNA compartment structure (data not shown). Repeated attempts to transfect the ES-harboring cell lines a second time using a different resistance marker cassette did not recover after application of the second selection drug or only after more than ten days, which is much longer than the typical 5-7 days of recovery observed in successful transfections. Clones from these very slowly recovering putative homozygous knockouts still showed one PCR product corresponding to the ETP wild type allele (data not shown), meaning that the second resistance cassette failed to replace the second copy of the ETP and in a rare off-target event inserted somewhere else. Also targeting alleles with flanking regions specific to each allele was not successful, as done in the case of ETP2 for Scaf3052 and Scaf3289. Hence, the generation of homozygous knockouts by conventional transfection strategy was not successful for ETP2 and ETP7 during this study. In the cases of the aposymbiotic cell line, no homozygous knockouts could be produced due to time constraints as this cell line grows much slower (Mundim and Roitman, 1977) than the ES harboring one and only heterozygous knockouts were achieved during the course of this thesis.

2.8 Verification of functionality of ETP2 fusion constructs

As all previous fusion constructs of ETPs with fluorescent proteins have been expressed from the amastin loci using Gapdh ir and the δ–amastin or γ–amastin 3' FR for mRNA splicing and stabilization instead of the endogenous locus it raised the question if the localization and abundance of the fluorescence signal may be an artifact of the experimental setup. To answer this question fusion constructs of *Etp*2 were produced with an *eGfp*-tag in the N- or C-terminus and transfected into *A. deanei* WT; transfected cassettes contained FR of the specific *Etp* for homologous recombination in the endogenous locus (Figure 2.14).

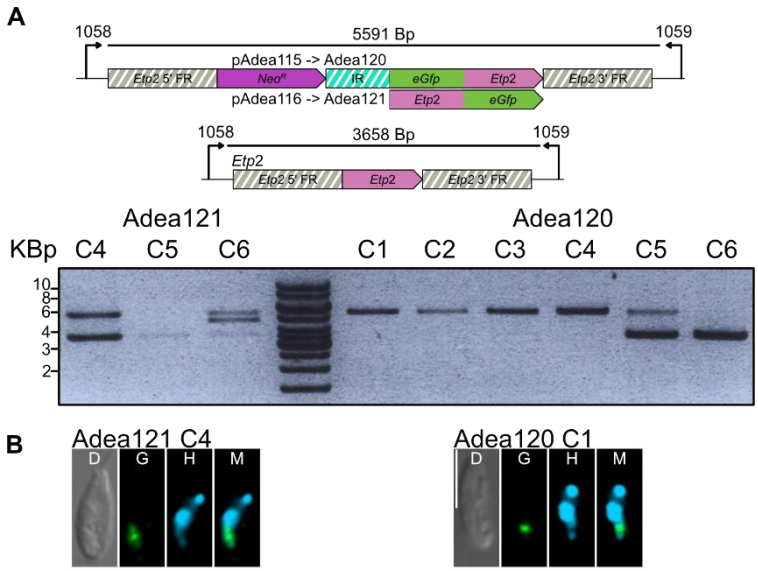

Figure 2.14 PCR verification of Adea120 and Adea121. (**A**) Diagnostic PCR using primes binding upstream and downstream of the FR used for homologous recombination on gDNA extracted from clonal cultures. Two main products were visible, corresponding to the WT allele of *Etp2* at 3658 Bp or the integrated cassette containing either *eGfp-Etp*2 (pAdea115 generating Adea120) or *Etp2-eGfp* (pAdea116 generating Adea121) at 5591 Bp. In Adea120 C1-C4 no WT band is visible, hinting on spontaneous homozygous insertion into both alleles of *Etp*2. (**B**) Epifluorescence microscopy of Adea120 and Adea121. D: Differential interference contrast, G: GFP, H: Hoechst 33342, M: Merge. Scale bar 5 µm.

Adea120 clones C1-C4 showed no PCR product corresponding to the WT *Etp*2 product, suggesting double insertion of the transfected cassette into both *Etp2* alleles which would speak for the functionality of the N-terminal fusion constructs in *A. deanei*. C5 showed one allele to be exchanged for the transfected cassette and C6 did not have any correct insertion into the *Etp*2 locus. In the case of Adea121 only C4 showed a singular insertion, while C5 did not show any insertion and C6 showed an irregular event with an additional product between WT *Etp*2 and the integrated cassette at the *Etp*2 locus. Southern blot analyses using a probe against *Etp2* should tell if any WT alleles of *Etp*2 were left in Adea120. Since the sequence information of the second allele of *Etp*2 (Scaf3052) was incomplete downstream of the 3' FR, gDNA of WT *A. deanei* was digested using several restriction enzyme combinations to test for suitability in a Southern blot using an *Etp2*-specific probe. It is to note that

KpnI contains a unique cutting site in the allele represented by Scaf3289, not found in Scaf3052 due to allelic variation. This creates two distinct signals in the Southern blot for WT *Etp*2 and allowed tracking which allele of *Etp*2 was replaced (Figure 2.15). In Adea120 C1 only one insertion took place into the allele corresponding to Scaf3289, while in C2 both alleles were replaced by the transfected cassette. Adea120 C2 expresses exclusively *eGfp-Etp*2 proving that N-terminal tagging of *Etp*2 produces functional fusion proteins in *A. deanei*.

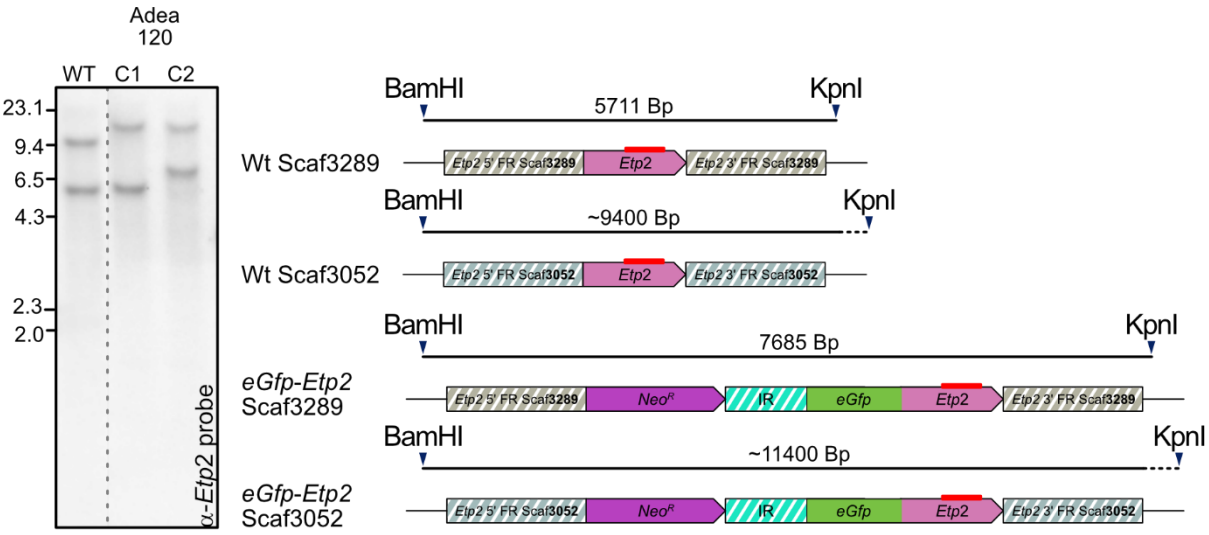

Figure 2.15 Southern blot of Adea120 C1 and C2. Probe (red bar) against *Etp*2 shows distinct signals for Scaf3289 (5.7 kBp, 1st. scheme) and Scaf3052 (9.4 kBp, 2nd scheme). Insertion into Scaf3052 leads to a shift to 11.4 kBp (4th scheme) and insertion into Scaf3289 to a shift to 7.7 kBp (3rd scheme) due to a unique KpnI cutting site in Scaf3289. Exact localization of the KpnI cutting site in Scaf3289 is not possible, as Scaf3289 sequence information is limited to 1 kBp downstream of *Etp*2 3' FR.

Repeated transfection attempts of Adea121 with pAdea093 or pAdea094 cassettes did not recover, which suggests that ETP2 is only functional when the C-terminus is not modified.

2.9 Conditional expression of ETP2 and ETP7

2.9.1 Degron

As generation of null mutants could not be achieved by conventional two step transfection (see section 2.8), a conditional system was to be established in *A. deanei*. To this end, three approaches were explored in this thesis. The first one, based on conditional protein degradation (section 2.9.1), the second one based on conditional gene deletions (section 2.9.2), and the third one based on conditional gene expression (section 2.9.3).

One strategy was the fusion of FKBP L106P (referred to as FKBP12 destabilizing domain, DDFKBP) to a POI which leads to its quick degradation; however, stabilization of the POI can be achieved by the addition of one of several synthetic ligands (Figure 2.16 A) (Banaszynski *et al.*, 2006). In *Leishmania major* this system allowed for depletion of UDP-glucose and UDP-galactose (Damerow *et al.*, 2015). This strategy was adapted by Rebecca Wolters during her master's thesis and applied to ETP2 and ETP7. Heterozygous knock-out strains of ETP2 (Adea087) and ETP7 (Adea103) were transfected with DDFKBP-V5-ETP2 and DDFKBP-V5-ETP7 to generate strains expressing only the conditionally stabilized protein in *A. deanei* (Figure 2.16 B, C). The V5-epitope allowed downstream Western blot and IFA analysis for determining protein abundance.

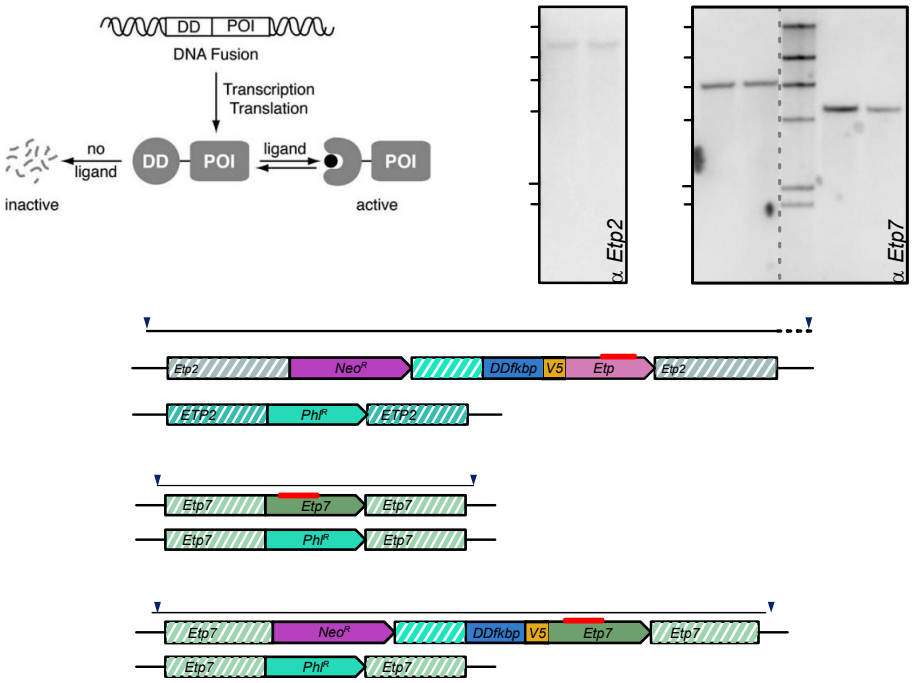

Figure 2.16 (A) Illustration of the degradation domain strategy adapted from Banaszynski et al., 2006 **and (B) Southern blot analysis of generated DDFKBP-V5-ETP2 (Adea175) and DDFKBP-V5-ETP7 (Adea177) expressing strains. (C) Schematic overview of strain genotypes shown in B.** (**A**) Fusion of a degradation domain (DD) to a POI leads to degradation of the fusion protein. Addition of a ligand stabilizes the DD which leads to active protein. (**B**) Southern blot analysis of Adea175 and Adea177

proves the strains are reliant on DDFKBP-V5-tagged copies of ETP2 and ETP7. Only bands corresponding to the inserted cassette are observed when a α–*Etp2* probe or α–*Etp7* probe are used for detection. Marker in kBp. (**C**) Adea175 was generated in the heterozygous *Etp2*/*Phl*^{R} strain Adea087. Adea177 was generated in the heterozygous *Etp7*/*Phl*^{R} strain Adea103 (used in the α–*Etp7* Southern blot, besides the WT, as a second control. Comparison to the WT shows a reduced signal strength, correlating to only one allele of *Etp7* left instead of two).

From the point of transfection, the ligand FK506 (200 µM) was added to the medium, to ensure stability of the fusion proteins, which in previous experiments allowed only for a total of 5-10% recovery of cytosolic eGFP tagged with FKBPDD in *A. deanei* (Wolters, 2019). Due to the essentiality of ETP2 and ETP7 it was assumed that low amounts of intact protein may be enough to avoid lethality, which seemed true as generation of Adea175 and Adea177 was possible. Removal of the ligand should lead to protein knock-down, expected to be paired with a reduced growth or collapse of the cultures. Transfer of Adea175 and Adea177 into ligand-free medium, however, did not show any change in growth behavior, even after several passages spanning more than two weeks. In NIH3T3 fibroblast cells within 4 h after ligand depletion DDFKBP levels were described as negligible and could not be tracked by Western blot anymore (Banaszynski *et al.*, 2006). IFA (4.4.6) and Western blot analysis (4.5.5) of Adea175 and Adea177 were performed (Figure 2.17).

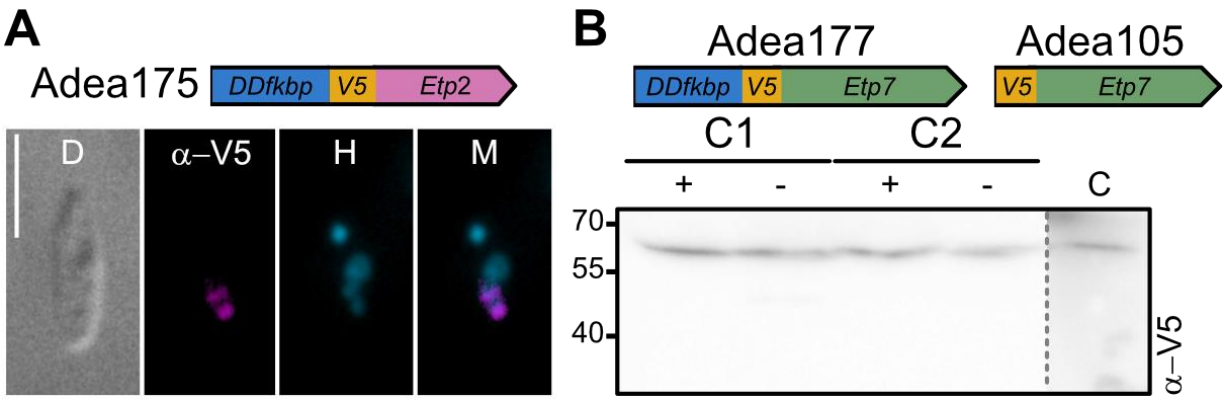

Figure 2.17 IFA of Adea175 (A) and Western blot analysis of Adea177 (B). (**A**) Fluorescence microscopy of Adea175 grown in medium without FK506. D: DIC, α–V5: 1st AB 1:1000 and 2nd AB 1:1000 m-IgGκ BP-CFL 594, H: Hoechst 33342, M: Merge of α–V5 and H channel. Scale bar 5 µm. **B:** Western blot of Adea177. +: lysate from cells grown in FK506 containing medium, -: lysate from cells grown without FK506 in the medium. C: control lysate from Adea105 producing V5-ETP7 without DDFKBP. 1st AB 1:2000, 2nd AB 1:5000 α–mouse HRP. Expected size for DDFKBP-V5-ETP7: 74.1 kDa. Expected size for V5-ETP7: 62.3 kDa.

IFA and Western blot confirmed DDFKBP-V5-ETP2 and DDFKBP-V5-ETP7 were still abundant enough without addition of FK506. DDFKBP-V5-ETP7 signal was too low during IFA (data not shown) but was still visible by Western blot. The expected size was bigger than V5-ETP7 at 74.1 kDa but instead, a signal was found at the same height at 62.3 kDa. Since depletion of FK506 did not decrease levels of ETP2 and ETP7, the degradation system based on DDFKBP was not compatible with both tested ETPs.

2.9.2 DiCre recombinase

As conditional protein degradation seemed to be difficult for ETP2 and ETP7, another conditional system was tested. This time it was based on the dimerizable Cre recombinase (DiCre), which excises a target GOI flanked by two identical 34 bp long sequences called loxP. The Cre recombinase was split into two moieties, each fused to either FKBP or FRB, which upon induction with rapamycin dimerize and reconstitute the Cre recombinase (Figure 2.18 A) (Jullien *et al.*, 2003; Andenmatten *et al.*, 2013; Collins *et al.*, 2013). This system has previously been adapted to *Leishmania mexicana* (Duncan *et al.*, 2016), to delete cyclin dependent kinase 3 (CDK3), which is crucial for completion of the cell cycle. Establishment of the DiCre system in *A. deanei* proved to be difficult as influx of FK506 and rapamycin is probably very slow. Experiments on *A. deanei* cultures required very high concentrations of the ligands to obtain any effect at all when compared to *L. major* (*L. major* 1 µM vs *A. deanei* 200 µM) (Damerow *et al.*, 2015; Wolters, 2019). Since excision of the gene should be a single event per cell, it was believed that extended incubation time and selection of clones in the presence of the ligand should allow to circumvent these limitations. In the case of essential genes, excision would be lethal, preventing attempts to generate clonal strains, by collapse of the culture during initial incubation with the ligand or during limiting dilution. As previous attempts to generate homozygous knockouts of ETP7 have failed (see section 2.8), it was expected that upon incubation with the ligand the growth rate of the induced cultures would decrease. $1x10^5$ cells of Adea311 + pAdea270 C1 and C2 (Figure 2.18 B, C) were transferred into fresh media containing 2% DMSO (final concentration of the solvent of FK506 and rapamycin in the culture), 200 µM FK506 or 200 µM rapamycin. After 48 h of incubation cell numbers in the cultures were measured again and limiting dilutions of all conditions were performed to observe if the number of viable cells in the rapamycin treated culture was decreased, which would indirectly hint that the applied strategy does impair growth (4.4.4). Clones in both conditions grew comparable, ranging from $9x10^6$ to $2.4x10^7$ cells/ml, which contradicted expectations as rapamycin treated cells should be inhibited in growth if loss of the single copy of ETP7 was lethal. gDNA of the generated clones, which recovered in the typical 5-7 days was extracted and tested if excision in the rapamycin treated cultures took place (Figure 2.18 D), as compared to the FK506 clones where dimerization should not have been possible since FK506 binds exclusively to FKBP but not to FRB (Jullien *et al.*, 2003). PCR produced the 4090 Bp long fragment of *eGfp-Etp7* flanked by loxP sites in the endogenous locus of *Etp7* in all clones with no difference between FK506 and rapamycin treatment. No excision events or growth impairments could be observed even when *A. deanei* cells were distributed throughout 96 well plates at a theoretical distribution of 1 cell per 5 wells, still cultures recovered within average recovery times of 7 days. The DiCre system did not work in this setup.

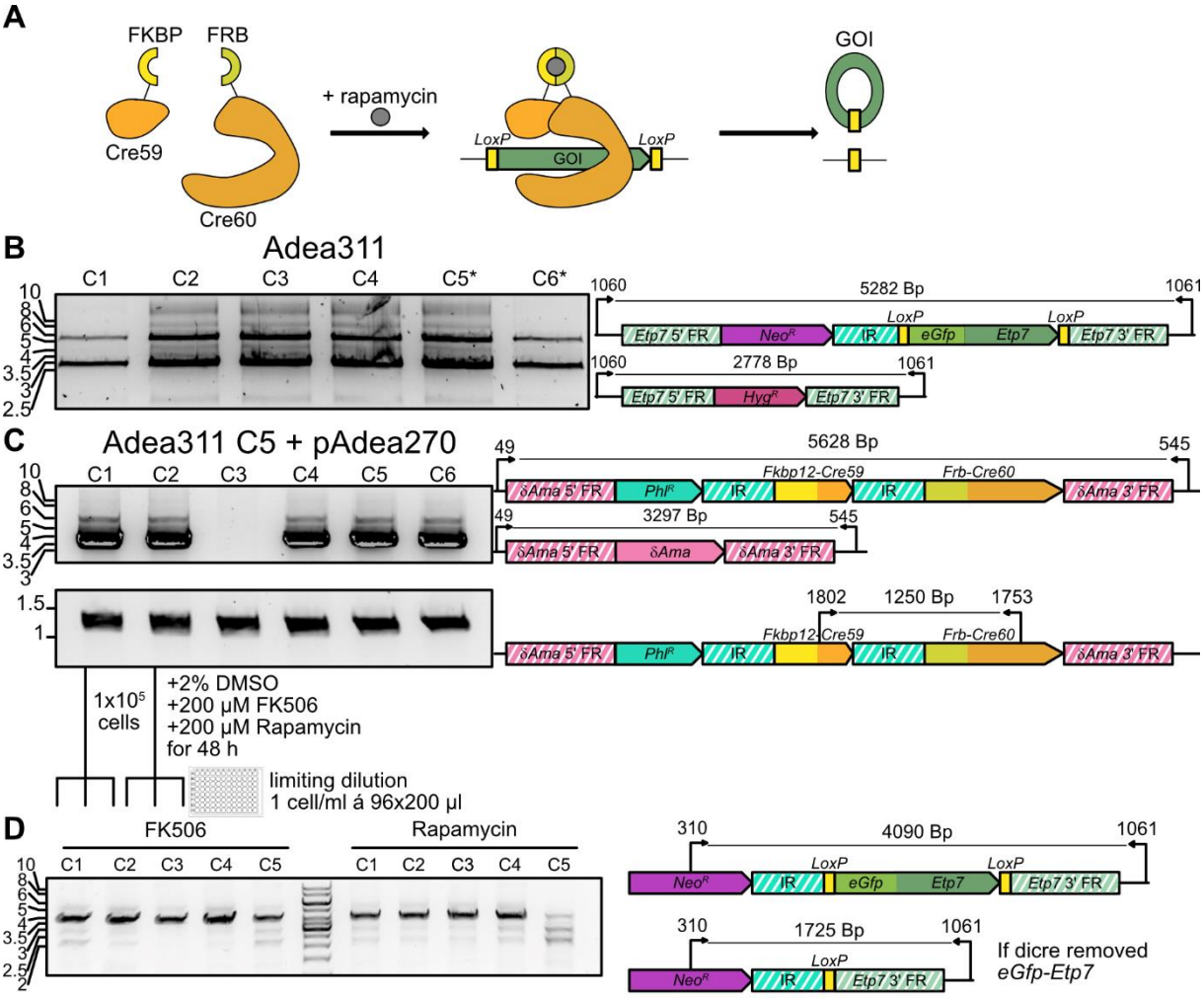

Figure 2.18 (A) Principle of DiCre system dimerization and GOI excision adapted from (Jullien *et al.*, 2003)**. (B) Generation of a floxed *eGfp-Etp7* strain (Adea311) and (C) Transfection with DiCre elements (pAdea270). (D) Incubation with dimerization inducer and limiting dilution.** (**A**) Inactive subunits of Cre are fused to FKBP and FRB. Addition of rapamycin leads to dimerization, activating the Cre recombinase, which binds to loxP-sites and loops out the GOI via recombination. (**B**) Heterozygous knock-out of *Etp7* Adea102 (*Etp7/Hyg*^{R}) was transfected with a linearized cassette containing floxed *eGfp-Etp7* to generate Adea311. PCR with primer 1060 and 1061 leads to two products, representing each of the two alleles. 2778 Bp for the *Hyg*^{R} insertion of the parental strain Adea102 and 5282 Bp for the cassette containing the floxed *eGfp-Etp7*. Sequencing of the inserted cassette revealed that only in C5* and C6* not only the upstream but also the downstream loxP site inserted. In the remaining clones (C1-C4) the downstream loxP site was missing. (**C**) PCR verification of clones after transfection of Adea311 C5 with the linearized cassette of pAdea270, containing the DiCre elements. Primer 49 + 545 verified insertion into the δ–Ama locus. 5628 Bp product corresponds to the transfected cassette. 3297 Bp product corresponds to the WT δ–Ama allele. As the band 5628 Bp product was relatively little a second PCR using primer 1802 and 1753, binding in Cre59 and Cre60, was performed to ensure availability of DiCre elements in the strain. 1x10^5 cells from a mid-log culture of Adea311 + pAdea270 C1 and C2 were incubated with 2 % DMSO, 200 µM FK506 and 200 µM rapamycin for 48 h before limiting dilution of all 6 conditions were performed. 2 % DMSO, 200 µM FK506 and 200 µM rapamycin was also added to each LD. (**D**) PCR of generated clones to test if excision of floxed *eGfp-Etp7* has occurred. All tested clones still produced full length products of 4090 Bp. Successfully excised *eGfp-Etp7* should produce a band of 1725 Bp, which was not visible in any of the tested clones. All marker in kBp.

2.9.3 TetR system

One of the first described conditional systems in trypanosomatids is based on the tetracycline binding repressor (TetR) and TetR binding operator (TetO) (Wirtz and Clayton, 1995). TetR binds to TetO and inhibits transcription of downstream genes. By heterologous expression of T7 polymerase and the addition of a T7 promotor in front of TetO an inducible system with high expression levels was developed in *Leishmania tarentolae* (Kushnir *et al.*, 2005) which is commercially available from Jena Bioscience. As tetracycline (TC) is an antibiotic effective against gram-negative and gram-positive bacteria application in *A. deanei* would inhibit its bacterial ES. Anhydrotetracycline (ATC) is a derivative of tetracycline, however, it has much lower antimicrobial activity and binds to TetR with a higher affinity (Oliva *et al.*, 1992; Gossen and Bujard, 1993). Incubation of *A. deanei* WT cells with 10 µg/ml ATC had no noticeable effect on the division rate of the culture (data not shown), which is the recommended concentration of TC for *L. tarentolae* (Kushnir *et al.*, 2005). Due to the higher binding affinity of ATC to TetR even lower concentrations of ATC should be enough for induction in *A. deanei*. A strain expressing TetR, and the T7 polymerase was generated (Figure 2.19).

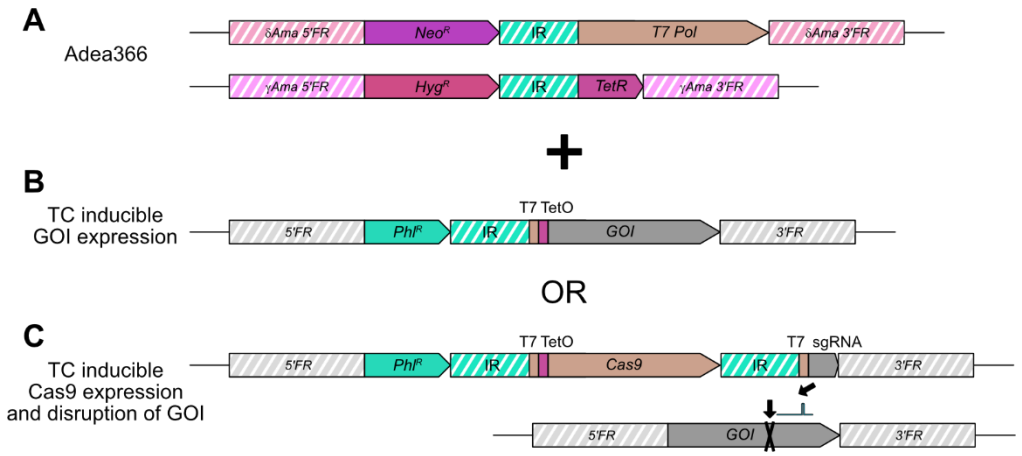

Figure 2.19 (A) Generation of Adea366, a strain for ATC-inducible protein expression (B) or Cas9-mediated gene disruption upon induction with ATC. (**A**) Adea366 expresses the T7 polymerase from δ–Ama and tetR from γ–Ama. (**B**) Upon transfection with a GOI lead by a T7P and TetO binding site, the GOI is only expressed during incubation with ATC if inserted into a silent locus. (**C**) Alternatively, the strain can be used to generate an irreversible disruption of the GOI if a cassette containing Cas9 lead by T7P and TetO binding site and the target sgRNA sequence for T7 polymerase driven expression. Induction with ATC would lead to the production of Cas9, which would bind to the sgRNA and create DNA double strand breaks at the target site of the sgRNA.

This strain is the basis for either protein overexpression in *A. deanei* (Figure 2.19 B), and conditional protein expression studies, as a heterozygous knock out expressing only one copy of an essential gene under control of the T7P and TetO. Transfer of the cell line from ATC containing medium to ATC-free medium should induce a homozygous knock-out-like state.

An alternative approach would be to express Cas9 under the control of T7P and TetO as well as one or several sgRNA templates. Induction with ATC would lead in this case to double strand breaks, which would be repaired by non-homologous end joining, which is often deleterious and targeting crucial sites may lead to inactive or unstable proteins due to a loss of sequence information. Targeting a GOI with several sgRNAs will lead to severe information loss in the ORF, effectively destroying the GOI upon induction.

2.10 Identification of ETP2 in *Strigomonas culicis*

As described in 2.1, no sequence homologues were found by BLAST analysis for ETP2 and ETP7. This may be partially also due to limited sequence information from other Strigomonadinae, as only *A. deanei*'s genome has been thoroughly sequenced and assembled to date (Davey *et al.*, 2021). Two whole genome sequencing analyses exist for *S. culicis* (João M P Alves *et al.*, 2013; Motta *et al.*, 2013), another family in the group of Strigomonadinae, but BLAST analysis is only able to identify the conserved ETP5 and ETP9 in these datasets.

Comparison of the ORFs upstream and downstream of *A. deanei Etp2* (*Ad*Etp2) to the *S. culicis* genome allowed for the localization of an ORF at the *S. culicis Etp2* equivalent locus. Alignment of this *StcEtp2* ORF to the *AdEtp2* ORF shows a pairwise identity of only 42.35% which translates into pairwise identity of just 20.07% on aa level. Observation of the protein sequences allowed for the identification of a long proline rich N-terminal domain, which contained three asparagine rich stretches in the case of *Ad*ETP2 and three glutamine rich stretches in *Stc*ETP2 (Figure 2.20 B). The C-termini of both proteins contain very little proline compared to the N-terminus and seem to be structured. Structure prediction by Alphafold (Jumper *et al.*, 2021) confirmed these observations (Figure 2.21).

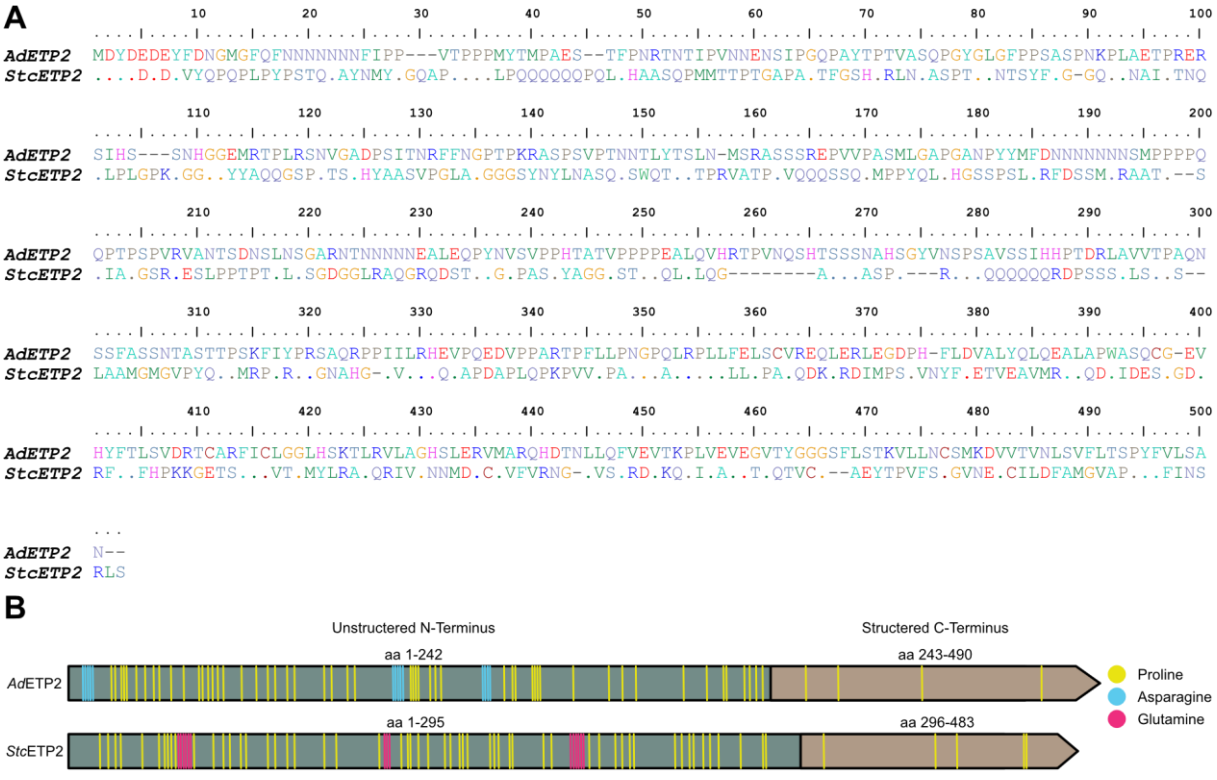

Figure 2.20 Alignment of AdETP2 vs StcETP2. (**A**) Pairwise alignment by clustal omega. Dots mark identical aa. (**B**) Schematic overview of *Ad*ETP2 and *Stc*ETP2. Green rectangle: unstructured N-terminus of ETP2, brown arrow: structured C-terminus of ETP2. Proline (yellow) asparagine (blue) and glutamine (red) have been highlighted.

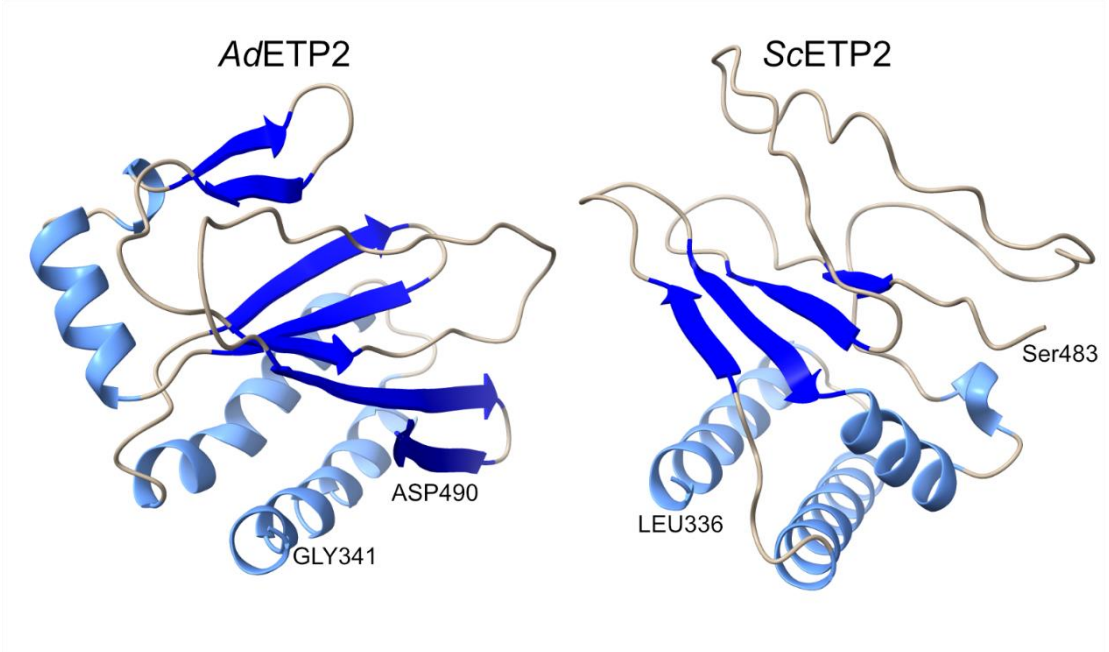

Figure 2.21 *Ad*ETP2 vs *Stc*ETP2 C-terminus shows a similar but mirrored orientation of α–helices and β–sheets. Alphafold prediction of *Ad*ETP2 and *Stc*ETP2. Only the structured C-terminus is displayed here. Unstructured aa: brown string, β–sheet: dark blue planes, α–helix: light blue helices. First and last displayed aa have been labeled by three letter code and aa position number based on the full-length protein sequence.

Despite the low amino acid sequence conservation between the two proteins, both ETP2s are similar in their predicted protein structures as both begin with two α–helices followed by two β–sheets and again leading into two shorter α–helices, ending with five more β–sheets for *Ad*ETP2 and just two more for *Stc*ETP2. These structures are mirrored in the prediction and do not produce any significant hit when compared to the PDB archive via PDBeFold (https://www.ebi.ac.uk/msd-srv/ssm/). Phyre2 prediction also failed to identify any high confidence hits for both full length sequences as well as only the C-terminal domain.

To test if the identified locus in *S. culicis* is in fact the *AdEtp2* equivalent, *StcEtp2* was amplified from *S. culicis* gDNA and cloned into pAdea043, the N-terminal eGFP-tagging vector for heterologous expression in *A. deanei*. This cassette was transfected into *A. deanei* WT cells (Adea216), and one clone of Adea216 had been transfected with a cassette for production of mSCARLET-ETP1 to label the ES (Adea217). *mScarlet-AdEtp2* was also transfected into Adea216 to assess if *Ad*ETP2 and *Stc*ETP2 do colocalize (Adea218) (Figure 2.22). During several microscopy sessions it was noticed that fluorescence intensity of eGFP-*Stc*ETP2 did fluctuate strongly between not being visible at all, to levels similar to mSCARLET-*Ad*ETP2. This observation could be linked to the cell density of the culture, as cultures in early to mid-log phase at 10^5-10^7 cells/ml showed no or mild fluorescence, often diffuse inside the host cell. Cultures in late-log to stationary phase (visible by a pellet at the bottom of the growth flask) showed strong fluorescence of eGFP-*Stc*ETP2 similar in intensity and distribution to mSCARLET-*Ad*ETP2.

The colocalization indicates strongly that *Stc*ETP2 is in fact *S. culicis* counterpart to *Ad*ETP2 even with low homology in the aa sequence and what seems to be a mirrored C-terminal protein structure based on Alphafold prediction. With this result the question arose if *Stc*ETP2 can complement *Ad*ETP2 in a heterozygous deletion background of *Ad*ETP2 (Adea272). To test this hypothesis *StcEtp2* replaced *AdEtp2* in pAdea115, to produce eGFP-*Stc*ETP2 from the endogenous locus of *AdEtp2*. Transfection into *A. deanei* WT cells was successful and clones could be obtained but exchange of the second *Etp2* allele with *Hyg*^{R} (following transfection of Adea272 with the *Etp2* locus-targeted Hyg^R cassette) could not be achieved (data not shown).

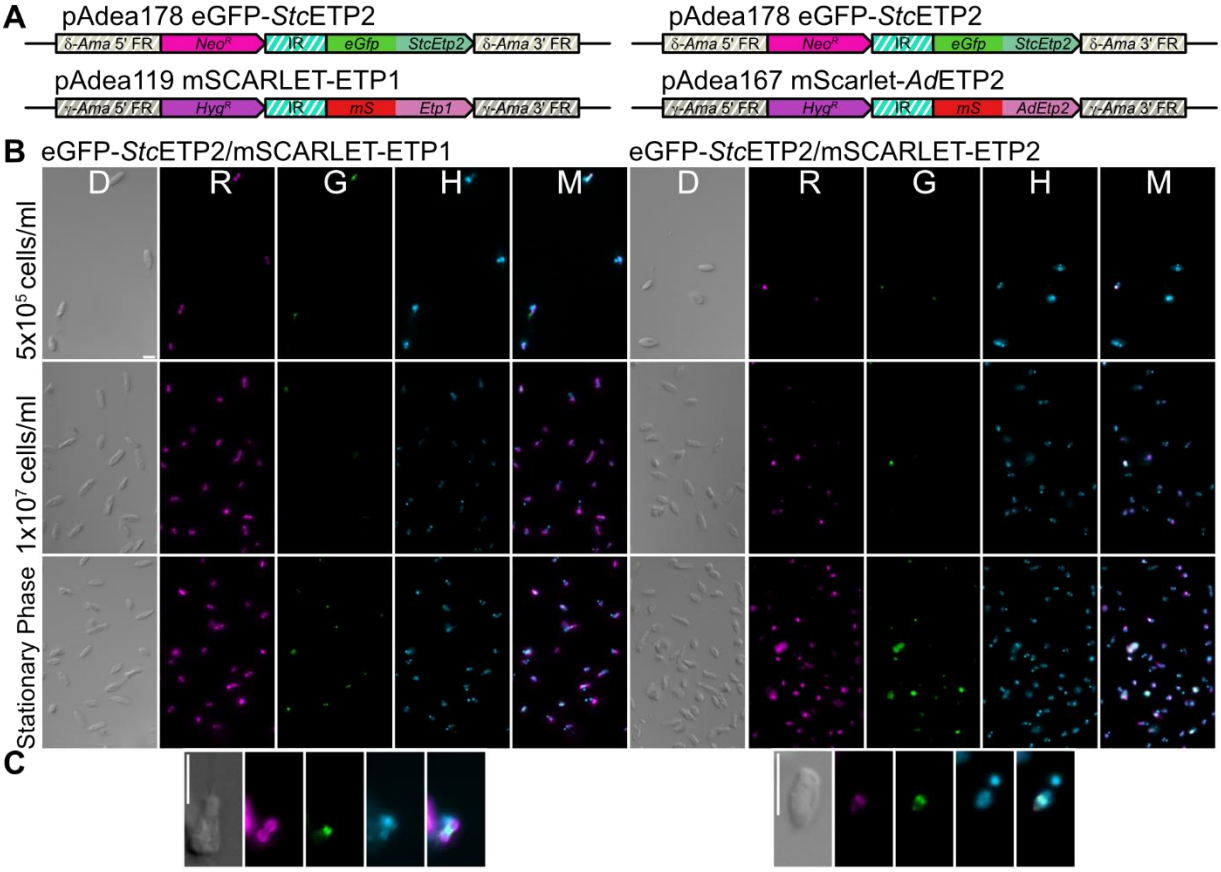

Figure 2.22 eGFP-*Stc*ETP2 fluorescence depends on the stage of the culture and does colocalize with mSCARLET-*Ad*ETP2. Epi-fluorescence microscopy of cell lines expressing eGFP-*Stc*ETP2 and mSCARLET-ETP1 or mSCARLET-*Ad*ETP2. (**A**) Schematic overview of transfected cassettes in the analyzed cell lines. (**B**) Microscopy of cultures throughout advancing culture age, indicated by rising *A. deanei* cell density. (**C**) Zoom-in on one cell to highlight the localization of eGFP-*Stc*ETP2 at the constriction site of the ES (left) and the colocalization with mSCARLET-*Ad*ETP2 (right). D: Differential interference contrast; R: red channel, mSCARLET, G: green channel, eGFP; H: cyan channel Hoechst 33342, M: Merge. Scale bar 5 µm.

2.11 Truncation of *Ad*ETP2 and *Stc*ETP2 to identify the ES-targeting domain

The low sequence similarity but identical localization of ETP2 raised the question whether the unstructured N-terminus or the structured C-terminus allow shuttling of the protein to the ES. *Ad*ETP2 was split at aa 242 and *Stc*ETP2 was split at aa 295. The N-terminal domains were fused at the C-terminus and the C-terminal domains at the N-terminus to eGFP and transfected into *A. deanei* WT.

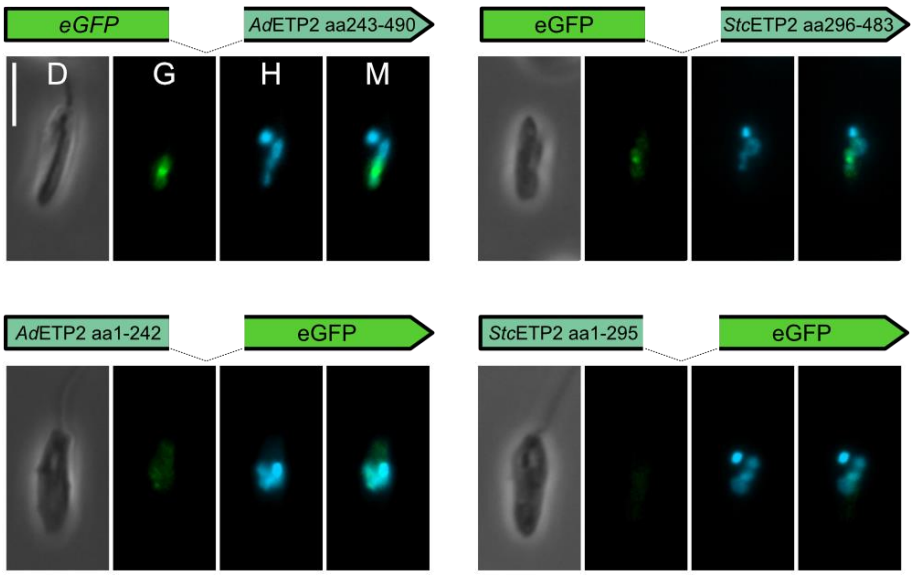

Figure 2.23 Epifluorescence of truncation constructs of *Ad*ETP2 and *Stc*ETP2 shows only the C-terminal domain is recruited to the ES. D: Differential interference contrast; G: green channel, eGFP; H: cyan channel, Hoechst 33342; M: Merge. Scale bar 5 µm.

Only late log cultures showed again fluorescence for the *Stc*ETP2 constructs (Figure 2.23). Fluorescence at the ES could only be observed for the C-terminal constructs of ETP2s, while very low, diffuse fluorescence throughout *A. deanei* was found for the N-terminal constructs, suggesting that the C-terminal domain shuttles to the ES independently of the N-terminal domain.

2.12 Phyre2 predicts a putative peptidoglycan hydrolyzing domain in ETP7

Due to the uniqueness of several ETPs to the Strigomonadinae no function from sequence similarity could be derived. Protein homology recognition by a web based secondary structure prediction (Kelley *et al.*, 2015) identified a high confidence hit based on $\phi 29$ phage tail lysozyme gp13 (Xiang *et al.*, 2008) for ETP7 aa358-518 with a confidence of 92.6. This domain contains specifically the invariable glutamic acid E45 in gp13, found to be essential for hydrolysis in hen egg lysozyme (E35) and T4 lysozyme (E11) (Atthews, 1999) which fits exactly with E369 of ETP7 (Figure 2.24). In the context of bacterial cell division in *A. deanei* some essential steps in PG restructuring are missing (see section 1.7), but due to sensitivity to β–lactam antibiotics a PG layer must exist (M. C. M. Motta *et al.*, 1997). The requirements of the division machinery of β–proteobacteria are poorly understood (Eswara and Ramamurthi, 2017)

but gaps in the division machinery of the ES that are compensated for by nucleus-encoded proteins may provide the host with control over the ES division.

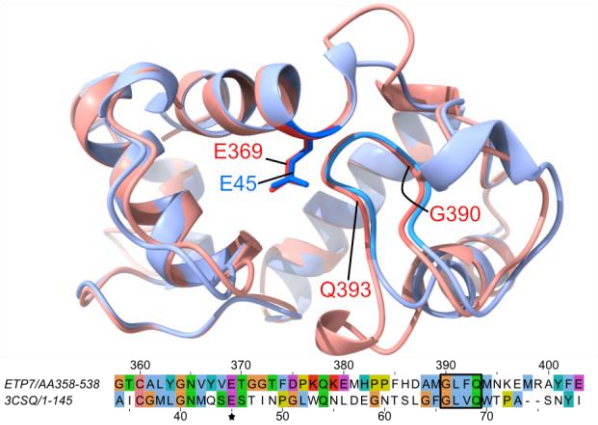

Figure 2.24 Superposition of the predicted structure of ETP7 aa 358-518 (red shades) and the gp13 NTD (PDB ID 3CSQ; blue shades). The predicted catalytically active glutamic acid (E369) and a conserved loop in proximity of the active site (G390-Q393) are highlighted. Amino acid conservation around E369 in the structure-based sequence alignment of ETP7 and gp13. E369 is marked by an asterisk, the conserved loop by a black box in the alignment.

To test this hypothesis PG-cleaving activity assays were to be performed with heterologously expressed ETP7.

2.13 Expression of ETP7 in *E. coli*

E. coli was chosen for heterologous expression of ETP7 due to ease and availability of the necessary strains and plasmids. From experience of endogenous expression of ETP7 in *A. deanei* a 6xHis-tag as well as a SUMO-tag (Butt *et al.*, 2005) for solubilization were cloned to the N-terminus of ETP7 and the C-terminus was left unaltered. Furthermore, a pelB-tag (Sockolosky and Szoka, 2013) for targeting of heterologous protein to the periplasm of *E. coli* was tested to test for PG-hydrolytic activity directly in *E. coli* (and to potentially increase the yield since ETP7 can be expected to localize in the periplasm of Ca. K. crithidii). *E. coli* BL21 (William Studier *et al.*, 1990)was chosen as expression strain and transformed with GPN131 for IPTG inducible expression of 6xHis-SUMO-ETP7 (Ec51) as well as GPN136, which contained an additional pelB-Tag at the N-terminus of the construct (pelB-6xHis-SUMO-ETP7, Ec52). Different temperatures, expression durations as well as media were tested to pin down optimal conditions (4.4.12). Induction at OD_{600} = 0.5 of the pelB-tagged construct with 1 mM IPTG and expression for 3 h at 28 °C yielded the highest protein amount (Figure 2.25 A, white arrowhead). Purification of 6xHis-SUMO-ETP7 was attempted via Immobilized metal affinity chromatography (IMAC) (Figure 2.25 B) but suffered from poor solubility of 6xHis-SUMO-ETP7 after ultracentrifugation at 120,000xg for 1 h at 4°C. Furthermore, 6xHis-SUMO-ETP7 elution showed

massive protein degradation in Western blot analysis. In Figure 2.25 B addition of 10% cOmplete proteinase inhibitor cocktail EDTA-free (Roche) and 0.05% BSA during all washing steps were attempted to reduce degradation.

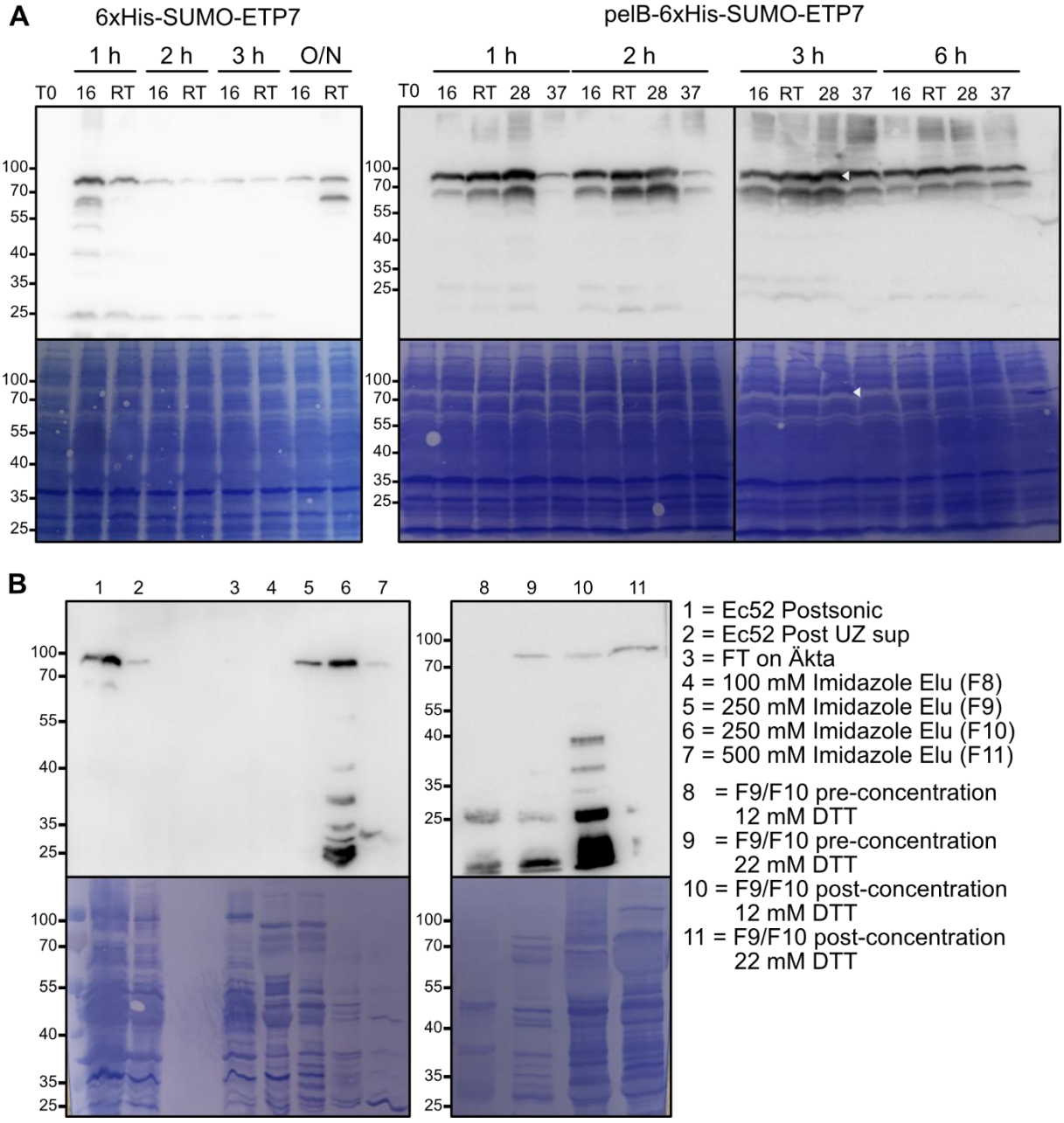

Figure 2.25 (A) Expression test of ETP7 constructs in BL21. α-His-HRP-antibody 1:5000 was used for detection of 6xHis-SUMO-ETP7 (74.4 kDa). T0 = sample before induction with 1 mM IPTG. Lane description in °C. Samples were taken each hour in the first three hours of induction, at 6 h and overnight (O/N). 1 ml of each culture was harvested, OD_{600} was measured and protein amount equivalent to OD_{600} = 0.5 were loaded on each lane. White arrowhead indicates condition deemed as optimal. **(B) Purification of 6xHis-SUMO-ETP7 by IMAC and concentration by Amicon 30 filter.** Cells were lysed by sonication (1), insoluble material was removed at 120,000xg 1 h 4°C and the supernatant (2) was injected into the Äkta pure system equipped with a 1 ml Histrap (GE healthcare). A sample of the unbound flow through (FT) was collected and 6xHis-SUMO-ETP7 eluted stepwise with 100-500 mM Imidazol (4-7). 250 mM elutions were pooled (8, 9) and concentrated via Amicon 30 (Millipore) from

8 ml to 500 µl (10, 11). Below each blot the staining of the PVDF membrane with CBB is shown. Marker in kDa.

Degradation was still high, but concentration via Amicon filter (cutoff 30 kDa) of 6xHis-SUMO-ETP7 still resulted in enough material to test for PG-hydrolyzing activity. Western blot analysis revealed that 6xHis-SUMO-ETP7 was degraded even further upon concentration attempts which resulted in a similar level of full length 6xHis-SUMO-ETP7 after 40x concentration compared to unconcentrated sample.

To test if protein degradation may be avoided by addition of protease inhibitors TLCK, E64, PMSF and cOmplete proteinase inhibitor cocktail EDTA-free in 1x and 0.1x concentration was tested over 24 h (Figure 2.26) at 4°C.

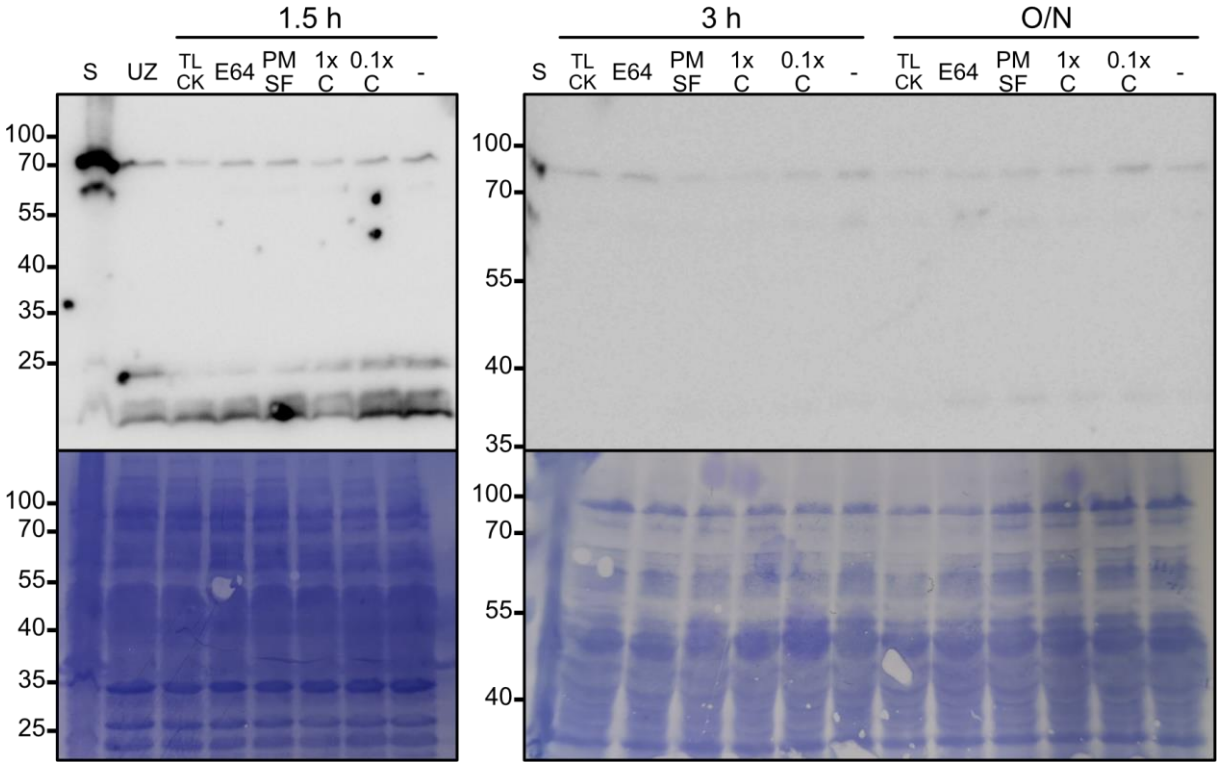

Figure 2.26 Comparison of different protease inhibitors against 6xHis-SUMO-ETP7 degradation. 6xHis-SUMO-ETP7 expressing cells were lysed by sonication (S) and the soluble proteins harvested by ultracentrifugation as before. To 1 ml of soluble proteins were 100 µM TLCK, 10 µM E64, 1 mM PMSF or cOmplete PI inhibitor cocktail in 1x or 0.1x concentration added (C). One was not treated with any PIs (-). 50 µl were taken at 1.5 h, 3 h and overnight (O/N) and mixed with sample buffer, heated for 5 min at 95°C and frozen until further analysis. α–His-HRP AB 1:5000, marker in kDa. Expected size of 6xHis-SUMO-ETP7: 74.4 kDa.

Irrespective of the added PI, degradation did not increase or decrease over the course of the experiment. 6xHis-SUMO-ETP7 is stable even overnight without addition of PIs, meaning degradation during the purification and concentration is not occurring due to exhaustion of PI and activity of proteases but possibly by autohydrolysis of ETP7 when the local concentration of ETP7 reached a certain level. As very little 6xHis-SUMO-ETP7 was soluble when expressed in BL21, more *E. coli* strains were tested to analyze if overall yield could still be improved. The *E. coli* strains C41(DE3) and C43(DE3)

(Miroux and Walker, 1996)were transformed with 6xHis-SUMO-ETP7 (C41, Ec58; C43, Ec60) and pelB-6xHis-SUMO-ETP7 (C41, Ec59; C43, Ec61) expression plasmids. Expression tests showed optimal conditions to be the same at 28°C 3 h in LB-Amp medium (Figure 2.27 A) for Ec58. In general, the C41 strains expressed more of the ETP7 constructs than the C43 strains, which were excluded from further analysis. The constructs lacking the pelB-tag were also more abundant in C41 compared to the previous results in BL21. Solubility of the ETP7 constructs expressed in BL21 and C41 were compared through differential centrifugation and solubilization with 0.1% of Na-deoxycholate (4.4.13) (Figure 2.27 B). Solubility of 6xHis-SUMO-ETP7 was still less than 50 % of the total protein amount produced independently of the chosen strain.

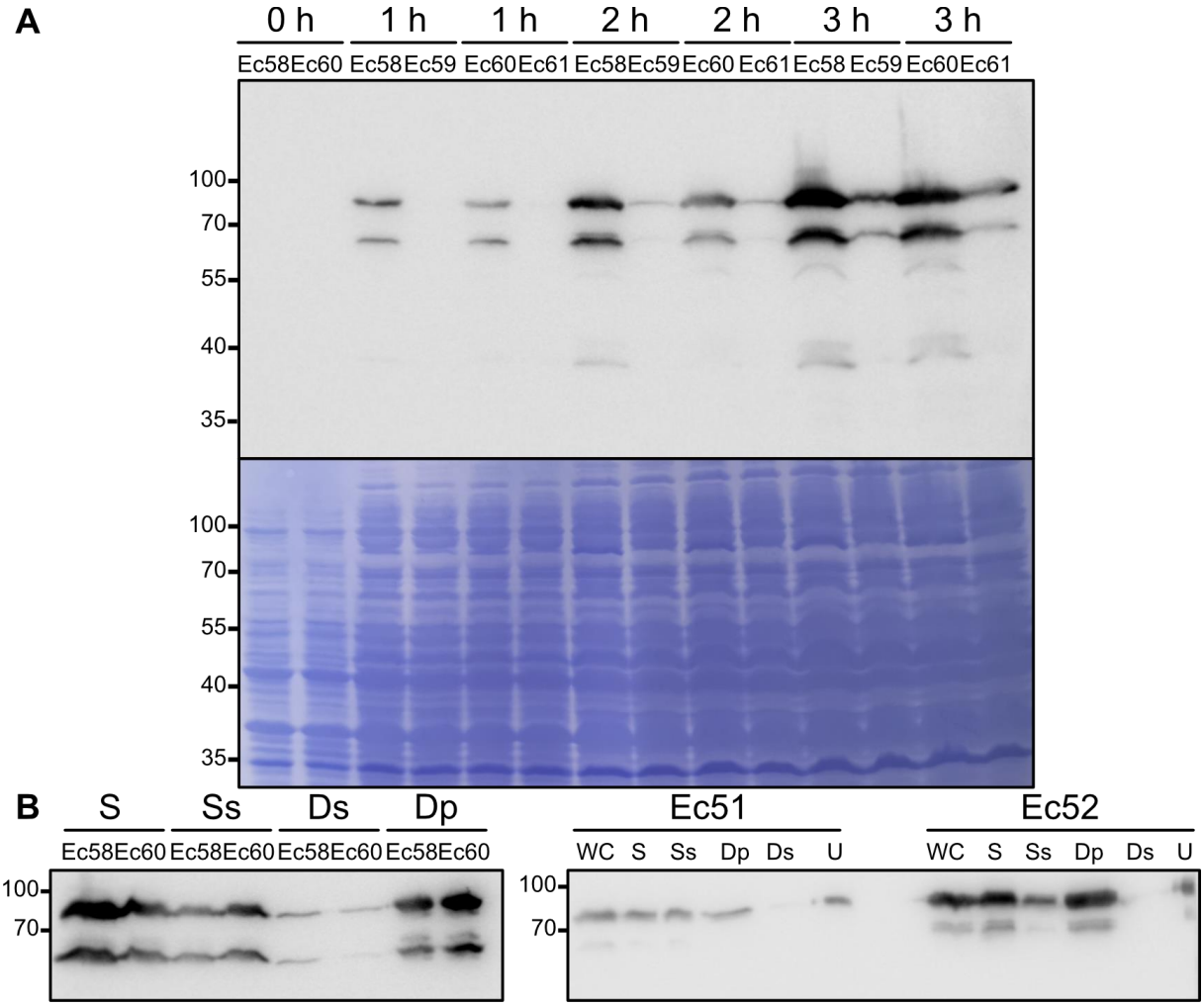

Figure 2.27 (A) Expression test of the C41 and C43 strains and (B) solubility test. Western blot of C41 and C43 strains expressing 6xHis-SUMO-ETP7 (C41, Ec58; C43, Ec60) or pelB-6xHis-SUMO-ETP7 C41, Ec59; C43, Ec61). Samples were taken every hour and used for Western blot analysis. CBB-stained membrane below (**B**) Intact cells (WC) were sonicated (S) and centrifuged at 12,000xg which resulted in the supernatant containing soluble proteins (Ss) and a pellet consisting of whole cells and insoluble material. This pellet was treated with Na-deoxycholate to solubilize membrane attached proteins (Ds) after another centrifugation. Still insoluble material (Dp) was resuspended in 8 M urea (U) and applied to the analysis of Ec51 and Ec52. α–His-HRP AB 1:5000, marker in kDa. Expected size of 6xHis-SUMO-ETP7: 74.4 kDa.

Several buffer conditions were tested as pH and detergents have a major influence on the solubility of the expressed protein. Buffers in a range between pH 5 and 8 were chosen. As the isoelectric point of ETP7 is 7.01, pH 7 was excluded since proteins are the least soluble at a pH corresponding to the isoelectric point of the protein. Ec58 was treated according to (4.4.14) and Western blot analysis was performed (Figure 2.28).

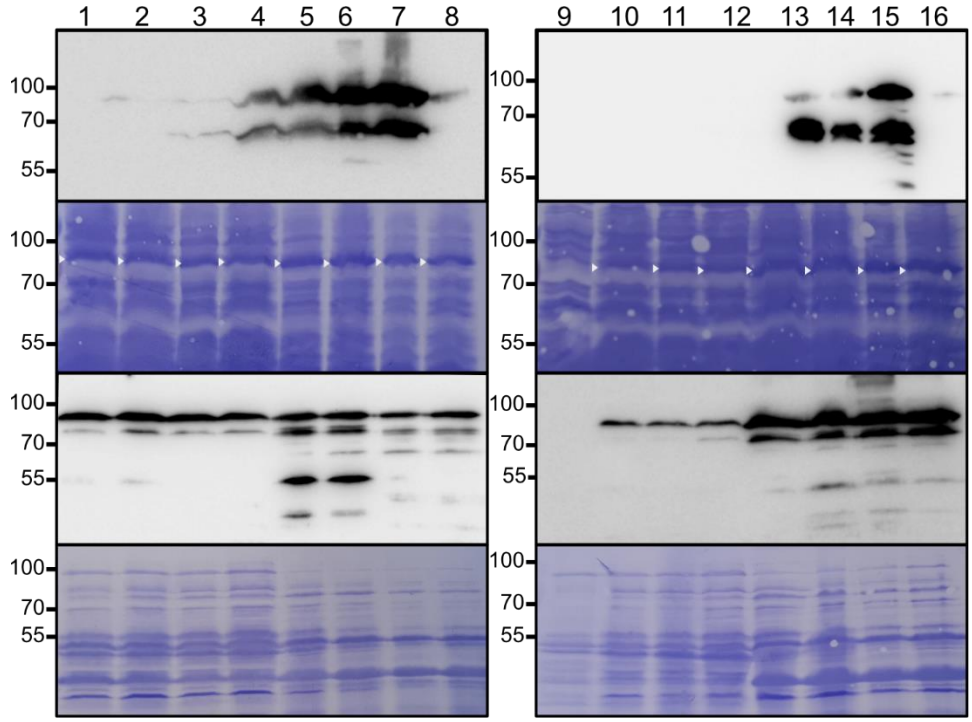

Figure 2.28 Influence of buffer and pH on the solubility of 6xHis-SUMO-ETP7. Upper row: 15 µl of samples were mixed with sample buffer and boiled for 5 min and run on a 12 % SDS-acrylamide gel and blotted on a PVDF membrane. White triangles highlight 6xHis-SUMO-ETP7 in CBB-stained membranes. Lower row: 2 µl of sample mixed with 8 M urea to a final concentration of 6.4 M before addition of sample buffer and boiling for 5 min. Samples 1 – 8 were collected after 12,000xg centrifugation. 1: pH 5 supernatant, 2: pH 5.5 supernatant, 3: pH 6.5 supernatant, 4: pH 8 supernatant, 5: pH 5 pellet, 6: pH 5.5 pellet, 7: pH 6.5 pellet, 8: pH 8 pellet. Samples 9 – 16 were collected after 120,000xg centrifugation. 9: pH 5 supernatant, 10: pH 5.5 supernatant, 11: pH 6.5 supernatant, 12: pH 8 supernatant, 13: pH 5 pellet, 14: pH 5.5 pellet, 15: pH 6.5 pellet, 16: pH 8 pellet. The pellets were resuspended in the same buffer and volume as the supernatant. α–His-HRP AB 1:5000, marker in kDa. Expected size of 6xHis-SUMO-ETP7: 74.4 kDa. CBB-stained PVDF membrane below each blot.

6xHis-SUMO-ETP7 is partly soluble at pH 5.5, 6.5 and 8 but pH 5 seemed to drastically decrease solubility, since after ultracentrifugation at 120,000xg signal corresponding to 6xHis-SUMO-ETP7 could not be observed (Figure 2.28, lane 9). Also, no band corresponding to 6xHis-SUMO-ETP7 was visible on the CBB stained membrane. A change of pH to increase solubility was deemed ineffective and the current buffer of 82.5 mM Tris-HCl pH 8.0 buffer was used for all further experiments. During this test it was noticed that detection of 6xHis-SUMO-ETP7 outside of whole cell *E. coli* lysate is highly influenced by the addition of urea. Without urea, 6xHis-SUMO-ETP7 can be only detected at very high

concentrations in Western blot, visible by eye on the CBB-stained membrane (Figure 2.28, white triangles).

As partial solubility would eventually be sufficient to conduct functionality assays with ETP7, this time column-based IMAC using Ni-NTA resin was tested (Figure 2.29) to purify ETP7.

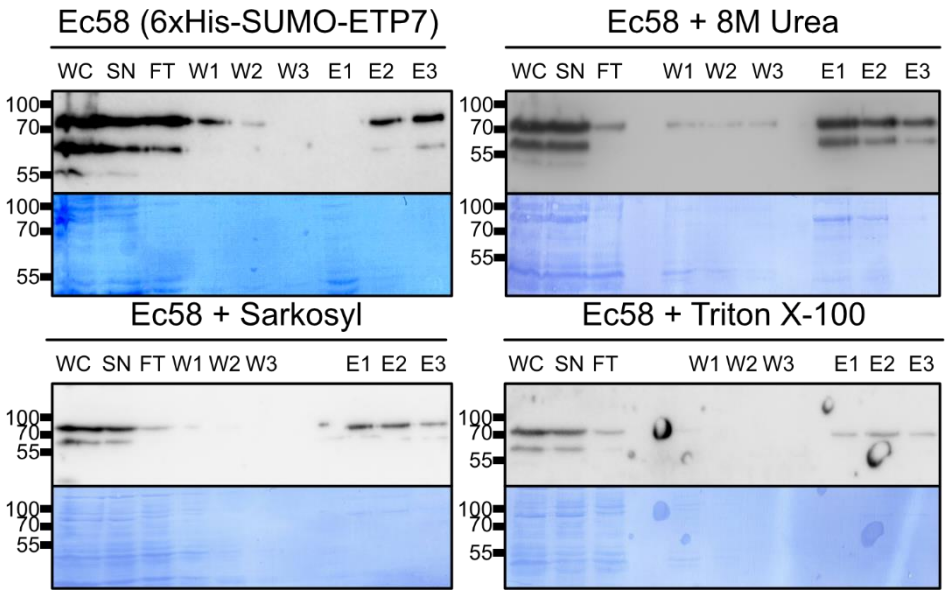

Figure 2.29 Column IMAC of 6xHis-SUMO-ETP7 treated with different detergents. Addition of 8 M urea, Sarkosyl or Triton X-100 in 1:1 protein:detergent mass ratio. All detergents were added after sonication. WC: whole cells; SN: sonicated; FT: flow through; W1-W3: wash step; E1-E3: elution steps with 50, 100 and 250 mM imidazole. α–His-HRP AB 1:5000, marker in kDa. Expected size of 6xHis-SUMO-ETP7: 74.4 kDa. CBB stained PVDF membranes are shown below each blot.

Without any additional detergents a major fraction of 6xHis-SUMO-ETP7 was left unbound and in the elution no band corresponding to 6xHis-SUMO-ETP7 could be observed on the CBB-stained membrane. Addition of 8 M urea improved binding and elution drastically but would also most likely affect the conformation of the protein as high levels of chaotropic agents tend to denature proteins.

Titration of anionic Sarkosyl and nonionic Triton X-100 in a 1:1 protein to detergent ratio were able to improve binding and elution similarly, which made Triton X-100 the preferred choice as nonionic detergents do not interfere with protein conformation, especially at very low concentrations. Testing of higher concentrations of Triton-X 100 did not improve solubility (data no shown) but for the sake of consistency and ease of preparation 0.1% (v/v) was set as standard concentration for future protein purification attempts.

Partial insolubility indicates suboptimal conditions which may affect the activity of the protein. Improving the solubility was further tested with a combination of Triton X-100 with NaCl, CHAPS and low concentrations of urea. Cells expressing 6xHis-SUMO-ETP7 were resuspended in buffer containing 82.5 mM Tris-HCl pH 8.0 and 300 mM NaCl with or without 0.1% Triton X-100 (Figure 2.30) and purified

by Ni-NTA. After purification, 2 ml of E2, which yielded the highest protein concentration according to Pierce 660 nm assay (4.5.3), was split into three 600 µl aliquots and detergents/chaotropic agents were added to the final concentrations described in Figure 2.30. All samples were then centrifuged at 120,000xg for 1 h at 4°C. The supernatant was collected, and the pellets resuspended in 600 µl of 82.5 mM Tris-HCl, pH 8.0. Apparently, addition of 300 mM NaCl drastically affected protein stability as now E2 shows massive protein degradation not observed previously during IMAC in batch protocol (Figure 2.29). Addition of CHAPS or 2 M urea did not improve solubility of 6xHis-SUMO-ETP7 any further.

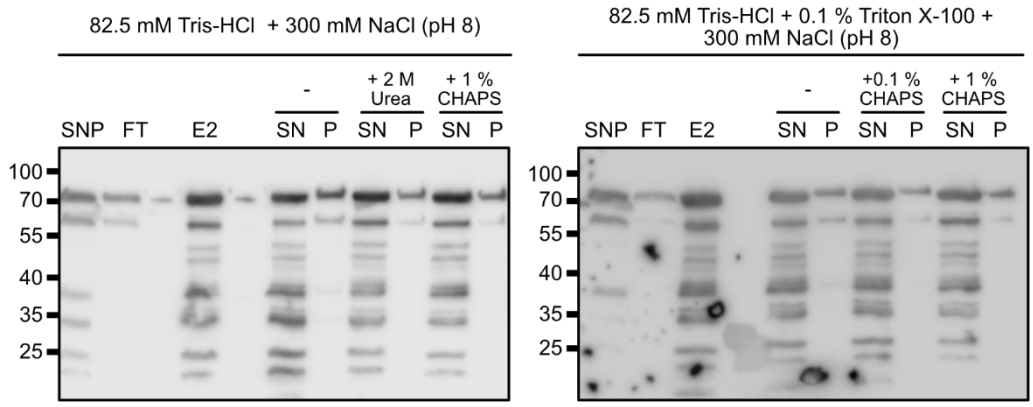

Figure 2.30 Effect of 300 mM NaCl, CHAPS and urea on the solubility of 6xHis-SUMO-ETP7. 6xHis-SUMO-ETP7 was isolated in 82.5 mM Tris-HCl + 300 mM NaCl pH 8.0 (left blot) and with the same buffer but additional 0.1% Triton X-100 (right blot). After elution, E2 was split into three reactions of 600 µl each and either 2 M Urea, or 0.1% or 1% CHAPS were added additionally before ultracentrifugation. One sample each was left untreated (-) before centrifugation. SNP: supernatant loaded on Ni-NTA, FT: flow through of unbound proteins after incubation with Ni-NTA, E2: 100 mM imidazole elution 2 of the Ni-NTA, previously seen to have the highest concentration of 6xHis-SUMO-ETP7, SN: supernatant after 120,000xg centrifugation, P: pellet after 120,000xg centrifugation. Marker in kDa. Expected size for 6xHis-SUMO-ETP7: 74.4 kDa.

2.13.1 Verification of pelB-mediated shuttling to the periplasm of *E. coli*

Expression of a PG-hydrolyzing enzyme may lead to impaired growth or lysis of *E. coli* cells during induction with IPTG, especially when targeted to the periplasm where the PG layer in gram negative bacteria is located. No reduction of the OD_{600} was observed in previous overexpression experiments of pelB-6xHis-SUMO-ETP7 independently of the *E. coli* strain used. This raised the question if the fusion protein may not reach the periplasm due to formation of inclusion bodies.

1 L of *E. coli* C41(DE3) expressing pelB-6xHis-SUMO-ETP7 was raised (4.4.12) and the periplasmic proteins released as described in (Quan *et al.*, 2013). Furthermore, *E. coli* membranes were isolated as described in 4.4.15 and separated by a linear sucrose gradient.

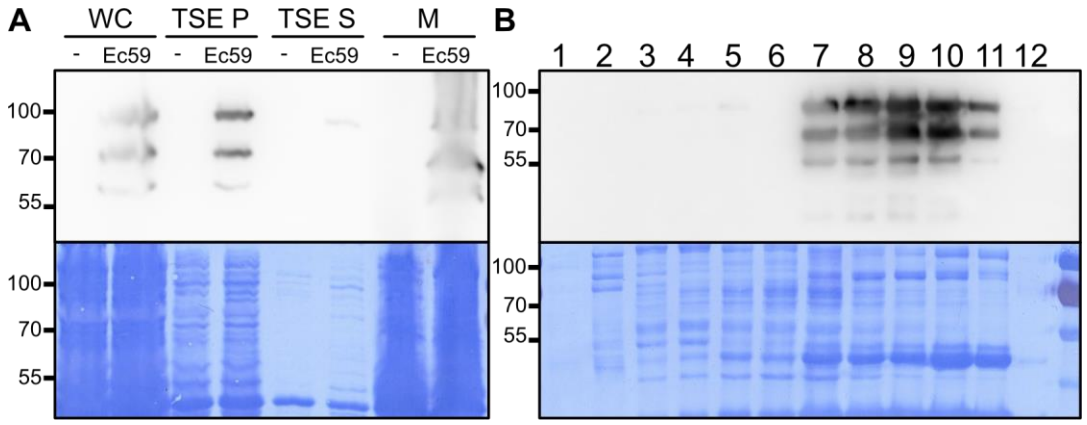

Figure 2.31 (A) Release of periplasmic proteins and (B) fractionation of *E. coli* membranes by linear sucrose gradient. (**A**) *E. coli* whole cells (WC) were treated with TSE buffer and insoluble material pelleted (TSE P) by centrifugation. This released periplasmic proteins into the supernatant (TSE S). Remaining cell material was lysed via cell disruptor and the membranes isolated (M). (**B**) A linear sucrose gradient was fractionated into 1 ml fractions (1-12) and protein precipitated using TCA. Half of the total precipitate was loaded onto the SDS-PAGE. 1-3: membrane associated proteins, 4-5 ribosomes. 6-8 inner membrane (main part in fraction 7), 9-10 outer membrane, 11 outer membrane mixed with inclusion bodies, 12 insoluble material and inclusion bodies. -: C41(DE3) cells containing an empty expression vector as a negative control. Ec59: C41(DE3) cell line expressing pelB-6xHis-SUMO-ETP7. α–His-HRP AB 1:5000, marker in kDa. Expected size of 6xHis-SUMO-ETP7: 74.4 kDa. CBB stained membrane below the respective blot.

6xHis-SUMO-ETP7 does reach the periplasm as some signal can be observed at TSE S (supernatant of TSE treated sample) in Ec59 (Figure 2.31 A) but still most of the 6xHis-SUMO-ETP7 is found in the membrane fraction of Ec59 cells. Separation of membrane fractions by linear sucrose gradient identifies the majority of 6xHis-SUMO-ETP7 in fraction 7-11 corresponding to the inner and outer membrane of *E. coli*. 6xHis-SUMO-ETP7 is indeed targeted to the periplasm of *E. coli* by addition of a pelB-tag but it is mainly found in association with the membranes and not as a soluble protein. The lack of 6xHis-SUMO-ETP7 in fraction 12 indicates no formation of inclusion bodies, which would not be desired anyway as proteins trapped in inclusion bodies are often misfolded and non-functional without further renaturation steps.

2.13.2 Identification of penicillin binding proteins by Bocillin FL staining of *E. coli* lysate

The ES of *A. deanei* lacks components of the divisome (Motta *et al.*, 2013) previously described as essential in other gram negative bacteria (see Figure 1.3). Some of those proteins belong to the group of penicillin binding proteins (PBPs). These are essential for modifications of the PG layer of bacteria during division. β–lactam antibiotics, such as penicillin which gave this class of proteins their name, are binding PBPs and inhibit bacterial growth by rendering the bacterium unable to remodel its PG layer.

Bocillin FL, a fluorescent derivative of penicillin V (Zhao *et al.*, 1999), allows for detection of PBPs. Due to the irreversible binding of Bocillin FL to PBPs, PBPs can then be separated via SDS-PAGE following

their incubation with Bocillin FL, and fluorescence detected inside the gel upon excitation. 6xHis-SUMO-ETP7 constructs were expressed in *E. coli* C41(DE3) for 3 h at 28°C induced with 1 mM IPTG and the lysate was incubated with Bocillin FL (Figure 2.32). After separation, the gel was briefly washed with water and imaged with the Chemidoc MP (Bio-Rad) with the Gel Pro-Q Emerald 488 program at auto exposure and 4x4 binning. A second gel loaded with the same samples was used to transfer the proteins to a PVDF membrane so that Western blot analysis could be performed.

It is known that Bocillin FL binds and stains *E. coli* PBP1a/b (~100 kDa), PBP2 (~66 kDa) and PBP4, 5 and 6 (~49 kDa, 42 kDa and 40 kDa) (Kocaoglu and Carlson, 2015) which served as internal controls. Additionally, a band corresponding to ETP7 constructs could be observed at the expected size for all constructs (Figure 2.32, white arrowheads) except the pelB-tagged constructs. The pelB-tagged constructs could probably not be observed due to much lower abundance of ETP7 in C41(DE3) compared to the pelB-lacking constructs as seen in the Western blot (Figure 2.32, Western blot).

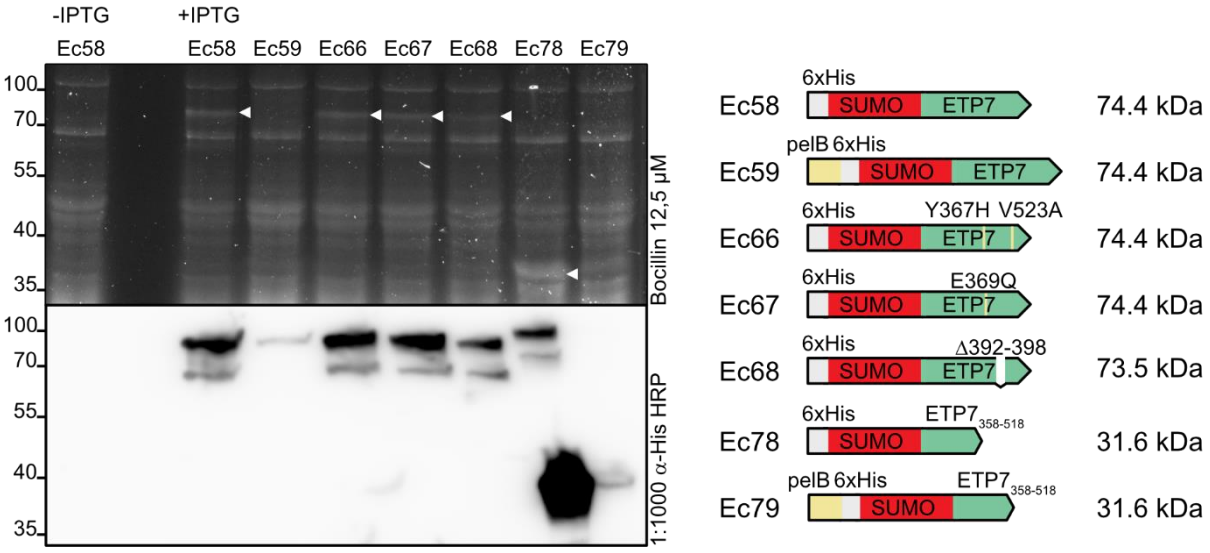

Figure 2.32 Incubation of Bocillin FL with lysate of *E. coli* expressing several constructs of ETP7. Lysate of uninduced Ec58 was treated with Bocillin FL to visualize *E. coli* endogenous PBPs. White arrowheads indicate additional bands corresponding to ETP7 constructs in the induced cell lines. Due to sample overflow during loading of the gel, Ec78 shows signal corresponding to a full length ETP7 construct in Western blot. ETP7 fusion constructs and the expected molecular weights are depicted in the scheme right of the Bocillin FL stained gel and Western blot. Bocillin FL gel was visualized under the Chemidoc MP (Bio-Rad) with the Gel Pro-Q Emerald 488 program at auto exposure and 4x4 binning. Western blot was performed by incubation with α–His-HRP 1:1000 (Santa Cruz Biotechnology). Marker in kDa.

ETP7 constructs were selected according to several features: ETP7 expressed in Ec66 contains exchanges at aa Y367H and V523A, which corresponds to the second allele of ETP7 in *A. deanei*. This construct was generated to compare overall functionality of encoded proteins of both alleles of ETP7. Ec67 contains an aa exchange at the predicted active site aa E369Q of the ETP7 hydrolase domain according to comparison of the structure based on the Phyre2 prediction to the ϕ29 tail hydrolase gp13 NTD (Figure 2.24). An overall reduction of binding affinity to β–lactams was not expected for this

construct. In Ec68 aa392-398 were deleted to interrupt a conserved loop found in gp13 NTD and observe if β–lactam binding affinity would decrease. Ec78 contains only the predicted hydrolase domain of ETP7 stretching from aa358-518. In Ec79, ETP7 possesses a pelB-tag at the N-terminus. Overall, 6xHis-SUMO-ETP7 does bind Bocillin FL, hinting towards a potential function in the restructuring of the PG layer in the ES. Binding may be slightly decreased in Ec68 but as the deletion did not abolish binding it was not further explored. The predicted Phyre2 PG hydrolase domain was able to bind Bocillin FL, which may suggest that instead of a PG-hydrolase activity this domain may facilitate a peptidase activity.

2.13.3 Hydrolase activity assays of ETP7

Hydrolysis of the β–1,4 glycosidic bond between N-acetylmuramic acid and N-acetylglucosamine in PG releases protons, which leads to a decrease of pH if enough PG is hydrolyzed. This shift in pH can be visualized by a pH sensitive dye in an in-gel assay, called zymogram (Bernadsky, Beveridge and Clarke, 1994). PG is embedded inside an acrylamide gel as a substrate for hydrolysis. After separation of the proteins according to their molecular weight by SDS-PAGE, the proteins in the gel are renatured and stained by the pH sensitive indicator methylene blue. Methylene blue changes its color from blue at a high pH to colorless at low pH. Hydrolytic activity of proteins accompanied by proton release inside the gel leads to a local decrease in pH which can be spotted as a clear band in a blue gel. Initially, the zymogram was used to test for PG hydrolysis activity as the POI does not need to be purified, if highly abundant in *E. coli* after induction. 2 µg BSA were used as a negative control and 2 µg of hen egg white lysozyme (LZ) as positive control. To observe if heating of samples during preparation reduces the renaturation rate one sample of LZ was not heated (LZ C1) and one was heated to 95°C for 5 min (LZ C2). LZ C3 is the same as LZ C2 but 10 µg were loaded instead of 2 µg. Ec27, expressing ETP2-6xHis should serve as a negative control, as no PG hydrolytic activity was predicted for ETP2. Finally, ETP7 was expressed in the BL21 strain with and without pelB, named Ec29 and Ec28. An equivalent of cell material to an OD_{600} =0.3 was resuspended in 15 µl 1x sample buffer and all loaded onto the zymogram (Figure 2.33 A). Renaturation and staining were performed according to (Zahrl *et al.*, 2005) and also described in (4.5.7).

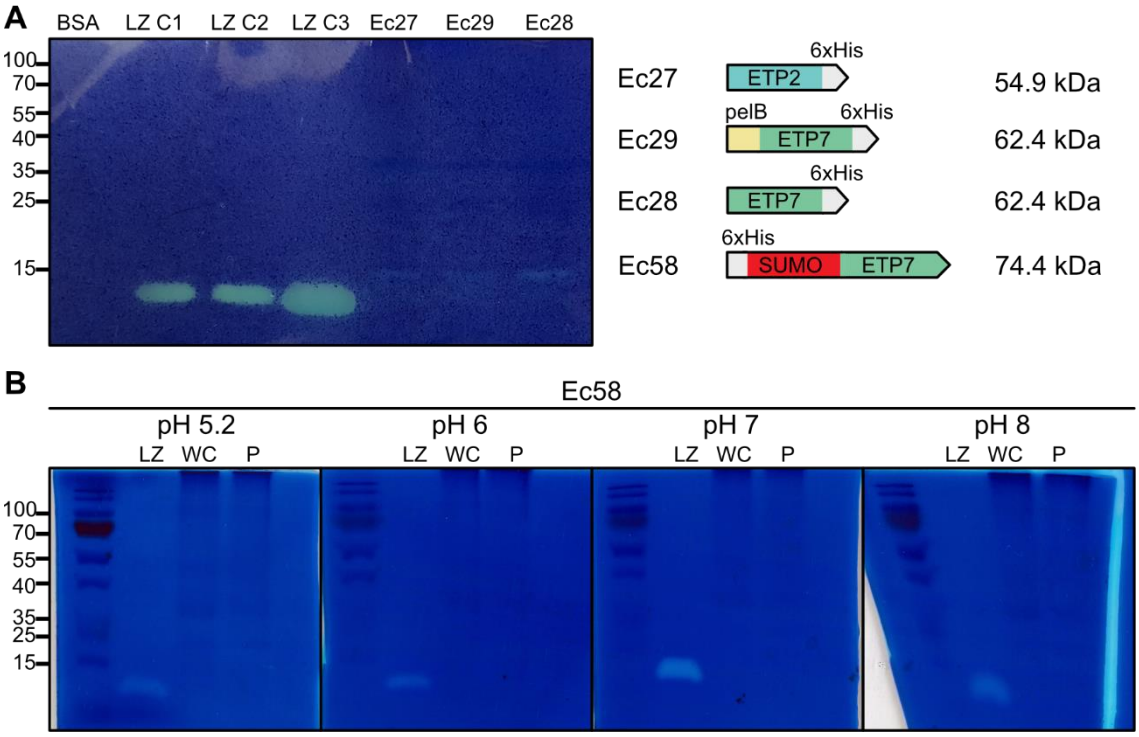

Figure 2.33 (A) Zymogram of ETP7-expressing cultures and test of different buffer conditions to improve renaturation rate (B). (**A)** 12% acrylamide gel embedded with PG and stained with methylene blue after renaturation at 4°C for 72 h at pH 5.2. Cleared zones are visible for LZ at 14 kDa and some very mild zones of clearing for some *E. coli* hydrolase at 15 kDa from the *E. coli* whole cell lysate of Ec27, Ec29 and Ec28. No clearing can be observed at the height of ETP7-6xHis (62.4 kDa). (**B)** Different buffer pH was tested to improve renaturation of 6xHis-SUMO-ETP7. No cleared zone could be observed at any tested pH inside the whole cell lysate (WC) or pellet (P) after clearing centrifugation of WC at 12,000xg 15 min (P). 3 µg lysozyme (LZ) was used as a positive control. Marker in kDa.

As previously stated, C-terminal fusion to ETP7 is undesirable, since endogenous expression of ETP7 and complementation in *A. deanei* was only possible with an N-terminal tag (Figure 2.18 B). Zymogram experiments started before this was known, which is why Ec29 (pelB-ETP7-6xHis) and Ec28 (ETP7-6xHis) were tested initially. The zymogram was repeated with the cell line Ec58, expressing 6xHis-SUMO-ETP7 instead. As successful renaturation of proteins can depend on several conditions, like pH (Marcyjaniak *et al.*, 2004) and availability of certain ions in the renaturation buffer. *E. coli* PG hydrolases seem to be mostly unaffected or even inhibited by cations other than $MgCl_2$ (Bernadsky, Beveridge and Clarke, 1994). A test of pH values ranging from 5.2 – 8 did not show any hydrolase activity for 6xHis-SUMO-ETP7 (nor any other endogenous *E. coli* PBPs) (Figure 2.33 B) under the tested zymogram conditions (Zahrl *et al.*, 2005). All tested zymogram protocols (Leclerc and Asselin, 1989; Bernadsky, Beveridge and Clarke, 1994; Marcyjaniak *et al.*, 2004; Zahrl *et al.*, 2005) failed to detected ETP7 PG hydrolase activity with any of the tested constructs.

To test a second independent assay and avoid denaturation of proteins, an in vitro PG-hydrolase assay was chosen (Shugar, 1952). In a 96-well plate PG is mixed with the POI and the OD_{450} is measured for a set period of time in triplicates. Cleavage of PG leads to a decrease in OD_{450}.

6xHis-SUMO-ETP7 was isolated via IMAC with addition of 0.1% Triton X-100 after sonication. The imidazole elutions were mixed with the PG solution as described in 4.5.9. 250 U/ml LZ in elution buffer were used as a positive control.

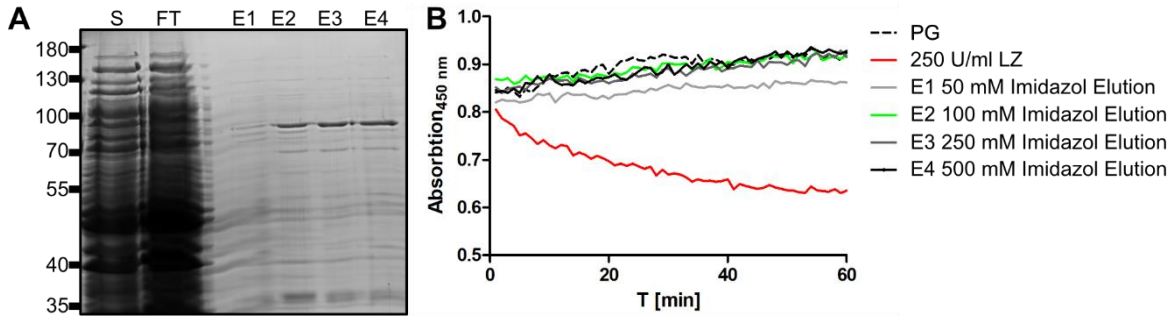

Figure 2.34 (A) IMAC purification of 6xHis-SUMO-ETP7 and (B) the subsequent PG-hydrolase assay. (A) CBB-stained SDS-PAGE after IMAC. S: supernatant after sonication and clearing of lysate, FT: flow through of unbound protein to the Ni-NTA resin, E1 to E4: eluates from elutions with an imidazole concentrations of 50, 100, 250, and 500 µM. Expected size for 6xHis-SUMO-ETP7: 74.4 kDa. Marker in kDa. **(B)** Cleavage of PG leads to a decrease of OD_{450} (vertical axis) over time (horizontal axis). Red line: 250 U/ml LZ (positive control), dashed line: PG solution without further additives (negative control), green line: 100 mM imidazole elution containing the highest concentration of 6xHis-SUMO-ETP7. Grey lines: 50, 250, and 500 mM imidazole elution.

The absorption at 450 nm decreased from an average of 0.805 to 0.635 in 60 min when lysozyme was added reflecting that the assay in general was suitable to detect lytic activity. In the same period of time no decrease could be observed for any of the elutions containing 6xHis-SUMO-ETP7 (Figure 2.34 B).

As sensitivity of the turbidimetric assay is relatively low, a 3 times more sensitive hydrolase assay based on the release of Remazol brilliant blue (RBB) from labeled PG was designed (Zhou, Chen and Recsei, 1988) and further streamlined (Ito, Yamada and Imoto, 1992). In this assay, PG is labeled with RBB which is released upon cleavage of the β-1,4-glycosidic bond between NAM and NAG. The released RBB increases the absorption at 600 nm, which can be measured in a plate reader assay similar to the turbidimetric assay (4.5.10). The RBB-release assay was tested with samples isolated (Figure 2.34 A) and also in the presence of urea as previously seen, binding and elution of ETP7 constructs from Ni-NTA was more effective in buffer containing 8 M urea.

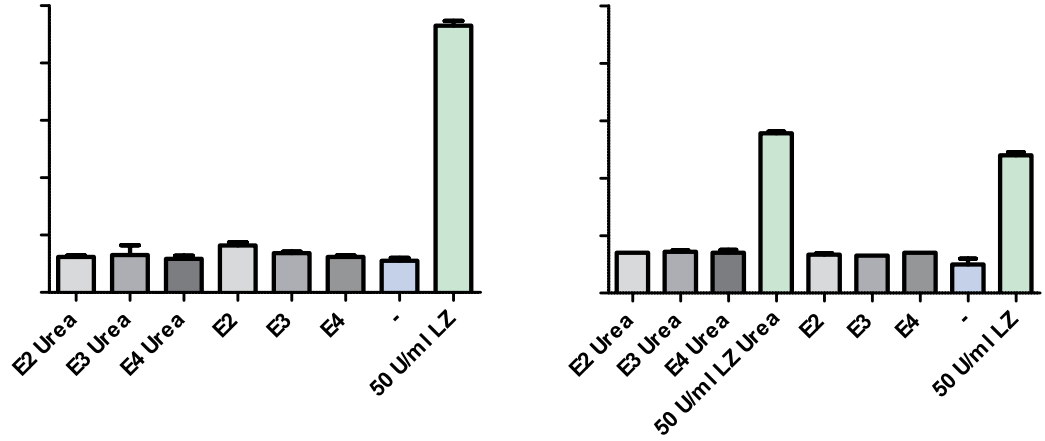

Figure 2.35 A: RBB-release hydrolase assay of 6xHis-SUMO-ETP7 and B: 6xHis-SUMO-ETP7$_{358-518}$. Incubation of E2-E4 in the presence of urea or 0.1% Triton X-100. All samples were incubated with RBB-labeled PG over night at 40°C. The absorption of released RBB was measured at 600 nm. 50 U of LZ was used as a positive control. -: Same volume of buffer was added to the RBB-labeled PG. E2-E4: 100, 250 and 500 mM imidazole elution of Ni-NTA. 3 technical replicates were measured.

None of the tested constructs showed any activity comparable to 50 U/ml LZ overnight. A very mild increase in absorption could be observed over several experiments but as the purification from Ni-NTA cannot exclude contamination with *E. coli* hydrolases, the activity was deemed too low for a highly enriched protein from IMAC purification to hint to any PG-hydrolase activity.

2.14 Expression of proteins in *L. tarentolae*

As ETP7 expressed in *E. coli* did not show any activity during PG hydrolysis assays, *L. tarentolae* was to be established as an alternative expression system. A tetracycline inducible strain specifically for the expression of heterologous proteins has been previously published (Kushnir *et al.*, 2005), which would be an ideal expression system for proteins of *A. deanei* as *L. tarentolae* is a close relative within the non-SHT group. The *L. tarentolae* strain expressing the T7 polymerase and TetR (available via Jena Bioscience) was termed Adea345. To test expression in Adea345, a plasmid for expression of eGFP-6xHis (pLEXSY_I-egfp-neo3, Jena Bioscience, termed pAdea348) was restricted according to manufacturer recommendations and the cassette for HR transfected (Vainio *et al.*, 2009) (4.4.3) generating Adea371LT. Furthermore 10xHis-ETP7 was cloned into pLEXSY_I-neo3 (pAdea347) producing pAdea349 and transfected into Adea345 as well generating Adea370LT. Both cell lines were grown and induced as described in 4.4.16 with 10 µM tetracycline and expressed for 48 h under agitation. 1 ml of culture were spun down, and the cells resuspended in 100 µl 1x SDS-sample buffer or 2x SDS-sample buffer containing 6.4 M Urea and boiled for 5 min. 20 µl of each sample was used for Western blot analysis (Figure 2.36). Expression of eGFP in Adea371LT was confirmed by α–GFP AB but

could not be detected using the α–His AB. 10xHis-ETP7 could not be detected in Adea370LT C1 and C2.

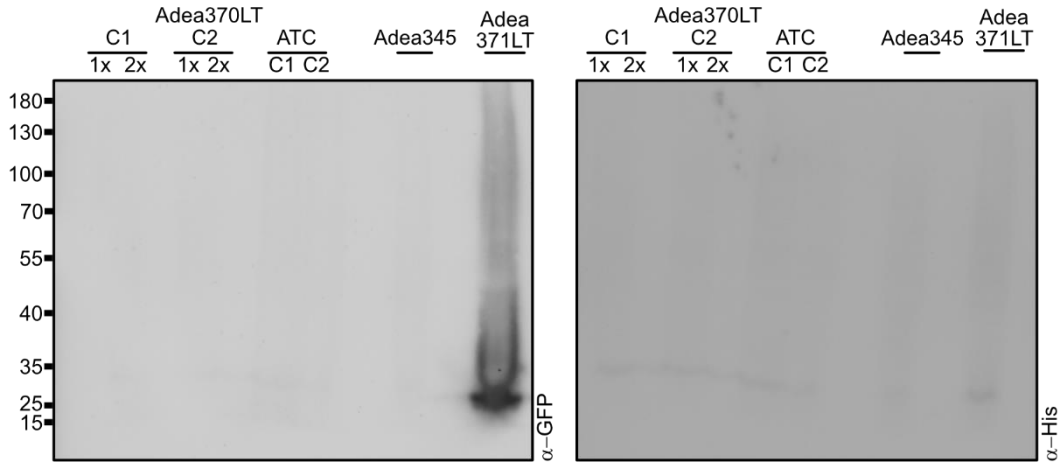

Figure 2.36 Western blot analysis of Adea370LT and Adea371LT. Two clones (C1 and C2) of Adea370LT were expressed by incubation with TC or ATC to compare the effect. Adea345 and Adea371LT were incubated only with TC. Left Western blot was incubated with rabbit α–GFP 1:1000 and α–rabbit HRP 1:5000 and the right blot with α–His-HRP 1:1000. Expected sizes: Adea370LT 10xHis-ETP7: 63.9 kDa; Adea371LT eGFP-6xHis: 28.3 kDa. ATC: Anhydrotetracycline. 1x and 2x relate to the concentration of SDS-sample buffer used to solubilize the samples. Marker in kDa corresponds to both Western blots.

3 Discussion

Ca. K. crithidii, the bacterial ES of *A. deanei* has undergone drastic reduction of genome size to just 10% compared to free-living relatives and about 50% of related intracellular pathogenic bacteria (João M.P. Alves *et al.*, 2013). Genomic reduction is common among intracellular pathogens, as host cells provide a stable environment. Most genes for core energy metabolism as well as biosynthetic capacity of some amino acids and cofactors such as proline, cysteine, and biotin were lost. Meanwhile biosynthetic pathways supporting host growth (aromatic aa, riboflavin, and heme) were retained and benefit the host by making SHTs nutritionally less fastidious than non-SHTs (Mundim and Roitman, 1977; João M P Alves *et al.*, 2013; João M.P. Alves *et al.*, 2013; Klein *et al.*, 2013).

The streamlining of the genome did not only make the ES nutritional requirements highly reliant on host-provided nutrients but also the ability of independent division has been lost as PG polymerization (FtsW), restructuring (PBP3) and outer membrane invagination (TolQ) are all lacking essential proteins (Figure 1.3). To sustain *Ca.* K. crithidii inside *A. deanei*, exchange of metabolites is not enough anymore as the host must provide proteins to the ES, which enable synchronized division granting tight control over the number of ES per cell and reliable inheritance to daughter cells – features still missing in the only other to date known SHT not belonging to the *Strigomonadinae*, *Novymonas esmeraldas* (Kostygov *et al.*, 2016).

3.1 Extent of host-encoded proteins found at the ES of *A. deanei*

With the ES highly intertwined with the host metabolism it was not clear how many proteins would be needed to orchestrate the metabolic cooperation of the symbiotic partners. In *P. chromatophora* several hundred proteins were found by a similar LC-MS/MS approach encoded by the host and targeted to the bacterial ES, the chromatophores (Singer *et al.*, 2017). In *A. deanei* however, only a total of 14 host-encoded candidates were found enriched at the ES (Table 2.1). The protein with the highest enrichment in the ES fraction from these 14 candidates, ETP1, was fused to eGFP and demonstrated in combination with fluorescence *in situ* hybridization (FISH) using a bacterium-specific probe a localization at the ES (Morales *et al.*, 2016). For the remaining 13 candidates, experimental analysis by eGFP fusion and expression in *A. deanei* revealed 6 more ETPs to be found at the ES (Figure 2.1). The ETPs are a diverse group of proteins. Yet from the seven ETPs total, three subgroups could be formed based on the observed localization. ETP1 and ETP5 are found homogenously distributed throughout the ES envelope. ETP2, ETP7 and ETP9 are all found at the constriction site of the ES possibly in a cell cycle stage dependent matter and ETP3 and ETP8, based on preliminary results, are able to cross the outer membrane and periplasm of the ES, likely attached to the inner membrane or

inside the cytosol of the ES. Furthermore, both accumulate between the nucleus and trans-Golgi in a dot-like spot.

The majority of the ETPs (ETP1, ETP2, ETP3 and ETP8) are all annotated as 'hypothetical proteins' with ETP1 and ETP2 not aligning with any proteins from other organisms in BLASTp analysis against the NCBI non-redundant (nr) database. 3D structure prediction by Phyre2 revealed no significant similarities in the case of ETP1, ETP2 and ETP8 and similarity to several long stretched α–helical proteins in highly diverse functions such as muscle contraction, PG hydrolysis and chromosome maintenance for ETP3, making a prediction of its cellular function impossible.

ETP5 shows 94% sequence identity to kinetoplastid membrane protein 11 (KMP-11) of *T. cruzi*, a protein of unknown function that is highly conserved among trypanosomatids (Stebeck *et al.*, 1995) and has been found to be essential for cytokinesis in *T. brucei* (Li and Wang, 2008). Just like the genes for KMP-11 in non-SHTs, ETP5 is the only ETP encoded by genes arranged in a tandem of four identical gene copies. ETP5 is found at the periphery of the ES and spans the host cell in a thread-like fashion connecting a ball-shaped structure at the anterior end of the cell close to the flagellar pocket, the kinetoplast and nucleus, down to the posterior end of the cell. It is speculated that the ball-shaped structure at the anterior end may be the basal body as KMP-11 was reported to be found in the basal body, the flagellar pocket and the flagellum in *T. brucei, T. cruzi* and *L. infantum* (Berberich *et al.*, 1998; Li and Wang, 2008; Finkelsztein *et al.*, 2015). The basal body in trypanosomatids is the nucleation site of the flagellum and in non-SHTs the first structure to initiate division by maturation of the probasal body, indicating the transition from G1- to S-phase (Elias *et al.*, 2007).

Previously reported localization of the basal body in *A. deanei* using an α–γ–tubulin antibody (Ríos *et al.*, 2004) was shown to locate between the kinetoplast and nucleus (Motta *et al.*, 2010) which does not fit exactly the localization of the ball-shaped structure found between the kinetoplast and anterior end of the cell. Instead of the basal body, eGFP-ETP5 may be found at the bilobe, a centrin-containing cytoskeletal structure found at the anterior end of the flagellar pocket and next to the flagellar pocket collar. Both complexes regulate the position of the flagellum in trypanosomatids but have not been described in SHTs yet (de Graffenried, Ho and Warren, 2008; Ikeda and De Graffenried, 2012). The bilobe is also essential for division and positioning of the Golgi which has been shown by depletion of Centrin2 in *T. brucei* (He, Pypaert and Warren, 2005; De Graffenried *et al.*, 2013). Inhibition of the bilobe-located polo-like kinase (PLK) leads to arrest of cell division (Ikeda and De Graffenried, 2012). The bilobe and flagellar pocket collar are therefore structures crucial to cell division in trypanosomatids and an adaption to the bacterial ES inside SHTs has yet to be explored. In the context of ETP5 localization, IFA of an eGFP-ETP5 expressing cell line using α–Centrin2 or α–PLK antibody and an

α–γ–tubulin antibody would allow to observe the bilobe and basal body, maybe answering the question in which other cellular structure ETP5 is located in *A. deanei*.

The remaining two ETPs with some resemblance to previously characterized proteins are ETP7 and ETP9. ETP7 is found exclusively in *A. deanei* when BLAST analysis against standard nr nucleotide collection is performed and Phyre2 predicts a PG-hydrolyzing domain with a confidence of 92.6 between aa 358-518 based on homology to the PG-hydrolyzing N-terminal domain of the bacteriophage ϕ29 protein gp13 (Xiang *et al.*, 2008). When comparing the aa sequences of both proteins the catalytically active glutamic acid found invariably in lysozymes (E45 in gp13 and E369 in ETP7) is conserved as well as a loop in proximity to the catalytic site. Combining this prediction with the localization of eGFP-ETP7 at the constriction site of the ES, which is missing PBP3, an essential transpeptidase for the restructuring of PG during division all support the claim that ETP7 does feature some function in PG processing.

ETP9 is annotated as a "dynamin family protein", which are self-assembling, polymer-forming GTPases involved in the division of membrane bearing structures. Trypanosomatids outside the *Strigomonadinae* encode only one dynamin-like protein (DLP) except for *T. brucei* which harbors two almost identical DLPs in tandem. *Tb*DLPs have been reported to function in mitochondrial division and proposed to take part in endocytosis and cytokinesis as well (Morgan, Goulding and Field, 2004; Chanez *et al.*, 2006; Benz *et al.*, 2017). Comparison of ETP9 to trypanosomatid DLPs reveals only 34% identity to *Tb*DLPs. Despite the low similarity, predicted domain organization seems to be conserved to *Tb*DLPs as well as DRP1 and Dnm1p from human and yeast (Morgan, Goulding and Field, 2004; Benz *et al.*, 2017). All domains necessary for GTPase activity and protein oligomerization are found in ETP9 (Morales *et al.*, 2023).

Even though currently no function for ETP3 and ETP8 can be predicted, their localization at the Golgi apparatus as observed in co-expression studies with the trans Golgi marker ARL1-V5 (Figure 2.4) may hint at a transport pathway through the Golgi to the ES. Targeting of Golgi-derived vesicles to secondary chloroplasts has been demonstrated in *Euglena gracilis* (Sláviková *et al.*, 2005), a Euglenid closely related to Symbiontida, Diplonemea and Kinetoplastea. So far, no transporters or import machineries have been identified between *A. deanei* and *Ca.* K. crithidii and no common targeting signal among the ETPs could be observed. The elevated level of the eukaryotic lipid phosphatidylcholine in the bacterial outer membrane of the ES may be another hint on vesicle transport to the ES as phosphatidylcholine is found enriched in the Golgi (Sleight and Pagano, 1984; Testerink *et al.*, 2009).

To understand their putative role in the context of endosymbiosis in *A. deanei*, this relatively small set of host-encoded proteins found enriched in the ES had to be further examined. Focus of this work were the ETPs ETP2 and ETP7 that localize at the constriction site of the endosymbiont.

3.2 Localization of ETP2, ETP7 and ETP9

Proteins recruited to the constriction site of bacteria are likely part of the divisome. From the 7 identified ETPs, three seem to be involved in division of the ES as heterologous fusion proteins are all found at the bacterial fission side. ETP7 has the overall weakest fluorescence intensity when comparing eGFP-fusion constructs of all three and is also found in only 40% of cells in a mid-log cell culture and is limited to the constriction site (Figure 2.5 B), indicating tight regulation and a highly time and space limited activity. Comparing eGFP-ETP7 at the ES to GFP-PBP3 in *E. coli* bears a striking resemblance in dividing cells (Weiss *et al.*, 1999).

ETP9 is found in about 50 % of the cells at the constriction site and in around 20% accumulating at the ES but dispersed around the periphery (Figure 2.5 B). Transport of ETP9 to the ES may begin before recruitment is initiated or after division eGFP-ETP9 is only slowly disassembled and partially persisting at the ES after successful separation. In the red alga *Cyanidioschyzon merolae* it has been shown that *Cm*Dnm1, a dynamin-related protein involved in mitochondrial fission, is found in patches surrounding the dividing mitochondrion and only recruited to the division site after assembly of the FtsZ ring and mitochondrial division ring (Miyagishima *et al.*, 2003; Nishida *et al.*, 2003). A similar process may occur at *Ca.* K. crithidii with ETP9 closely surrounding the ES until all prerequisites have been met. In this context, the co-localization of ETP7 and ETP9 makes sense, as only when divisome assembly has been initiated, ETP7 is recruited to the ES constriction site with ETP9 assembling into a ring surrounding the constriction site of the ES and separating the two daughter cells in parallel with the FtsZ ring on the inside.

ETP2 with its four different distribution patterns (Figure 2.5 A) and no homology to any characterized protein allows only for speculation on a possible function. The distribution at the poles and center of the cell resembles the MinCDE system, an inhibitory complex preventing aberrant division at the cell poles (de Boer, Crossley and Rothfield, 1989). In *E. coli* MinC and MinD accumulate at a cell pole preventing formation of an FtsZ ring anywhere but the center of the cell by oscillating between the poles of the cells due to constant release of polymerized MinC and MinD by MinE (Loose *et al.*, 2011). The oscillation between the poles is not essential however, as *B. subtilis* maintains static concentration of MinC and MinD at the poles (Marston *et al.*, 1998). Since MinC, MinD and MinE are still encoded in the ES it seems unlikely that ETP2 complements a conserved system. Involvement in the correct

recruitment of the divisome or FtsZ ring placement is still a likely function for ETP2 as it has been shown that even in the absence of the Min system cells are still viable, strongly implicating other redundant systems previously overlooked (Wu and Errington, 2004; Bernhardt and De Boer, 2005; Rodrigues and Harry, 2012). Several proteins have been reported for recruitment of soluble factors or linkage of chloroplasts and mitochondria division machinery to host-derived components (Osteryoung and Pyke, 2014; Miyagishima, 2017; Voleman and Dolezăl, 2019).

Alternatively ETP2 may also feature some role in the recruitment and incorporation of new PG as the distribution of ETP2 bears striking resemblance to the fluorescent D-amino acid (HADA) sites of PG synthesis throughout the cell cycle in *Agrobacterium tumefaciens* (Figueroa-Cuilan and Brown, 2018).

3.3 Immunogold TEM visualizes envelope specific localization of ETP1 at the ES

Most ETPs are found at the periphery of the ES but their exact location has not been explored yet. The ES is surrounded by two bacterial membranes and a reduced PG-layer in between. The composition of these two membranes is asymmetrical with respect to lipid and protein composition as the two membranes fulfill different functions. Host proteins that interact with the endosymbiont should have to some degree the capacity to overcome the protective abilities of the ES envelope. In this context, there is a major difference if a host-derived protein is interacting with the outside of the outer membrane, i.e. strictly speaking not entering the ES, or is able to translocate across the outer membrane into the intermembrane space or across both membranes and the PG layer to affect cytosol-localized cellular processes in the ES directly. Nowadays, several membrane dyes are available but their application inside *A. deanei* has not been tested and the short distance between inner and outer ES membrane likely makes it impossible to distinguish between these two membranes with light microscope-based methods. TEM on the other hand offers enough resolution to distinguish between outer and inner membrane and does not rely on specific membrane staining. Porin, a major protein of the outer membrane of bacteria was revealed to sit in the outer membrane of *Ca*. K. crithidii by immuno-TEM (Andrade *et al.*, 2011), proving that immuno-TEM on membrane components of the bacterium is possible.

In the work leading to this thesis, *A. deanei* cells embedded in LR-White showed in general relatively low amounts of gold particles after immunogold staining, which is most likely caused by loss of the epitopes during heat curing. To visualize porin, Andrade et al. used curing of embedded cells at -20°C under UV light, which preserves epitopes much better than heat treatment. During the course of this thesis no capable device to perform cryo-UV curing was available.

Heat curing does affect the epitope availability by masking a high proportion, which increases proportional to the temperature used for curing. Lower temperatures however suffer from the risk of incomplete curing of the resin, leading to crumbly, instable blocks and sensitive sections. Downstream immuno steps often introduced warping of the sections, producing wrinkles in the cells ((B). A balance had to be found between keeping as many epitopes as accessible as possible, but ensuring curing was successful.

Ultimately, all these drawbacks made it necessary to test alternative embedding strategies, as heat curing in LR-White was inconsistent and difficult to handle. Epitope preservation was of highest priority for any alternative strategy. Ultracryotomy of cells in sucrose suspension as described by Tokuyasu (Tokuyasu, 1973)does not depend on strong fixatives or heat-cured resins. Furthermore, Tokuyasu embedding has been used previously in *T. brucei* to study the formation of cristae and protein import into mitochondria by immunogold-TEM of V5-labeled *Tb*Mic10-1/2 (Kaurov *et al.*, 2018).

As before, ETP1 fused to a V5 tag was used for assessment of the best immuno-TEM conditions in ultracryosectioned cells, due to the high and specific protein abundance found at the membrane of the ES. Various protocols were tested with several combinations of 1st AB concentrations and different strategies for detection. From all tested combinations only Protein A fused to 15 nm colloidal gold particles (condition 3) allowed for consistent labeling, meeting the expectations set by the results obtained from fluorescence microscopy of V5-, eGFP- and mSCARLET-ETP1 and STED-microscopy of SNAP-ETP1 (Ehret, 2017) that ETP1 is found at the membrane of the ES (Figure 2.9).

A rough estimate by comparison of the size of the 15 nm gold particles and the membrane structure leaves the ES membrane at what appears to be around 20 nm in width as the inner and outer membrane are only divided by a reduced PG layer and a small intermembrane space. The 15 nm gold particles attached to a chain of 1st AB, bridge AB and Protein A are a big structure in comparison and offer insufficient resolution to determine whether ETP1 is exclusive to the outer membrane of the ES or may be able to travel up to the intermembrane space or even associate with the inner membrane. Antibodies with smaller colloidal gold particles should be tested next to improve resolution and help answer this question.

In sum, immunogold-TEM has been successfully established for cryosectioned *A. deanei* cells and confirms ETP1 to be restricted to the ES envelope. This technique may be used in the future to study subcellular protein localization where fluorescence microscopy offers insufficient resolution or other cellular structures are to be analyzed.

3.4 All ETPs are retained in aposymbiotic *A. deanei*

Attempts to generate an aposymbiotic *A. deanei* cell line (Mundim and Roitman, 1977) based on ATCC PRA-265 have been unsuccessful, but an aposymbiotic strain of *A. deanei* has been made available via the American type culture collection. Comparison between the aposymbiotic strain and the ES-harboring strain of *A. deanei* allows analysis of the effect of the ES on the host transcriptome and proteome. Previous studies revealed changes in host structures to improve attachment to insect guts e.g., enlarged flagella allowing tighter adhesion. Colonization of the mosquito *Aedes aegypti* was only possible for the ES-harboring strain in feeding experiments (Fampa *et al.*, 2003). Another study was also able to demonstrate ES-induced increase in host ornithine decarboxylase activity (Frossard *et al.*, 2006).

After successful verification of the identity of ATCC-30969 as *A. deanei* by sequencing of the 18S rRNA gene (Figure 2.10) the presence of the ETPs genes were examined. Primers designed for amplification of the ETP-coding genes from the ES-harboring *A. deanei* strain were used in PCR on gDNA of aposymbiotic *A. deanei* and the PCR products were cloned into pJET 1.2 and sequenced. All ETP genes could be amplified from aposymbiotic *A. deanei* gDNA, and except for *Etp3*, were identical to any of the previously analyzed alleles found in the ES-harboring *A. deanei*. *Etp3* shows the highest level of allelic variation between the two alleles of ES-harboring *A. deanei* with a total of 40 nucleotide mismatches, resulting in a pairwise nucleotide identity of 98.59% and a total of 8 out of 943 aa exchanges (Figure 2.11). All other ETP genes showed a pairwise nucleotide identity of >99% between the two alleles, except for *Etp1* due to the 21 Bp insertion found in the Q+ termed allele. The nucleotide exchanges in ETP3 are most common in the first third and the last quarter of the gene. The sequenced allele of ETP3 of aposymbiotic *A. deanei* has also seven more aa exchanges, which are all found from the center to the last quarter of the gene. With so many exchanges between alleles ETP3 may still be evolving rapidly compared to the other ETPs.

For ETP7, ETP8 and ETP9 sequence information from a draft whole-genome assembly (Morales *et al.*, 2016) and the chromosome-level assembled genome (Davey *et al.*, 2021) did not match fully to just two alleles. It has been shown that *A. deanei* comprises four infraspecific genotypes (Dea1-Dea4) with high genetic diversity ranging from 12% between Dea1 and Dea2 and 20% between Dea1 and Dea3/Dea4 based on internal transcribed spacer 1 rDNA. Even within a single genotype sequence divergencies ranging from 1-6% were reported (Teixeira *et al.*, 2011; Borghesan *et al.*, 2018). This range of divergence also fits the observed number of unique exchanges found in any of the alleles.

Nonetheless, all ETPs are retained in the aposymbiotic *A. deanei* strain even though ETP5 as KMP-11 is the only conserved protein found in non-SHTs. The selective pressure to remove these genes from the genome seems to be low or not enough time has passed to allow for deleterious mutations to occur

since the generation of the strain and its storage at the ATCC. Additionally, no documentation is available describing how long the strains stored at the ATCC have been in culture before cryopreservation. A long-term culturing experiment to compare the evolution of the aposymbiotic *A. deanei* and the ES-harboring strain may reveal some genomic rearrangements the more time passes without an ES to sustain.

Previous attempts to generate an aposymbiotic cell line based on ATCC PRA-265 may have been unsuccessful due to genetic variation in between the four genotypes of *A. deanei* as currently it is not clear which genotypes are found in ATCC PRA-265 compared to ATCC 30255 which was used previously to generate the aposymbiotic *A. deanei* cell line. The strain ATCC 30255 was removed in 2009 from the ATCC as the strain did not represent the symbiont-bearing *A. deanei* anymore (Yurchenko *et al.*, 2009).

3.5 Generation of ETP2 and ETP7 homozygous knockouts

A universally common approach in identification of possible function of a novel and uncharacterized gene is the removal from the genome to observe any phenotype triggered. Previous attempts to generate homozygous knockouts of *Etp1* in ES-harboring *A. deanei* have failed (Kokkori, 2018), but as the ETPs are a highly diverse group this result cannot be extrapolated to other ETPs. During this thesis ETP2 and ETP7 were chosen for homozygous knockout attempts. Two consecutive rounds of transfection of resistance markers flanked by either ETP2 or ETP7 FR should exchange both copies of the gene and produce ETP2 or ETP7-deficient cell lines. Generation of heterozygous knockout cell lines was straight forward in both cases and produced cell lines without any noticeable phenotype under regular culture conditions. Exchange of one allele may not necessarily translate into halved mRNA and protein amounts per cell as trypanosomatids control protein expression by post-transcriptional methods (Clayton, 2002; Haile and Papadopoulou, 2007). No analysis regarding mRNA abundance and stability were performed, however. Correct insertion of the transfected cassette was verified by PCR using primers upstream and downstream of the cassette used for homologous recombination. This produced two products during PCR, corresponding to the WT allele and the exchanged cassette (Figure 2.13 A). To ensure insertion did not occur at off-target sites as well, Southern blot analysis was performed (Figure 2.13 B). No off-target insertion could be detected in all tested heterozygous clones. Repeated attempts to transfect verified heterozygous knockout clonal cell lines with a transfection cassette targeting the same locus containing a second resistance marker never resulted in recovery of homozygous knockout cell lines. Flanking regions adapted specifically for each allele in transfected cassettes did not lead to successful transfection events either.

Generation of homozygous knockouts in aposymbiotic *A. deanei* were initiated with successful generation of heterozygous knockouts but could not be repeatedly transfected in time as growth of the aposymbiotic *A. deanei* is much slower compared to ES-harboring *A. deanei* and severe shipping delay of the strain from the ATCC to Germany resulted in a very late start of the project. If ETPs are only essential when *Ca.* K. crithidii is harbored inside *A. deanei,* generation of homozygous knockouts should be relatively simple to achieve.

3.6 Tags fused to the N-terminus of ETP2 and ETP7 do not interfere with protein function in *A. deanei*

With all previously generated cell lines expressing fusion constructs from either the γ– or δ–amastin loci using the Gapdh ir spliced leader sequence and the respective amastin locus 3' maturation site for mRNA processing it was never tested if the observed protein localizations may be an overexpression artifact, as the amastin loci were chosen specifically due to the high corresponding mRNA abundance levels and absence of phenotype of amastin null mutants under culture conditions. Furthermore, subcellular localization may be altered and interaction with protein partners sterically prevented due to the size of the chosen eGFP and mSCARLET tags. Transfection of *A. deanei* WT cells with a cassette containing either *eGfp-Etp2* or *Etp2-eGfp* containing FRs to the ETP2 locus resulted in clones depending exclusively on the *eGfp*-tagged *Etp2*, as PCR and Southern blot confirmed spontaneous exchange of both alleles of *Etp2* with *eGfp-Etp2* as seen in Adea120 C2 (Figure 2.15). For *Etp2-eGfp*, exchange of one allele of *Etp2* was possible (Figure 2.14) but transfection attempts of verified clones to exchange the second allele for a resistance cassette did not produce the anticipated cell line. Epifluorescence of both cell lines was consistent with the previously observed localization of *Etp2* constructs expressed from the amastin locus, which means recruitment to the constriction site does not depend on an unoccupied C-terminus but some essential interaction or activity must be impaired. Instead of eGFP the degron domain DDFKBP in tandem with the V5-tag could also be fused to the N-terminus of ETP2 and ETP7.

Confirmation of localization of ETP2 and ETP7 expressed from their endogenous loci and successful verification of viability of N-terminal fusion constructs was a prerequisite to ensure that previous and future results obtained in heterologous cell lines are of biological relevance in *A. deanei*.

3.7 Current limits of conditional expression systems in *A. deanei*

Characterization of essential genes in cellular processes is always difficult as knockouts are only possible if rescue strategies can be applied to avoid premature and uncontrolled cell death. Since all previous knockout attempts of ETPs have never resulted in a homozygous knockout cell line the ETPs found in *A. deanei* may be crucial for maintenance of the ES that is obligate for survival of *A. deanei* (at least in this strain and under the culture conditions used in this work). In *Trypanosoma*, studies of such genes have been successfully performed by coupling of a tetracycline-inducible operator coupled to RNAi (Wirtz and Clayton, 1995; Shi *et al.*, 2000; Wang *et al.*, 2000; Alibu *et al.*, 2005). RNAi is not conserved universally among all trypanosomatids as most *Leishmania spp.* lack parts of the RNAi pathway (Roberts, 2011). A study in *A. deanei* achieved knock-down of specific genes by transfection of double stranded RNAs (Catta-Preta *et al.*, 2016) but attempts to perform RNAi through genomic double strand RNA expression failed in our group (Kokkori, 2018) and have not been reported to have been repeated in the literature.

Protein destabilization through fusion of DDFKBP to target proteins as an alternative to RNAi has been successfully established in *L. major* and was the first system to be adopted in *A. deanei* (Results 2.10.1) after RNAi attempts. Degradation of DDFKBP-eGFP was effective but stabilization of the protein through addition of any of the tested ligands FK506, shield1 and rapamycin all resulted in relatively poor recovery rates as measured by fluorescence intensity in a plate reader-based assay (Wolters, 2019). Despite concerns regarding protein concentrations that can be achieved under stabilizing conditions with the DDFKBP system, which may be critical for essential proteins, ETP2 and ETP7 were still fused to DDFKBP and expressed from the respective endogenous loci in a heterozygous knockout background. Irrespective of addition of stabilizing ligand both cell lines proliferated against the set expectations. Western blot analysis and IFA confirmed DDFKBP-V5-ETP2 and DDFKBP-V5-ETP7 were still detectable in both cell lines (Figure 2.17). The effect of the degron domain seemed proven by previous work, so how were ETP2 and ETP7 constructs able to avoid degradation? One possible explanation lies in the nature of the FKBP derived origin as a eukaryotic protein. In bacteria proteasomes are not universal (De Mot *et al.*, 1999; Müller and Weber-Ban, 2019) and a previous report used DDFKBP in *E. coli* to decrease folding speed of proteins instead and observed only some decrease in proteins levels when compared to constructs without DDFKBP (Schwarz *et al.*, 2012).

This means that probably any DDFKBP-V5-ETPs reaching the inside of the bacterium may be protected from eukaryotic degradation processes. The localization of ETP3 and ETP8 close to the trans-site of the Golgi may be a hint that ETPs are shuttled via vesicles to the ES, potentially protecting them from cytosolic degradation pathways. Electron micrographs of Strigomonadinae have already observed potential fusion of vesicles to the outer membrane of the ES (Chang, 1974). ETP9 would be a prime

target to test this hypothesis, as a potential ring structure would sit outside of the ES outer membrane, potentially becoming a target for eukaryotic degradation processes. The limited influx of ligands FK506 and rapamycin into the cells however may still pose a problem for downstream application of the system.

Conditional gene excision of a GOI should circumvent the problem of proteins escaping degradation, which led to the application of the DiCre-recombinase in *A. deanei* (Results section 2.9.2). So far, it is unclear why gene excision has not been observed in any of the constructs. Western blot analysis using α–Cre antibody (69050, Merck) detected low protein levels and could only detect the Cre60 domain, as the α–Cre antibody was raised specifically against the C-terminal end of the Cre recombinase. Furthermore, the plasmids containing constructs flanked by LoxP sites which were used for the generation of transfection cassettes could be successfully excised by application of commercially available Cre and separation on an agarose gel (Wolters, 2019). Detection and abundance problems were addressed at the same time by generation of cell lines expressing codon optimized versions of V5-tagged constructs of Cre59 and Cre60, enabling detection and comparison to non-optimized Cre domains by students in our laboratory (Dreesbach, 2022; Stirba, 2022). A noticeable increase in overall protein amounts for both domains was achieved but still no GOI could be excised from *A. deanei*. The successful application of the DiCre in *L. mexicana* (Duncan *et al.*, 2016) but the lack of any traceable activity in *A. deanei* is puzzling. Preliminary experiments performed by Lena Kröninger give a strong hint that the FK506-induced dimerization through FKBP and FRB fails in *A. deanei*, as constitutive expression of a restored single fragment Cre-recombinase resulted in gene excision of a genomically integrated LoxP-flanked *eGfp*.

In the future, the application of the tetracycline inducible system in combination with ATC should allow for easy and fast protein expression when combined with a T7 polymerase and a T7 promotor upstream of a target gene inserted into a silent genomic locus. The necessary plasmids for Tet-inducible expression of ETP7 and eGFP in *A. deanei* have already been produced and are currently under investigation. In combination with Cas9 the process could also be inverted and induction with ATC would allow for double strand DNA breaks of GOIs. This strategy will become of particular importance if multicopy genes such as ETP5 are to be knocked out as the current strategy for homologous recombination against a resistance cassette may not effectively exchange all copies. Alternatively, a reconstituted Cre-recombinase could be expressed under TetO control, allowing for ATC-inducible expression of Cre-recombinase. This would allow to use the previously constructed plasmids and *A. deanei* strains which contain loxP-flanked copies of essential genes for the conditional gene excision strategy but omitting FK506 and the dimerization domains.

3.8 ETP2 is highly divergent between *A. deanei* and *S. culicis*

The monophyletic origin of the Strigomonadinae (Souza *et al.*, 1999; Votýpka *et al.*, 2014) by invasion of a β–proteobacterium means that the genera *Strigomonas*, *Angomonas* and *Kentomonas* must have derived from the same ancestor and underwent similar evolutionary pressure, since all Strigomonadinae harbor the same ecological niche as parasites in the guts of insects. Genomes of all *Ca.* Kinetoplastibacterium spp. vary less than 3% in total genome length between each other and show overall similar streamlining (João M.P. Alves *et al.*, 2013). A recent report postulates horizontal transmission of the ES has occurred between *A. ambiguous* and *A. deanei* (Skalický *et al.*, 2021). With the same essential genes missing for cellular processes such as division (Figure 1.3) mechanisms for adaption to the ES inside the host must be similar. Evolution of ETPs must have occurred in all Strigomonadinae but BLASTn analysis of the ETPs was only able to identify ETP5 and ETP9 in *S. culicis*. Initially this was thought to be due to incomplete genomic data for most Strigomonadinae, but more in-depth analysis by comparing upstream and downstream loci instead of the GOI itself revealed an ORF roughly fitting in length to *AdEtp2*. The found gene, termed *StcEtp2*, was highly divergent from *AdEtp2* but shared its unique features among the ETPs. The high proline content in the N-terminus, three asparagine stretches, substituted with glutamine in *StcETP*2, and what appears to be a structured C-terminus (Figure 2.20). Structure prediction by Alphafold revealed a similar structure, consisting of a total of 4 α–helices and 7 β–sheets for *Ad*ETP2 and 4 for *StcETP*2 (Figure 2.21). With no significant hit of the PDB files against the PDB archive no clues on the function of these proteins could be obtained from the Alphafold-predicted structure. Direct comparison of the two structure predictions against each other revealed that the proteins are in fact mirrored. This may be an explanation why ETP2 in *A. deanei* and *S. culicis* are highly diverse in sequence even though the genes likely evolved from the same progenitor and fulfill the same function in the ES. Localization seems also to be conferred in both proteins by the C-terminal domain as N-terminal ETP2 domains fused to eGFP showed only very mild cytosolic fluorescence (*Ad*ETP2$_{aa1\text{-}242}$-eGFP) or no fluorescence at all (*StcETP*2$_{aa1\text{-}295}$-eGFP) (Figure 2.23).

The identical localization of both *Ad*ETP2 and *StcETP*2 in *A. deanei* proves that recruitment to the ES and the constriction site takes place and the structures necessary for correct targeting of *StcETP*2 are recognized in *A. deanei* but functional complementation is not possible as no Δ–*AdEtp2*$^{eGfP\text{-}StcEpt2/HygR}$ strain could be generated. *Stc*ETP2 is recruited to the same intracellular localization as *Ad*ETP2, but the divergent evolution of the protein seems to interfere with essential functions *in vivo*. eGFP-*StcETP*2 was overall less abundant in cells than mSCARLET-*Ad*ETP2 when epifluorescence microscopy was performed but an increase in eGFP-*StcETP*2-positive cells was observed in stationary phase cultures (Figure 2.22). Which factors stabilize eGFP-*StcETP*2 in stationary cultures is not clear, but the same effect was not observed for any of the *Ad*ETP2 fusion constructs. As *S. culicis* was already successfully

transfected in our institute, *Stc*ETP2 will be analyzed in the future in *S. culicis* as well. Production of *Ad*ETP2 and *Stc*ETP2 in *S. culicis* will elucidate if this late recruitment does occur in *S. culicis* too or if it is an artifact of heterologous gene expression in *A. deanei.*

The identification of *StcEtp*2 outside of conventional screening methods in the genome of *S. culicis* proves that searching for ETP homologs in other SHTs may not be trivial, even with full sequence information available as evolution of ETPs that are not highly conserved throughout trypanosomatids (such as ETP5) may have resulted in considerable sequence divergence.

3.9 Experimental analysis of the putative PG hydrolase activity of ETP7

Peptidoglycan restructuring is not only crucial in free-living bacteria but even in intracellular species only very few bacteria lack a cell wall such as the genus *Mycoplasma*. Peptidoglycan as a target for nuclear control of plastid division has been found in Glaucophyte algae and some basally branching Viridiplantae (Miyagishima *et al.*, 2014). The absence of several crucial proteins of the divisome in *Ca* K. crithidii strongly suggests host-encoded proteins fill the gaps. Annotation of ETP7 as a putative 'phage tail lysozyme' makes it a likely candidate to take part in the divisome.

An *in vitro* approach was chosen to study interaction of ETP7 with PG. Since purified ETP7 was to be tested for its catalytic activity, denaturing agents were avoided in all purification steps. Production of ETP7 in *E. coli* led to formation of inclusion bodies, which contain high concentrations of the heterologous protein but are not correctly folded (Fahnert, Lilie and Neubauer, 2004). This could be alleviated by targeting of ETP7 to the periplasm via a pelB-tag in *E. coli* BL21 (Sockolosky and Szoka, 2013) or expression with a SUMO-tag in *E. coli* C41 to increase solubility of the construct (Butt *et al.*, 2005). *E. coli* growth under overexpression is not affected as neither the cytosolic expression nor periplasmic targeting led to any observable growth impairment based on OD_{600} measurement and microscopy.

During initial expression tests it was noticed that detection of ETP7 by Western blot in whole cell lysates was only achieved consistently when 6 M urea was added to the protein sample buffer. The addition of urea in the sample buffer has been reported to improve solubility for non-histone nucleus proteins and membrane proteins previously (Takeya *et al.*, 2018). Even though ETP7 does not contain any predicted transmembrane domains (Hallgren *et al.*, 2022) or amphipathic helices according to HELIQUEST (Gautier *et al.*, 2008), urea is necessary for Western blot based detection of ETP7.

Purification attempts under native conditions with or without Triton X-100 at 0.1% (v/v) via IMAC lead to massive protein degradation irrespective of protease inhibitor addition when high protein amounts

were loaded (Figure 2.25 B). When eluted ETP7 was concentrated, most remaining ETP7 was also degraded. As ETP7 seemed stable in *E. coli* whole cell lysate, ETP7 is most likely proteolytic at high concentrations.

Incubation with Bocillin FL allowed for detection of penicillin binding activity. ETP7 showed binding to Bocillin FL in all tested constructs, although affinity seemed reduced in the ETP7$_{\Delta 392\text{-}398}$ construct, which was anticipated as deletion of this domain should have destabilized the putative PG binding pocket (Figure 2.32). These results indicate that ETP7 may have evolved additional abilities outside from lysozyme-like protein as lysozymes are not affected by β–lactams. In fact, lysozymes have been shown to counteract the activity of β–lactams by degradation of the sacculus and prohibiting the build-up of osmotic pressure in bacteria (Kawai, Mickiewicz and Errington, 2018).

Hydrolytic activity of ETP7 against PG was tested by two independent methods. The zymogram allows screening of PG hydrolases in whole cell lysates as well as in purified proteins, but due to treatment with SDS and reducing agents to separate the proteins via SDS-PAGE, denaturation of protein samples will occur. Successful in-gel renaturation depends on the individual protein and extensive screening of different buffers can be necessary to find suitable experimental conditions. This results in a lot of uncertainties if the POI is rendered dysfunctional due to failed renaturation or a lack of predicted activity. ETP7 did not exhibit any PG-hydrolytic activity under any conditions tested for the zymograms. However, also endogenous *E. coli* PBPs showed only very low or no recognizable PG hydrolytic activity in these assays (Figure 2.36), suggesting that further optimization of the procedure might be necessary.

The second method was incubation of crude IMAC elutions with either PG from *M. luteus* sacculi to measure lytic activity by a decline in turbidity or with RBB-labeled PG to measure lytic activity by a release of the dye. Both approaches rely on purified proteins but for exploratory experiments the crude IMAC elutions were considered acceptable. Both experiments did not show any lytic activity for any of the tested ETP7 containing elutions. Even addition of 100 µl of Elution 2-4 instead of 8 µl as described in 4.5.9 did not show any increase in PG degradation (data not shown). An extremely faint increase during the RBB release assay could be observed for E2 (Figure 2.35) but as the tested elutions are still relatively crude a contamination with *E. coli*-derived hydrolases cannot be excluded.

Currently none of the assays detected a hydrolytic activity for ETP7. Reasons are manifold, as heterologously expressed ETP7 may rely on eukaryotic protein expression and folding mechanisms, not found in *E. coli*. Maybe ETP7 exhibits function only when in complex with other proteins, as has been shown for FtsW (Taguchi *et al.*, 2019). Or maybe ETP7 is not able to cleave mature PG and instead interacts with newly synthesized lipid II, which would also fit better into the role of the missing PBP3

from *Ca.* K. crithidii genome. PBP3 has transpeptidase activity cleaving the D-Ala-D-Ala peptide bond allowing crosslinking of nascent PG through the peptide side chains (Schleifer and Kandler, 1972).

To tackle the issue of expression of ETP7 in *E. coli*, the trypanosomatid *L. tarentolae* may become a suitable expression system in the future as expression in another closely related trypanosomatid should avoid problems regarding protein confirmation and inclusion body formation. Currently it seems simply due to detection issues of the current α–His AB in *L. tarentolae*-expressed proteins that ETP7 failed to be detected. This should be simple to solve as cloning of eGFP-ETP7 into *L. tarentolae* expression vectors will ensure the currently used α–eGFP antibody will allow detection of the expressed protein. Furthermore, cleavage of the eGFP for downstream assays is unnecessary since functional complementation could be proven by generation of a Δ–*Etp7*$^{eGfp\text{-}Etp7/HygR}$ *A. deanei* cell line.

PG hydrolases vary greatly in their cleaving targets (Delcour *et al.*, 1999). Instead of cleaving of PG future assays could first focus on the questions if ETP7 is able to bind PG (Firczuk and Bochtler, 2007; Wehbi *et al.*, 2011; Sauvage *et al.*, 2014) or lipid II (Bolla *et al.*, 2018). Assays covering activities of other hydrolases should be tested out in the future as well such as e.g. glucosaminidase and N-acetylmuramoyl-L-alanine amidase activity (García-Cano *et al.*, 2015).

3.10 Outlook

In this thesis the previously developed molecular toolbox for *A. deanei* has been used to identify and study the function of several host-encoded proteins targeted to the bacterial ES. From a total of 14 candidates, 7 proved to be in proximity to the ES. Some proteins evolved from genes of trypanosomatid origin or probably gained new functions related to the control of ES. Most of the ETPs are novel, uncharacterized proteins exclusive to the Strigomonadinae. Exploration of their function is key to understand how host and ES can communicate, exchange metabolites, and divide in synchrony. Of particular interest here is the trio of ETP2, ETP7 and ETP9 based on their concentration at the constriction site of the ES. *A. deanei* as a genetically tractable emerging model organism to study endosymbiosis on the verge to organellogenesis is still very young and the family of Strigomonadinae obtained a lot of subtle but impactful changes to their metabolism most likely influenced by the acquisition and establishment of the ES.

There are many unanswered questions how *A. deanei* is controlling the ES. A clear answer to some of these questions is directly related to the function of the ETPs identified during the course of this study. It is now crucial to test new strategies and molecular tools allowing for the observation of the effects that the loss of specific protein has in the organism. Due to their essential role in the *A. deanei* strain ATCC-PRA 265 under the current culture conditions used, establishment of a conditional system is key

to further investigate the function of the ETPs. Several strategies have been tested but suffered from severe limitations or were incompatible with *A. deanei* under the tested conditions altogether.

Our understanding of SHTs is still limited but at the same time offers a plethora of new discoveries in the field of endosymbiosis. Unraveling the mechanisms and structures involved in metabolite exchange and cell cycle orchestration in *A. deanei* may become a prime example how an organelle-like tight endosymbiont integration without massive protein import can be achieved.

4 Materials

4.1 Reagents and Kits

Table 4.1 Enzymes

Name	Function	Manufacturer
DNAse I	cleavage of DNA / removal of DNA	Thermo Fisher
Lysozyme	β– 1,4 glycosidic bond hydrolysis between NAM and NAG	Sigma-Aldrich
Phusion DNA Polymerase	amplification of DNA during PCR	New England Biolabs
Restriction enzymes	Restriction of DNA	New England Biolabs
T4-DNA Ligase	DNA ligation	New England Biolabs
T5 exonuclease	creates single-strand DNA 3' overhangs	New England Biolabs

Table 4.2 Protease inhibitors

Name	Application	Manufacturer
cOmplete EDTA-free Protease Inhibitor Cocktail	Preparation of cell extracts from protein overexpression in *E. coli* or *A. deanei* endosymbiont isolation	Roche
E64	Preparation of cell extracts for ES isolation from *A. deanei*	Sigma-Aldrich
Tosyllysine Chloromethyl Ketone (TLCK)	Preparation of cell extracts for ES isolation from *A. deanei*	Sigma-Aldrich
Phenylmethylsulfonylfluorid (PMSF)	Preparation of cell extracts for ES isolation from *A. deanei*	Sigma-Aldrich
SIGMAFAST EDTA-free Protease Inhibitor Cocktail	Preparation of cell extracts from protein overexpression in *E. coli*	Sigma-Aldrich

Table 4.3 Kits

Name	Application	Manufacturer
Monarch DNA Gel Extraction Kit	Extraction of PCR products from agarose gels	New England Biolabs
DNeasy Blood and Tissue Kit	Extraction of gDNA from *A. deanei*	Qiagen
NucleoSpin Gel and PCR Clean-up Kit	Purification of DNA from PCR reactions and extraction from agarose gels	Macherey-Nagel
NucleoSpin Plasmid Mini Kit for plasmid DNA	Purification of plasmids from *E. coli*	Macherey-Nagel
Plasmid Plus Midi Kit	High-yield purification of plasmids	Qiagen
Gold conjugation kit ab201808	Colloidal gold labeling of antibodies	Aurion

Table 4.4 Antibodies

Name	Application	Manufacturer
mouse-α–V5 ab27671	Western blot, IFA, immunogold-TEM	Abcam
rabbit-α–GFP ab6556	Western blot, immunogold-TEM	Abcam
mouse-α–His IgG-HRP	Western blot	Santa Cruz Biotechnology
α–mouse HRP #7076	Western blot	Cellsignal
α–rabbit HRP #7074	Western blot	Cellsignal
α–RFP [5F8]	Western blot	Chromotek
Rabbit-α–V5 V8137	Western blot	Sigma-Aldrich
Goat-α–mouse Alexa fluor 594 nm	IFA	Thermo Fisher
Rabbit-α–mouse 315-005-048	immunogold-TEM	Dianova
goat-α–mouse 6 nm gold 115-195-146	immunogold-TEM	Jackson ImmunoResearch

goat-α–mouse 15 nm gold 815.022	immunogold-TEM	Aurion
Protein A 15 nm gold	immunogold-TEM	Cell Biology Utrecht
anti-digoxigenin-AP fab fragments	Southern blot	Roche

Table 4.5 Antibiotics

Name	final concentration in culture	Manufacturer
Ampicillin	*E. coli*: 50 µg/ml	Carl Roth
Hygromycin	*A. deanei* ATCC-PRA-265: 500 µg/ml	Invivogen
	A. deanei ATCC-30969: 500 µg/ml	
	L. tarentolae: 100 µg/ml	
Phleomycin	*A. deanei* ATCC-PRA-265: 200 µg/ml	Invivogen
Chloramphenicol	*A. deanei*: 4 µg/ml	Carl Roth
G418 (Geneticin)	*A. deanei* ATCC-PRA-265: 500 µg/ml	Sigma-Aldrich
	A. deanei ATCC-30969: 500 µg/ml	
	L. tarentolae: 50 µg/ml	
Tetracycline	*L. tarentolae*: 10 µg/ml	Sigma-Aldrich
Nourseothricin	*L. tarentolae*: 100 µg/ml	Carl Roth

4.2 Media and Culture Conditions

4.2.1 Cultivation of trypanosomatids

The ES-harboring strain *A. deanei* ATCC PRA-265 was grown in Brain Heart Infusion (BHI) broth supplemented with 10 % heat-inactivated horse serum (HS) and hemin (10 µg/ml) after transfection **(Motta *et al.*, 2013)**. After limiting dilution ATCC PRA 265 was grown without HS. Cultures were grown at 28°C without agitation.

The aposymbiotic strain *A. deanei* ATCC 30969 was initially recovered in ATCC 1034 medium. Since growth in BHI and ATCC 1034 was indistinguishable, BHI supplemented with 10 % heat-inactivated HS and 10 µg/ml hemin was used in all further analyses. Cultures were grown at 28°C without agitation.

Leishmania tarentolae was grown at 28°C without agitation in BHI + 10% heat-inactivated HS with 20 µg/ml hemin.

Table 4.6 Media for trypanosomatids

Name	Component and stock solution	
	BHI (completed) 1 L	**Manufacturer**
BHI powder	37 g of 5 g/L beef heart (infusion from 250 g), 12.5 g/L calf brains (infusion from 200 g), 2.5 g/L disodium hydrogen phosphate, 2 g/L D(+)-glucose, 10 g/L peptone, 5 g/L sodium chloride, powder	Sigma-Aldrich
Hemin	4 ml of 2.5 mg/ml stock solution in 50 mM NaOH, sterile filtered	Sigma-Aldrich
Horse serum	100 ml, heat-inactivated at 56°C for 30 min	Sigma-Aldrich
Preparation	37 g BHI were dissolved in 900 ml dH_2O and autoclaved. After cooling to RT 10 % of inactivated HS and 10 µg/ml hemin were added. Completed medium was stored at 4°C.	
	ATCC 1034	**Manufacturer**
Peptone	10 g, powder	Carl Roth
Yeast Extract	10 g, powder	Gibco
Yeast nucleic acid	1 g, powder	Thermo Fisher
Folic acid	7.5 ml of stock solution (2 mg/ml in DMSO)	Sigma-Aldrich
Hemin	400 µl of stock solution (2.5 mg/ml in 50 mM NaOH, sterile filtered)	Sigma-Aldrich
Fetal bovine serum	100 ml of heat-inactivated at 56°C for 30 min	Sigma-Aldrich
Buffer solution	20 ml of stock solution (18.1 g KH_2PO_4, 25.0 g Na_2HPO_4, dissolved in 1.0 L of dH_2O, pH adjusted to 6.5, autoclaved)	
Preparation	10 g peptone, 10 g yeast extract, 1 g yeast nucleic acid were dissolved in 880 ml of dH_2O and autoclaved. 100 ml of fetal bovine serum, 20 ml of buffer solution, 15 mg folic acid and 1 mg of hemin were added aseptically to the medium. Completed medium was stored at 4°C.	

4.2.2 Cultivation of *Escherichia coli*

Cultures for plasmid generation

E. coli Top10 cells were grown in LB medium supplemented with 100 µg/ml ampicillin at 37°C at 180 rpm or on plates supplemented with 2 % agar.

Cultures for ETP7 expression

E. coli BL21 (DE3), C41, C43 and LOBSTR were grown in LB medium or 2xYT medium with 100 µg/ml ampicillin at 180 rpm at 37°C until an OD_{600}= 0.5 was reached and then transferred to 28°C at 180 rpm.

Table 4.7 *E. coli* growth media

Name	**Component and stock solution**	
	Lysogeny broth (LB) 1 L	**Manufacturer**
Tryptone	10 g, powder	Gibco
Yeast extract	5 g, powder	Gibco
Sodium chloride	5 g, powder	Merck
Agar	20 g, powder	Carl Roth
Preparation	10 g or tryptone, 5 g of yeast extract and 5 g of sodium chloride are dissolved in 1 L of dH_2O and autoclaved. When plates were to be poured, 20 g of agar were added before autoclaving.	
	2xYT 1 L	**Manufacturer**
Tryptone	16 g, powder	Gibco
Yeast extract	10 g, powder	Gibco
Sodium chloride	5 g, powder	Merck
Preparation	16 g tryptone, 10 g yeast extract and 5 g sodium chloride are dissolved in dH_2O, and the pH adjusted to 7.0. Sterilized by autoclaving.	

4.3 Molecular biology methods

4.3.1 Polymerase chain reaction

DNA was amplified via PCR. Depending on the application the reaction volume was adjusted. For trypanosomatid gDNA PCR betaine was added to the reaction when needed (Henke *et al.*, 1997). Annealing temperature and elongation times were calculated depending on the primer properties and the expected PCR product length according to manufacturer recommendations.

For *E. coli* colony PCR some cells were scratched with a pipette tip off an agar plate and transferred into 10 µl of a reaction mix.

Verification of clonal cultures of trypanosomatids was performed via touchdown PCR (Don *et al.*, 1991; Korbie and Mattick, 2008). This PCR uses initially an annealing temperature above the calculated optimum of the primers for the initial PCR cycles and then decreases the temperature stepwise, to enforce high binding specificity.

Site directed mutagenesis to alter single bases within a sequence or to obtain truncation of genes was achieved by modification of primers.

Table 4.8 PCR components

Reagents	**gDNA PCR reaction volume (10 µl) [final concentration]**	**Fragment PCR reaction volume (10 µl) [final concentration]**
ddH_2O	3.2 µl	5.7 µl
5x HF oder GC Puffer	2 µl [1x]	2 µl [1x]
5 M betaine	2.5 µl [1.25 M]	-
10 mM dNTPs	0.2 µl [200 µM]	0.2 µl [200 µM]
10 µM forward primer	0.5 µl [0.5 µM]	0.5 µl [0.5 µM]
10 µM reverse primer	0.5 µl [0.5 µM]	0.5 µl [0.5 µM]
Phusion (New England Biolabs) DNA-Polymerase	0.1 µl [0.5 units]	0.1 µl [0.5 units]
Template-DNA	1 µl [50-250 ng]	1 µl [20-100 ng]

Table 4.9 PCR program

Step	Time [s]	Temperature [°C]	
1. Initial denaturation	180	98	
2. Denaturation	10	98	30x cycles
3. Annealing	10	50-72	
4. Extension	30 s per kBp	72	
5. Final extension	300	72	
6. Storage	∞	16	

4.3.2 Separation of DNA by agarose gels

DNA was mixed with loading dye containing 5% glycerol and 0.005% bromophenolblue final concentration and loaded onto a 1-2% TAE agarose gel (depending on the size of the expected fragment) containing SYBR Safe for staining (Thermo Scientific). The gel was separated in 1x TAE buffer at 120 V for 30 min to 1 h.

Table 4.10 50x TAE buffer

Reagent	Quantity
Tris	242 g
Acetic acid	57.1 ml
Na_2EDTA	7.43 g
Preparation	Dissolve in dH_2O and adjust volume to 1 L.

4.3.3 Gel extraction of nucleic acids

The agarose gel was illuminated with UV light or blue light and the DNA product was excised. DNA was extracted from the gel via Monarch Gel Extraction kit (New England Biolabs) or NucleoSpin Gel and PCR Clean-up Kit (Macherey-Nagel) according to the manufacturer's protocol.

4.3.4 Construction of plasmids

Plasmids were assembled via Golden Gate (Engler, Kandzia and Marillonnet, 2008) or Gibson assembly (Gibson *et al.*, 2009). All gene fragments were amplified from previously assembled plasmids or from gDNA extracted from *A. deanei*, *S. culicis* or *L. tarentolae*. Resistance cassettes and regulatory elements were amplified as described previously (Kokkori, 2018). 20 fmol of fragments was added in equimolar

ratio in a 15 µl volume. When the size of one fragment was less than one fifth of another fragment, 60 fmol of the smaller fragment were added instead (backbone:insert ratio of 1:3). For Gibson assembly the assembly master mix was completed with 5 µl of the DNA fragments and dH_2O to 20 µl and incubated at 50°C for 1 h. 5 µl of the reaction mix were transformed into *E. coli* Top10.

For Golden Gate assembly T4 ligase was mixed with T4 ligase buffer, BsaI-HFv2 and the DNA fragments, adjusted to 15 µl with dH_2O. The reaction was incubated alternating between 37°C and 16°C for restriction and ligation of the fragments. After inactivation of the reaction at 80°C 5 µl of the reaction mix were transformed into *E. coli* Top10.

Table 4.11 Gibson assembly mix

Reagent	Quantity	Reagent	Quantity
5x isothermal reaction buffer (6 ml)		**Assembly master mix**	
1 M Tris-HCl pH7.5	3 ml	5x isothermal reaction buffer	320 µl
2 M $MgCl_2$	150 µl	1U/µl T5 exonuclease	6.4 µl
100 mM dGTP	60 µl	2 U/µl Phusion DNA polymerase	20 µl
100 mM dATP	60 µl	40 U/µl Taq DNA ligase	160 µl
100 mM dCTP	60 µl	**Preparation**	
100 mM dTTP	60 µl		
1 M DTT	300 µl	Adjust the total volume to 1.2 ml with dH_2O and mix. Aliquot the assembly master mix in 15 µl aliquots each and store at -20°C.	
PEG-8000	1.5 g		
100 mM NAD	300 µl		

Table 4.12 Golden Gate mix

Golden Gate mix (15 µl)		Ligation protocol	
10x T4 ligase buffer	1.5 µl	37°C 2 min	30x

T4 ligase (400,000 units/ml) (New England Biolabs)	0.75 µl	16°C 5 min	
BsaI-HFv2 (New England Biolabs)	0.5 µl	37°C	5 min
DNA fragments	x µl	16°C	∞
dH_2O	up to 15 µl	80 °C	5 min

4.3.5 Measurement of DNA concentration

The DNA concentration was measured with a Nanodrop 2000c (Thermo Scientific) or a NP80 (Implen) nanophotometer at 260 nm. Impurities were estimated by 260/280 nm and 260/230 nm ratios.

4.3.6 Sequencing of plasmid DNA

Sanger sequencing of DNA was performed by Eurofins Genomics and Microsynth. Around 1 µg of plasmid DNA or 100 ng of PCR product were mixed with 20 pmol of a primer in a total volume of 15 µl and send to the respective company. The results were aligned via Benchling or Bioedit by MAFFT (Katoh, 2002) or Clustal Omega **(Sievers *et al.*, 2011)** algorithm.

4.3.7 Southern blot analysis

Genomic integration of transfected genetic elements was verified by Southern blot (Southern, 1975) as previously described (Kokkori, 2018). 5 µg gDNA was digested with appropriate restriction enzymes overnight. Digested DNA samples were separated at 100 V in a 1% TAE agarose gel for 2 h. The digest of the gDNA was confirmed briefly under UV light, creating the typical 'smear' pattern. The gel was then incubated for 20 min in 0.25 M HCl, followed by 20 min in denaturation buffer and lastly 20 min in renaturation buffer. The DNA is transferred through capillary action to a positively charged nylon membrane (0.45 µm, GE Healthcare Life Sciences) using 20xSSPE transfer buffer through a Whatman filter paper salt-bridge overnight. On the next day the DNA was fixed on the membrane using 120 mJ UV-irradiation using a UVP hybrilinker oven (Analytic Jena). The membranes were incubated with hybridization buffer for 20 min at 65°C in a hybridization tube. A digoxigenin-11-dUTP (DIG) labeled gene-specific probe was prepared by exchanging half of the reaction volume of dNTPs with a DIG DNA-labeling mix (Roche). The PCR reaction was mixed with hybridization buffer and denatured at 98°C for 5 min. This mix was applied to the membrane and incubated at the calculated hybridization temperature T_{opt} (see below) under continuous agitation overnight.

$$T_m = 49.82 + 0.41(\%G + C) - \left(\frac{600}{l}\right)$$

$$T_{opt} = Tm - 20\ to\ 25°C$$

With T_m = melting point of probe-target hybrid; (%G+C) = percent of G and C content in probe sequence; l = length of the probe in base pairs; T_{opt}= optimal temperature for hybridization of the probe to the target.

The hybridization probe was removed, and the membrane was washed once with Southern-wash I, II and III solution at 65°C each for 15 min. Afterwards the membrane was washed for 5 min with DIG-wash solution at RT and then blocked in DIG-2 for 30 min. The membrane was then incubated with anti-digoxigenin-AP fab fragments (Roche) diluted 1:10,000 in DIG-2 solution for 90 min and then washed thrice with DIG-wash solution for 5 min and once for 15 min. The membrane was then equilibrated in DIG3 solution for 5 min and finally incubated with CDP-star solution (Roche) diluted 1:100 in DIG3 solution at 37°C. Excess solution was removed and the chemiluminescence was detected in a Chemidoc MP+ (Bio-Rad).

Table 4.13 Southern blot buffers

Name	**Components**
Denaturation Solution	1.5 M NaCl 0.4 M NaOH
Neutralization solution	0.5 M Tris, pH 7.0 3.0 M NaCl
20x SSPE buffer (Transfer buffer)	3 mM NaCl 227 mM NaH2PO4 x H20 20 mM Na2EDTA x 2H2O, Set pH to 7.4 with NaOH
Denhardt's solution	2% (w/v) BSA fraction V 2% (w/v) Ficoll 2% (w/v) PVP (Polyvinyl Pyrrolidone, SIGMA PVP-360)
Southern Hybridization buffer	26% (v/v) SSPE (20x) 5% (v/v) Denhardt's solution 5% (v/v) SDS (10%)
Southern wash Buffer I	2x SSPE (20x) 0.1% SDS (10%)

Southern wash Buffer II	1x SSPE (20x) 0.1% SDS (10%)
Southern wash Buffer III	0.1x SSPE (20x) 0.1% SDS (10%)
DIG-1	0.1 M maleic acid 0.15 M NaCl, Set pH to 7.5 using NaOH
DIG-wash	0.3% (v/v) Tween20 in DIG1 solution
DIG-2	1% (w/v) skimmed milk powder in DIG1
DIG-3	0.1 M Tris-HCl 0.1 M NaCl, Set pH to 9.5

4.4 Microbiological methods and imaging techniques

4.4.1 Transformation of *E. coli*

50 µl of chemically competent *E. coli* Top10 cells were thawed on ice for 5 min and transformed with 5 µl of the Golden Gate or Gibson assembly reaction mix or 10 ng of purified plasmid, and incubated for 30 min on ice. Cells were heat shocked at 42°C for 45 s and placed on ice for 2 min. 40 µl of the competent cells were plated directly on LB-amp plates and incubated overnight at 37°C.

4.4.2 Isolation of plasmid DNA from *E. coli*

Plasmid DNA was extracted from 5 ml of *E. coli* overnight cultures in LB-amp medium by Miniprep Kits (Qiagen or Macherey-Nagel) according to manufacturer protocol. Qiagen Midiprep Kit Plus was used for isolation of plasmids from 35 ml *E. coli* culture to obtain high amounts of plasmid for transfection of *A. deanei*.

4.4.3 Transfection of *A. deanei* and *L. tarentolae*

A. deanei was transfected essentially as described previously (Morales *et al.*, 2016) with some modifications. $1x10^7$ cells were resuspended in 20 µl of solution P3 (Lonza) containing 5 µg of restricted cassette. The cells were electroporated using the program FP-158 in the Nucleofector 4D (Lonza). After transfection the cells were transferred into 5 ml of supplemented BHI medium and grown at 28°C for 6 h. Antibiotics were added to the culture according to the stated concentrations in Table 4.5 and 2.5 ml were used for limiting dilution. The remaining 2.5 ml were grown at 28°C for 7 days.

$1x10^7$ cells of *L. tarentolae* were transfected the same way as *A. deanei* but the cells were transferred into 10 ml of supplemented BHI medium and grown at 28°C for 24 h before addition of antibiotics. After 5-7 days limiting dilution was performed.

4.4.4 Limiting dilution

To generate clones in liquid medium, cultures were diluted to 1 cell per ml and distributed in aliquots of 200 µl into a sterile 96-well plate and grown at 28°C for seven days. When limiting dilution was performed 6 h after transfection, 2.5 ml of the culture was added to 22.5 ml of supplemented BHI medium containing the respective antibiotics and distributed in 200 µl aliquots into a sterile 96-well plate. Clones were identified by turbid wells, from which a few microliter were used for inoculation of 2 ml of fresh medium and 150 µl were used for gDNA extraction and PCR verification of the cassette insertion.

4.4.5 Extraction of gDNA from trypanosomatids

To verify clonal cultures via PCR, gDNA was isolated using DNAzol (Thermo Scientific). 150-400 µl of a mid- to late-log culture was pelleted at 7000xg for 5 min and resuspended in 200 µl DNAzol. Released DNA was separated from cell debris at 10,000xg for 10 min. The supernatant was transferred to a new tube and mixed with 200 µl of 100% ethanol. After 3 min at RT the DNA was pelleted at 4000xg for 3 min, the supernatant discarded, and the pellet was washed twice with 75% ethanol. The DNA was resuspended in 10 µl of dH_2O.

DNA extraction for Southern blots was done by DNeasy Blood and Tissue Kit (Qiagen) from 2 ml of mid- to late-log culture. Cells were pelleted at 7000xg 5 min and resuspended in 200 µl of PBS pH 7.4, 20 µl of Proteinase K and 200 µl of buffer AL. Cells were vigorously vortexed for one minute three times with a break of one minute. All downstream steps were done according to manufacturer protocol.

4.4.6 Fluorescence microscopy

100 µl of *A. deanei* cultures at mid log phase were pelleted at 7000xg for 5 min and resuspended in 100 µl of PBS and 100 µl 4% PFA. Cells were fixed protected from light at RT for 10 min and washed twice with PBS to remove the PFA. ~10^5 cells were spotted on poly-L-lysine covered slides and incubated with 10 µg/ml Hoechst 33342 for 10 min. The slide was washed twice with PBS to remove unbound Hoechst and covered with Slow Fade Diamond (Thermo Fisher) or Prolong Diamond (Thermo Fisher). The cells were imaged at a Zeiss Axio Imager.A2 using Zen 2.5 blue edition or Leica TCS SP8 STED 3X (LAS X). Images were processed with ZEN, ImageJ, and Affinity designer.

Table 4.14 Preparation of 4% PFA

4% PFA (10ml)	
0.4 g PFA	
20 µl 1 M NaOH	**Preparation**
0.4 g of PFA are dissolved in 60°C warm 1xPBS on a magnetic stirrer under a fume hood. 20 µl of 1 M NaOH are added and stirred continuously at 60°C until all PFA has dissolved. The solution is filtered through a 0.2 µm sterile filter and stored light protected at 4°C.	

4.4.7 Immunofluorescence assay (IFA)

A. deanei cells were fixed and spotted on poly-L-lysine covered slides as described before. The cells were permeabilized with 0.1% Triton X-100 in PBS (PBST) for 20 min. The slide was then incubated with blocking solution (BS) (10% goat serum (Aurion) in PBS) for 30 min. After that, the 1st antibody was diluted in BS and incubated for 30 min on the slide. The slide was washed three times with BS. A 2nd AB conjugated to a fluorophore was diluted in BS and incubated for another 30 min on the slide. The slide was washed again 3x with BS and then stained with Hoechst 33342 and covered with Slow Fade or Prolong Diamond as described above (see section 4.4.6).

4.4.8 Fluorescence in situ hybridization

~10^5 cells were fixed as described above (see section 4.4.6) and spotted on slides coated with gelatin. The cells were dehydrated with 50%, 80% and 100% ethanol for 3 min each. 90 µl of hybridization buffer (Table 4.15) mixed with 10 µl of the universal bacterial probe Eub338 at a concentration of 50 ng/µl, binding to bacterial 16S rRNA and coupled to Cy3 (Amann, Krumholz and Stahl, 1990; Cottrell and Kirchman, 2000; Amann and Fuchs, 2008), was pipetted onto the cells and incubated, protected from light, for 90 min in a humid chamber at 46°C. Unbound probe was removed by rinsing the slides with wash buffer (Table 4.15) at 48°C and then incubated with wash buffer for 25 min at 48°C light protected. The slides are then rinsed with dH_2O and incubated with Hoechst 33342 as described above (see section 4.4.6). Finally, the slides were covered with Slow Fade or Prolong Diamond as described above (see section 4.4.6).

Table 4.15 Hybridization buffer and wash buffer composition

Reagent	Hybridization buffer	Wash buffer
NaCl	900 mM	80 mM
Tris-HCl pH 7.2	20 mM	20 mM
Formamide	35%	-
SDS	0.01%	0.01%

4.4.9 Embedding of cells in LR-white resin

5 ml of mid-log phase culture was pelleted at 7000xg for 5 min and resuspended in 0.1% OsO_4, 2% PFA, 0.5% glutaraldehyde in 0.1 M cacodylate buffer pH 7.4 for 45 min on ice. The cells were washed three times with cacodylate buffer and resuspended in 10 µl of the same buffer. 5 µl of this highly concentrated cell emulsion was injected into liquid 6% low melting agarose solution in a reaction tube to form a small, enclosed sphere and cooled on ice until the agarose solidified. The sphere was then cut out from the agarose block without disrupting it, leaving only a small layer of agarose around. The pellet was dehydrated in 15 min-steps at 15%, 30%, 45% ethanol on ice and then at 60%, 75%, 90% and 100% ethanol at -20°C. The last step was performed overnight. The ethanol was then exchanged on a roller with LR white resin (medium grade, London resin company) mixed with ethanol stepwise at 20%, 33%, 50%, 67%, 80%, and 100% at RT. The final step was again performed overnight. The next day, the LR white was exchanged once more with fresh LR white and incubated for 1 h. The pellet was transferred into a gelatin capsule and LR white was added on top. The capsule was sealed with a gelatin cap, placed in a reaction tube, and incubated at 50°C for 72 h for polymerization. 50 nm thin sections were placed on formvar-coated nickel grids and stored until further immunosteps were performed.

4.4.10 Fixation of cells for cryosectioning

10 ml of mid-log phase *A. deanei* cultures were pelleted at 2000xg for 10 min and washed twice with 0.1 M phosphate buffer (PB) pH 7.2. The cells were fixed in 4% PFA in 0.1 M PB for 2 h at RT. The fixation buffer was exchanged afterwards and then incubated at 4°C overnight. All further downstream steps were performed according to (Tokuyasu, 1973) by Miriam Bäumers from the Center of Advanced Imaging (CAi, Heinrich Heine university Düsseldorf).

4.4.11 IFA of 250 nm rough sections of Tokuyasu embedded cells

Cryosections were initially incubated with dH_2O at 37°C for 30 min to remove the protective methyl cellulose layer. The sections were then transferred to droplets of PBS-T (0.05% Tween 20) and equilibrated for 30 min at RT. The PBS-T was removed and the sections blocked with blocking solution (BS, Aurion) for 1 h at RT. BS was exchanged with α–V5 AB (Abcam) diluted 1:20 in BS and incubated

for 1 h. The sections were then washed three times for 5 min with PBS-T to remove unbound AB. A drop of ready-to-use goat α–mouse Alexa fluor 594 nm was applied on top of the sample and incubated for 30 min protected from light. The samples were again washed with PBS-T three times for 5 min, residual buffer was removed and the samples covered with Prolong Diamond for imaging the next day.

4.4.12 *E. coli* overexpression optimization

E. coli overexpression strains were inoculated in 20 ml of either LB-amp or 2YT-amp medium and grown overnight at 37°C at 180 rpm. The main culture (100 ml) was inoculated with 2 ml of the overnight culture and grown under the same conditions until an OD_{600}= 0.6 was reached (approximately 2 h). 1 mM IPTG was then added to induce overexpression and the cultures were grown at temperatures ranging from 16°C to 37°C to identify the optimal overexpression conditions. The cell material was spun down at 6000xg for 15 min at 4°C, resuspended in SDS-sample buffer containing 50 mM DTT, boiled for 5 min at 95°C and stored at -20°C until further use.

Final overexpression conditions used for ETP7 constructs: 20 ml overnight cultures grown at 37°C, 180 rpm were used to inoculate 1 L of LB-amp medium and grown under the same conditions until an OD_{600}=0.6 was reached. The culture was then induced with 1 mM IPTG and transferred to 28°C, 180 rpm for 3 h. Finally, the cells were harvested at 6000xg 15 min 4°C and frozen in liquid N_2. The frozen material was stored at -80°C until further use.

4.4.13 Solubilization by Na-deoxycholate

1 g of *E. coli* wet pellet was resuspended in PBS supplemented with 1x protease inhibitor cocktail and 10 µg/ml DNAse I. The cells were disrupted by sonication for 8 min with cycles of 30 s of sonication and 30 s of cooldown on ice. Soluble and insoluble material were separated by centrifugation at 12,000xg for 15 min at 4°C. The pellet was resuspended in PBS + 0.1% (w/v) Na-deoxycholate and again separated at 12,000xg for 15 min at 4°C. The supernatant contained the membrane associated proteins solubilized by Na-deoxycholate.

4.4.14 Testing of buffer conditions for solubilization of ETP7

1 g of *E. coli* cells were resuspended in 10 ml of 50 mM sodium acetate pH 5, 50 mM MES pH 5.5, 50 mM bis-tris pH 6.5, and 50 mM Tris-HCl pH 8 + 1x protease inhibitor cocktail (Roche) each. The cells were opened by sonication as described in 4.4.15 and separated at 12,000xg for 15 min at 4°C. The supernatant was again ultracentrifuged at 120,000xg for 1 h at 4°C. Samples were taken from all supernatants and pellets.

4.4.15 Isolation of *E. coli* membranes

The periplasmic proteins were isolated according to "isolation of bacterial cell surfaces" (Quan *et al.*, 2013). 1 L of Ec59 culture and 1 L of a *E. coli* C41 transformed with the empty expression vector GPN001 were harvest after expression (4.4.12). 1 g of each pellet were resuspended very gently in ice cold TSE buffer (Tris, Sucrose, and EDTA) + 1x protease inhibitor cocktail (Roche) and the remaining 4 g of the pellets were frozen in liquid N_2 and stored at -80°C for preparation of *E. coli* membranes. The cells resuspended in TSE buffer were incubated on ice for 30 min, during which the outer membrane was disrupted. The supernatant, containing periplasmic proteins, was harvested by centrifugation at 16,000xg for 30 min at 4°C.

The membranes of the remaining *E. coli* 4 g pellets were isolated essentially as described previously (Kanonenberg *et al.*, 2019). The pellets were resuspended in 15 ml of ice cold 85.5 mM Tris-HCl pH 8.0 + 1x protease inhibitor cocktail (Roche) and homogenized through a cell disrupter (Microfluidics) four times at 100 bar. Cell debris was removed by centrifugation at 6000xg for 10 min at 4°C. The membranes in the supernatant were pelleted at 200,000xg for 1 h at 4°C. A continuous sucrose gradient (20-70% in Tris-HCl pH 8.0 + 1x protease inhibitor cocktail (Roche), prepared at a Gradient Station (BioComp Instruments)) was used to fractionate the membranes at 110,000xg for 16 h at 4°C. From the total gradient volume of 12 ml, 11 ml were fractioned from top to bottom, with the bottom 1 ml consisting of non-separated material, excluded from further analysis. The 1 ml fractions were TCA-precipitated (4.5.1) and resuspended in 100 µl of 50 mM Tris-HCl pH 8.0 + 8 M Urea + 2 mM β–mercaptoethanol, 150 mM NaCl. 25 µl of 5x SDS-SB + 50 mM DTT were added to each sample and boiled for 5 min at 95°C and stored at -20°C until further analysis.

4.4.16 Tet-inducible expression in *L. tarentolae*

Transformed *L. tarentolae* cells were grown at 28°C in 10 ml of BHI supplemented with 10% inactivated horse serum and 20 µg/ml hemin and antibiotics for selection. 20 ml of the same medium were inoculated with 10% of mid-log phase culture and immediately induced by addition of 10 µg/ml of tetracycline. The induced cultures were grown either at 28°C without agitation for up to three days or at 120 rpm for two days. 1 ml of culture was pelleted by centrifugation at 7000xg for 5 min and the cells immediately resuspended in 100 µl of buffer containing 6 M Urea and 1x SDS-SB + 50 mM DTT and boiled at 95°C.

4.5 Protein biochemical methods

4.5.1 TCA precipitation

Protein samples were precipitated by addition of 10% trichloroacetic acid (w/v). The samples were incubated on ice for 20 min and afterwards pelleted at 21,000xg for 15 min at 4°C. The pellet was washed with ice cold acetone twice and then dried at RT. Volume and buffer for resuspension were chosen depending on the downstream application.

4.5.2 Immobilized metal affinity chromatography

Isolation of recombinant proteins expressed in *E. coli* were isolated by IMAC using nickel-nitrilotriacetic acid (Ni-NTA).

E. coli cells after overexpression of ETP7 constructs were resuspended in 82.5 mM Tris-HCl pH 8.0 + 1x protease inhibitor cocktail (Roche) (purification buffer), opened by sonication and the supernatant after centrifugation at 12,000xg for 10 min at 4°C was mixed with Ni-NTA. The Ni-NTA loaded with the supernatant was incubated for 1 h at 4°C under agitation and afterwards gently spun down at 1,000xg for 3 min at 4°C. The supernatant was discarded and the Ni-NTA was washed with purification buffer + 20 mM imidazole three times. A range of 50 to 500 mM imidazole in purification buffer was applied to the Ni-NTA to elute bound proteins. ETP7 fusion proteins usually eluted at 100 mM imidazole.

4.5.3 Protein concentration measurement by Pierce™ 660 nm assay

Calibration curves were prepared by BSA of rising concentrations from 50 µg/ml to 2 mg/ml in dH_2O. 10 µl of each protein sample were mixed with 150 µl of Pierce™ 660 nm reagent and incubated for 10 min at RT in a 96-well plate. The absorption was measured at 660 nm in a plate reader.

4.5.4 SDS-PAGE

Proteins were separated according to their molecular weight by sodium dodecyl sulfate polyacrylamide gel electrophoresis (SDS-PAGE) (Laemmli, 1970). Tris-glycine-based polyacrylamide gels were prepared according to Bio-Rad handcasting polyacrylamide protocol consisting of a 4 % acrylamide stacking gel and 10 or 12 % resolving gel (https://www.bio-rad.com/sites/default/files/webroot/web/pdf/lsr/literature/Bulletin_6201.pdf). Protein samples were treated with SDS-sample buffer containing reducing agents (31.5 mM Tris-HCl pH 6.8, 10% glycerol, 1% SDS, 0.005% bromophenol blue, 10-50 mM DTT) and denatured by heat treatment, usually at 95°C for 5 min if not stated otherwise.

Proteins samples were separated in gels running in tris glycine running buffer with 0.1% SDS at 180 V 35 mA per gel for 1 h. For the preparation of figure 2.2 A and 2.3 discontinuous 4-12% bis-tris plus gels (Thermo Fisher) were used and proteins separated in 1x MES running buffer (50 mM MES (2-[N-

morpholino] ethanesulfonic acid), 50 mM Tris, 1 mM EDTA, 0.1% (w/v) SDS, pH 7.4) at 180 V for around 30-45 min.

4.5.5 Western blot analysis

Following SDS-PAGE, gels were briefly washed with water and equilibrated in Towbin transfer buffer (25 mM Tris, 192 mM glycine pH 8.3. 20% MeOH) for 10 min. 6 pieces of 0.8 mm Whatman paper (GE Healthcare) were soaked in Towbin transfer buffer in parallel. A PVDF membrane (Thermo Fisher) was activated in ethanol for 30 s, briefly washed in water and equilibrated for 10 min in Towbin transfer buffer. Three pieces of Whatman paper were placed in a transfer cassette of a Trans-Blot Turbo Transfer System (Bio-Rad), with the PVDF membrane, the gel and three more pieces of Whatman paper stacked on top. The transfer was performed using the standard SD transfer protocol for 30 min. After transfer, the membrane was briefly washed in water and placed in a blot holder, which was placed in a cartridge of the SNAP i.d.® Protein Detection System (Merck Millipore). The membrane was blocked by passing of PBS-T (0.1% tween 20) + 0.1 % skimmed milk powder (BS) through the blot holder by application of vacuum. The 1st AB was then diluted in the same buffer depending on the antibody and incubated for 10 min on the membrane. The membrane was washed four times with PBS-T and incubated with a 2nd AB coupled to HRP diluted in the BS. The membrane was again washed four times with PBS-T and incubated with HRP-substrate Luminata^{TM} Classico (Merck Millipore). Detection was performed in a Chemidoc MP (Bio-Rad) using the chemiluminescence program.

4.5.6 Coomassie staining of SDS-polyacrylamide gels and PVDF membranes

To stain all proteins separated in a polyacrylamide gel or transferred on the PVDF membranes, Coomassie Brilliant Blue R-250 (CBB) dissolved in 40% EtOH and 10% acetic acid was used. A gel was incubated in CBB solution for 30 min at RT under agitation and then transferred into destaining solution (40% EtOH + 10% acetic acid) for 30 min and exchanged twice. PVDF membranes were stained for 5 min in CBB solution and briefly rinsed twice with destaining solution and twice with dH_2O.

4.5.7 Zymogram

Zymograms were tested according to several protocols (Bernadsky, Beveridge and Clarke, 1994; Zahrl *et al.*, 2005; Vaz and Filipe, 2015). The best results were achieved with PG isolated from *Micrococcus luteus* based on the protocol by Zahrl.

Acrylamide gels were casted with 0.05% PG (w/v) embedded as a substrate for hydrolysis. After protein separation by SDS-PAGE the gels were incubated with dH_2O for 1 h at 4°C under agitation. The gels were transferred into renaturation buffers of varying pH containing 0.1% Trition X-100 for 1 h at 4°C. The buffer was replaced once and incubated at 4°C under agitation for 72 h to renature the proteins.

The gel was stained with 0.1% methylene blue in 0.01% KOH for 1 h at 4°C and destained with dH_2O until zones of clearing became visible.

4.5.8 Bocillin assay

100 ml *E. coli* cultures were harvested, and the pellets resuspended in 5 ml of 82.5 mM Tris-HCl pH 8.0 + 1x protease inhibitor cocktail (Roche) and 1 µg/ml of DNAse. 200 µl of lysate were treated with 12.5 µM Bocillin-FL and incubated light-protected at 35°C for 30 min. Protein concentration was measured by Pierce 660 nm assay of all samples. 25 µg of protein were separated until the running front left the acrylamide gel. The gel was briefly rinsed in dH_2O and imaged in the Chemidoc MP (Bio-Rad) using the Alexa fluor 488 program.

4.5.9 Turbidity-based hydrolase assay

Hydrolase activity defined as lysis of PG can be measured by a decrease in absorption at 450 nm (Shugar, 1952). 0.015% (w/v) of PG was dissolved in 50 mM potassium phosphate buffer, pH 6.24 which should result in an A_{450}=0.6-0.7. 8 µl of sample or 250 U/ml of hen egg white LZ (40,000 units = 1 mg LZ) as a positive control was added to 192 µl of PG solution and the A_{450} was measured every 5 min for 1 h at 25°C. Measurements were performed in triplicates.

4.5.10 Remazol brilliant blue labeled peptidoglycan release assay

Turbidity-based measurement is relatively insensitive and thus, may fail to identify low activity hydrolases. Sensitivity was increased by labeling of PG with Remazol brilliant blue (RBB), which is released again when PG is cleaved and the absorption at 595 nm of the cleared supernatant was measured (Zhou, Chen and Recsei, 1988; Santin and Cascales, 2017).

To label PG with RBB, 250 µl of PG were mixed with 200 µl of 400 mM NaOH for 30 min at 37°C. 25 mM RBB was added and incubated further overnight at 37°C. On the next morning 500 µl of 1 M HCl were added to stop the reaction. PG was pelleted at 400,000xg at 25°C for 30 min and resuspended in 2 ml of dH_2O. The labeled PG was washed until the supernatant became clear, but at least three times. The final labeled PG was resuspended in 250 µl of PBS and stored at 4°C.

10 µl of labeled PG was diluted with 90 µl of PBS and incubated for 37°C at 30 min to measure hydrolase activity. The POI (typically 0.2-0.5 nmol) were added to triplicates of diluted PG and incubated for set periods of time. The reaction was stopped by addition of 100 µl of EtOH and the undigested PG was pelleted at 400,000xg for 30 min at 25°C. The absorption of the supernatant was measured at 595 nm.

5 References

Alibu, V.P. *et al.* (2005) 'A doubly inducible system for RNA interference and rapid RNAi plasmid construction in *Trypanosoma brucei*', *Molecular and Biochemical Parasitology*, 139(1), pp. 75–82. Available at: https://doi.org/10.1016/j.molbiopara.2004.10.002.

Alves, João M P *et al.* (2013) 'Endosymbiosis in trypanosomatids: the genomic cooperation between bacterium and host in the synthesis of essential amino acids is heavily influenced by multiple horizontal gene transfers.', *BMC Evolutionary Biology*, 13, p. 190. Available at: https://doi.org/10.1186/1471-2148-13-190.

Alves, João M.P. *et al.* (2013) 'Genome Evolution and Phylogenomic Analysis of *Candidatus* Kinetoplastibacterium, the Betaproteobacterial Endosymbionts of *Strigomonas* and *Angomonas*', *Genome Biology and Evolution*, 5(2), pp. 338–350. Available at: https://doi.org/10.1093/gbe/evt012.

Amann, R. and Fuchs, B.M. (2008) 'Single-cell identification in microbial communities by improved fluorescence in situ hybridization techniques', *Nature Reviews Microbiology*, 6(5), pp. 339–348. Available at: https://doi.org/10.1038/nrmicro1888.

Amann, R.I., Krumholz, L. and Stahl, D.A. (1990) 'Fluorescent-oligonucleotide probing of whole cells for determinative, phylogenetic, and environmental studies in microbiology', *Journal of Bacteriology*, 172(2), pp. 762–770. Available at: https://doi.org/10.1128/jb.172.2.762-770.1990.

Andenmatten, N. *et al.* (2013) 'Conditional genome engineering in *Toxoplasma gondii* uncovers alternative invasion mechanisms', *Nature Methods*, 10(2), pp. 125–127. Available at: https://doi.org/10.1038/nmeth.2301.

Andrade, I. d. S. *et al.* (2011) 'Characterization of a porin channel in the endosymbiont of the trypanosomatid protozoan *Crithidia deanei*', *Microbiology*, 157(10), pp. 2818–2830. Available at: https://doi.org/10.1099/mic.0.049247-0.

Anselme, C. *et al.* (2008) 'Identification of the Weevil immune genes and their expression in the bacteriome tissue', *BMC Biology*, 6(1), p. 43. Available at: https://doi.org/10.1186/1741-7007-6-43.

Atthews, B.R.W.M. (1999) 'Structural basis of the conversion of T4 lysozyme into a transglycosidase by reengineering the active site', *Biochemistry*, 96, pp. 8949–8954.

de Azevedo-Martins, A.C. *et al.* (2015) 'Biochemical and phylogenetic analyses of phosphatidylinositol production in *Angomonas deanei*, an endosymbiont-harboring trypanosomatid', *Parasites & Vectors*, 8(1), p. 247. Available at: https://doi.org/10.1186/s13071-015-0854-x.

Banaszynski, L.A. *et al.* (2006) 'A Rapid, Reversible, and Tunable Method to Regulate Protein Function in Living Cells Using Synthetic Small Molecules', *Cell*, 126(5), pp. 995–1004. Available at: https://doi.org/10.1016/j.cell.2006.07.025.

Bennett, G.M. and Moran, N.A. (2015) 'Heritable symbiosis: The advantages and perils of an evolutionary rabbit hole', *Proceedings of the National Academy of Sciences*, 112(33), pp. 1–8. Available at: https://doi.org/10.1073/pnas.1421388112.

Benz, C. *et al.* (2017) 'Dynamin-like proteins in *Trypanosoma brucei*: A division of labour between two paralogs?', *PLOS ONE*. Edited by J. Mata, 12(5), p. e0177200. Available at: https://doi.org/10.1371/journal.pone.0177200.

Berberich, C. *et al.* (1998) 'The expression of the *Leishmania infantum* KMP-11 protein is developmentally regulated and stage specific', *Biochimica et Biophysica Acta - Gene Structure and Expression*, 1442(2–3), pp. 230–237. Available at: https://doi.org/10.1016/S0167-4781(98)00176-6.

Bernadsky, G., Beveridge, T.J. and Clarke, A.J. (1994) *Analysis of the Sodium Dodecyl Sulfate-Stable Peptidoglycan Autolysins of Select Gram-Negative Pathogens by Using Renaturing Polyacrylamide Gel Electrophoresis*, *JOURNAL OF BACTERIOLOGY*.

Bernhardt, T.G. and De Boer, P.A.J. (2005) 'SlmA, a nucleoid-associated, FtsZ binding protein required for blocking septal ring assembly over chromosomes in *E. coli*', *Molecular Cell*, 18(5), pp. 555–564. Available at: https://doi.org/10.1016/j.molcel.2005.04.012.

Bhattacharya, D. *et al.* (2012) 'Single cell genome analysis supports a link between phagotrophy and primary plastid endosymbiosis', *Scientific Reports*, 2, pp. 1–8. Available at: https://doi.org/10.1038/srep00356.

de Boer, P.A.J., Crossley, R.E. and Rothfield, L.I. (1989) 'A division inhibitor and a topological specificity factor coded for by the minicell locus determine proper placement of the division septum in *E. coli*', *Cell*, 56(4), pp. 641–649. Available at: https://doi.org/10.1016/0092-8674(89)90586-2.

Bolla, J.R. *et al.* (2018) 'Direct observation of the influence of cardiolipin and antibiotics on lipid II binding to MurJ', *Nature Chemistry*, 10(3), pp. 363–371. Available at: https://doi.org/10.1038/nchem.2919.

Bombaça, A.C.S. *et al.* (2017) 'Hydrogen peroxide resistance in *Strigomonas culicis*: Effects on mitochondrial functionality and Aedes aegypti interaction', *Free Radical Biology and Medicine*, 113(October), pp. 255–266. Available at: https://doi.org/10.1016/j.freeradbiomed.2017.10.006.

Borghesan, T.C. *et al.* (2018) 'Genetic Diversity and Phylogenetic Relationships of Coevolving Symbiont-Harboring Insect Trypanosomatids, and Their Neotropical Dispersal by Invader African Blowflies (Calliphoridae)', *Frontiers in Microbiology*, 9, p. 131. Available at: https://doi.org/10.3389/fmicb.2018.00131.

Brum, F.L. *et al.* (2014) 'Structural characterization of the cell division cycle in *Strigomonas culicis*, an endosymbiont-bearing trypanosomatid', *Microscopy and Microanalysis*, 20(1), pp. 228–237. Available at: https://doi.org/10.1017/S1431927613013925.

Brunoro, G.V.F. *et al.* (2019) 'Quantitative Proteomic Map of the Trypanosomatid *Strigomonas culicis*: The Biological Contribution of its Endosymbiotic Bacterium', *Protist*, 170(6), p. 125698. Available at: https://doi.org/10.1016/j.protis.2019.125698.

Buddelmeijer, N. *et al.* (2002) 'YgbQ, a cell division protein in *Escherichia coli* and *Vibrio cholerae* , localizes in codependent fashion with FtsL to the division site', *Proceedings of the National Academy of Sciences*, 99(9), pp. 6316–6321. Available at: https://doi.org/10.1073/pnas.092128499.

Butt, T.R. *et al.* (2005) 'SUMO fusion technology for difficult-to-express proteins', *Protein Expression and Purification*, 43(1), pp. 1–9. Available at: https://doi.org/10.1016/j.pep.2005.03.016.

Carvalho, A.L.M. and Deane, M.P. (1974) 'Trypanosomatidae Isolated from *Zelus leucogrammus* (Perty, 1834) (Hemiptera, Reduviidae), with a Discussion on Flagellates of Insectivorous Bugs*', *The Journal of Protozoology*, 21(1), pp. 5–8. Available at: https://doi.org/10.1111/j.1550-7408.1974.tb03605.x.

Catta-Preta, C.M.C. *et al.* (2016) 'Reduction of Tubulin Expression in *Angomonas deanei* by RNAi Modifies the Ultrastructure of the Trypanosomatid Protozoan and Impairs Division of Its Endosymbiotic Bacterium', *Journal of Eukaryotic Microbiology*, pp. 1–10. Available at: https://doi.org/10.1111/jeu.12326.

Chanez, A.-L. *et al.* (2006) 'Ablation of the single dynamin of *T. brucei* blocks mitochondrial fission and endocytosis and leads to a precise cytokinesis arrest', *Journal of Cell Science*, 119(14), pp. 2968–2974. Available at: https://doi.org/10.1242/jcs.03023.

Chang, K. -P. (1974) 'Ultrastructure of Symbiotic Bacteria in Normal and Antibiotic-Treated *Blastocrithidia culicis* and *Crithidia oncopelti*', *The journal of eukaryotic microbiology*, 21(5), pp. 699–707. Available at: https://doi.org/10.1111/j.1550-7408.1974.tb03733.x.

Clark, C.G. (1997) 'Riboprinting: a tool for the study of genetic diversity in microorganisms.', *The Journal of eukaryotic microbiology*, 44(4), pp. 277–83. Available at: https://doi.org/10.1111/j.1550-7408.1997.tb05667.x.

Clayton, C.E. (2002) 'Life without transcriptional control? From fly to man and back again', *The EMBO Journal*, 21(8), pp. 1881–1888. Available at: https://doi.org/10.1093/emboj/21.8.1881.

Collins, C.R. *et al.* (2013) 'Robust inducible Cre recombinase activity in the human malaria parasite *Plasmodium falciparum* enables efficient gene deletion within a single asexual erythrocytic growth cycle', *Molecular Microbiology*, 88(4), pp. 687–701. Available at: https://doi.org/10.1111/mmi.12206.

Cottrell, M.T. and Kirchman, D.L. (2000) 'Community composition of marine bacterioplankton determined by 16S rRNA gene clone libraries and fluorescence in situ hybridization', *Applied and Environmental Microbiology*, 66(12), pp. 5116–5122. Available at: https://doi.org/10.1128/AEM.66.12.5116-5122.2000.

Damerow, S. *et al.* (2015) 'Depletion of UDP-Glucose and UDP-Galactose Using a Degron System Leads to Growth Cessation of *Leishmania major*', *PLoS Neglected Tropical Diseases*, 9(11), pp. 1–15. Available at: https://doi.org/10.1371/journal.pntd.0004205.

Davey, J.W. *et al.* (2021) 'Chromosomal assembly of the nuclear genome of the endosymbiont-bearing trypanosomatid *Angomonas deanei*', *G3 Genes|Genomes|Genetics*. Edited by B. Andrews, 11(1), pp. 1–7. Available at: https://doi.org/10.1093/g3journal/jkaa018.

d'Avila-Levy, C.M. *et al.* (2003) 'A metalloproteinase extracellularly released by *Crithidia deanei*', *Canadian Journal of Microbiology*, 49(10), pp. 625–632. Available at: https://doi.org/10.1139/w03-081.

d'Avila-Levy, C.M. *et al.* (2008) '*Crithidia deanei*: Influence of parasite gp63 homologue on the interaction of endosymbiont-harboring and aposymbiotic strains with *Aedes aegypti* midgut', *Experimental Parasitology*, 118(3), pp. 345–353. Available at: https://doi.org/10.1016/j.exppara.2007.09.007.

Delaye, L., Valadez-Cano, C. and Pérez-Zamorano, B. (2016) 'How Really Ancient Is Paulinella Chromatophora?', *PLoS Currents*, 8. Available at: https://doi.org/10.1371/CURRENTS.TOL.E68A099364BB1A1E129A17B4E06B0C6B.

Delcour, J. *et al.* (1999) 'The biosynthesis and functionality of the cell-wall of lactic acid bacteria.', *Antonie van Leeuwenhoek*, 76(1–4), pp. 159–84. Available at: https://doi.org/10.1023/A:1002089722581.

Don, R.H. *et al.* (1991) '"Touchdown" PCR to circumvent spurious priming during gene amplification', *Nucleic Acids Research*, 19(14), pp. 4008–4008. Available at: https://doi.org/10.1093/nar/19.14.4008.

Dreesbach, M. (2022) 'Analysis of expression and localization of the DiCre system in *Angomonas deanei*', *Master thesis* [Preprint].

Duhamel, R.C. *et al.* (1979) 'pH gradient elution of human IgG1, IgG2 and IgG4 from protein A-Sepharose', *Journal of Immunological Methods*, 31(3–4), pp. 211–217. Available at: https://doi.org/10.1016/0022-1759(79)90133-9.

D'Ulisse, V. *et al.* (2007) 'Three functional subdomains of the *Escherichia coli* FtsQ protein are involved in its interaction with the other division proteins', *Microbiology*, 153(1), pp. 124–138. Available at: https://doi.org/10.1099/mic.0.2006/000265-0.

Duncan, S.M. *et al.* (2016) 'Conditional gene deletion with DiCre demonstrates an essential role for CRK3 in *Leishmania mexicana* cell cycle regulation', *Molecular Microbiology*, 100(6), pp. 931–944. Available at: https://doi.org/10.1111/mmi.13375.

Duncan, S.M., Jones, N.G. and Mottram, J.C. (2017) 'Recent advances in *Leishmania* reverse genetics: Manipulating a manipulative parasite', *Molecular and Biochemical Parasitology*, 216, pp. 30–38. Available at: https://doi.org/10.1016/j.molbiopara.2017.06.005.

Dworzanski, J.P. *et al.* (2005) 'Novel biomarkers for Gram-type differentiation of bacteria by pyrolysis-gas chromatography-mass spectrometry', *Journal of Analytical and Applied Pyrolysis*, 73(1), pp. 29–38. Available at: https://doi.org/10.1016/j.jaap.2004.09.003.

Egan, A.J.F. (2018) 'Bacterial outer membrane constriction', *Molecular Microbiology*, 107(6), pp. 676–687. Available at: https://doi.org/10.1111/mmi.13908.

Ehret, G. (2017) 'Determination of the subcellular localization and identification of the targeting signals of the endosymbiont-targeted proteins 1 and 2 in *Angomonas deanei*', *Master thesis* [Preprint].

Elias, M. *et al.* (2007) 'Morphological Events during the *Trypanosoma cruzi* Cell Cycle', *Protist*, 158(2), pp. 147–157. Available at: https://doi.org/10.1016/j.protis.2006.10.002.

Embley, T.M. and Martin, W. (2006) 'Eukaryotic evolution, changes and challenges', *Nature*, 440(7084), pp. 623–630. Available at: https://doi.org/10.1038/nature04546.

Engler, C., Kandzia, R. and Marillonnet, S. (2008) 'A one pot, one step, precision cloning method with high throughput capability', *PLoS ONE*, 3(11). Available at: https://doi.org/10.1371/journal.pone.0003647.

Eswara, P.J. and Ramamurthi, K.S. (2017) 'Annual Review of Microbiology Bacterial Cell Division: Nonmodels Poised to Take the Spotlight', *Annu. Rev. Microbiol*, 71(1), pp. 393–411. Available at: https://doi.org/10.1146/annurev-micro-102215.

Fahnert, B., Lilie, H. and Neubauer, P. (2004) 'Inclusion bodies: formation and utilisation.', *Advances in biochemical engineering/biotechnology*, 89, pp. 93–142. Available at: https://doi.org/10.1007/b93995.

Fampa, P. *et al.* (2003) 'Interaction of insect trypanosomatids with mosquitoes, sand fly and the respective insect cell lines', *International Journal for Parasitology*, 33(10), pp. 1019–1026. Available at: https://doi.org/10.1016/S0020-7519(03)00124-3.

Figueroa-Cuilan, W.M. and Brown, P.J.B. (2018) 'Cell Wall Biogenesis During Elongation and Division in the Plant Pathogen Agrobacterium tumefaciens', in *Current Topics in Microbiology and Immunology*. Springer Verlag, pp. 87–110. Available at: https://doi.org/10.1007/82_2018_92.

Finkelsztein, E.J. *et al.* (2015) 'Altering the motility of *Trypanosoma cruzi* with rabbit polyclonal anti-peptide antibodies reduces infection to susceptible mammalian cells', *Experimental Parasitology*, 150, pp. 36–43. Available at: https://doi.org/10.1016/j.exppara.2015.01.007.

Firczuk, M. and Bochtler, M. (2007) 'Mutational Analysis of Peptidoglycan Amidase MepA †', *Biochemistry*, 46(1), pp. 120–128. Available at: https://doi.org/10.1021/bi0613776.

Flaspohler, J.A. *et al.* (1997) 'Functional identification of a *Leishmania* gene related to the peroxin 2 gene reveals common ancestry of glycosomes and peroxisomes', *Molecular and Cellular Biology*, 17(3), pp. 1093–1101. Available at: https://doi.org/10.1128/mcb.17.3.1093.

Flegontov, P. *et al.* (2013) '*Paratrypanosoma* is a novel early-branching trypanosomatid', *Current Biology*, 23(18), pp. 1787–1793. Available at: https://doi.org/10.1016/j.cub.2013.07.045.

Frossard, M.L. *et al.* (2006) 'An endosymbiont positively modulates ornithine decarboxylase in host trypanosomatids', *Biochemical and Biophysical Research Communications*, 343(2), pp. 443–449. Available at: https://doi.org/10.1016/j.bbrc.2006.02.168.

Gabr, A., Grossman, A.R. and Bhattacharya, D. (2020) '*Paulinella* , a model for understanding plastid primary endosymbiosis', *Journal of Phycology*. Edited by B. Palenik, 56(4), pp. 837–843. Available at: https://doi.org/10.1111/jpy.13003.

Gale, M., Carter, V. and Parsons, M. (1994) 'Translational control mediates the developmental regulation of the *Trypanosoma brucei* Nrk protein kinase.', *Journal of Biological Chemistry*, 269(50), pp. 31659–31665. Available at: https://doi.org/10.1016/S0021-9258(18)31746-0.

Ganyukova, A.I., Malysheva, M.N. and Frolov, A.O. (2020) 'Life cycle, ultrastructure and host-parasite relationships of *Angomonas deanei* (Kinetoplastea: Trypanosomatidae) in the blowfly *Lucilia sericata*

(Diptera: Calliphoridae)', *Protistology*, 14(4), pp. 204–218. Available at: https://doi.org/10.21685/1680-0826-2020-14-4-2.

García-Cano, I. *et al.* (2015) 'Expression, purification, and characterization of a bifunctional 99-kDa peptidoglycan hydrolase from *Pediococcus acidilactici* ATCC 8042', *Applied Microbiology and Biotechnology*, 99(20), pp. 8563–8573. Available at: https://doi.org/10.1007/s00253-015-6593-2.

Gautier, R. *et al.* (2008) 'HELIQUEST: a web server to screen sequences with specific -helical properties', *Bioinformatics*, 24(18), pp. 2101–2102. Available at: https://doi.org/10.1093/bioinformatics/btn392.

Gerding, M.A. *et al.* (2007) 'The trans -envelope Tol–Pal complex is part of the cell division machinery and required for proper outer-membrane invagination during cell constriction in *E. coli*', *Molecular Microbiology*, 63(4), pp. 1008–1025. Available at: https://doi.org/10.1111/j.1365-2958.2006.05571.x.

Ghuysen, J.-M. and Goffin, C. (1999) 'Lack of Cell Wall Peptidoglycan versus Penicillin Sensitivity: New Insights into the Chlamydial Anomaly', *Antimicrobial Agents and Chemotherapy*, 43(10), pp. 2339–2344. Available at: https://doi.org/10.1128/AAC.43.10.2339.

Gibson, D.G. *et al.* (2009) 'Enzymatic assembly of DNA molecules up to several hundred kilobases', *Nature Methods*, 6(5), pp. 343–345. Available at: https://doi.org/10.1038/nmeth.1318.

Gonçalves, C.S. *et al.* (2021) 'Importance of *Angomonas deanei* KAP4 for kDNA arrangement, cell division and maintenance of the host-bacterium relationship', *Scientific Reports*, 11(1), p. 9210. Available at: https://doi.org/10.1038/s41598-021-88685-8.

Gossen, M. and Bujard, H. (1993) 'Anhydrotetracycline, a novel effector for tetracycline controlled gene expression systems in eukaryotic cells', *Nucleic Acids Research*, 21(18), pp. 4411–4412. Available at: https://doi.org/10.1093/nar/21.18.4411.

De Graffenried, C.L. *et al.* (2013) 'Polo-like kinase phosphorylation of bilobe-resident TbCentrin2 facilitates flagellar inheritance in *Trypanosoma brucei*', *Molecular Biology of the Cell*, 24(12), pp. 1947–1963. Available at: https://doi.org/10.1091/mbc.E12-12-0911.

de Graffenried, C.L., Ho, H.H. and Warren, G. (2008) 'Polo-like kinase is required for Golgi and bilobe biogenesis in *Trypanosoma brucei*', *Journal of Cell Biology*, 181(3), pp. 431–438. Available at: https://doi.org/10.1083/jcb.200708082.

Haile, S. and Papadopoulou, B. (2007) 'Developmental regulation of gene expression in trypanosomatid parasitic protozoa', *Current Opinion in Microbiology*, 10(6), pp. 569–577. Available at: https://doi.org/10.1016/j.mib.2007.10.001.

Hajduk, S.L., Klein, V.A. and Englund, P.T. (1984) 'Replication of kinetoplast DNA maxicircles', *Cell*, 36(2), pp. 483–492. Available at: https://doi.org/10.1016/0092-8674(84)90241-1.

Hakoyama, T. *et al.* (2009) 'Host plant genome overcomes the lack of a bacterial gene for symbiotic nitrogen fixation', *Nature*, 462(7272), pp. 514–517. Available at: https://doi.org/10.1038/nature08594.

Hallgren, J. *et al.* (2022) 'DeepTMHMM predicts alpha and beta transmembrane proteins using deep neural networks', *bioRxiv*, p. 2022.04.08.487609. Available at: https://doi.org/10.1101/2022.04.08.487609.

Hansen, L. (Heinrich-H.-U. (2021) 'Establishment of a Golgi marker for the Trypanosomatid *Angomonas deanei* and its application in colocalization studies with Endosymbiont-targeted protein 8', *Bachelor Thesis*.

He, C.Y., Pypaert, M. and Warren, G. (2005) 'Cell biology: Golgi duplication in *Trypanosoma brucei* requires Centrin2', *Science*, 310(5751), pp. 1196–1198. Available at: https://doi.org/10.1126/science.1119969.

Heidrich, C. *et al.* (2001) 'Involvement of N-acetylmuramyl-l-alanine amidases in cell separation and antibiotic-induced autolysis of *Escherichia coli*', *Molecular Microbiology*, 41(1), pp. 167–178. Available at: https://doi.org/10.1046/j.1365-2958.2001.02499.x.

Heidrich, C. *et al.* (2002) 'Effects of multiple deletions of murein hydrolases on viability, septum cleavage, and sensitivity to large toxic molecules in *Escherichia coli*', *Journal of Bacteriology*, 184(22), pp. 6093–6099. Available at: https://doi.org/10.1128/JB.184.22.6093-6099.2002.

Henke, W. *et al.* (1997) 'Betaine improves the PCR amplification of GC-rich DNA sequences', *Nucleic Acids Research*, 25(19).

Ikeda, K.N. and De Graffenried, C.L. (2012) 'Polo-like kinase is necessary for flagellum inheritance in *Trypanosoma brucei*', *Journal of Cell Science*, 125(13), pp. 3173–3184. Available at: https://doi.org/10.1242/jcs.101162.

Ito, Y., Yamada, H. and Imoto, T. (1992) 'Colorimetric Assay for Lysozyme Using *Micrococcus luteus* Labeled with a Blue Dye, Remazol Brilliant Blue R, as a Substrate.', *Chemical and Pharmaceutical Bulletin*, 40(6), pp. 1523–1526. Available at: https://doi.org/10.1248/cpb.40.1523.

Jackson, A.P. (2015) 'Genome evolution in trypanosomatid parasites', *Parasitology*, 142, pp. S40–S56. Available at: https://doi.org/10.1017/S0031182014000894.

Johnson, D.C. *et al.* (2005) 'STRUCTURE, FUNCTION, AND FORMATION OF BIOLOGICAL IRON-SULFUR CLUSTERS', *Annual Review of Biochemistry*, 74(1), pp. 247–281. Available at: https://doi.org/10.1146/annurev.biochem.74.082803.133518.

Jullien, N. *et al.* (2003) 'Regulation of Cre recombinase by ligand-induced complementation of inactive fragments.', *Nucleic acids research*, 31(21). Available at: https://doi.org/10.1093/nar/gng131.

Jumper, J. *et al.* (2021) 'Highly accurate protein structure prediction with AlphaFold', *Nature*, 596(7873), pp. 583–589. Available at: https://doi.org/10.1038/s41586-021-03819-2.

Kalyanaraman, D. (2018) 'Characterization of ETP7 - A putative endosymbiont regulator in the trypanosomatid *Angomonas deanei*', *Master thesis*.

Kanonenberg, K. *et al.* (2019) 'Shaping the lipid composition of bacterial membranes for membrane protein production', *Microbial Cell Factories*, 18(1), p. 131. Available at: https://doi.org/10.1186/s12934-019-1182-1.

Katoh, K. (2002) 'MAFFT: a novel method for rapid multiple sequence alignment based on fast Fourier transform', *Nucleic Acids Research*, 30(14), pp. 3059–3066. Available at: https://doi.org/10.1093/nar/gkf436.

Kaurov, I. *et al.* (2018) 'The Diverged Trypanosome MICOS Complex as a Hub for Mitochondrial Cristae Shaping and Protein Import', *Current Biology*, 28(21), pp. 3393-3407.e5. Available at: https://doi.org/10.1016/j.cub.2018.09.008.

Kawai, Y., Mickiewicz, K. and Errington, J. (2018) 'Lysozyme Counteracts β-Lactam Antibiotics by Promoting the Emergence of L-Form Bacteria', *Cell*, 172(5), pp. 1038-1049.e10. Available at: https://doi.org/10.1016/j.cell.2018.01.021.

Kelley, L.A. *et al.* (2015) 'The Phyre2 web portal for protein modeling, prediction and analysis', *Nature Protocols*, 10(6), pp. 845–858. Available at: https://doi.org/10.1038/nprot.2015.053.

Klein, C.C. *et al.* (2013) 'Biosynthesis of vitamins and cofactors in bacterium-harbouring trypanosomatids depends on the symbiotic association as revealed by genomic analyses', *PLoS ONE*, 8(11). Available at: https://doi.org/10.1371/journal.pone.0079786.

Kocaoglu, O. and Carlson, E.E. (2015) 'Profiling of β-Lactam Selectivity for Penicillin-Binding Proteins in *Escherichia coli* Strain DC2', *Antimicrobial Agents and Chemotherapy*, 59(5), pp. 2785–2790. Available at: https://doi.org/10.1128/AAC.04552-14.

Kokkori, S. (2018) 'Genetic tools for the trypanosomatid *Angomonas deanei* help to dissect host-endosymbiont interactions', *Dissertation*.

Kooter, J.M. and Borst, P. (1984) 'α-Amanitin-insensitive transcription of variant surface glycoprotein genes provides further evidence for discontinuous transcription in trypanosomes', *Nucleic Acids Research*, 12(24), pp. 9457–9472. Available at: https://doi.org/10.1093/nar/12.24.9457.

Korbie, D.J. and Mattick, J.S. (2008) 'Touchdown PCR for increased specificity and sensitivity in PCR amplification', *Nature protocols*, 3(9), pp. 13–15. Available at: https://doi.org/10.1038/nprot.2008.133.

Kostygov, A.Y. *et al.* (2016) 'Novel Trypanosomatid-Bacterium Association: Evolution of Endosymbiosis in Action', *mBio*. Edited by K. Gull, 7(2). Available at: https://doi.org/10.1128/mBio.01985-15.

Kostygov, A.Y. *et al.* (2017) 'Genome of *Ca.* Pandoraea novymonadis, an Endosymbiotic Bacterium of the Trypanosomatid *Novymonas esmeraldas*', *Frontiers in Microbiology*, 8(October), pp. 1–13. Available at: https://doi.org/10.3389/fmicb.2017.01940.

Kupper, M. *et al.* (2014) 'Versatile roles of the chaperonin GroEL in microorganism-insect interactions', *FEMS Microbiology Letters*, 353(1), pp. 1–10. Available at: https://doi.org/10.1111/1574-6968.12390.

Kushnir, S. *et al.* (2005) 'Development of an inducible protein expression system based on the protozoan host *Leishmania tarentolae*', *Protein Expression and Purification*, 42(1), pp. 37–46. Available at: https://doi.org/10.1016/j.pep.2005.03.004.

Laemmli, U.K. (1970) 'Cleavage of Structural Proteins during the Assembly of the Head of Bacteriophage T4', *Nature*, 227(5259), pp. 680–685. Available at: https://doi.org/10.1038/227680a0.

Leclerc, D. and Asselin, A. (1989) 'Detection of bacterial cell wall hydrolases after denaturing polyacrylamide gel electrophoresis', *Canadian Journal of Microbiology*, 35(8), pp. 749–753. Available at: https://doi.org/10.1139/m89-125.

Lee, M.G.-S. and Van der Ploeg, L.H.T. (1990) 'Homologous Recombination and Stable Transfection in the Parasitic Protozoan *Trypanosoma brucei*', *Science*, 250(4987), pp. 1583–1587. Available at: https://doi.org/10.1126/science.2177225.

Li, Z. and Wang, C.C. (2008) 'KMP-11, a basal body and flagellar protein, is required for cell division in *Trypanosoma brucei*', *Eukaryotic Cell*, 7(11), pp. 1941–1950. Available at: https://doi.org/10.1128/EC.00249-08.

Liechti, G.W. *et al.* (2014) 'A new metabolic cell-wall labelling method reveals peptidoglycan in *Chlamydia trachomatis*', *Nature*, 506(7489), pp. 507–510. Available at: https://doi.org/10.1038/nature12892.

Loose, M. *et al.* (2011) 'Min protein patterns emerge from rapid rebinding and membrane interaction of MinE', *Nature Structural and Molecular Biology*, 18(5), pp. 577–583. Available at: https://doi.org/10.1038/nsmb.2037.

Loyola-Machado, A.C. *et al.* (2017) 'The Symbiotic Bacterium Fuels the Energy Metabolism of the Host Trypanosomatid *Strigomonas culicis*', *Protist*, 168(2), pp. 253–269. Available at: https://doi.org/10.1016/j.protis.2017.02.001.

Lukeš, J. *et al.* (2002) 'Kinetoplast DNA Network: Evolution of an Improbable Structure', *Eukaryotic Cell*, 1(4), pp. 495–502. Available at: https://doi.org/10.1128/EC.1.4.495-502.2002.

Lukeš, J. *et al.* (2018) 'Trypanosomatids Are Much More than Just Trypanosomes: Clues from the Expanded Family Tree', *Trends in Parasitology*, 34(6), pp. 466–480. Available at: https://doi.org/10.1016/j.pt.2018.03.002.

Mair, G. *et al.* (2000) 'A new twist in trypanosome RNA metabolism: cis-splicing of pre-mRNA', *RNA*, 6(2), p. S135583820099229X. Available at: https://doi.org/10.1017/S135583820099229X.

Marcyjaniak, M. *et al.* (2004) 'Peptidoglycan amidase MepA is a LAS metallopeptidase', *Journal of Biological Chemistry*, 279(42), pp. 43982–43989. Available at: https://doi.org/10.1074/jbc.M406735200.

Marin, B., Nowack, E.C.M.M. and Melkonian, M. (2005) 'A plastid in the making: Evidence for a second primary endosymbiosis', *Protist*, 156(4), pp. 425–432. Available at: https://doi.org/10.1016/j.protis.2005.09.001.

Marston, A.L. *et al.* (1998) 'Polar localization of the MinD protein of *Bacillus subtilis* and its role in selection of the mid-cell division site', *Genes and Development*, 12(21), pp. 3419–3430. Available at: https://doi.org/10.1101/gad.12.21.3419.

Maslov, D.A. *et al.* (2013) 'Diversity and phylogeny of insect trypanosomatids: All that is hidden shall be revealed', *Trends in Parasitology*, 29(1), pp. 43–52. Available at: https://doi.org/10.1016/j.pt.2012.11.001.

Maslov, D.A. *et al.* (2019) 'Recent advances in trypanosomatid research: genome organization, expression, metabolism, taxonomy and evolution', *Parasitology*, 146(1), pp. 1–27. Available at: https://doi.org/10.1017/S0031182018000951.

Mayho, M. *et al.* (2006) 'Post-transcriptional control of nuclear-encoded cytochrome oxidase subunits in *Trypanosoma brucei*: evidence for genome-wide conservation of life-cycle stage-specific regulatory

elements', *Nucleic Acids Research*, 34(18), pp. 5312–5324. Available at: https://doi.org/10.1093/nar/gkl598.

de Menezes, M.C.N.D. and Roitmanz, I. (1991) 'Nutritional Requirements of *Blastocrithidia culicis* , a Trypanosomatid with an Endosymbiont 1', *The Journal of Protozoology*, 38(2), pp. 122–123. Available at: https://doi.org/10.1111/j.1550-7408.1991.tb06030.x.

Mereschkowsky, K. (1905) 'Über Natur und Ursprung der Chromatophoren im Pflanzenreiche', *Biologisches Centralblatt. Bd. 25*, 25(July), pp. 593–604.

Miroux, B. and Walker, J.E. (1996) 'Over-production of Proteins in *Escherichia coli*: Mutant Hosts that Allow Synthesis of some Membrane Proteins and Globular Proteins at High Levels', *Journal of Molecular Biology*, 260(3), pp. 289–298. Available at: https://doi.org/10.1006/jmbi.1996.0399.

Miyagishima, S. (2017) 'Chloroplast division: A handshake across membranes', *Nature Plants*, 3(3), p. 17025. Available at: https://doi.org/10.1038/nplants.2017.25.

Miyagishima, S. ya *et al.* (2014) 'DipM is required for peptidoglycan hydrolysis during chloroplast division', *BMC Plant Biology*, 14(1), pp. 1–15. Available at: https://doi.org/10.1186/1471-2229-14-57.

Miyagishima, S.Y. *et al.* (2003) 'A plant-specific dynamin-related protein forms a ring at the chloroplast division site', *Plant Cell*, 15(3), pp. 655–665. Available at: https://doi.org/10.1105/tpc.009373.

Morales, J. *et al.* (2016) 'Development of a toolbox to dissect host-endosymbiont interactions and protein trafficking in the trypanosomatid *Angomonas deanei*', *BMC Evolutionary Biology*, 16(1), p. 247. Available at: https://doi.org/10.1186/s12862-016-0820-z.

Morales, J. *et al.* (2023) 'Host-symbiont interactions in *Angomonas deanei* include the evolution of a host-derived dynamin ring around the endosymbiont division site', *Current Biology*, 33(1), pp. 28-40.e7. Available at: https://doi.org/10.1016/j.cub.2022.11.020.

Morgan, G.W., Goulding, D. and Field, M.C. (2004) 'The Single Dynamin-like Protein of *Trypanosoma brucei* Regulates Mitochondrial Division and Is Not Required for Endocytosis', *Journal of Biological Chemistry*, 279(11), pp. 10692–10701. Available at: https://doi.org/10.1074/jbc.M312178200.

De Mot, R. *et al.* (1999) 'Proteasomes and other self-compartmentalizing proteases in prokaryotes', *Trends in Microbiology*, 7(2), pp. 88–92. Available at: https://doi.org/10.1016/S0966-842X(98)01432-2.

Motta, M.C. *et al.* (1997) 'Ultrastructural and biochemical analysis of the relationship of *Crithidia deanei* with its endosymbiont.', *European journal of cell biology*, 72(4), pp. 370–7.

Motta, M.C.M. *et al.* (1997) 'Detection of penicillin-binding proteins in the endosymbiont of the trypanosomatid *Crithidia deanei*', *Journal of Eukaryotic Microbiology*, 44(5), pp. 492–496. Available at: https://doi.org/Doi 10.1111/J.1550-7408.1997.Tb05729.X.

Motta, M.C.M. *et al.* (2010) 'The bacterium endosymbiont of *Crithidia deanei* undergoes coordinated division with the host cell nucleus', *PLoS ONE*, 5(8), pp. 20–21. Available at: https://doi.org/10.1371/journal.pone.0012415.

Motta, M.C.M. *et al.* (2013) 'Predicting the Proteins of *Angomonas deanei*, *Strigomonas culicis* and Their Respective Endosymbionts Reveals New Aspects of the Trypanosomatidae Family', *PLoS ONE*, 8(4). Available at: https://doi.org/10.1371/journal.pone.0060209.

Moya, A. *et al.* (2008) 'Learning how to live together: genomic insights into prokaryote–animal symbioses', *Nature Reviews Genetics*, 9(3), pp. 218–229. Available at: https://doi.org/10.1038/nrg2319.

Mueller, E.A. and Levin, P.A. (2020) 'Bacterial Cell Wall Quality Control during Environmental Stress', *mBio*. Edited by D.A. Garsin, 11(5), pp. 1–15. Available at: https://doi.org/10.1128/mBio.02456-20.

Müller, A.U. and Weber-Ban, E. (2019) 'The bacterial proteasome at the core of diverse degradation pathways', *Frontiers in Molecular Biosciences*, 6(APR), pp. 1–7. Available at: https://doi.org/10.3389/fmolb.2019.00023.

Mundim, M.H. and Roitman, I. (1977) 'Extra Nutritional Requirements of Artificially Aposymbiotic *Crithidia deanei* *', *The Journal of Protozoology*, 24(2), pp. 329–331. Available at: https://doi.org/10.1111/j.1550-7408.1977.tb00988.x.

Nardelli, S.C. *et al.* (2007) 'Small-Subunit rRNA Processome Proteins Are Translationally Regulated during Differentiation of *Trypanosoma cruzi*', *Eukaryotic Cell*, 6(2), pp. 337–345. Available at: https://doi.org/10.1128/EC.00279-06.

Nishida, K. *et al.* (2003) 'Dynamic recruitment of dynamin for final mitochondrial severance in a primitive red alga', *Proceedings of the National Academy of Sciences of the United States of America*, 100(4), pp. 2146–2151. Available at: https://doi.org/10.1073/pnas.0436886100.

Nowack, E.C.M. *et al.* (2011) 'Endosymbiotic gene transfer and transcriptional regulation of transferred genes in *Paulinella chromatophora*', *Molecular Biology and Evolution*, 28(1), pp. 407–422. Available at: https://doi.org/10.1093/molbev/msq209.

Nowack, E.C.M. (2014) '*Paulinella chromatophora* - Rethinking the transition from endosymbiont to organelle', *Acta Societatis Botanicorum Poloniae*, 83(4), pp. 387–397. Available at: https://doi.org/10.5586/asbp.2014.049.

Nowack, E.C.M. *et al.* (2016) 'Gene transfers from diverse bacteria compensate for reductive genome evolution in the chromatophore of *Paulinella chromatophora*', *Proceedings of the National Academy of Sciences of the United States of America*, 113(43), pp. 12214–12219. Available at: https://doi.org/10.1073/pnas.1608016113.

Nowack, E.C.M. and Grossman, A.R. (2012) 'Trafficking of protein into the recently established photosynthetic organelles of *Paulinella chromatophora*', *Proceedings of the National Academy of Sciences of the United States of America*, 109(14), pp. 5340–5345. Available at: https://doi.org/10.1073/pnas.1118800109.

Nowack, E.C.M., Melkonian, M. and Glöckner, G. (2008) 'Chromatophore Genome Sequence of Paulinella Sheds Light on Acquisition of Photosynthesis by Eukaryotes', *Current Biology*, 18(6), pp. 410–418. Available at: https://doi.org/10.1016/j.cub.2008.02.051.

Oberleitner, L. *et al.* (2020) 'The Puzzle of Metabolite Exchange and Identification of Putative Octotrico Peptide Repeat Expression Regulators in the Nascent Photosynthetic Organelles of *Paulinella chromatophora'*, *Frontiers in Microbiology*, 11(November), pp. 1–15. Available at: https://doi.org/10.3389/fmicb.2020.607182.

Oliva, B. *et al.* (1992) 'Evidence that tetracycline analogs whose primary target is not the bacterial ribosome cause lysis of *Escherichia coli*', *Antimicrobial Agents and Chemotherapy*, 36(5), pp. 913–919. Available at: https://doi.org/10.1128/AAC.36.5.913.

Osellame, L.D., Blacker, T.S. and Duchen, M.R. (2012) 'Cellular and molecular mechanisms of mitochondrial function', *Best Practice and Research: Clinical Endocrinology and Metabolism*, 26(6), pp. 711–723. Available at: https://doi.org/10.1016/j.beem.2012.05.003.

Osteryoung, K.W. and Pyke, K.A. (2014) 'Division and Dynamic Morphology of Plastids', *Annual Review of Plant Biology*, 65(1), pp. 443–472. Available at: https://doi.org/10.1146/annurev-arplant-050213-035748.

Otten, C. *et al.* (2018) 'Peptidoglycan in obligate intracellular bacteria', *Molecular Microbiology*, 107(2), pp. 142–163. Available at: https://doi.org/10.1111/mmi.13880.

Palmié-Peixoto, I.V. *et al.* (2006) 'Effects of sterol biosynthesis inhibitors on endosymbiont-bearing trypanosomatids', *FEMS Microbiology Letters*, 255(1), pp. 33–42. Available at: https://doi.org/10.1111/j.1574-6968.2005.00056.x.

Parsons, M. *et al.* (1984) 'Trypanosome mRNAs share a common 5' spliced leader sequence', *Cell*, 38(1), pp. 309–316. Available at: https://doi.org/10.1016/0092-8674(84)90552-X.

Parsons, M. (2004) 'Glycosomes: Parasites and the divergence of peroxisomal purpose', *Molecular Microbiology*, 53(3), pp. 717–724. Available at: https://doi.org/10.1111/j.1365-2958.2004.04203.x.

Pichoff, S. and Lutkenhaus, J. (2005) 'Tethering the Z ring to the membrane through a conserved membrane targeting sequence in FtsA', *Molecular Microbiology*, 55(6), pp. 1722–1734. Available at: https://doi.org/10.1111/j.1365-2958.2005.04522.x.

Price, D.R.G. *et al.* (2014) 'Aphid amino acid transporter regulates glutamine supply to intracellular bacterial symbionts', *Proceedings of the National Academy of Sciences*, 111(1), pp. 320–325. Available at: https://doi.org/10.1073/pnas.1306068111.

Quan, S. *et al.* (2013) 'Isolation of Bacterial Cell Surfaces', *Bacterial Cell Surfaces: Methods and Protocols*, 966, pp. 359–366. Available at: https://doi.org/10.1007/978-1-62703-245-2.

Ríos, R.M. *et al.* (2004) 'GMAP-210 Recruits γ-Tubulin Complexes to cis-Golgi Membranes and Is Required for Golgi Ribbon Formation', *Cell*, 118(3), pp. 323–335. Available at: https://doi.org/10.1016/j.cell.2004.07.012.

Roberts, S.C. (2011) 'The genetic toolbox for *Leishmania* parasites', *Bioengineered Bugs*, 2(6). Available at: https://doi.org/10.4161/bbug.2.6.18205.

Rodrigues, C.D.A. and Harry, E.J. (2012) 'The Min System and Nucleoid Occlusion Are Not Required for Identifying the Division Site in *Bacillus subtilis* but Ensure Its Efficient Utilization', *PLoS Genetics*. Edited by W.F. Burkholder, 8(3), p. e1002561. Available at: https://doi.org/10.1371/journal.pgen.1002561.

Sagan, L. (1967) 'On the origin of mitosing cells', *Journal of theoretical biology*, 14(3), pp. 255–74. Available at: https://doi.org/10.1016/0022-5193(67)90079-3.

Sahin, A. *et al.* (2008) 'The *Leishmania* ARL-1 and Golgi Traffic', *PLoS ONE*. Edited by N. Ahmed, 3(2), p. e1620. Available at: https://doi.org/10.1371/journal.pone.0001620.

Santin, Y.G. and Cascales, E. (2017) 'Measure of Peptidoglycan Hydrolase Activity', in *Bacterial protein secretion systems*. Springer, pp. 151–158. Available at: https://doi.org/10.1007/978-1-4939-7033-9.

Sauvage, E. *et al.* (2014) 'Crystal structure of penicillin-binding protein 3 (PBP3) from *Escherichia coli*', *PLoS ONE* [Preprint]. Available at: https://doi.org/10.1371/journal.pone.0098042.

Schimper, A. (1883) 'Uber die Entwicklung der Chlorophyllkorner und Farbkorper', *Botanie Zeitung*, 41, pp. 105–114. Available at: https://doi.org/10.1038/028267a0.

Schleifer, K.H. and Kandler, O. (1972) 'Peptidoglycan types of bacterial cell walls and their taxonomic implications', *Bacteriological Reviews*, 36(4), pp. 407–477. Available at: https://doi.org/10.1128/br.36.4.407-477.1972.

Schmidt, K.L. *et al.* (2004) 'A Predicted ABC Transporter, FtsEX, Is Needed for Cell Division in *Escherichia coli*', *Journal of Bacteriology*, 186(3), pp. 785–793. Available at: https://doi.org/10.1128/JB.186.3.785-793.2004.

Schwarz, C.K.W. *et al.* (2012) 'Using an E. coli Type 1 secretion system to secrete the mammalian, intracellular protein IFABP in its active form', *Journal of Biotechnology*, 159(3), pp. 155–161. Available at: https://doi.org/10.1016/j.jbiotec.2012.02.005.

Sharma, V. *et al.* (2020) 'Molecular Basis of Root Nodule Symbiosis between *Bradyrhizobium* and "Crack-Entry" Legume Groundnut (*Arachis hypogaea L.*)', *Plants*, 9(2), p. 276. Available at: https://doi.org/10.3390/plants9020276.

Shi, H. *et al.* (2000) 'Genetic interference in *Trypanosoma brucei* by heritable and inducible double-stranded RNA', *Rna*, 6(7), pp. 1069–1076. Available at: https://doi.org/10.1017/S1355838200000297.

Shigenobu, S. and Stern, D.L. (2012) 'Aphids evolved novel secreted proteins for symbiosis with bacterial endosymbiont', *Proceedings of the Royal Society B: Biological Sciences*, 280(1750), pp. 20121952–20121952. Available at: https://doi.org/10.1098/rspb.2012.1952.

Shugar, D. (1952) 'The measurement of lysozyme activity and the ultra-violet inactivation of lysozyme', *BBA - Biochimica et Biophysica Acta*, 8(C), pp. 302–309. Available at: https://doi.org/10.1016/0006-3002(52)90045-0.

Sievers, F. *et al.* (2011) 'Fast, scalable generation of high-quality protein multiple sequence alignments using Clustal Omega', *Molecular Systems Biology*, 7(1), p. 539. Available at: https://doi.org/10.1038/msb.2011.75.

Silva, F.M. *et al.* (2014) 'Aphid gene of bacterial origin encodes a protein transported to an obligate endosymbiont', *Eukaryotic Cell*, 8(2), pp. 352–362. Available at: https://doi.org/10.1017/S0031182014001139.

Simarro, P.P. *et al.* (2012) 'Estimating and Mapping the Population at Risk of Sleeping Sickness', *PLoS Neglected Tropical Diseases*. Edited by J.M. Ndung'u, 6(10), p. e1859. Available at: https://doi.org/10.1371/journal.pntd.0001859.

Singer, A. *et al.* (2017) 'Massive Protein Import into the Early-Evolutionary-Stage Photosynthetic Organelle of the Amoeba *Paulinella chromatophora*', *Current Biology*, 27(18), pp. 2763-2773.e5. Available at: https://doi.org/10.1016/j.cub.2017.08.010.

Singh, S.K. *et al.* (2012) 'Three redundant murein endopeptidases catalyse an essential cleavage step in peptidoglycan synthesis of *Escherichia coli* K12', *Molecular Microbiology*, 86(5), pp. 1036–1051. Available at: https://doi.org/10.1111/mmi.12058.

Skalický, T. *et al.* (2021) 'Endosymbiont capture, a repeated process of endosymbiont transfer with replacement in Trypanosomatids *Angomonas Spp.*', *Pathogens*, 10(6), pp. 1–13. Available at: https://doi.org/10.3390/pathogens10060702.

Sláviková, S. *et al.* (2005) 'Homologous and heterologous reconstitution of Golgi to chloroplast transport and protein import into the complex chloroplasts of *Euglena'*, *Journal of Cell Science*, 118(8), pp. 1651–1661. Available at: https://doi.org/10.1242/jcs.02277.

Sleight, R.G. and Pagano, R.E. (1984) 'Transport of a fluorescent phosphatidylcholine analog from the plasma membrane to the golgi apparatus', *Journal of Cell Biology*, 99(2), pp. 742–751. Available at: https://doi.org/10.1083/jcb.99.2.742.

Soares, M.J. and De Souza, W. (1988) 'Freeze-Fracture Study of the Endosymbiont of *Blastocrithidia culicis* 1', *The Journal of Protozoology*, 35(3), pp. 370–374. Available at: https://doi.org/10.1111/j.1550-7408.1988.tb04109.x.

Sockolosky, J.T. and Szoka, F.C. (2013) 'Periplasmic production via the pET expression system of soluble, bioactive human growth hormone', *Protein Expression and Purification*, 87(2), pp. 129–135. Available at: https://doi.org/10.1016/j.pep.2012.11.002.

Southern, E.M. (1975) 'Detection of Specific Sequences Among DNA Fragments Separated by Gel Electrophoresis', in *Molecular Biology*. Elsevier, pp. 503–517. Available at: https://doi.org/10.1016/B978-0-12-131200-8.50041-1.

Souza, W. *et al.* (1999) 'Endosymbiosis in protozoa of the Trypanosomatidae family', *FEMS Microbiology Letters*, 173(1), pp. 1–8. Available at: https://doi.org/10.1016/S0378-1097(99)00005-1.

Sprent, J.I. (2007) 'Evolving ideas of legume evolution and diversity: a taxonomic perspective on the occurrence of nodulation', *New Phytologist*, 174(1), pp. 11–25. Available at: https://doi.org/10.1111/j.1469-8137.2007.02015.x.

Stebeck, C.E. *et al.* (1995) 'Kinetoplastid membrane protein-11 (KMP-11) is differentially expressed during the life cycle of African trypanosomes and is found in a wide variety of kinetoplastid parasites', *Molecular and Biochemical Parasitology*, 71(1), pp. 1–13. Available at: https://doi.org/10.1016/0166-6851(95)00022-S.

Stirba, F.P. (2022) 'Optimization of the DiCre system and establishment of a blasticidin resistance marker for their use in *Angomonas deanei*', *Bachelor Thesis*.

Taguchi, A. *et al.* (2019) 'FtsW is a peptidoglycan polymerase that is functional only in complex with its cognate penicillin-binding protein', *Nature Microbiology*, 4(4), pp. 587–594. Available at: https://doi.org/10.1038/s41564-018-0345-x.

Takeya, K. *et al.* (2018) 'Addition of urea and thiourea to electrophoresis sample buffer improves efficiency of protein extraction from TCA/acetone-treated smooth muscle tissues for phos-tag SDS-PAGE', *ELECTROPHORESIS*, 39(2), pp. 326–333. Available at: https://doi.org/10.1002/elps.201700394.

Teixeira, M.M.G. *et al.* (2011) 'Phylogenetic validation of the genera *Angomonas* and *Strigomonas* of Trypanosomatids harboring bacterial endosymbionts with the description of new species of trypanosomatids and of proteobacterial symbionts', *Protist*, 162(3), pp. 503–524. Available at: https://doi.org/10.1016/j.protis.2011.01.001.

Teng, S. chun, Wang, S.X. and Gabriel, A. (1995) 'A new non-LTR retrotransposon provides evidence for multiple distinct site-specific elements in *Crithidia fasciculata* miniexon arrays.', *Nucleic acids research*, 23(15), pp. 2929–36. Available at: https://doi.org/10.1093/nar/23.15.2929.

Terfrüchte, M. *et al.* (2014) 'Establishing a versatile Golden Gate cloning system for genetic engineering in fungi', *Fungal Genetics and Biology*, 62, pp. 1–10. Available at: https://doi.org/10.1016/j.fgb.2013.10.012.

Testerink, N. *et al.* (2009) 'Depletion of phosphatidylcholine affects endoplasmic reticulum morphology and protein traffic at the Golgi complex', *Journal of Lipid Research*, 50(11), pp. 2182–2192. Available at: https://doi.org/10.1194/jlr.M800660-JLR200.

Timmis, J.N. *et al.* (2004) 'Endosymbiotic gene transfer: Organelle genomes forge eukaryotic chromosomes', *Nature Reviews Genetics*, 5(2), pp. 123–135. Available at: https://doi.org/10.1038/nrg1271.

Tokuyasu, K.T. (1973) 'a Technique for Ultracryotomy of Cell Suspensions and Tissues', *The Journal of Cell Biology*, 57(2), pp. 551–565. Available at: https://doi.org/10.1083/jcb.57.2.551.

Typas, A. *et al.* (2012) 'From the regulation of peptidoglycan synthesis to bacterial growth and morphology', *Nature Reviews Microbiology*, 10(2), pp. 123–136. Available at: https://doi.org/10.1038/nrmicro2677.

Urban, J.M. and Cryan, J.R. (2012) 'Two ancient bacterial endosymbionts have coevolved with the planthoppers (Insecta: Hemiptera: Fulgoroidea)', *BMC Evolutionary Biology*, 12(1), p. 87. Available at: https://doi.org/10.1186/1471-2148-12-87.

Vainio, S. *et al.* (2009) 'Evidence that J-binding protein 2 is a thymidine hydroxylase catalyzing the first step in the biosynthesis of DNA base J', *Molecular and Biochemical Parasitology*, 164(2), pp. 157–161. Available at: https://doi.org/10.1016/j.molbiopara.2008.12.001.

Vaz, F. and Filipe, S. (2015) 'Preparation and Analysis of Crude Autolytic Enzyme Extracts from *Staphylococcus aureus*', *BIO-PROTOCOL*, 5(24). Available at: https://doi.org/10.21769/BioProtoc.1687.

Voleman, L. and Doležăl, P. (2019) 'Mitochondrial dynamics in parasitic protists', *PLoS Pathogens*, 15(11), pp. 1–15. Available at: https://doi.org/10.1371/journal.ppat.1008008.

Votýpka, J. *et al.* (2014) '*Kentomonas* gen. n., a New Genus of Endosymbiont-containing Trypanosomatids of Strigomonadinae subfam. n.', *Protist*, 165(6), pp. 825–838. Available at: https://doi.org/10.1016/j.protis.2014.09.002.

Wang, Z. *et al.* (2000) 'Inhibition of *Trypanosoma brucei* gene expression by RNA interference using an integratable vector with opposing T7 promoters', *Journal of Biological Chemistry*, 275(51), pp. 40174–40179. Available at: https://doi.org/10.1074/jbc.M008405200.

Webster, R.E. (1991) 'The tol gene products and the import of macromolecules into *Escherichia coli*', *Molecular Microbiology*, 5(5), pp. 1005–1011. Available at: https://doi.org/10.1111/j.1365-2958.1991.tb01873.x.

Wehbi, H. *et al.* (2011) 'The Peptidoglycan-Binding Protein FimV Promotes Assembly of the *Pseudomonas aeruginosa* Type IV Pilus Secretin', *Journal of Bacteriology*, 193(2), pp. 540–550. Available at: https://doi.org/10.1128/JB.01048-10.

Weiss, D.S. *et al.* (1999) 'Localization of FtsI (PBP3) to the septal ring requires its membrane anchor, the Z ring, FtsA, FtsQ, and FtsL.', *Journal of bacteriology*, 181(2), pp. 508–20.

William Studier, F. *et al.* (1990) 'Use of T7 RNA polymerase to direct expression of cloned genes', in *Proc. Natl. Acad. Sci. U.S.A*, pp. 60–89. Available at: https://doi.org/10.1016/0076-6879(90)85008-C.

Wirtz, E. and Clayton, C. (1995) 'Inducible Gene Expression in Trypanosomes Mediated by a Prokaryotic Repressor', *Science*, 268(5214), pp. 1179–1183. Available at: https://doi.org/10.1126/science.7761835.

Wolters, R. (2019) 'Exploring inducible genetic systems for the functional characterization of endosymbiosis-related genes in the trypanosomatid *Angomonas deanei*', *Master thesis*.

Wu, L.J. and Errington, J. (2004) 'Coordination of cell division and chromosome segregation by a nucleoid occlusion protein in *Bacillus subtilis'*, *Cell*, 117(7), pp. 915–925. Available at: https://doi.org/10.1016/j.cell.2004.06.002.

Xiang, Y. *et al.* (2008) 'Crystal and cryoEM structural studies of a cell wall degrading enzyme in the bacteriophage ϕ29 tail', *Proceedings of the National Academy of Sciences*, 105(28), pp. 9552–9557. Available at: https://doi.org/10.1073/pnas.0803787105.

Yurchenko, V.Y. *et al.* (2009) 'Selective recovery of the cultivation-prone components from mixed trypanosomatid infections: A case of several novel species isolated from Neotropical Heteroptera', *International Journal of Systematic and Evolutionary Microbiology*, 59(4), pp. 893–909. Available at: https://doi.org/10.1099/ijs.0.001149-0.

Zahrl, D. *et al.* (2005) 'Peptidoglycan degradation by specialized lytic transglycosylases associated with type III and type IV secretion systems', *Microbiology*, 151(11), pp. 3455–3467. Available at: https://doi.org/10.1099/mic.0.28141-0.

Zakharova, A. *et al.* (2021) 'A New Model Trypanosomatid, *Novymonas esmeraldas* : Genomic Perception of Its " *Candidatus* Pandoraea novymonadis" Endosymbiont', *mBio*. Edited by L.D. Sibley, 12(4). Available at: https://doi.org/10.1128/mBio.01606-21.

Zhao, G., Meier, T. I., Kahl, S. D., Gee, K. R., & Blaszczak, L. C. (1999). BOCILLIN FL, a Sensitive and Commercially Available Reagent for Detection of Penicillin-Binding Proteins. *Antimicrobial Agents and Chemotherapy*, *43*(5), 1124–1128. https://doi.org/10.1128/AAC.43.5.1124

Zhou, R., Chen, S. and Recsei, P. (1988) 'A dye release assay for determination of lysostaphin activity', *Analytical Biochemistry*, 171(1), pp. 141–144. Available at: https://doi.org/10.1016/0003-2697(88)90134-0.

6 Appendix

Table 6.1 Overview of all created plasmids, cell lines and the individual contribution of all involved researchers. Name of the person generating the plasmid, *A. deanei* cell line based on Adea126 (light red background) and the experimental data, divided into epifluorescence microscopy, isolation of ES of the corresponding cell line and Western blot analyses of purified ES and whole cell lysate. Only if ETP candidates showed ES located eGFP signal during epifluorescence microscopy and enrichment in the ES fraction was observed via Western blot, confocal microscopy was performed. Grey background: N-terminally tagged eGFP constructs, white background, C-terminal eGFP constructs. X: analysis not performed.

Accession (ETP)	Plasmid (generator)	Cell line (generator)	Epifluorescence microscopy (generator)	ES Isolation + WB (generator)	Confocal microscopy (generator)
CAD2220707.1 (ETP1)	pAdea119 (Jorge Morales)	Adea126 (Davide Zanini)	(Jorge Morales)	X	(Georg Ehret/Jorge Morales)
CAD2221027.1 (ETP2)	pAdea035 (Georg Ehret)	Adea142 (Jorge Morales)	(Jorge Morales)	(Georg Ehret)	(Georg Ehret/Jorge Morales)
	pAdea036 (Georg Ehret)	Adea157 (Jan. Wieneke)	(Jorge Morales)	(Georg Ehret)	(Georg Ehret/Jorge Morales)
CAD2213480.1 (ETP3)	pAdea024 (Sofia Kokkori)	Adea155 (Jan Wieneke)	(Jorge Morales)	(Jorge Morales)	(Georg Ehret/Jorge Morales)
	pAdea025 (Sofia Kokkori)	Adea158 (Jan Wieneke)	(Georg Ehret)	(Georg Ehret)	(Georg Ehret/Jorge Morales)
CAD2216595.1	pAdea248 (Lena Kröninger)	Adea281 (Lena Kröninger)	(Lena Kröninger)	(Georg Ehret/Lena Kröninger)	X
	pAdea249 (Lena Kröninger)	Adea282 (Lena Kröninger)	(Lena Kröninger)	(Georg Ehret/Lena Kröninger)	X
CAD2216818.1; CAD2216819.1; CAD2216820.1;	pAdea052 (Jorge Morales)	Adea283 (Lena Kröninger)	(Georg Ehret)	(Georg Ehret)	(Georg Ehret)

CAD2216821.1 (ETP5)	pAdea236 (Lena Kröninger)	Adea277 (Lena Kröninger)	(Georg Ehret)	(Georg Ehret)	(Georg Ehret)
CAD2220712.1	pAdea053 (Jorge Morales)	Adea284 (Lena Kröninger)	(Georg Ehret)	(Georg Ehret)	X
	pAdea237 (Lena Kröninger)	Adea274 (Lena Kröninger)	(Georg Ehret)	(Georg Ehret)	X
CAD2217314.1 (ETP7)	pAdea054 (Jorge Morales)	Adea144 (Jorge Morales)	(Jorge Morales)	(Rebecca Wolters)	(Georg Ehret/Jorge Morales)
	pAdea238 (Lena Kröninger)	Adea279 (Lena Kröninger)	(Georg Ehret)	(Georg Ehret)	(Georg Ehret)
CAD2216283.1 (ETP8)	pAdea117 (Michael Krakovka)	Adea150 (Michael Krakovka)	(Michael Krakovka)	(Michael Krakovka)	(Georg Ehret/Jorge Morales)
	pAdea266 (Georg Ehret)	Adea303 (Georg Ehret)	(Georg Ehret)	(Georg Ehret)	(Georg Ehret)
CAD2212698.1 (ETP9)	pAdea258 (Tobias Reinicke)	Adea305 (Tobias Reinicke)	(Tobias Reinicke)	(Georg Ehret)	(Georg Ehret)
	pAdea259 (Tobias Reinicke)	Adea306 (Tobias Reinicke)	(Tobias Reinicke)	(Georg Ehret)	(Georg Ehret)
CAD2220896.1	pAdea250 (Georg Ehret)	Adea292 (Georg Ehret)	(Georg Ehret)	(Georg Ehret)	X
	pAdea251 (Georg Ehret)	Adea293 (Georg Ehret)	(Georg Ehret)	(Georg Ehret)	X

CAD2222258.1	pAdea252 (Georg Ehret)	Adea294 (Georg Ehret)	(Georg Ehret)	(Georg Ehret)	X
	pAdea253 (Georg Ehret)	Adea295 (Georg Ehret)	(Georg Ehret)	(Georg Ehret)	X
CAD2222840.1	pAdea254 (Georg Ehret)	Adea296 (Georg Ehret)	(Georg Ehret)	(Georg Ehret)	X
	pAdea255 (Georg Ehret)	Adea297 (Georg Ehret)	(Georg Ehret)	(Georg Ehret)	X
CAD2218427.1	pAdea256 (Tobias Reinicke)	Adea298 (Tobias Reinicke)	(Tobias Reinicke)	(Georg Ehret)	X
	pAdea257 (Tobias Reinicke)	Adea299 (Tobias Reinicke)	(Tobias Reinicke)	(Georg Ehret)	X
CAD2216215.1	pAdea274 (Tobias Reinicke)	Adea310 (Tobias Reinicke)	(Tobias Reinicke)	(Georg Ehret)	X
	pAdea273 (Tobias Reinicke)	Adea309 (Tobias Reinicke)	(Tobias Reinicke)	(Georg Ehret)	X

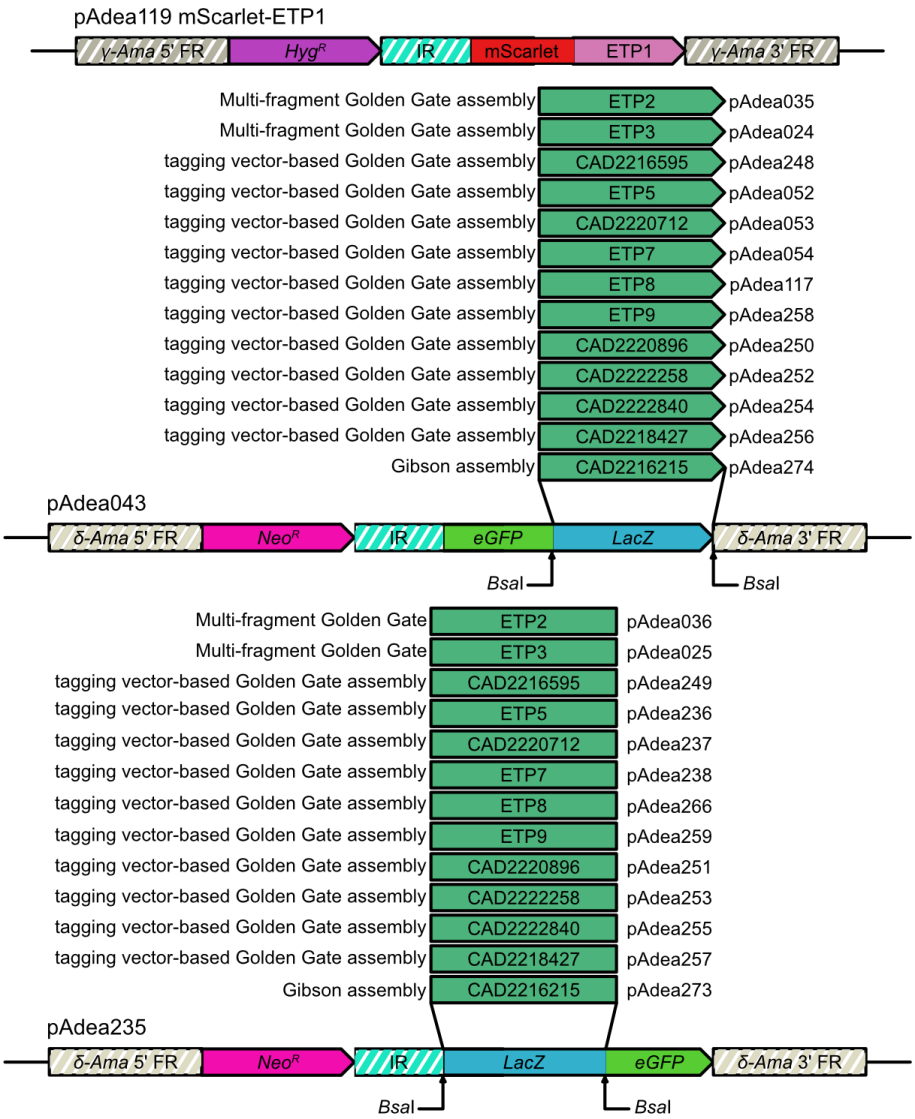

Figure 6.1: Cassettes used for the expression of recombinant proteins. The plasmid pAdea119 contains a cassette for the expression of ETP1 (pink arrow) fused to the C-terminus of mSCARLET (red rectangle) from the γ–amastin locus; the γ–amastin flanking regions (FRs) used for homologous recombination (HR) are represented by hatched grey bars. The plasmids pAdea043 and pAdea235 contain cassettes for expression from the δ–amastin locus; FRs used for HR are represented by hatched brown bars. By replacement of the lacZα expression cassette with the POI (dark green rectangles) at the BsaI sites, the POI is scarlessly fused to the C-terminus (pAdea043) or N-terminus (pAdea235) of eGFP (green rectangle/arrow). The absence/presence of the lacZα cassette allows for blue/white selection of the resulting plasmids. Hygromycin resistance gene (hyg, violet arrow); neomycin resistance gene (neo, fuchsia arrow); the intergenic region between the glyceraldehyde 3-phosphate dehydrogenase I and II from *A. deanei* (IR, hatched cyan bar); lacZα expression cassette (lacZ, blue-green rectangle).

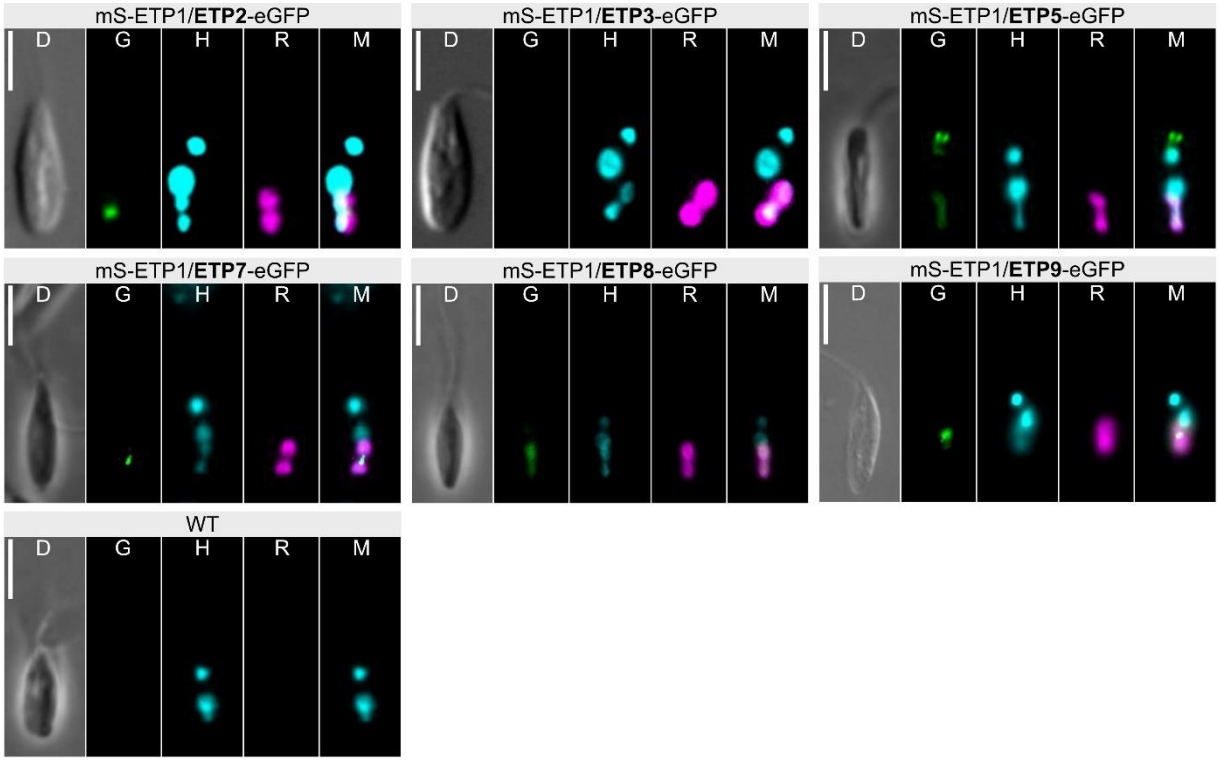

Figure 6.2: Subcellular location of the various ETPs with a C-terminal eGFP tag in *A. deanei.* The recombinant ETPs with C-terminal eGFP tags show a green fluorescence signal corresponding to the subcellular localization observed when the eGFP tag was placed at their N-terminus. Only for ETP3-eGFP no fluorescence signal was detected. WT, wildtype; mS, mSCARLET; D, differential interference contrast; R, red channel; G, green channel; H, blue channel visualizing Hoechst 33342 staining; M, merge between the three fluorescence channels. Scale bar is 5 μm.

```
CAD2220707.1 (-> ETP1)
CAD2220707.1   ---------- ---------- ---------- ---------- ---------- ---------- ---------- ---------- ---------- --------MR
a814;735 K:    MTEPNAQTPP RPEQDSNNNQ TNEEEEDPRL VHPIMPAALP PPEGQIPKYL NAVYYGGRLA GIKRPVKAEL EAMGEEEAAR QKIEREERKE IKAIEKDFMR

CAD2220707.1   GVMDEERRVA KEKKEAEKKE RKEKKEAEKK RKEEEKQQQE EQQEEQTPAA EQPEAPAEEV PAQEGEEGAA TKEGGCKMCQ WLPSLHLPQL PRLPWFAKDG
a814;735 K:    GVMDEERRVA KEKKEAEKKE RKEKKEAEKK RKEEEKQQQE EQQEEQTPAA EQPEAPAEEV PAQEGEEGAA TKEGGCKMCQ WLPSLHLPQL PRLPWFAKDG

CAD2220707.1   ETPAEGEEQE EKPKVVPRRS VIGPRPNATK RPYLMIMAEE DLPPEEEVEK WRQEQRILAE EEKARQELEK ARKAEAKKAE KEAKKLAKQA KKDSKKYAKE
a814;735 K:    ETPAEGEEQE EKPKVVPRRS VIGPRPNATK RPYLMIMAEE DLPPEEEVEK WRQEQRILAE EEKARQELEK ARKAEAKKAE KEAKKLAKQA KKDSKKYAKE

CAD2220707.1   HKNDPPKEEE EEKKEEVATP QPSASPAASK AATPSPARPA YVPKAATPAA SRDASPSQPA TTAAAEPAAT PASDVVEKKD A
a814;735 K:    HKNDPPKEEE EEKKEEVATP QPSASPAASK AATPSPARPA YVPKAATPAA SRDASPSQPA TTAAAEPAAT PASDVVEKKD A

CAD2221027.1 (-> ETP2)
CAD2221027.1   MDYDEDEYFD NGMGFQFNNN NNNNFIPPVT PPPMYTMPAE STFPNRTNTI PVNNENSIPG QPAYTPTVAS QPGYGLGFPP SASPNKPLAE TPRERSIHSS
a8985;116 K:   MDYDEDEYFD NGMGFQFNNN NNNNFIPPVT PPPMYTMPAE STFPNRTNTI PVNNENSIPG QPAYTPTVAS QPGYGLGFPP SASPNKPLAE TPRERSIHSS

CAD2221027.1   NHGGEMRTPL RSNVGADPSI TNRFFNGPTP KRASPSVPTN NTLHTSLNMS RASSSREPVV PASMLGAPGA NPYYMFDNNN NNSMPPPPQQ PTPSPVRVAN
a8985;116 K:   NHGGEMRTPL RSNVGADPSI TNRFFNGPTP KRASPSVPTN NTLYTSLNMS RASSSREPVV PASMLGAPGA NPYYMFDNNN NNNE...... ..........

CAD2221027.1   TSDNSLNSGA RNTNNNNNEA LEQPYNVSVP PHTATVPPPP EALQVHRTPV NQSHTSSSNA HSGYVNSPSA VSSIHHPTDR LAVVTPAQNS SFASSNTAST
a8985;116 K:   .......... .......... .......... .......... .......... .......... .......... .......... .......... ..........

CAD2221027.1   TPSKFIYPRS AQRPPIILRH EVPQEDVPPA RTPFCYRRSS AAAIAV
a8985;116 K:   .......... .......... .......... .......... ......

CAD2213480.1 (-> ETP3)
CAD2213480.1   MIDTKFHCLI TSKERNVFDR KKSVLSVKTP SNPFSFSYNA VVSECQAWFD SWLGSVSTSS NHCVLMHAMN TESGIRLFEG TVNQIRTKLA ATGPLEIAVS
a2301;422 K:   MIDTKFHCLI TSKERNVFDR KKSVLSVKTP SNPFSFSYNA VVSECQAWFD SWLGSVSTSS NHCVLMHAMN TESGIRLFEG TVNQIRTKLA ATGPLEIAVS

CAD2213480.1   RVYSWGCMDF ISDSCIEENR HVDAGVNNLL TELSFKALES ADFHKLLKKC TSMMSGHCIV HVEIQCGNAR CSINLVPPLK DTNVILLKDL LRLRSQLLSS
a2301;422 K:   RVYSWGCMDF ISDSCIEENR HVDAGVNNLL TELSFKALES ADFHKLLKKC TSMMSGHCIV HVEIQCGNAR CSINLVPPLK DTNVILLKDL LRLRSQLLSS

CAD2213480.1   SAENSECRLF PLLIPHHDTK APCQLHVISL DDRDSSSDFH LSAWFGSSST TDDEFWQSKF RKLQTVSPAA NARKNEFKCD AQMAEKLRST RRTTDRCVSL
a2301;422 K:   SAENSECRLF PLLIPHHDTK APCQLHVISL DDRDSSSDFH LSAWFGSSST TDDEFWQSKF RKLQTVSPAA NARKNEFKCD AQMAEKLRST RRTTDRCVSL

CAD2213480.1   GAVENTDQSE QSLDPVLNAS SIEENCEQVS RTLALIKAML EEHNRREVKE HIPLSERSVP KGEDGEKRDF KVNSCADLVP LIKAKLSALE RERRKYERAV
a2301;422 K:   GAVENTDQSE QSLDPVLNAS SIEENCEQVS RTLALIKAML EEHNRREVKE HIPLSERSVP KGEDGEKRDF KVNSCADLVP LIKAKLSALE RERRKYERAV

CAD2213480.1   EDLRSAIPDS RSEVGNDDRA EDEGEECESV HSNNSLSAAG KPVEPIGVLS PSQPSLLSPD STISGSPYFD PFVSKVKKHI IKTTEEAKQM RHAIDVTFEA
a2301;422 K:   EDLRSAIPDS RSEVGNDDRA EDEGEECESV HSNNSLSAAG KPVEPIGVLS PSQPSLLSPD STISGSPYFD PFVSKVKKHI IKTTEEAKQM RHAIDVTFEA

CAD2213480.1   LGGDSSIAKA DPIIATKSLI ELAGDTSESI TQVKQLLDLE NDAVEHREKM STVLDGVREK LKKVDEVQKE ATTIVESFTK ADEEETTSVS GEGGAAVVER
a2301;422 K:   LGGDSSIAKA DPIIATKSLI ELAGDTSESI TQVKQLLDLE NDAVEHREKM STVLDGVREK LKKVDEVQKE ATTIVESFTK ADEEETTSVS GEGGAAVVER

CAD2213480.1   KHIQRKVKPM SPEEAASDAN MTLTSTLYFG VLPRSIKQNP STSLVLADIT PEAVRNFKRE MKQKMQELDE ANNALQVCVK LMKPGGKAPS THRDLVTEAL
a2301;422 K:   KHIQRKVKPM SPEEAASDAN MTLTSTLYFG VLPRSIKQNP STSLVLADIT PEAVRNFKRE MKQKMQELDE ANNALQVCVK LMKPGGKAPS THRDLVTEAL

CAD2213480.1   RLCQDANKAL TLTDQLFDDF APDDDGASPQ STITSLSGET IPKNKLTLAT RTEALVEAMK TLQNDSESCF EENDNLQRRV VFLLQQEERL QEEREAAVKR
a2301;422 K:   RLCQDANKAL TLTDQLFDDF APDDDGASPQ STITSLSGET IPKNKLTLAT RTEALVEAMK TLQNDSESCF EENDNLQRRV VFLLQQEERL QEEREAAVKR

CAD2213480.1   EQFLGNIQEK LNETEEELTT RDEELKRLQE ELKEATQKCE EATKASEMKD NIRNKRDSLL TETEYLQQDV EDLLMTKGAI EEVLGDILVS LESAVEDLEV
a2301;422 K:   EQFLGNIQEK LNETEEELTT RDEELKRLQE ELKEATQKCE EATKASEMKD NIRNKRDSLL TETEYLQQDV EDLLMTKGAI EEVLGDILVS LESAVEDLEV

CAD2213480.1   QESAMLTEVQ RAESVLRLSS TSAYAQEQKV LAKLLEAVEK QSN
a2301;422 K:   QESAMLTEVQ RAESVLRLSS TSAYAQEQKV LAKLLEAVEK QSN

CAD2216595.1
CAD2216595.1   MLKGASEVEL RKFQQLVNHW HDPNGALRSL HLFNPIRVGY INDMVRRYGR RVAATGDQSS GNFDYLLRSG ANGSQAGYSA FLANTSDGSK LRVLDVGCGG
a2685;461 K:   MLKGASEVEL RKFQQLVNHW HDPNGALRSL HLFNPIRVGY INDMVRRYGR RVAATGDQSS GNFDYLLRSG ANGSQAGYSA FLANTSDGSK LRVLDVGCGG

CAD2216595.1   GILSESLFRL GASVTGIDLV EESVAVANER KGMVLANLNQ SSPLYREEDL TFRQASLFEV LEEESKADGG YDVVVASEVV EHVDDARAFV KALGDVTKAR
a2685;461 K:   GILSESLFRL GASVTGIDLV EESVAVANER KGMVLANLNQ SSPLYREEDL TFRQASLFEV LEEESKADGG YDVVVASEVV EHVDDARAFV KALGDVTKAR

CAD2216595.1   GGLLIVSTME KSICSFLSHI VVAETLTGIV APRHPTTGGK FINKKDLSEY LAQHNHIAEV DHKYIASFPD PFQSAATRNL QLQFKLTNAV NTGHYLWTGL
a2685;461 K:   GGLLIVSTME KSICSFLSHI VVAETLTGIV APGTHDW-GK FINKKDLSEY LAQHNHIAEV DHKYIASFPD PFQSAATRNL QLQFKLTNAV NTGHYLWTGL

CAD2216595.1   KQ
a2685;461 K:   KQ

CAD2216818.1-CAD2216821.1 (-> ETP5)
CAD2216818.1   MATTLEEFSA KLDRLDQEFA KKMEEQNKKF FADKPDDSTL SPEMKEHYEK FEKMIQEHTD KFNNKMHEHS EHFKQKFAEL LEQQKNAQLP K
CAD2216819.1   MATTLEEFSA KLDRLDQEFA KKMEEQNKKF FADKPDDSTL SPEMKEHYEK FEKMIQEHTD KFNNKMHEHS EHFKQKFAEL LEQQKNAQLP K
CAD2216820.1   MATTLEEFSA KLDRLDQEFA KKMEEQNKKF FADKPDDSTL SPEMKEHYEK FEKMIQEHTD KFNNKMHEHS EHFKQKFAEL LEQQKNAQLP K
CAD2216821.1   MATTLEEFSA KLDRLDQEFA KKMEEQNKKF FADKPDDSTL SPEMKEHYEK FEKMIQEHTD KFNNKMHEHS EHFKQKFAEL LEQQKNAQLP K
a45;12605 K:   MATTLEEFSA KLDRLDQEFA KKMEEQNKKF FADKPDDSTL SPEMKEHYEK FEKMIQEHTD KFNNKMHEHS EHFKQKFAEL LEQQKNAQLP K

CAD2220712.1
CAD2220712.1   MLRRFSPRLC AAHHQNDHYT NNFFQKLRTR LMDRIPQTGH ETTARYKWAT HVYWYLLDPL LRCHHYYYRR KVVVDRFLER NSVFANTIFG ILLGLTVYFL
a8234;114 K:   MLRRFSPRLC AAHHQNDHYT NNFFQKLRTR LMDRIPQTGH ETTARYKWAT HVYWYLLDPL LRCHHYYYRR KVVVDRFLER NSVFANTIFG ILLGLTVYFL

CAD2220712.1   LAELVLPTAA DDEHNKNKIM HPHNMEIYSP QDNAQIVVDC IGTSTTKELP AFQLMRLKRI IMGRVLEVAD LSEVRRQREE TEKLKALLAK
a8234;114 K:   LAELVLPTAA DDEHNKNKIM HPHNMEIYSP QDNAQIVVDC IGTSTTKELP AFQLMRLKRI IMGRVLEVAD LSEVRRQREE TEKLKALLAK

CAD2217314.1 (-> ETP7)
CAD2217314.1   MLQSLRDKYD DHKRRVDERE RLRNDPTSDP NYYQDVINRS LLGEEVAGRP NVTPKTRRPH HDPTADPNYH QDVINRSLLN FNSETTPPPK EPKKGWFGLN
a3942;267 K:   MLQSLRDKYD DHKRRVDERE RLRNDPTSDP NYYQDVINRS LLGEEVAGRP NVTPKTRRPH HDPTADPNYH QDVINRSLLN FNSETTPPPK EPKKGWFGLN

CAD2217314.1   NVVQGALEKC KLLKEELFDD DKTDDPYDSE SNRAYRSKFA DYGDAGIPFS LCDNLNGDST YYYAKSNSCS SSRLPSSSKS KSRSTKHSSS PETVMSNNGR
a3942;267 K:   NVVQGALEKC KLLKEELFDD DKTDDPYDSE SNRAYRSKFA DYGDAGIPFS LCDNLNGDST YYYAKSNSCS SSRLPSSSKS KSRSTKHSSS PETVMSNNGR

CAD2217314.1   EYSHSRPPLD PPIKSYVGSN LNVVNNSNNT SSAFYYYHHC NRQSESNTHS SVNVDLSNIE NQVAPSVPPT APPFVLEKME SEVSTRKSYS VLPSNSDRVP
a3942;267 K:   EYSHSRPPLD PPIKSYVGSN LNVVNNSNNT SSAFYYYHHC NRQSESNTHS SVNVDLSNIE NQVAPSVPPT APPFVLEKME SEVSTRKSYS VLPSNSDRVP

CAD2217314.1   PYTIEEMHSK SRVNRVSFLD SSRSPSVAPS VYYKVMETPE ERRHLFIVKC LPHLGVVGTC ALYGNVYVET GGTFDPKQKE MHPPFHDAMG LFQMNKEMRA
a3942;267 K:   PYTIEEMHSK SRVNRVSFLD SSRSPSVAPS VYYKVMETPE ERRHLFIVKC LPHLGVVGTC ALYGNVYVET GGTFDPKQKE MHPPFHDAMG LFQMNKEMRA

CAD2217314.1   YFEKYCAEFY IRSHHLTATI VTTPSTAGGV RRDFLDPDTM DAQLTFVINE IATGSYIGAG NAATLRKSFY LLKKDISHND MRVTLTKKEY VSPPMVEAAA
a3942;267 K:   YFEKYCAEFY IRSHHLTATI VTTPSTAGGV RRDFLDPDTM DAQLTFVINE IATGSYIGAG NAATLRKSFY LLKKDISHND MRVTLTKKEY VSPPMVEAAA

CAD2217314.1   EMFCNLFERP SIPHLDRRKI SSVECLEYIR EQGLTVRM
a3942;267 K:   EMFCNLFERP SIPHLDRRKI SSVECLEYIR EQGLTVRM
```

Supplementary Fig. 6.3 (continues)

CAD2216283.1 (-> ETP8)

```
CAD2216283.1   ---------- ---------- ---------- ---------- ---------- ---------- ---------- ---------- ---------- ----------
RACE a6023;145 MSVVSANSNV RTVTGGNYVA QNVAVEVVKG TPFDHMIPVI TDLETKEGEP SNPSSEAKIK KLEDAGLKVQ RLPISYKGKN GDEIHEQLLP FVIHYKMQLL

CAD2216283.1   ---------- ---------- --MTSFHFGI PLKEKILLQF STLEARKLLG NTTESMNDEE TVDFSATRHL APEDLGVIND SIVNFESTVN KLLELTQTPG
RACE 6023;145  LLSERTQRKV VSNGEMTSRS NIMTSFHFGI PLKEKILLQF STLEARKLLG NTTESMNDEE TVDFSATRHL APEDLGVIND SIVNFESTVN KLLELTQTPG

CAD2216283.1   KSSK
RACE 6023;145  KSSK
```

CAD2212698.1 (->ETP9)

```
CAD2212698.1   MNTFIEAVNR LQDIVSGSDV SLDLTLPQIA VVGSQSSGKS SVLEHIVGEE FLPRGPTMVT RCPIVLQLHQ LPKNDKRKWG EFLHLPNKRF TDFNLIREEI
a3170;304 K:   MNTFIEAVNR LQDIVSGSDV SLDLTLPQIA VVGSQSSGKS SVLEHIVGEE FLPRGPTMVT RCPIVLQLHQ LPKNDKRKWG EFLHLPNKRF TDFNLIREEI

CAD2212698.1   LRYTRELIGD RTVTSQSITL KISSAAVANL TLVDLPGLVT TPIRGQPETI VTDIEDMVRR YVADKNTVIL AITPANQDVA TSAALSVSRM VDPHGERTMG
a3170;304 K:   LRYTRELIGD RTVTSQSITL KISSAAVANL TLVDLPGLVT TPIRGQPETI VTDIEDMVRR YVADKNTVIL AITPANQDVA TSAALSVSRM VDPHGERTMG

CAD2212698.1   VLTKLDLMDR GTTAHRTLMG DEYELKFGFI GVVNRSQESI NSGQTMSDAR AAEEEFINEY YPELSGRMGT KYLTAVLNSV LVSRIKECLP FIRQQISDKV
a3170;304 K:   VLTKLDLMDR GTTAHRTLMG DEYELKFGFI GVVNRSQESI NSGQTMSDAR AAEEEFINEY YPELSGRMGT KYLTAVLNSV LVSRIKECLP FIRQQISDKV

CAD2212698.1   NDASVVLKEL GPRMPPEDGP EKTKYVRDLL QRFELCVTSE IEGRMALATP GLKAGARIGA VVRHRYWTEV ADLEVSDKVE DQFLRETYHS TSGVYQPHLH
a3170;304 K:   NDASVVLKEL GPRMPPEDGP EKTKYVRDLL QRFELCVTSE IEGRMALATP GLKAGARIGA VVRHRYWTEV ADLEVSDKVE DQFLRETYHS TSGVYQPHLH

CAD2212698.1   GDAAIRPICA TCLIEMERPS ANCVREVKGV LKDVAMKALE SLRFPLLQHS TMEEVDRFYD QQTEACLRAI DSLFEREKSF INISHPLMEC TLPELRLIVQ
a3170;304 K:   GDAAIRPICA TCLIEMERPS ANCVREVKGV LKDVAMKALE SLRFPLLQHS TMEEVDRFYD QQTEACLRAI DSLFEREKSF INISHPLMEC TLPELRLIVQ

CAD2212698.1   GMRQSFGRSR PAGARQALQQ SPLQQYYAQL HFQQFTQQQQ YEQAQKQPAQ GDKSVQENQP QERRAAASEP TPADPTAPSV SLNAQRGGRT MDERNIEIVK
a3170;304 K:   GMRQSFSRSR PAGARQALQQ SPLQQYYAQL HFQQFTQQQQ YEQAQKQPAQ GDKSVQENQP QERRAAASEP TPADPTAPSV SLNAQRGGRT MDERNIEIVK

CAD2212698.1   DSILKYFEIS KLTLGDQVHK LINFYLVYEV CRNLRNVLMD FLTEEVISTV SEPEERARMR KEFNSKLDRL LMCRRALDDF ATDLI
a3170;304 K:   DSILKYFEIS KLTLGDQVHK LINFYLVYEV CRNLRNVLMD FLTEEVISTV SEPEERARMR KEFNSKLDRL LMCRRALDDF ATDLI
```

CAD2220896.1

```
CAD2220896.1   ---------- ---------- ---------- ---------- ---------- ---------- ---------- ---------- ---------- ----------
a5402_199 K:   MRSFARRSLV PCLASMTHGL QRPSPSWCSG RSCQSAPPPQ EEDSHHHHVE ERPRQFQQDM ELRQLVQSAV PLQSTEDIKT MLHGVKNAKE VRHILETVVY

CAD2220896.1   ---------- ---------- ---------- ---------- ---------- ---------- ---------- ---------- ---------- ----------
a5402_199 K:   RHHLCGDVLN GHGFRVTIVQ SLTLVAPRVQ AMEEWFDCLG RFRKLNFLLT RTFAAEGLHL IKEWLTHRFN TEGRTPFLLT TGTAYIRELM YWCHEDKLVF

CAD2220896.1   ---------- ---------- ---------- ---------- ---------- ---------- ---MEEVLDL LRNDIPSRPN FNLLFRLMDY YFATDNVEKL
a5402_199 K:   DHVLYTRIVF LLTIIVSFFD RQNLYRTSFP SDFVKRDGIV TEWIHTNERC VDYDECVVQC DALMEEVLDL LRNDIPSRPN FNLLFRLMDY YFATDNVEKL

CAD2220896.1   IAVMEDAHEY GVTVAESSTA KLMQLACAFN YPTAPELFLR WRVSLPQCAI ASPDISRLLF YYSRSGGGLP CPACGEKYNH RNVNVYHWMA TPPHQRQCPV
a5402_199 K:   IAVMEDAHEY GVTVAESSTA KLMQLACAFN YPTAPELFLR WRVSLPQCAI ASPDISRLLF YYSRSGGGLP CPACGEKYNH RNVNVYHWMA TPPHQRQCPV

CAD2220896.1   LHMARNRKGD LEADPALPQN RDWSERALQL RELSTARSIE WGTQEWRGFL GCFMFAPTEK AMQAKALLDQ SMGAAQMDDF LRAAYIRLLR YHAPELSLPV
a5402_199 K:   LHMARNRKGD LEADPALPQN RDWSERALQL RELSTARSIE WGTQEWRGFL GCFMFAPTEK AMQAKALLDQ SMGAAQMDDF LRAAYIRLLR YHAPELSLPV

CAD2220896.1   LRQWEDSGIR MSPIVLQEAL MAAVTLDDSV QRLESLTHTW DLLREKGSYV MPFTRRYVER RRDALQQQAP LSGEESHIIR EVVEMRPRTV SLLDRKDSSS
a5402_199 K:   LRQWEDSGIR MSPIVLQEAL MAAVTLDDSV QRLESLTHTW DLLREKGSYV MPFTRRYVER RRDALQQQAP LSEEESHIIR EVVEMRPRTV SLLDRKDSSS

CAD2220896.1   DFVIGTSKKN IYIPKRSLKE SERRRDQRRQ RSQSE
a5402_199 K:   DFVIGTSKKN IYIPKRSLKE SERRRDQRRQ RSQSE
```

CAD2222258.1

```
CAD2222258.1   ---------- ---------- ---------- ---------- ---------- ---------- ---------- ---------- ---------- ----------
a5695_215 K:   MTDSDQHLSN ETQLEFTNND SNDQNPATDV ADMNLSEFRR VVQESQPQDN HLPAPPRAVL KYIPEVTDDF IRNFLLRNNM LKTLEQFEVE WYSRFGSAAS

CAD2222258.1   ---------- ---------- ---------- ---------- ---------- ---------- ---------- ---------- -----MKRRC DGLLKQKTVL
a5695_215 K:   RDVPLVPDNY LETAQLSHRI ELLERDLREH AELTTTLNKQ WRQAKKERDF HKANHSRVVQ EKNKLTKVLK QTDRNAADLT PTLEEMKRRC DGLLKQKTVL

CAD2222258.1   SLEKDKLAAQ VEQLEKRLSE AERRLEGEEG ESSTTSGKPK RSKSSQKKEN TSSSAARKRG VAAAVSAART GTSTTKTADG STTDGFVWPP DERPNTEAAP
a5695_215 K:   SLEKDKLAAQ VEQLEKRLSE AERRLEGEEG ESSTTSGKPK RSKSSQKKEN TSSSAARKRG VAAAVSAART GTSTTKTADG STTDGFVWPP DERPNTEAAP

CAD2222258.1   PSLPSHVTQW SNTHTFTAHA MSVTKIALHP RKPAVASCSD DGTWRLSTVP EGELILSGEG HQNWVAAVAM HPAGTMVATG SGDKTVKLWD FATNSCANTL
a5695_215 K:   PSLPSHVTQW SNTHTFTAHA MSVTKIALHP RKPAVASCSD DGTWRLSTVP EGELILSGEG HQNWVAAVAM HPAGTMVATG SGDKTVKLWD FATNSCANTL

CAD2222258.1   RSHTDGVWSV DFQETGALLA SGSLDTTARV WDVEMGKCRQ TLRGHVEAVN AVQWCVGTNI LCTGSGDKTV SLWDTRMNCC ATTLYGHRSP VLSVSTLPGN
a5695_215 K:   RSHTDGVWSV DFQETGALLA SGSLDTTARV WDVEMGKCRQ TLRGHVEAVN AVQWCVGTNI LCTGSGDKTV SLWDTRMNCC ATTLYGHRSP VLSVSTLPGN

CAD2222258.1   QVLASCDTEG TVVVWDIRKL EQKQSFACGP SPANCVTFDG VGEWLAVGSD DSILRLIDLE KETVSELRGH EDGVLCCAFD PAMRFLVSSG SDCTVRYWN
a5695_215 K:   QVLASCDTEG TVVVWDIRKL EQKQSFACGP SPANCVTFDG VGEWLAVGSD DSILRLIDLE KETVSELRGH EDGVLCCAFD PAMRFLVSSG SDCTVRYWN
```

CAD2222840.1

```
CAD2222840.1   MTILENPAPS SSFRNWQNIA TGYGAFCVQE RTAAARRPSV ISFAPAEKPF RIIFSHCPID FLSLTEKLSA KSSTTGLPSS AGSGNKRFVV AVASSLATIL
a5888_177 K:   MTILENPAPS SSFRNWQNIA TGYGAFCVQE RTAAARRPSV ISFAPAEKPF RIIFSHCPID FLSLTEKLSA KSSTTGLPSS AGSGNKRFVV AVASSLATIL

CAD2222840.1   EDWGWVMKGW QTVGQRTDSA MKRRTRTSRT AGSSDDALTR EEWSEVVQVI KEQLEVEREA EYVETTTENM LDEEDGGKKP LSPSASVRDA ALLVSRDRRL
a5888_177 K:   EDWGWVMKGW QTVGQRTDSA MKRRTRTSRT AGSSDDALTR EEWSEVVQVI KEQLEVEREA EYVETTTENM LDEEDGGKKP LSPSASVRDA ALLVSRDRRL

CAD2222840.1   SVDDSLDTTP EVSGAPTRDD TFLAELEEEP ANKVTGVYFY TSDIFDIILL RHIDVWAWSS PHVTILMIMV CFAFPWNQAL VILLAEALPL SLLQRRRAVD
a5888_177 K:   SVDDSLDTTP EVSGAPTRDD TFLAELEEEP ANKVTGVYFY TSDIFDIILL RHIDVWAWSS PHVTILMIMV CFAFPWNQAL VILLAEALPL SLLQRRRAVD

CAD2222840.1   KRTKKRDQRH LETFSKLFSK LGHLKEEEPE TKVNPFKQES DVSVGEEEEE PVKPEDPLVT RVGNFMGTFL AKVLFVAVLL FALFNLILPR SVDLLAVADA
a5888_177 K:   KRTKKRDQRH LETFSKLFSK LGHLKEEEPE TKVNPFKQES DVSVGEEEEE PVKPEDPLVT RVGNFMGTFL AKVLFVAVLL FALFNLILPR SVDLLAVADA

CAD2222840.1   VVGKVVGAAL LLCGVRQVLK PPVVNRRPLS RKAITNLLAS TQRNIHPHID NPSHRYVRPE LSESEKSMVD QLRNFGAPYP LILLRPLRDL SVATGWTPVV
a5888_177 K:   VVGKVVGAAL LLCGVRQVLK PPVVNRRPLS RKAITNLLAS TQRNIHPHID NPSHRYVRPE LSESEKSMVD QLRNFGAPYP LILLRPLRDL SVATGWTPVV

CAD2222840.1   LGEKVRCEHR YSNNDTVHSI RYSVNVPLAN VGTMQAVLLD DVDGQFDELH SSNLYTWDTL LQSRQILKKL DYNLYVVRYQ RRSSMWGVPS SDLDQFVIPA
a5888_177 K:   LGEKVRCEHR YSNNDTVHSI RYSVNVPLAN VGTMQAVLLD DVDGQFDELH SSNLYTWDTL LQSRQILKKL DYNLYVVRYQ RRSSMWGVPS SDLDQFVIPA

CAD2222840.1   VVLNSEQQKA LNISDITPRP PAAEGRRKGH GNLRAFLQCA IPCPESFSAP YVEEAAEGKG RSPTSKEEPT KIAATSLLLG LEEADGSLTL CLYRSYSGVT
a5888_177 K:   VVLNSEQQKA LNISDITPRP PAAEGRRKGH GNLRAFLQCA IPCPESFSAP YVEEAAEGKG RSPTSKEEPT KIAATSLLLG LEEADGSLTL CLYRSYSGVT

CAD2222840.1   RSKFLEEQRL IMGEASTHCL AYLLEATGYQ PSQIADFSNA SGFQPFFCRQ PFTDLPAEEE ENVDPGDDTL ELPAMGARNG VSPERDQGDG MIKRQRSLRF
a5888_177 K:   RSKFLEEQRL IMGEASTHCL AYLLEATGYQ PSQIADFSNA SGFQPFFCRQ PFTDLPAEEE ENVDPGDDTL ELPAMGARNG VSPERDQGDG MIKRQRSLRF

CAD2222840.1   MSTLPLPTVC QTVVRDALQS NLWRLRKTRG GVRVMECTRT VPGIWDGTPH VSVFCAQVVV SCNFFHVMRT LSRNSAVTVY NDAVESRVPL GSQIPVAELL
a5888_177 K:   MSTLPLPTVC QTVVRDALQS NLWRLRKTRG GVRVMECTRT VPGIWDGTPH VSVFCAQVVV SCNFFHVMRT LSRNSAVTVY NDAVESRVPL GSQIPVAELL

CAD2222840.1   ATVEEESSDE EEAALTGVTS VNVSPPVSTV LKQVGEVRGT GSGVYHTAFR GKFGAVARDA ITKEHGPYFF TAKSLREHLF DATQSAEMDL LRELPNDTRM
a5888_177 K:   ATVEEESSDE EEAALTGVTS VNVSPPVSTV LKQVGEVRGT GSGVYHTAFR GKFGAVARDA ITKEHGPYFF TAKSLREHLF DATQSAEMDL LRELPNDTRM

CAD2222840.1   CVRVEEDPTL DDGETVQAGK TKNTTKKPKK KREIVPPLMD YERCHVHRRG VLCYEIPSKK EGVPQTMVMH YSCAEPSGWL PKLYANVIEV EQLLLSAEKF
a5888_177 K:   CVRVEEDPTL DDGETVQAGK TKNTTKKPKK KREIVPPLMD YERCHVHRRG VLCYEIPSKK EGVPQTMVMH YSCAEPSGWL PKLYANVIEV EQLLLSAEKF

CAD2222840.1   KTLVEYSNKE K
a5888_177 K:   KTLVEYSNKE K
```

Supplementary Figure 6.3 (continues)

Figure 6.3 Alignments of candidate ETP gene models in genome assembly GCA_903995115.1 with corresponding 5' full-length *A. deanei* transcripts. N-terminal extensions of ORFs deduced from transcript sequences are highlighted in blue. The transcript sequence of ETP2 is incomplete at the C-terminal end.

Table 6.2 Primer used for sequencing analysis

Number	Sequence
2	GGAGAGGGAGCCTGAGAAAT
3	GGACGTAATCGGCACAGTTT
49	ACTCCTCCACCACTACCACC
253	GAGGCACTGCAGGTGCATCG
254	CGATGCACCTGCAGTGCCTC
271	CGTGTCTCCCGCGGCAAACG
272	AAGTAAAGCAGTTACTAGAC
310	CGAAACATCGCATCGAGCG
311	ATCGACAAGACCGGCTTCC
411	ATGCTGCAATCCTTACGGGAC
412	TCACATGCGTACCGTTAACCC
545	CTCCCTAAGCGCCAATATCA

1060	CACTGATATTATCTCCCTCACC
1061	GCATCCTGCAGGTACAGC
1109	CGACTCACTATAGGGAGAGCGGC
1110	AAGAACATCGATTTTCCATGGCAG
1278	GGTCTCGCCAAATGAGTGTAGTGTCCGCCAACTCC
1279	GGTCTCTTCACCTTGGACGACTTTCCAGGAGTCTG
1753	GATGCGGGCAATCTCGGCGATG
1802	GTCAGGAAGAACCTGATGGACATG
1845	ATGGCCACCACCCTTGAGG
1874	ggtctcacaagATGAACACATTCATCGAGGCAGTCA
1875	ggtctcatcttCTAAATCAAGTCTGTGGCAAAGTCA
2004	GGTCTCGTTTAttacttggggagctgggcgtt

Table 6.3 Generated *E. coli* strains for storage of trypanosomatid transfection plasmids

***E. coli* strain**	**Description of nucleic acids**	**Resistance**	**Generator**	**Progenitor**
Top10	F- Δ(-hsdRMS-) φ Z Δ Δ X nupG recA1 Δ(-leu)7697 galE15 g s ( ) λ -	strep	Invitrogen	K-12
Ec_pAdea024	δ-Amastin 5‘ FR, *Neo*^{R}, Gapdh ir, eGfp-Etp3, δ-Amastin 3‘ FR	amp	Sofia Kokkori	Top10
Ec_pAdea025	δ-Amastin 5‘ FR, *Neo*^{R}, Gapdh ir, Etp3-*eGfp*, δ-Amastin 3‘ FR	amp	Sofia Kokkori	Top10
Ec_pAdea035	δ-Amastin 5‘ FR, *Neo*^{R}, Gapdh ir, *eGfp-Etp2*, δ-Amastin 3‘ FR	amp	Georg Ehret	Top10
Ec_pAdea036	δ-Amastin 5‘ FR, *Neo*^{R}, Gapdh ir, *Etp2-eGfp*, δ-Amastin 3‘ FR	amp	Georg Ehret	Top10
Ec_pAdea043	δ-Amastin 5‘ FR, *Neo*^{R}, Gapdh ir, *eGfp* (nostop),LacZ , δ-Amastin 3‘ FR	amp	Eva Nowack	Top10

Ec_pAdea052	δ-Amastin 5’ FR, *Neo*^{R}, Gapdh ir, *eGfp*-Etp5, δ-Amastin 3’ FR	amp	Jorge Morales	Top10
Ec_pAdea053	δ-Amastin 5’ FR, *Neo*^{R}, Gapdh ir, *eGfp*-Etp6, δ-Amastin 3’ FR	amp	Morales	Top10
Ec_pAdea054	δ-Amastin 5’ FR, *Neo*^{R}, Gapdh ir, *eGfp*-Etp7, δ-Amastin 3’ FR	amp	Morales	Top10
Ec_pAdea058	δ-Amastin 5‘ FR, *Neo*^{R}, Gapdh ir, *Etp1*-V5, δ-Amastin 3‘ FR	amp	Georg Ehret	Top10
Ec_pAdea059	δ-Amastin 5‘ FR, *Neo*^{R}, Gapdh ir, V5-*Etp1*, δ-Amastin 3‘ FR	amp	Georg Ehret	Top10
Ec_pAdea080	δ-Amastin 5‘ FR, *Neo*^{R}, Gapdh ir, V5-*Etp2*, δ-Amastin 3‘ FR	amp	Georg Ehret	Top10
Ec_pAdea081	δ-Amastin 5‘ FR, *Neo*^{R}, Gapdh ir, *Etp2*-V5, δ-Amastin 3‘ FR	amp	Georg Ehret	Top10
Ec_pAdea092	Etp2 5‘ FR, *Neo*^{R}, Etp2 3‘ FR	amp	Georg Ehret	Top10
Ec_pAdea093	Etp2 5' FR, *Hyg*^{R}, Etp2 3' FR	amp	Georg Ehret	Top10
Ec_pAdea094	Etp2 5‘ FR, *Phleo*^{R}, Etp2 3‘ FR	amp	Georg Ehret	Top10
Ec_pAdea102	Etp7 5‘ FR, *Hyg*^{R}, Etp7 3‘ FR	amp	Dhevi Kalyanaraman	Top10
Ec_pAdea103	Etp7 5‘ FR, *Phleo*^{R}, Etp7 3‘ FR	amp	Dhevi Kalyanaraman	Top10
Ec_pAdea115	Etp2 5‘ FR, *Neo*^{R}, Gapdh ir, Egfp-*Etp2*, Etp2 3‘ FR	amp	Georg Ehret	Top10
Ec_pAdea116	Etp2 5‘ FR, *Neo*^{R}, Gapdh ir, *Etp2*-eGfp, Etp2 3‘ FR	amp	Georg Ehret	Top10
Ec_pAdea117	δ-Amastin 5‘ FR, *Neo*^{R}, Gapdh ir, eGfp-Etp8, δ-Amastin 3‘ FR	amp	Michael Krakovka	Top10
Ec_pAdea119	δ-Amastin 5‘ FR, *Hyg*^{R}, Gapdh ir, mScarlet-*Etp1*, δ-Amastin 3‘ FR	amp	Jorge Morales	Top10
Ec_pAdea120	Etp2 5‘ FR, *Neo*^{R}, Gapdh ir, *V5-Etp2*, Etp2 3‘ FR	amp	Georg Ehret	Top10
Ec_pAdea149	Etp2 5‘ FR (scaf3289), *Hyg*^{R}, Etp2 3‘ FR (scaf3289)	amp	Georg Ehret	Top10
Ec_pAdea151	Etp2 5' FR (Scaff3289), *Neo*^{R}, Etp2 3' FR (Scaff3289)	amp	Georg Ehret	Top10
Ec_pAdea165	δ-Amastin 5‘ FR, *Neo*^{R}, Gapdh ir, adk-eGfp, δ-Amastin 3‘ FR	amp	Davide Zanini	Top10

Ec_pAdea167	γ-Amastin 5‘ FR, *Hyg*^{R}, Gapdh ir, *mScarlet-Etp2*, γ-Amastin 3‘ FR	amp	Georg Ehret	Top10
Ec_pAdea178	δ-Amastin 5‘ FR, *Neo*^{R}, Gapdh ir, *eGfp-ScEtp2*, δ-Amastin 3‘ FR	amp	Georg Ehret	Top10
Ec_pAdea189	δ-Amastin 5‘ FR, *Neo*^{R}, Gapdh ir, *AdEtp2*$_{aa1-242}$*-eGfp*, δ -Amastin 3‘ FR	amp	Georg Ehret	Top10
Ec_pAdea190	δ-Amastin 5‘ FR, *Neo*^{R}, Gapdh ir, *eGfp-AdEtp2*$_{aa243-490}$, δ -Amastin 3‘ FR	amp	Georg Ehret	Top10
Ec_pAdea198	δ-Amastin 5‘ FR, *Neo*^{R}, Gapdh ir, *ScEtp2*$_{aa1-295}$*-eGfp*, δ -Amastin 3‘ FR	amp	Georg Ehret	Top10
Ec_pAdea213	δ-Amastin 5‘ FR, *Neo*^{R}, Gapdh ir, *ScEtp2*$_{aa1-295}$*-eGfp*, δ -Amastin 3‘ FR	amp	Georg Ehret	Top10
Ec_pAdea229	Etp2 5' FR, *Neo*^{R}, Gapdh ir, *eGfp-ScEtp2*, Etp2 3' FR	amp	Georg Ehret	Top10
Ec_pAdea235	δ-Amastin 5’ FR, *Neo*^{R}, Gapdh ir, *lacZ*, *eGfp*, δ-Amastin 3’ FR	amp	Lena Kröninger	Top10
Ec_pAdea236	δ-Amastin 5’ FR, *Neo*^{R}, Gapdh ir, *Etp5-eGfp*, δ-Amastin 3’ FR	amp	Lena Kröninger	Top10
Ec_pAdea237	δ-Amastin 5’ FR, *Neo*^{R}, Gapdh ir, *Etp6-eGfp*, δ-Amastin 3’ FR	amp	Lena Kröninger	Top10
Ec_pAdea238	δ-Amastin 5’ FR, *Neo*^{R}, Gapdh ir, *Etp7-eGfp*, δ-Amastin 3’ FR	amp	Lena Kröninger	Top10
Ec_pAdea248	δ-Amastin 5’ FR, *Neo*^{R}, Gapdh ir, e*Gfp-NodS*, δ-Amastin 3’ FR	amp	Lena Kröninger	Top10
Ec_pAdea249	δ-Amastin 5’ FR, *Neo*^{R}, Gapdh ir, *NodS-GFP*, δ-Amastin 3’ FR	amp	Lena Kröninger	Top10
Ec_pAdea250	δ-Amastin 5’ FR, *Neo*^{R}, Gapdh ir, *eGfp-CAD2220896*, δ-Amastin 3’ FR	amp	Georg Ehret	Top10
Ec_pAdea251	δ-Amastin 5’ FR, *Neo*^{R}, Gapdh ir, *CAD2220896-eGfp*, δ-Amastin 3’ FR	amp	Georg Ehret	Top10
Ec_pAdea252	δ-Amastin 5’ FR, *Neo*^{R}, Gapdh ir, *eGfp-CAD2222258*, δ-Amastin 3’ FR	amp	Georg Ehret	Top10

Ec_pAdea253	δ-Amastin 5’ FR, *Neo*^{R}, Gapdh ir, *CAD2222258-eGfp*, δ-Amastin 3’ FR	amp	Georg Ehret	Top10
Ec_pAdea254	δ-Amastin 5’ FR, *Neo*^{R}, Gapdh ir, *eGfp-CAD2222840*, δ-Amastin 3’ FR	amp	Georg Ehret	Top10
Ec_pAdea255	δ-Amastin 5’ FR, *Neo*^{R}, Gapdh ir, *CAD2222840-eGfp*, δ-Amastin 3’ FR	amp	Georg Ehret	Top10
Ec_pAdea256	δ-Amastin 5’ FR, *Neo*^{R}, Gapdh ir, *eGfp-CAD2218427*, δ-Amastin 3’ FR	amp	Tobias Reinicke	Top10
Ec_pAdea257	δ-Amastin 5’ FR, *Neo*^{R}, Gapdh ir, *CAD2218427-eGfp*, δ-Amastin 3’ FR	amp	Tobias Reinicke	Top10
Ec_pAdea258	δ-Amastin 5’ FR, *Neo*^{R}, Gapdh ir, *eGfp-Etp9*, δ-Amastin 3’ FR	amp	Tobias Reinicke	Top10
Ec_pAdea259	δ-Amastin 5’ FR, *Neo*^{R}, Gapdh ir, *Etp9-eGfp*, δ-Amastin 3’ FR	amp	Tobias Reinicke	Top10
Ec_pAdea266	δ-Amastin 5’ FR, *Neo*^{R}, Gapdh ir, *Etp8-eGfp*, δ-Amastin 3’ FR	amp	Georg Ehret	Top10
Ec_pAdea270	δ-Amastin 5’ FR, *Phleo*^{R}, Gapdh ir, *fkbp12*-linker-*cre59*, Gapdh ir, *frb*-linker-*cre60* (opt.), δ-Amastin 3‘ FR	amp	Georg Ehret	Top10
Ec_pAdea271	Etp2 5' FR, *Neo*^{R}, Gapdh ir, *loxP_eGfp-Etp2_loxP*, Etp2 3' FR	amp	Georg Ehret	Top10
Ec_pAdea272	Etp7 5' FR, *Neo*^{R}, Gapdh ir, *loxP_eGfp-Etp7_loxP*, Etp7 3' FR	amp	Georg Ehret	Top10
Ec_pAdea273	δ-Amastin 5’ FR, *Neo*^{R}, Gapdh ir, *CAD2216215-eGfp*, δ-Amastin 3’ FR	amp	Tobias Reinicke	Top10
Ec_pAdea274	δ-Amastin 5’ FR, *Neo*^{R}, Gapdh ir, *eGfp-CAD2216215*, δ-Amastin 3’ FR	amp	Tobias Reinicke	Top10
Ec_pAdea283	γ-Amastin 5‘ FR, *Hyg*^{R}, Gapdh ir, *ARL1-V5*, γ-Amastin 3‘ FR	amp	Lucie Hansen	Top10
Ec_pAdea294	γ-Amastin 5‘ FR, *Hyg*^{R}, Gapdh ir, *V5-Flag-Cas9*, γ-Amastin 3‘ FR	amp	Georg Ehret	Top10

Ec_pAdea302	δ-Amastin 5’ FR, *Neo*^{R}, Gapdh ir, *T7 pol*, δ-Amastin 3’ FR	amp	Anay Kumar	Top10
Ec_pAdea349	L.t. ODC 5' FR,T7 Promotor, Tet Operator, L.t. 5' aprt,*10xHis-Etp7*, cam operon IR, *Neo*R, L.t. 5' UTR dhfr-ts, L.t. ODC 3' FR	amp	Georg Ehret	Top10
Ec_pAdea351	γ-Amastin 5' FR, *Hyg*^{R}, Gapdh ir, *TetR,* γ-Amastin 3' FR	amp	Georg Ehret	Top10
Ec_pAdea353	pLexsy-neo3-*eGfp* derived from Jena Bioscience	amp	Georg Ehret	Top10
Ec_pAdea354	L.t. ODC 5' FR, T7 Promotor, Tet Operator, L.t. 5' aprt,*10xHis-Etp7*, cam operon IR, *Neo*^{R}, L.t. 5' UTR dhfr-ts, L.t. ODC 3' FR	amp	Georg Ehret	Top10

Table 6.4 Generated *A. deanei* strains

Adea	Transferred nucleic acid	Transfected plasmid
025	δ-Amastin 5‘ FR, *Neo*^{R}, Gapdh ir, *eGfp-Etp3*, δ-Amastin 3‘ FR	pAdea024
029	δ-Amastin 5‘ FR, *Neo*^{R}, Gapdh ir, *Etp2-eGfp*, δ-Amastin 3‘ FR	pAdea036
030	δ-Amastin 5‘ FR, *Neo*^{R}, Gapdh ir, *eGfp-Etp2*, δ-Amastin 3‘ FR	pAdea035
040	δ-Amastin 5‘ FR, *Neo*^{R}, Gapdh ir, *Etp1-V5*, δ-Amastin 3‘ FR	pAdea058
041	δ-Amastin 5‘ FR, *Neo*^{R}, Gapdh ir, *V5-Etp1*, δ-Amastin 3‘ FR	pAdea059
042	δ-Amastin 5’ FR, *Neo*^{R}, Gapdh ir, *eGfp-Etp5*, δ-Amastin 3’ FR	pAdea052
043	δ-Amastin 5’ FR, *Neo*^{R}, Gapdh ir, *eGfp-Etp6*, δ-Amastin 3’ FR	pAdea053
044	δ-Amastin 5’ FR, *Neo*^{R}, Gapdh ir, *eGfp-Etp7*, δ-Amastin 3’ FR	pAdea054
060	δ-Amastin 5‘ FR, *Neo*^{R}, Gapdh ir, *V5-Etp2*, δ-Amastin 3‘ FR	pAdea080
061	δ-Amastin 5‘ FR, *Neo*^{R}, Gapdh ir, *Etp2-V5*, δ-Amastin 3‘ FR	pAdea081
086	Etp2 5‘ FR, *Neo*^{R}, Etp2 3‘ FR	pAdea092
087	Etp2 5‘ FR, *Phleo*^{R}, Etp2 3‘ FR	pAdea094
102	Etp7 5‘ FR, *Hyg*^{R}, Etp7 3‘ FR	pAdea102

103	Etp7 5‘ FR, *Phleo*^{R}, Etp7 3‘ FR	pAdea103
113	Etp2 5' FR, *Hyg*^{R}, Etp2 3' FR	pAdea093
120	Etp2 5‘ FR, *Neo*^{R}, Gapdh ir, *eGfp-Etp2*, Etp2 3‘ FR	pAdea115
121	Etp2 5‘ FR, *Neo*^{R}, Gapdh ir, *Etp2-eGfp*, Etp2 3‘ FR	pAdea116
126	γ-Amastin 5’ FR, *Hyg*^{R}, Gapdh ir, *mScarlet-Etp1*, γ-Amastin 3’ FR	pAdea119
142	γ-Amastin 5’ FR, *Hyg*^{R}, Gapdh ir, *mScarlet-Etp1*, γ-Amastin 3’ FR, δ-Amastin 5’ FR, *Neo*^{R}, Gapdh ir, *eGfp-Etp2*, δ-Amastin 3’ FR	pAdea119/ pAdea035
143	γ-Amastin 5’ FR, *Hyg*^{R}, Gapdh ir, *mScarlet-Etp1*, γ-Amastin 3’ FR, δ-Amastin 5’ FR, *Neo*^{R}, Gapdh ir, *eGfp-Etp5*, δ-Amastin 3’ FR	pAdea119/ pAdea052
144	γ-Amastin 5’ FR, *Hyg*^{R}, Gapdh ir, *mScarlet-Etp1*, γ-Amastin 3’ FR / δ-Amastin 5’ FR, *Neo*^{R}, Gapdh ir, *eGfp-Etp7*, δ-Amastin 3’ FR	pAdea119/ pAdea054
146	Etp2 5‘ FR, *Neo*^{R}, Gapdh ir, *V5-Etp2*, Etp2 3‘ FR	pAdea120
148	γ-Amastin 5’ FR, *Hyg*^{R}, Gapdh ir, mScarlet-*Etp1*, γ-Amastin 3’ FR, δ-Amastin 5’ FR, *Neo*^{R}, Gapdh ir, *eGfp-Etp6*, δ-Amastin 3’ FR	pAdea119/ pAdea053
150	δ-Amastin 5‘ FR, *Neo*^{R}, Gapdh ir, *eGfp-Etp8*, δ-Amastin 3‘ FR	pAdea117
152	γ-Amastin 5’ FR, *Hyg*^{R}, Gapdh ir, *mScarlet-Etp1*, γ-Amastin 3’ FR / δ-Amastin, *Neo*^{R}, Gapdh ir, *Etp3-eGfp*, γ-Amastin 3’ FR	pAdea119/ pAdea025
153	Etp2 5‘ FR (scaf3289), *Hyg*^{R}, Etp2 3‘ FR (scaf3289)	pAdea149
155	γ-Amastin 5’ FR, *Hyg*^{R}, Gapdh ir, *mScarlet-Etp1*, γ-Amastin 3’ FR / γ-Amastin 3’ FR / δ-Amastin 5’ FR, *Neo*^{R}, Gapdh ir, *eGfp-Etp3*, δ-Amastin 3’ FR	pAdea119/ pAdea024
157	γ-Amastin 5’ FR, *Hyg*^{R}, Gapdh ir, *mScarlet-Etp1*, γ-Amastin 3’ FR / γ-Amastin 3’ FR/ 5’ FR δ-Amastin, *Neo*^{R}, Gapdh ir, *Etp2-eGfp*, γ-Amastin 3’ FR	pAdea119/ pAdea036
158	γ-Amastin 5’ FR, *Hyg*^{R}, Gapdh ir, *mScarlet-Etp1*, γ-Amastin 3’ FR / 5’ FR δ-Amastin, *Neo*^{R}, Gapdh ir, *Etp3-eGfp*, γ-Amastin 3’ FR	pAdea024/ pAdea119
169	γ-Amastin 5’ FR, *Hyg*^{R}, Gapdh ir, *mScarlet-Etp1*, δ-Amastin, *Neo*^{R}, Gapdh ir, *Etp7-eGfp*, γ-Amastin 3’ FR	pAdea109/ pAdea119

170	γ-Amastin 5’ FR, *Hyg*^{R}, Gapdh ir, *mScarlet-Etp1*, δ-Amastin, *Neo*^{R}, Gapdh ir, *Etp8-eGfp*, γ-Amastin 3’ FR	pAdea117/ pAdea119
181	γ-Amastin 5‘ FR, *Hyg*^{R}, Gapdh ir, *mScarlet-Etp2*, γ-Amastin 3‘ FR	pAdea167
205	δ-Amastin 5’ FR, *Neo*^{R}, Gapdh ir, *eGfp-Etp7*, δ-Amastin 3’ FR / γ-Amastin 5‘ FR, *Hyg*^{R}, Gapdh ir, *mScarlet-Etp2*, γ-Amastin 3‘ FR	pAdea054/ pAdea167
216	δ-Amastin 5‘ FR, *Neo*^{R}, Gapdh ir, *eGfp-ScEtp2*, δ-Amastin 3‘ FR	pAdea178
217	δ-Amastin 5‘ FR, *Neo*^{R}, Gapdh ir, *eGfp-ScEtp2*, δ-Amastin 3‘ FR / γ-Amastin 5‘ FR, *Hyg*^{R}, Gapdh ir, *mScarlet-Etp1*, γ-Amastin 3‘ FR	pAdea178/ pAdea119
218	δ-Amastin 5‘ FR, *Neo*^{R}, Gapdh ir, *eGfp-ScEtp2*, δ-Amastin 3‘ FR / γ-Amastin 5‘ FR, *Hyg*^{R}, Gapdh ir, mScarlet-*AdEtp2*, γ-Amastin 3‘ FR	pAdea178/ pAdea167
219	δ-Amastin 5‘ FR, *Neo*^{R}, Gapdh ir, *AdEtp2*$_{aa1-242}$-*eGfp*, δ -Amastin 3‘ FR	pAdea189
220	δ-Amastin 5‘ FR, *Neo*^{R}, Gapdh ir, *eGfp-AdEtp2*$_{aa243-490}$, δ -Amastin 3‘ FR	pAdea190
221	δ-Amastin 5‘ FR, *Neo*^{R}, Gapdh ir, *ScEtp2*$_{aa1-295}$-*eGfp*, δ -Amastin 3‘ FR	pAdea198
222	δ-Amastin 5‘ FR, *Neo*^{R}, Gapdh ir, *ScEtp2*$_{aa1-233and290-295}$-*eGfp*, δ -Amastin 3‘ FR	pAdea199
271	δ-Amastin 5’ FR, *Neo*^{R}, Gapdh ir, *eGfp-Etp6*, δ -Amastin 3‘ FR	pAdea053
272	*Etp2* 5' FR, *Neo*^{R}, Gapdh ir, *eGfp*-Sc*Etp2*, *Etp2* 3' FR	pAdea229
277	γ-Amastin FR, *Hyg*^{R}, Gapdh ir, *mScarlet-Etp1* / δ-Amastin 5’ FR, *Neo*^{R}, Gapdh ir, *Etp5-eGfp*, δ-Amastin 3’ FR	pAdea119/ pAdea236
278	γ-Amastin FR, *Hyg*^{R}, Gapdh ir, *mScarlet-Etp1* / δ-Amastin 5’ FR, *Neo*^{R}, Gapdh ir, *Etp6-eGfp*, δ-Amastin 3’ FR	pAdea119/ pAdea237
279	γ-Amastin FR, *Hyg*^{R}, Gapdh ir, *mScarlet-Etp1* / δ-Amastin 5’ FR, *Neo*^{R}, Gapdh ir, *Etp7-eGfp*, δ-Amastin 3’ FR	pAdea119/ pAdea238
281	γ-Amastin FR, *Hyg*^{R}, Gapdh ir, *mScarlet-Etp1* / δ-Amastin 5’ FR, *Neo*^{R}, Gapdh ir, *eGfp-NodS*, δ-Amastin 3’ FR	pAdea119/ pAdea248

282	γ-Amastin FR, *Hyg*^{R}, Gapdh ir, *mScarlet-Etp1* / δ-Amastin 5’ FR, *Neo*^{R}, Gapdh ir, *NodS-eGfp*, δ-Amastin 3’ FR	pAdea119/ pAdea249
283	γ-Amastin FR, *Hyg*^{R}, Gapdh ir, mScarlet-*Etp1* / δ-Amastin 5’ FR, *Neo*^{R}, Gapdh ir, *eGfp-Etp5*, δ-Amastin 3’ FR	pAdea119/ pAdea052
284	γ-Amastin FR, *Hyg*^{R}, Gapdh ir, *mScarlet-Etp1* / δ-Amastin 5’ FR, *Neo*^{R}, Gapdh ir, *eGfp-Etp6*, δ-Amastin 3’ FR	pAdea119/ pAdea053
292	γ-Amastin FR, *Hyg*^{R}, Gapdh ir, *mScarlet-Etp1*/ δ-Amastin 5’ FR, *Neo*^{R}, Gapdh ir, *eGfp-CAD2220896*, δ-Amastin 3’ FR	pAdea119/ pAdea250
293	γ-Amastin FR, *Hyg*^{R}, Gapdh ir, *mScarlet-Etp1* / δ-Amastin 5’ FR, *Neo*^{R}, Gapdh ir, *CAD2220896-eGfp*, δ-Amastin 3’ FR	pAdea119/ pAdea251
294	γ-Amastin FR, *Hyg*^{R}, Gapdh ir, *mScarlet-Etp1* / δ-Amastin 5’ FR, *Neo*^{R}, Gapdh ir, *eGfp-CAD2222258*, δ-Amastin 3’ FR	pAdea119/ pAdea252
295	γ-Amastin FR, *Hyg*^{R}, Gapdh ir, *mScarlet-Etp1* / δ-Amastin 5’ FR, *Neo*^{R}, Gapdh ir, *CAD2222258-eGfp*, δ-Amastin 3’ FR	pAdea119/ pAdea253
296	γ-Amastin FR, *Hyg*^{R}, Gapdh ir, *mScarlet-Etp1* / δ-Amastin 5’ FR, *Neo*^{R}, Gapdh ir, *eGfp-CAD2222840*, δ-Amastin 3’ FR	pAdea119/ pAdea254
297	γ-Amastin FR, *Hyg*^{R}, Gapdh ir, *mScarlet-Etp1* / δ-Amastin 5’ FR, *Neo*^{R}, Gapdh ir, *CAD2222840-eGfp*, δ-Amastin 3’ FR	pAdea119/ pAdea255
298	γ-Amastin FR, *Hyg*^{R}, Gapdh ir, *mScarlet-Etp1* / δ-Amastin 5’ FR, *Neo*^{R}, Gapdh ir, *eGfp-CAD2218427*, δ-Amastin 3’ FR	pAdea119/ pAdea256
299	γ-Amastin FR, *Hyg*^{R}, Gapdh ir, *mScarlet-Etp1*/ δ-Amastin 5’ FR, *Neo*^{R}, Gapdh ir, *CAD2218427-eGfp*, δ-Amastin 3’ FR	pAdea119/ pAdea257
303	γ-Amastin FR, *Hyg*^{R}, Gapdh ir, *mScarlet-Etp1* / δ-Amastin 5’ FR, *Neo*^{R}, Gapdh ir, *Etp8Full-eGfp*, δ-Amastin 3’ FR	pAdea119/ pAdea266
305	γ-Amastin FR, *Hyg*^{R}, Gapdh ir, *mScarlet-Etp1* / δ-Amastin 5’ FR, *Neo*^{R}, Gapdh ir, *eGfp-Etp9*, δ-Amastin 3’ FR	pAdea119/ pAdea258
306	γ-Amastin FR, *Hyg*^{R}, Gapdh ir, *mScarlet-Etp1* / δ-Amastin 5’ FR, *Neo*^{R}, Gapdh ir, *Etp9-eGfp*, δ-Amastin 3’ FR	pAdea119/ pAdea259

309	γ-Amastin FR, *Hyg*^{R}, Gapdh ir, *mScarlet-Etp1* / δ-Amastin 5’ FR, *Neo*^{R}, Gapdh ir, *CAD2216215-eGfp*, δ-Amastin 3’ FR	pAdea119/ pAdea273
310	γ-Amastin FR, *Hyg*^{R}, Gapdh ir, *mScarlet-Etp1* / δ-Amastin5’ FR, *Neo*^{R}, Gapdh ir, *eGfp-CAD2216215*, δ-Amastin3’ FR	pAdea119/ pAdea274
311	Etp7 5' FR, *Neo*^{R}, Gapdh ir, *loxP_eGfp-Etp7_loxP*, Etp7 3' FR	pAdea102/ pAdea272
313	γ-Amastin 5‘ FR, *Hyg*^{R}, Gapdh ir, *V5-Flag-Cas9*, γ-Amastin 3‘ FR	pAdea294
317	γ-Amastin 5‘ FR, *Hyg*^{R}, Gapdh ir, *ARL1-V5*, γ-Amastin 3‘ FR / δ-Amastin 5’ FR, *Neo*^{R}, Gapdh ir, *Etp8Full-eGfp*, δ-Amastin 3’ FR	pAdea283/ pAdea266
318	Etp7 5' FR, *Neo*^{R}, Gapdh ir, *loxP_eGfp-Etp7_loxP*, Etp7 3' FR / Etp7 5‘ FR, *Hyg*^{R}, Etp7 3‘ FR / δ-amastin 5’ FR, *Phleo*^{R}, Gapdh ir, *fkbp12*-linker-*cre59*, Gapdh ir, *frb*-linker-*cre60* (opt.), δ-amastin 3‘ FR	pAdea102/ pAdea272/ pAdea270
319	δ-Amastin 5’ FR, *Neo*^{R}, Gapdh ir, *T7pol*, δ-Amastin 3’ FR	pAdea302
327	γ-Amastin 5‘ FR, *Hyg*^{R}, Gapdh ir, *V5-Flag-Cas9*, γ-Amastin 3‘ FR / δ-Amastin 5’ FR, *Neo*^{R}, Gapdh ir, *T7pol*, δ-Amastin 3’ FR	pAdea294/ pAdea302
344	*Etp2* 5' FR, *Neo*^{R}, Gapdh ir, loxP_*eGfp-Etp2_loxP*, *Etp2* 3' FR	pAdea271
361 ATCC-30969	*Etp2* 5‘ FR, *Neo*^{R}, *Etp2* 3‘ FR	pAdea092
362 ATCC-30969	γ-Amastin 5‘ FR, *Hyg*^{R}, Gapdh ir, *mScarlet-Etp2*, γ-Amastin 3‘ FR	pAdea167
363 ATCC-30969	Etp9 5' FR, *Hyg*^{R}, Etp9 3' FR	pAdea303
364 ATCC-30969	Etp7 5‘ FR, *Hyg*^{R}, Etp7 3‘ FR	pAdea102
366	δ-Amastin 5’ FR, *Neo*^{R}, Gapdh ir, *T7pol*, δ-Amastin 3’ FR / γ-Amastin 5' FR, *Hyg*^{R}, Gapdh ir, *TetR*, γ-Amastin 3' FR	pAdea302/ pAdea351

370LT	L.t. ODC 5' FR,T7 Promotor, Tet Operator, L.t. 5' aprt, *10xHis-Etp7*, cam operon IR, *Neo*^{R}, L.t. 5' UTR dhfr-ts, L.t. ODC 3' FR	pAdea349
371LT	L.t. ODC 5' FR,T7 Promotor, Tet Operator, L.t. 5' aprt, *eGfp-6xHis*, cam operon IR, *Neo*^{R}, L.t. 5' UTR dhfr-ts, L.t. ODC 3' FR	pAdea348

Table 6.5 Primers used for generation of pAdea plasmids

Number	Sequence	Fragment	pAdea
1083	GGTCTCAGTAATAAAAAACATACAAAACAAAAC	3'-γ-Amastin FR/ pUMA1467 backbone/5'-γ-Amastin FR/*Hyg*^{R}/Gapdh ir/	
348	GGTCTCCTTGGATAACTGTGTTTTTTGATGAA		
1085	GGTCTCACCAAATGGTGAGCAAGGGCGAGGC	*mScarlet*	119
1086	GGTCTCACCGTCTTGTACAGCTCGTCCATGC		
1087	GGTCTCTACGGAACCCAACGCCCAAAC	*Etp1* "allele Q-"	
1088	GGTCTCGTTACGCATCCTTCTTCTCTA		
598	CACGGTACCGGTCTCTAAGAGGGGGGAGAGAGACGTG	BsaI/3'-δ-Amastin FR/pUMA1467 backbone/5'-δ-Amastin FR/*neo*^{R}/Gapdh ir/*eGfp*/BsaI	043
599	CACCTCGAGGGTCTCGCTTGTACAGCTCGTCCATGC		
596	CACCTCGAGTTTACACTTTATGCTTCCGG	XhoI/LacZ alpha with promoter/KpnI	
597	CACGGTACCTTAATGCGCCGCTACAG		
493	GGTCTCGCCAAATGGGCAAACCGATTCCGAACCCGCTGCTGGGCCTGGATAGCACCACGGAACCCAACGCCCAAAC	*V5-Etp1*	
467	GGTCTCCCTTTTACGCATCCTTCTTCTCTAC		059
469	GGTCTCGAAAGAGGGGGGAGAGAGACGTGA	3'-δ-Amastin FR/pUMA1467 backbone/5'-δ-Amastin FR/*neo*^{R}/Gapdh ir	
492	GGTCTCCTTGGATAACTGTGTTTTTTGATGAAAGAAGACTTAAAGAACTGTAGTGGATGAGGG		
491	GGTCTCCCCAAATGACGGAACCCAACGCC	*Etp1-V5*	058

463	GGTCTCCTTGGTGCTATCCAGGCCCAGCAGCGGGTTCGGAATCGGTTTGCCCGCATCCTTCTTCTCTACAA		
465	GGTCTCCCCAAGAGGGGGGAGAGAGAC	3'-δ-Amastin FR/pUMA1467 backbone/5'-δ-Amastin FR/*neo*^{R}/Gapdh ir/	
490	GGTCTCGTTGGATAACTGTGTTTTTTGATGAAAGAAGACTTAAAGAACTGTAGTGGATGAGGGAGA		
763	CACGGTACCGGTCTCTGTGAGCAAGGGCGAGGAG	BsaI/*eGfp*/3'-δ-Amastin FR/pUMA1467 backbone/5'-δ-Amastin FR/*Neo*^{R}/Gapdh ir/BsaI	235
764	CACCTCGAGGGTCTCGTTGGATAACTGTGTTTTTTGATGAAAG		
596	CACCTCGAGTTTACACTTTATGCTTCCGG	XhoI/LacZ alpha with promoter/KpnI	
597	CACGGTACCTTAATGCGCCGCTACAG		
121	GGTCTCGCCTGCAGTGCGTCGCCCGGCTA	5'-δ-Amastin FR/*Neo*^{R}/Gapdh ir/*eGfp*	
362	GGTCTCGTCCTTGTACAGCTCGTCCAT		
363	GGTCTCGAGGACTACGACGAGGATGAAT	*Etp2*	035
364	GGTCTCGCTTTTAGTTCGCCGAAAGCAC		
365	GGTCTCCAAAGAGGGGGGAGAGAGACGT	3'-δ-Amastin FR	
126	GGTCTCGCTGCGTCGCGGGGGCTGTCGCA		
121	GGTCTCGCCTGCAGTGCGTCGCCCGGCTA	5'-δ-Amastin FR/*neo*/Gapdh ir/*eGfp*	
354	GGTCTCCCTTGTACAGCTCGTCCATG		
355	GGTCTCGCAAGATCGACACGAAATTTCATTGT	*Etp3*	024
356	GGTCTCGTTCTAGTTGGACTGCTTTTCTAC		
357	GGTCTCCAGAAGAGGGGGGAGAGAGACG	3'-δ-Amastin FR	
126	GGTCTCGCTGCGTCGCGGGGGCTGTCGCA		
612	GGTCTCGCAAGATGGCCACCACCCTTGAGGAA	*Etp5*	052
613	GGTCTCGTCTTTTACTTGGGGAGCTGGGCGT		

614	GGTCTCGCAAGATGCTCCGTCGATTTTCCCCA	*CAD2220712*	053
615	GGTCTCGTCTTCTACTTGGCCAGCAGTGCCT		
616	GGTCTCGCAAGATGCTGCAATCCTTACGGGAC	*Etp7*	054
617	GGTCTCGTCTTTCACATGCGTACCGTTAACC		
1280	GGTCTCGCAAGAGTGTAGTGTCCGCCAACTCCAAC	*Etp8*	117
1281	GGTCTCGTCTTTTACTTGGACGACTTTCCAGGAGT		
121	GGTCTCGCCTGCAGTGCGTCGCCCGGCTA	5'-δ-Amastin FR/*neo*^{R}/Gapdh ir	
303	GGTCTCGTTTGGATAACTGTGTTTTTTGATGA		
263	GGTCTCGCAAATGGACTACGACGAGGAT	*Etp2*	036
264	GGTCTCGGTTCGCCGAAAGCACAAA		
265	GGTCTCCGAACGTGAGCAAGGGCGAGGAG	*eGfp*/3'-δ-Amastin FR	
126	GGTCTCGCTGCGTCGCGGGGGCTGTCGCA		
121	GGTCTCGCCTGCAGTGCGTCGCCCGGCTA	5'-δ-Amastin FR/*neo*^{R}/Gapdh ir	
273	GGTCTCCTCATTTGGATAACTGTGTTTTTTGATGAAAGAAGAC		
274	GGTCTCGATGATCGACACGAAATTTCAT	*Etp3*	025
275	GGTCTCGGTTGGACTGCTTTTCTACTG		
276	GGTCTCCCAACGTGAGCAAGGGCGAGGAG	*eGfp*/3'-δ-Amastin FR	
126	GGTCTCGCTGCGTCGCGGGGGCTGTCGCA		
630	GGTCTCGCCAAATGGCCACCACCCTTGAGGAA	*Etp5*	236
893	GGTCTCGTCACCTTGGGGAGCTGGGCGT		
632	GGTCTCGCCAAATGCTCCGTCGATTTTCCCCA	*CAD2220712*	237
894	GGTCTCGTCACCTTGGCCAGCAGTGCCT		
634	GGTCTCGCCAAATGCTGCAATCCTTACGGGAC	*Etp7*	238

895	GGTCTCGTCACCATGCGTACCGTTAACC		
1278	GGTCTCGCCAAATGAGTGTAGTGTCCGCCAACTCC	*Etp8*	266
1279	GGTCTCTTCACCTTGGACGACTTTCCAGGAGTCTG		
863	GGTCTCGTGTGACTGTCAGAAAGCGGC	5' FR scaffold 1854	
844	GGTCTCCTTAGAAGAACTCGTCAAGAAGG		
524	GGTCTCCCTAAGGAAAAGATAAATAGACGTTAAAAAAG	*neo*^{R}/3' FR scaffold 1854	156
595	GGTCTCCGCACAAATAATGGTTTTGAGGCT		
590	GGTCTCGGTGCAGGTCTAGATATCGGATC	pUMA 1467	
862	GGTCTCGCACAGGTGAGCTCGAATTCA		
1835	ATGGTAGGTCTCACAAGATGCTGAAAGGCGCCTCTGAGGTGG	*CAD2216595*	248
1836	ATGGTAGGTCTCATCTTTTACTGTTTCAGTCCAGTCCACAGA		
1837	ATGGTAGGTCTCACCAAATGCTGAAAGGCGCCTCTGAGGTGG	*CAD2216595*	249
1838	AGTGTAGGTCTCATCACCTGTTTCAGTCCAGTCCACAGATAG		
1849	GGTCTCACAAGATGAGAAGTTTCGCTAGAAGGTC	*CAD2220896*	250
1850	GGTCTCAtcttTTACTCACTTTGTGATCGTTGGC		
1851	GGTCTCACCAAATGAGAAGTTTCGCTAGAAGGTC	*CAD2220896*	251
1852	GGTCTCATCACCTCACTTTGTGATCGTTGG		
1853	GGTCTCACAAGATGACAGACAGCGATCAACAC	*CAD2222258*	252
1854	GGTCTCAtcttCTAATTCCAGTAGCGCACCGTA		
1855	GGTCTCACCAAATGACAGACAGCGATCAACAC	*CAD2222258*	253

1856	GGTCTCATCACATTCCAGTAGCGCACCGTAC		
1857	GGTCTCACAAGATGACGATCTTGGAGAATCCAGC		
1858	GGTCTCAtcttTTACTTTTCTTTATTCGAATACTCCACG	*CAD2222840*	254
1859	GGTCTCACCAAATGACGATCTTGGAGAATCCAG		
1860	GGTCTCATCACCTTTTCTTTATTCGAATACTCCACGA	*CAD2222840*	255
1861	ggtctcacaagATGCTCAAAAATGAATCCAAACCACC	*CAD2218427*	256
1862	ggtctcatcttTCACTCTCTGCTGTTATGATTCTTCCG		
1863	ggtctcaccaaATGCTCAAAAATGAATCCAAACCACC	*CAD2218427*	257
1864	ggtctcaTCACCTCTCTGCTGTTATGATTCTTCCG		
1874	ggtctcacaagATGAACACATTCATCGAGGCAGTCA	*Etp9*	258
1875	ggtctcatcttCTAAATCAAGTCTGTGGCAAAGTCA		
1876	ggtctcaccaaATGAACACATTCATCGAGGCAGTCA	*Etp9*	259
1877	ggtctcatcacAATCAAGTCTGTGGCAAAGTCATCT		
1945	ttcatcaaaaaacacagttatccaaATGTTTAGCAGCCCGTTCAA	*CAD2216215*	273
1946	tgaacagctcctcgcccttgctcacTTTGAATGTCACCACATGATCTGC		
1943	tctcggcatggacgagctgtacaagATGTTTAGCAGCCCGTTCAA	*CAD2216215*	274
1944	cactcacgtctctctccccctcttTTATTTGAATGTCACCACATGATCTG		
733	GGTCTCGTGCGCCAAAGCTGCACTGCA	5'-Etp2 FR	092
734	GGTCTCGCATTTTGGTGTGTATGATTGTATT		
845	GGTCTCGCTAATAATATATATTTATCTCGTTCGGTGTTG	3‘-Etp2 FR	

846	GGTCTCGCGGtACGGATCTCATTGCC		
731	GGTCTCGACCGCAGGTCTAGATATCGGATC	pUMA1467	
732	GGTCTCGCGCAGGTGAGCTCGAATTCA		
735	GGTCTCGAATGATTGAACAAGATGGATTGC	*Neo*^{R}	
844	GGTCTCCTTAGAAGAACTCGTCAAGAAGG		
733	GGTCTCGTGCGCCAAAGCTGCACTGCA	5'-Etp2 FR	
739	GGTCTCCTTGGTGTGTATGATTGTATTT		
740	GGTCTCCCCAAAatgaaaaagcctgaactcac	*Hyg*^{R}	
847	GGTCTCGttgccctcggacgagtgc		093
848	GGTCTCGgcaaagaaataaTAATATATATTTATCTCGTTCGGTGTT	3‘-Etp2 FR	
849	GGTCTCGCGGtACGGATCTCATTGCC		
871	GGTCTCGCTGATAATATATATTTATCTCGTTCGGTGTT	3‘-Etp2 FR/pUMA1467/5‘-Etp2 FR	
872	GGTCTCGCCATTTTGGTGTGTATGATTGTATTTTTC		094
873	GGTCTCGATGGCCAAGTTGACCAGT	*Phleo*^{R}	
874	GGTCTCGTCAGTCCTGCTCCTCGGC		
948	GGTCTCCGCAGGTCTAGATATCGGATC	pUMA1467	
949	GGTCTCCCAGGTGAGCTCGAATTCA		
950	GGTCTCGCCTGTTGACGAGGACGAGACGG	5‘-Etp7 FR	
951	GGTCTCCTCACGGTGGTTTGTTTGT		102
952	GGTCTCGGTGAATGAAAAAGCCTGAACTCAC	*Hyg*^{R}	
953	GGTCTCGACTTATTTCTTTGCCCTCGGA		
954	GGTCTCCAAGTTGAATCACTTTATATACGACAAGG	3‘-Etp7 FR	

955	GGTCTCCCTGCCATCACATCCTCGAGGGA		
950	GGTCTCGCCTGTTGACGAGGACGAGACGG	5‘-Etp7 FR	
956	GGTCTCGTCACGGTGGTTTGTTTGT		
957	GGTCTCCGTGAATGGCCAAGTTGACCAGT	*Phleo*^{R}	103
958	GGTCTCCCAACTCAGTCCTGCTCCTCGGC		
959	GGTCTCCGTTGAATCACTTTATATACGACAAGG	3‘-Etp7 FR	
955	GGTCTCCCTGCCATCACATCCTCGAGGGA		
2011	TTCATCAAAAAACACAGTTATCCAAATGGGAGCG TGGCTGACGT	*Arl1*	
2012	GGTGCTATCCAGGCCCAGCAGCGGGTTCGGAATC GGTTTGCCCTTGCCGTTCGTTGCGGTC		283
2013	CCCGCTGCTGGGCCTGGATAGCACCTAAAAAACA TACAAAACAAAACAAAAAAACAGAC	3'-γ-amastin FR/ pUMA1467 backbone/5'-γ-amastin FR/*Hyg*^{R}/Gapdh ir/	
2014	TTGGATAACTGTGTTTTTTGATGAAAGAAG		
714	GGTCTCGAAAGAGGGGGGAGAGAGAC	3'-δ-amastin FR/ pUMA1467 backbone/5'-δ-amastin FR/*Neo*^{R}/Gapdh ir/*V5*	080
715	GGTCTCGTCGGTGCTATCCAGGCCCAG		
716	GGTCTCGCCGACTACGACGAGGATGAAT	*Etp2*	
717	GGTCTCGCTTTTAGTTCGCCGAAAGCAC		
710	GGTCTCCACGGCAAACCGATTCCGAAC	*V5*/3'-δ-amastin FR/ pUMA1467 backbone/5'-δ-amastin FR/*Neo*^{R}/Gapdh ir	81
711	GGTCTCCTTTGGATAACTGTGTTTTTTGATGAAAG A		
712	GGTCTCCCAAATGGACTACGACGAGGAT	*Etp2*	
713	GGTCTCCCCGTTCGCCGAAAGCACAAA		
1022	GGTCTCCATGATTGAACAAGATGGATTGC	*Neo*^{R}/Gapdh ir/*eGfp-Etp2*	115
1023	GGTCTCCTTAGTTCGCCGAAAGCAC		

1015	GGTCTCCCTAATAATATATATTTATCTCGTTCGGTGTT	Etp2 3’ FR/pUMA1467 backbone/Etp2 5’ FR	
1016	GGTCTCCTCATTTTGGTGTGTATGATTGTATTTTTC	(Same fragment used for pAdea115/120)	
1020	GGTCTCCATGATTGAACAAGATGGATTGC	*Neo*^{R}/Gapdh ir/*Etp2-eGfp*	
1021	GGTCTCCTTACTTGTACAGCTCGTCC		
1019	GGTCTCGGTAATAATATATATTTATCTCGTTCGGTGTT	Etp2 3’ FR/pUMA1467 backbone/Etp2 5’ FR	116
1016	GGTCTCCTCATTTTGGTGTGTATGATTGTATTTTTC		
1024	GGTCTCCATGATTGAACAAGATGGATTGC	*Neo*^{R}/Gapdh ir/*V5-Etp2*	120
1025	GGTCTCCTTAGTTCGCCGAAAGCAC		
733	GGTCTCGTGCGCCAAAGCTGCACTGCA	Etp2 5’ FR (Scaf3289)	
739	GGTCTCCTTGGTGTGTATGATTGTATTT		
740	GGTCTCCCCAAAatgaaaaagcctgaactcac	*Hyg*^{R}	
847	GGTCTCGttgccctcggacgagtgc		
848	GGTCTCGgcaaagaaataaTAATATATATTTATCTCGTTCGGTGTT	3’ FR (Scaf3289)	149
849	GGTCTCGCGGtACGGATCTCATTGCC		
731	GGTCTCGACCGCAGGTCTAGATATCGGATC	pUMA1467 (same fragment used for pAdea151)	
732	GGTCTCGACCGCAGGTCTAGATATCGGATC		
1394	GGTCTCGagGACTACGACGAGGATGAAT	*Etp2*	
1395	GGTCTCGTTAGTTCGCCGAAAGCAC		
187	GGTCTCCCTGCAGTGATTCAATAGCGGTAATAAAC	3'-γ–Amastin	167
1396	GGTCTCCCTAATAAAAAACATACAAAACAAAAC		
259	GGTCTCGCCTGGATGATTTGCAAGTGCATGT		

1393	GGTCTCCTCcttgtacagctcgtccat	5’-γ-Amastin/*Hyg*^{R}/Gapdh ir/*mScarlet*	
1409 1410	GGTCTCCCAAGATGGACTACGACGACGACGATT GGTCTCCTCTTTCAAGAGAGGCGGGAGTTAATG	*StcEtp2*	178
1569 1570	GGTCTCACCAAATGGACTACGACGAGGATGAATAC GGTCTCATCACTGGTGGGGGTGGCAC	*AdEtp2*$_{aa\ 1\text{-}242}$	189
1567 1568	GGTCTCACAAGGAGGCACTGCAGGTGCAT GGTCTCAtcttTTAGTTCGCCGAAAGCACAAAATAGGG	*AdEtp2*$_{aa\ 243\text{-}490}$	190
1573 1574	GGTCTCACCAAATGGACTACGACGACGACGATT GGTCTCATCACCTGGTACGGCACGC	*StcEtp2*$_{aa\ 296\text{-}483}$	198
1571 1572	GGTCTCACAAGACACCGATGCGGCCCATC GGTCTCAtcttTCAAGAGAGGCGGGAGTTAATGAAGA	*StcEtp2*$_{aa\ 1\text{-}295}$	213
1662 1663 1664 1665	TCTCGGCATGGACGAGCTGTACAAGATGGACTACGACGACGACGAT CACCGAACGAGATAAATATATATTATCAAGAGAGGCGGGAGTTAAT ATTAACTCCCGCCTCTCTTGATAATATATATTTATCTCGTTCGGTG ATCGTCGTCGTCGTAGTCCATCTTGTACAGCTCGTCCAT	*StcEtp2* pUMA1467 backbone/Etp2 5’ FR /*Neo*^{R}/Gapdh ir/*eGfp*/Etp2 3’ FR/	229
1956 1957	TGGCCGAGGAGCAGGACTGAaagtgctagtgagagtttgact CGGCACTGGTCAACTTGGCCATTTTCTTGTGAGATGATTATAAAAAGTGT	δ-amastin 5’ FR/Gapdh ir/*fkbp12*-linker-*cre59*/Gapdh ir/*frb*-linker-*cre60* (opt.)/δ-amastin 3‘ FR	270

1958	TTTTTATAATCATCTCACAAGAAAATGGCCAAGTTGACCAGTGCCG	*Phleo*^{R}	
1633	TCAAACTCTCACTAGCACTTTCAGTCCTGCTCCTCGGCCA		
1954	GGTCTCAatagcatacattatacgaagttatTAATATATATTTATCTCGTTCGGTGTTGT	*LoxP*/3’ Etp2 FR/pUMA1467/5’ Etp2 FR/*Neo*^{R}/Gapdh ir/*LoxP*	271
1953	GGTCTCAatgtatgctatacgaagttatttggataactgtgtttttttgatgaaag		
1950	GGTCTCAacattatacgaagttatATGGTGAGCAAGGGCGAG	*eGfp-Etp2*	
1955	GGTCTCActatacgaagttatTTAGTTCGCCGAAAGCACAAAATAGG		
1952	GGTCTCAtcgtatagcatacattatacgaagttatGTTGAATCACTTTATATACGAC	*LoxP*/3’ Etp7 FR/pUMA1467/5’ Etp7 FR/*Neo*^{R}/Gapdh ir/*LoxP*	272
1953	GGTCTCAatgtatgctatacgaagttatttggataactgtgtttttttgatgaaag		
1950	GGTCTCAacattatacgaagttatATGGTGAGCAAGGGCGAG	*eGfp-Etp7*	
1951	GGTCTCAacgaagttatTCACATGCGTACCGTTAACCC		
2017	GGTCTCACACCatggactataaggaccacgacg	*Cas9*	294
2018	GGTCTCATTTAttacttttttctttttgcctggcc		
2088	GGTCTCAatggagacgattaacatcgctaagaa	entire plasmid amplified omitting V5-tag	302
2089	GGTCTCAccatttggataactgtgtttttttgatgaa		
2409	ACCAgatctatgggccatcatcatcatca	*10xHis*/TEV/*Etp7*	349
2410	AGGGCGGCCGCTCACATGCGTACCGTTAACC		
2429	GGTCTCCttaaTAAAAAACATACAAAACAAAACAAAAAAACAGAC		351

2430	GGTCTCGacatTTGGATAACTGTGTTTTTTGATGAAA	γ-Amastin 5' FR/pUMA1467/*Hyg*^{R}/Gapdh ir/γ-Amastin 3' FR	
2427	GGTCTCTatgtctagattagataaaagtaaagtgattaaca	*TetR*	
2428	GGTCTCGttaagacccactttcacatttaagttg		
2461	ggatCCAATATGGCCAAGTTGACCAGTGC	*Phleo*^{R}	353/ 354
2462	ACTAGtTCAGTCCTGCTCCTCGGC		

Table 6.6 *E. coli* strains generated for protein expression

EC ID	*E. coli* strain	Expressed protein
28	BL21 (DE3)	ETP7-6xHis
29	BL21 (DE3)	pelB-ETP7-6xHis
50	BL21 (DE3)	pelB-10xHis-TEV-ETP7
51	BL21 (DE3)	6xHis-SUMO-ETP7
52	BL21 (DE3)	pelB-6xHis-SUMO-ETP7
58	C41 (DE3)	6xHis-SUMO-ETP7
59	C41 (DE3)	pelB-6xHis-SUMO-ETP7
60	C43 (DE3)	6xHis-SUMO-ETP7
61	C43 (DE3)	pelB-6xHis-SUMO-ETP7
66	C41 (DE3)	6xHis-SUMO-ETP7$_{Y367H,\ V523A}$
67	C41 (DE3)	6xHis-SUMO-ETP7$_{E369Q}$
68	C41 (DE3)	6xHis-SUMO-ETP7$_{\Delta 392\text{-}398}$
74	C41 (DE3)	6xHis-SUMO-ETP7$_{aa1\text{-}269}$
75	C41 (DE3)	pelB-6xHis-SUMO-ETP7$_{aa1\text{-}269}$
76	C41 (DE3)	6xHis-SUMO-ETP7$_{aa270\text{-}538}$
77	C41 (DE3)	pelB-6xHis-SUMO-ETP7$_{aa270\text{-}538}$
78	C41 (DE3)	6xHis-SUMO-ETP7$_{aa358\text{-}518}$
79	C41 (DE3)	pelB-6xHis-SUMO-ETP7$_{aa358\text{-}518}$
93	LOBSTR (DE3)	6xHis-SUMO-ETP7
94	LOBSTR (DE3)	pelB-6xHis-SUMO-ETP7
95	LOBSTR (DE3)	6xHis-SUMO-ETP7$_{aa358\text{-}518}$
96	LOBSTR (DE3)	pelB-6xHis-SUMO-ETP7$_{aa358\text{-}518}$

Table 6.7 Primers used for generation of *E. coli* plasmids

Number	Sequence	Fragment	GPN
1179	tacatATGCTGCAATCCTTACGGG	NdeI/*Etp7*/HindIII	086
1180	gcaagcttCATGCGTACCGTTAACC		
1180	gcaagcttCATGCGTACCGTTAACC	BamHI/*Etp7*/HindIII	087
1181	tcggatccgCTGCAATCCTTACGGGA		
1381	atgaaaacctgtattttcagggacatatgCTGCAATCCTTACGGGA	NdeI/*Etp7*/BamHI	121
1382	gttagcagccggatcctcgagTCACATGCGTACCGTTAACC		
1575	gtgatgatgatgatgatgatgatgatgggccatcgccggctgg	GPN001	130
1576	GGTTAACGGTACGCATGTGAtgagatccggctgctaacaaagc		
1577	gctgcccagccggcgatggcccatcatcatcatcatcatcatcatcatcac	*10xHis*/TEV/*Etp7*	
1578	gctttgttagcagccggatctcaTCACATGCGTACCGTTAACC		
1677	GGTCTCCATGGGCAGCAGCCATCATCA	*SUMO*	131
1678	GGTCTCCACCACCAATCTGTTCTCTGTGAG		
1675	GGTCTCCTGGTatgCTGCAATCCTTACGGGAC	GPN130	
1676	GGTCTCACCATatgtatatctccttcttaaagt		
1696	GGTCTCAggccGGCAGCAGCCATC	*6xHis/SUMO/Etp7*	136
1697	GGTCTCATCACATGCGTACCGTTAACCCC		
1698	GGTCTCAGTGAtgagatccggctgctaacaaagc	pET22b	
1699	GGTCTCAggccatcgccggctggg		

1788	CTCACAGAGAACAGATTGGTGGTatgCTGCAATCC TTACGGGACAAGTACGA	Depending on the template used *Etp7*$_{Y367H,\ V523A}$, *Etp7*$_{E369Q}$, *Etp7*$_{\Delta 392\text{-}398}$	138, 139, 140
1789	gggctttgttagcagccggatctcaTCACATGCGTACCGTT AACCCCTGC		
1784	ACCACCAATCTGTTCTCTGTG	GPN131 without *Etp7*	
1785	gagatccggctgctaacaaa		
1678	GGTCTCCACCACCAATCTGTTCTCTGTGAG	GPN131/GPN136 omitting *Etp7*	148, 149
1919	GGTCTCAtgagatccggctgctaacaa		
1675	GGTCTCCTGGTatgCTGCAATCCTTACGGGAC	*Etp7*$_{aa1\text{-}269}$	
1920	GGTCTCActcaTCAGGGAGGGACCGAC		
1921	GGTCTCActcaTCACATGCGTACCGTTAACCC	*Etp7*$_{aa270\text{-}538}$	150, 151
1922	GGTCTCATGGTACCGCCCCTCCGTTC		
1923	GGTCTCATGGTGGTACATGTGCCTTATACGG	*Etp7*$_{aa358\text{-}518}$	152, 153
1924	GGTCTCActcaTCAACGCCGGTCCAGG		

7 Manuscript

The following manuscript was published online ahead of print on December 07, 2022 in the journal Current Biology:

"Host-symbiont interactions in *Angomonas deanei* include the evolution of a host-derived dynamin ring around the endosymbiont division site"

Authors: Jorge Morales[*], Georg Ehret[*], Gereon Poschmann, Tobias Reinicke, Anay K. Maurya, Lena Kröninger, Davide Zanini, Rebecca Wolters, Dhevi Kalyanaraman, Michael Krakovka, Miriam Bäumers, Kai Stühler, and Eva C. M. Nowack

* Contributed equally

Figures and tables from the manuscript that were modified and displayed in this dissertation are listed below:

Number of or table in manuscript	Number of figure or table in Dissertation
Figure 1	Figure 2.1
Figure 2	Figure 2.2, Figure 2.9
Figure 3 a	2.5 B
Figure 3 b/c	Figure 2.27
Supplementary Figure 1	Figure 2.3
Supplementary Figure 3	Figure 2.16 B
Supplementary Figure 4	Figure 6.1
Supplementary Table S2	Table 2.1
Supplementary Table S3	Table 6.5

LC-MS/MS data of *A. deanei* samples was generated by Dr. Gereon Poschmann from the Institute of Molecular Medicine, Heinrich Heine University Düsseldorf, and proteome analysis of the data presented in 2.1 was performed by Dr. Jorge Morales and Prof. Dr. Eva C. M Nowack.

Plasmids, cell lines and contributions to experiments from Dhevi Kalyanaraman, Rebecca Wolters, Davide Zanini, Michael Krakovka, Lucie Hansen, Tobias Reinicke, Anay K. Maurya, Dr. Miriam Bäumers, Dr. Lena Kröninger and Dr. Jorge Morales were indicated in Table 6.1, Table 6.3 and the respective chapters covering the experiments.

8 Acknowledgements

Nach einer langen Reise möchte ich nun allen danken die mich während der Promotion mit Rat und Tat unterstützt haben.

Ich danke meiner Chefin Prof. Dr. Eva Nowack und Prof. Dr. Johannes Hegemann, die mit ihrer Leidenschaft an der Wissenschaft stets Vorbilder für mich waren. Sie ermöglichten mir auch im Rahmen der Graduate School „Molecules of Infection III“ (MOI III) die Promotion an einem außerordentlich spannenden Thema in einer sehr harmonischen und familiären Arbeitsgruppe unter Evas Leitung, in der ich mich über die Jahre stets wohlgefühlt habe.

Im Zuge dessen möchte ich natürlich auch der MOI III und der Jürgen Manchot Stiftung danken, die mit ihrem Curriculum und der ausgezeichneten wissenschaftlichen Unterstützung in allen Bereichen einen unbeschwerten Focus auf die Forschung ermöglichte. Die sehr anregende und großartige Atmosphäre zwischen Professoren und Stipendiaten bei den regelmäßigen Treffen waren immer Highlights, auf die man sich freuen konnte.

Natürlich möchte ich auch all meinen Laborkollegen danken, mit denen es durch die Höhen und Tiefen des Laboralltags ging. Angefangen mit Jorge und Sofia, die mir das Handwerk von *Angomonas* beigebracht haben, Jan der aus irgendwelchen Gründen schon seit meiner Bachelorarbeit zufällig immer im gleichen Institut als TA gearbeitet hat und mir auch mal unter die Arme greifen konnte, wenn wieder alles auf einmal fertig musste. Auch danke ich Luis und Linda die von der grünen Seite der Gruppe immer wussten was noch zu probieren ist, wenn mal wieder die Proteine auf dem Tisch was anderes gemacht haben als im Kopf. Ich danke auch Lena, Vika und Tobi, die später dazustießen aber eine große Hilfe waren und mit denen ich auch immer gern Zeit verbracht habe. Ich danke auch den vielen Studenten, die ich selbst betreut habe, denn mit jedem bin ich auch selbst ein Stück gewachsen.

Ich danke auch der Unterstützung von dem Cai-Team, die mir so viel über die verschiedenen Mikroskope und deren Handhabung beigebracht haben.

Der letzte Abschnitt richtet sich an meine Freunde und Familie, die immer ein sicherer Hafen der guten Stimmung waren, wenn das Labor und die Experimente es nicht waren. Danke an meine Eltern, die stets an meine Fähigkeiten geglaubt und mich immer ohne Wenn und Aber nach allen Möglichkeiten unterstützt haben.

Zuletzt danke ich auch Rin. Sie half mir auf und motivierte mich als es mir wirklich schlecht ging und ich freue mich über jeden Tag, den ich mit ihr verbringe.

Ich werde auf die Zeit des Studiums und der Promotion stets gern zurückblicken.